AN ABSTRACT OF THE DISSERTATION OF

Arne E. Skaugset III for the degree of Doctor of Philosophy in Forest Engineering presented on January 24, 1997. Title: Modeling Root Reinforcement in Shallow Forest Soils.

Abstract approved: _____

Marvin R. Pyles

A hypothesis used to explain the relationship between timber harvesting and landslides is that tree roots add mechanical support to soil, thus increasing soil strength. Upon harvest, the tree roots decay which reduces soil strength and increases the risk of management -induced landslides. The technical literature does not adequately support this hypothesis. Soil strength values attributed to root reinforcement that are in the technical literature are such that forested sites can't fail and all high risk, harvested sites must fail. Both unstable forested sites and stable harvested sites exist, in abundance, in the real world thus, the literature does not adequately describe the real world.

An analytical model was developed to calculate soil strength increase due to root reinforcement . Conceptually, the model is composed of a reinforcing element with high tensile strength, i.e. a conifer root, embedded in a material with little tensile strength, i.e. a soil. As the soil fails and deforms, the reinforcing element also deforms and stretches. The lateral deformation of the reinforcing element is treated analytically as a laterally loaded pile in a flexible foundation and the axial deformation is treated as an axially loaded pile. The governing

differential equations are solved using finite-difference approximation techniques.

The root reinforcement model was tested by comparing the final shape of steel and aluminum rods, parachute cord, wooden dowels, and pine roots in direct shear with predicted shapes from the output of the root reinforcement model. The comparisons were generally satisfactory, were best for parachute cord and wooden dowels, and were poorest for steel and aluminum rods.

A parameter study was performed on the root reinforcement model which showed reinforced soil strength increased with increasing root diameter and soil depth. Output from the root reinforcement model showed a strain incompatibility between large and small diameter roots. The peak increase in soil strength attributed to roots was controlled by the small (< 4mm) diameter root fraction.

These results were used to calculate the effect of timber harvesting on a small, approximately 7.6 m^3 (10 yd^3) , hypothetical landslide in a shallow, cohesionless, forest soil. The root reinforcement model predicted a post-harvest reduction in soil strength of 14 and 19 percent for a soil with and without 5 kPa (105 lbs/ft^2) of cohesion, respectively.

Modelling Root Reinforcement in Shallow Forest Soils

by

Arne E. Skaugset III

A DISSERTATION

submitted to

Oregon State University

in partial fulfillment of
the requirements for the
degree of

Doctor of Philosophy

Completed January 24, 1997

Commencement June 1997

Doctor of Philosophy dissertation of Arne E. Skaugset III presented on January 25, 1997

APPROVED:

Major Professor, representing Forest Engineering

Head of Department of Forest Engineering

Dean of Graduate School

I understand that my dissertation will become part of the permanent collection of Oregon State University libraries. My signature below authorizes release of my dissertation to any reader upon request.

Arne Skaugset, Author

ACKNOWLEDGMENTS

Initially, this project was supported by the Forest Engineering Department through the Forest Research Laboratory. However, for most of its life this project was supported by the Adaptive COPE Program. That support is gratefully acknowledged.

This odyssey started, probably about 12 years ago, when Dr. Marvin Pyles took a chance by accepting as a Ph.D. student an older than average, "dirt forester" made good. Since that decision, I have enjoyed a 12 year association with Marv Pyles. During that time he has filled the roles of mentor, associate, colleague, peer, and friend to me. It is not understating the case to say that without Marv and his support, I would not be in the position I am. For all the risks he took and the efforts he has expended on my behalf, I am beholden. I look forward to a long and prosperous career and friendship with Marv.

I would like to acknowledge the rest of my committee; Dr. Lee Schroeder, Dr. Bob Beschta, Dr. Pete Klingeman, and Dr. Dave Paine. I would like to thank them for their help and support and for sticking with me. Specifically I would like to thank Dave Paine and Lee Schroeder, whose circumstances changed significantly during the life of this project, for sticking with me to the final defense. It certainly made my task easier.

My colleagues at both the Adaptive COPE Program and in the Forest Engineering Department have had to persevere while I finish this dissertation. I acknowledge their patience, help, and support

My children must also be acknowledged. The fact that I was still in college was a source of acute embarrassment to my first grade son, 10 years ago, when the parents of all his classmates already had degrees. He has turned the tables on me repeatedly since then by accompanying any family discussions regarding the completion my dissertation with multiple derogatory comments which associate any such accomplishment up there with the Beavers winning the Rose Bowl. My children spent their adolescence with a father who was perpetually either working on or planning to work on his dissertation most evenings and weekends. Well kids, its finally done.

It is customary at this point to acknowledge the love, support, and encouragement of one's spouse. That sentiment certainly holds in this case. I must acknowledge the uncomplaining support and unfailing love of my wife, Janet, throughout the decade it has taken me to complete this dissertation. However, my debt to her does not come close to being fulfilled with this simple statement, no matter how heartfelt, because this dissertation and the steps along life's road that it has facilitated, simply would not have been possible without my wife. It was my wife, a full time mother and homemaker, who grudgingly allowed her babies to be put in daycare and then went to work full time in order to support my desire to obtain a Ph.D. This dissertation would not have been possible and simply would have occurred without her . Dissertations should be allowed to have co-authors and mine would be Janet Skaugset.

TABLE OF CONTENTS

TABLE OF CONTENTS (Continued)

LIST OF FIGURES

LIST OF FIGURES (Continued)

LIST OF FIGURES (Continued)

LIST OF FIGURES (Continued)

LIST OF FIGURES (Continued)

LIST OF FIGURES (Continued)

LIST OF FIGURES (Continued)

LIST OF TABLES

LIST OF TABLES (Continued)

LIST OF APPENDIX FIGURES

LIST OF SYMBOLS

S	soil strength; kPa, lbs/in^2
ΔS	change in soil strength; kPa, lbs/in^2
S_{comp}	composite soil strength; kPa, lbs/in^2
S_r	soil strength attributed to roots; kPa, lbs/in^2
c	soil cohesion; kPa, lbs/in^2
c'	effective soil cohesion; kPa, lbs/in^2
ϕ	internal angel of friction; °
ϕ'	effective internal angle of friction °
σ_n	total normal stress; kPa, lbs/in^2
σ_n'	effective normal stress; kPa, lbs/in^2
u	pore water pressure; kPa, lbs/in^2
T	tension in the reinforcing element; kN, lbs
T_{max}	maximum allowable tension in the reinforcing element; kN, lbs
T_r	increased tension in root; kN, lbs
T_x	applied tensile load perpendicular to failure surface; kN, lbs
T_y	y-component of reinforcing element tension; kN, lbs
ΔT	change in the tensile force; kN, lbs
t_r	root tensile stress; kPa, lbs/in^2
$t_{r_{ult}}$	average ultimate root stress; kPa, lbs/in^2
V	shear in the reinforcing element; kN, lbs
r_t	total tensile strength per unit soil area; kN/m^2, lbs/in^2
A	soil cross sectional area; m^2, ft^2
A_r	total cross sectional area in roots; cm^2, in^2
A_s	reinforcing element surface area; cm^2, in^2
K	a horizontal earth pressure coefficient
σ_v	vertical soil pressure; kPa, lbs/in^2
X	reinforcing element horizontal spacing; m, ft
Y	reinforcing element vertical spacing; m, ft
Z	shear zone width; cm, inches
FS_R	factor of safety in rupture
FS_p	factor of safety in pull-out
R_t	maximum allowable tensile stress in reinforcing elements; kPa, lbs/in^2
t	reinforcing element thickness; cm, inches
μ^*	apparent coefficient of friction
L_e	effective length of reinforcing element to resist pullout; m, ft.
y	reinforcing element lateral deformation; cm, inches
x	distance along the reinforcing element; m, ft
z	movement of reinforcing element through the soil; m, ft

LIST OF SYMBOLS (Continued)

θ	angle the deflected reinforcing element makes with its original vertical position; °
Δl	change in reinforcing element length; cm, inches
E	modulus of elasticity; kPa, lbs^2
dy	differential lateral deflection of the reinforcing element
dx	differential length of the reinforcing element
E_s	secant modulus of the soil response; kN/cm, lbs/in
E_{s_i}	initial tangent modulus of soil reaction; kN/cm, lbs/in
h	discrete element length; cm, inches
Δh	change in discrete element length; mm, inches
n	number of nodes in the reinforcing element
[A]	coefficients matrix
[b]	constants matrix
[x]	matrix of unknowns
[U]	upper triangular matrix
[L]	lower triangular matrix
V_y	applied force parallel to failure surface on the reinforcing element; kN, lbs
b	reinforcing element width and diameter; cm, inches
k_h	coefficient of horizontal subgrade reaction; kN/cm^3, lbs/in^3
k	constant of subgrade reaction; kN/cm^3, lbs/in^3
p	soil pressure; kN/cm, lbs/in
p_{ult}	ultimate soil resistance; kN/cm, lbs/in
p_{uf}	adjusted ultimate soil resistance; kN/cm, lbs/in
p_f	ultimate pullout capacity; kN, lbs
γ	soil density; kN/m^3, lbs/in^3
N_q	bearing capacity factor
K_a	active earth pressure coefficient
K_o	at-rest earth pressure coefficient
β	complement of the passive earth pressure coefficient
l	reinforcing element length; m, ft
l_o	original reinforcing element length; m, ft
F_s	shear-stress transfer force; kN, lbs
Ψ	shear-stress transfer function
τ	shear stress; kPa, lbs/in^2
τ_{ult}	ultimate shear-stress transfer; kPa, lbs/in^2
z	axial deformation of discrete element; cm, inches
δ	apparent friction angle
a_o, a_1, a_2	shear-stress transfer function empirical coefficients
SC	scaling coefficient

LIST OF UNITS AND THEIR CONVERSION FACTORS

Length

1 inch = 25.4 mm
1 inch = 2.54 cm
1 foot = 0.3048 m
1 yard = 0.9144 m

Area

1 in^2 = 6.45 cm^2
1 ft^2 = 929.03 cm^2
1 ft^2 = 0.029 m^2
1 yd^2 = 0.836 m^2

Volume

1 in^3 = 16.387 cm^3
1 ft^3 = 28,316.85 cm^3
1 ft^3 = 0.0283 m^3
1 yd^3 = 0.765 m^3

Mass

1 lb mass = 452.6 gms
1 lb mass = 0.4536 kg

Force

1 lb force = 4.448 N
1 kg force = 9.807 N
1 kip = 1,000 lbs force
1,000 lbs force = 4.448 kN

Pressure

1 lb/in^2 = 6.89 kPa
1lb/ft^2 = 0.048 kPa

This dissertation is dedicated to the
patience and longsuffering
of my wife and children

Janet, Eric, and Kari

Modeling Root Reinforcement in Shallow Forest Soils

INTRODUCTION

Forested headwater streams of the Pacific Northwest continue to be the focus of ongoing forest resource management conflict. At issue is whether or not it is possible to simultaneously manage the forests of these headwater watersheds and maintain a viable and productive fishery in the streams. Of particular interest to this project are the small, steeply-sloping, first order watersheds which are the source areas for many naturally occurring landslides from forested areas. These watersheds are of particular interest for a number of reasons. First of all, they are the most numerous of all other size and order watersheds, thus, most forest management activities occur on them. Secondly, being topographically at the highest elevations in a large watershed, the rest of the stream system is downstream of these steeply-sloping, first order watersheds. Finally, forest management activities on these watersheds can cause accelerated erosion by increasing the size and/or frequency of landslides from these watersheds. Thus the resource management conflict.

Landslides associated with forest management from the steeply-sloping headwater watersheds are divided into two categories; road-related landslides and in-unit landslides or landslides occurring in harvest units apparently unrelated to roads. The causes of road-related landslides are fairly

straightforward and improvements in forest road design, layout, construction, and maintenance appear to have reduced the rate of accelerated erosion due to landslides from forest roads. In the case of landslides from forest roads, it appears that definite steps can be taken to reduce the incidence of these landslides with the promise of positive results. This same positive statement can not be made regarding in-unit landslides and headwater watersheds. Even the certainty of an increase in landslide rate in harvest units relative to forests can be and is debated. If such an increase exists, its cause or causes are less than straightforward and the steps to be taken to reduce the increase are less than definite and certainly don't necessarily promise definite results. The one statement that can be made regarding the occurrence of landslides within harvest units it that they have served to establish a perception of the importance of tree roots and, in particular, reinforcement from tree roots to the overall stability of steep, forested slopes.

One of the reasons this project was undertaken was to investigate the magnitude of the importance of root reinforcement to the overall stability of steep, forested slopes. As an example, consider the graph in Figure 1-1. This graph portrays the change in the stability of a forested slope, as represented by a factor of safety, against a time line which shows years since timber harvest. The annual reduction in hillslope stability due to positive pore water pressure from seasonal winter storms is portrayed as a series of sharp valleys between relatively straight line segments which represent summers. The reduction in

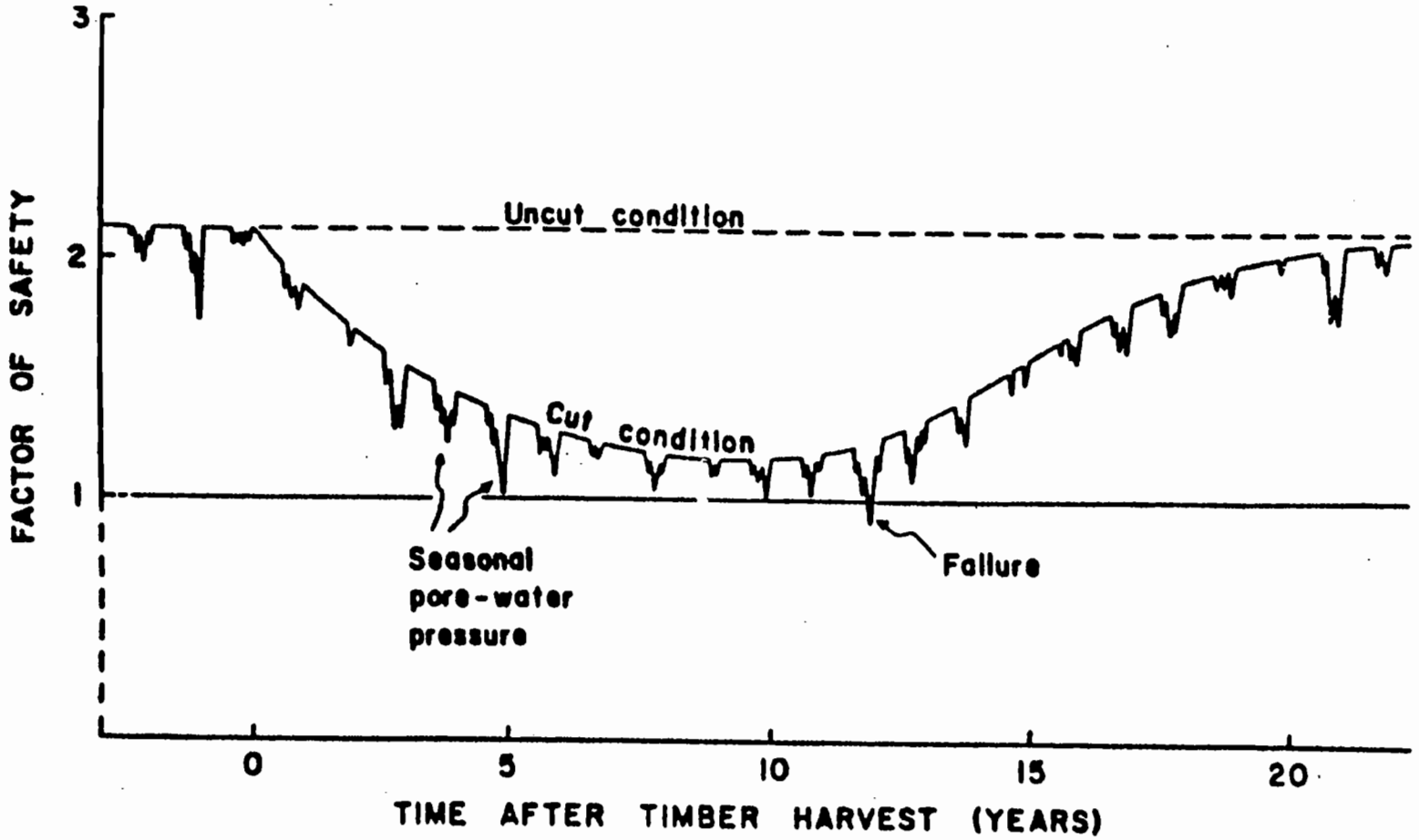

Figure 1-1. A graph showing the hypothesized relationship between seasonal pore water pressure and the loss and recovery of soil strength due to root reinforcement on the factor-of-safety of a landslide-prone slope as a function of time since timber harvest (Ziemer, 1981b).

hillslope stability due to loss of root reinforcement caused by timber harvesting is portrayed by a larger scale, smooth valley which starts descending at age 0, reaches a minimum at about 10 years, and approaches an uncut condition again at about 20 years. If this is a true portrayal of the relative magnitude of the factors affecting hillslope stability, it is clear that the magnitude of the influence of root reinforcement to slope stability is three to four times the magnitude of the seasonal reduction in slope stability due to winter storms. From the information portrayed in Figure 1-1, it would appear to be almost impossible to have a forested site fail during winter as a result of pore water pressure changes alone. Yet the forested slopes of headwater watersheds fail regularly during large, slide-producing winter storms. The content of the graph in Figure 1-1 is counterintuitive in that it doesn't explain the real world as it is observed and the author of the graph (Ziemer, 1981b) provides no data to support its construction.

The technical literature can be searched to find data to confirm the hypothesis implicit in Figure 1-1. Sidle et. al. (1985) presents a table which summarizes research results quantifying the magnitude of soil strength attributed to root reinforcement. That information is summarized in Table 1-1. The change in soil strength attributed to root reinforcement ranges from a high of 17.5 kPa to a low of 1.0 kPa with a median value in the range of 8.0 to 10.0 kPa.. This information is of value only when compared with the inherent strength of steeply-sloping forested slopes. From Schroeder and Alto (1983), average values

Table 1-1. Research results showing the soil strength increase attributed to root reinforcement displayed as an apparent cohesion term, C_a, in kPa (adapted from Sidle et, al., 1985).

Literature Source	Soil, Vegetation, & Location	C_a (kPa)
Endo & Tsuruta (1969)	nursery loam soil w/alder	2.0-12.0
Swanston (1970)	forest soil w/conifers - SE Alaska	3.4 - 4.4
O'Loughlin (1974)	forest soil w/conifers - B.C.	1.0 - 3.0
Burroughs and Thomas (1977)	forest soil w/conifers - W OR & ID	3.1 - 17.5
Wu, et. al. (1979)	forest soils w/conifers - SE Alaska	5.9
Waldron & Dakessian (1981)	clay loam w/pine seedlings - laboratory	5.0
Gray & Megahan (1981)	forest soil w/conifers - Idaho	10.3
O'Loughlin, et. al. (1982)	forest soil w/mixed evergreen forest - N.Z.	3.3
Sidle & Swanston (1982)	forest soil w/conifers & brush - SE Alaska	2.2
Waldron, et. al. (1983)	clay loam w/pine seedlings - laboratory	8.9 - 11.8

of internal angle of friction, saturated unit weight, and unit weight of *in situ* soils at field moisture content are 35.4°, 18.2 kN/m^3, and 16.0 kN/m^3, respectively. The frictional component of the inherent soil strength is 11.4 kPa and the frictional component of the soil saturated with water is 6.0 kPa. It is commonly accepted that the effect of saturating a soil profile reduces the frictional component of soil strength by roughly half. In this particular case the reduction is 53 percent which is roughly what is expected. From Table 1-1, soil strength attributed to root reinforcement ranges from a high of 17.5 kPa, which is 154 percent of inherent soil strength, to a low of 1.0 kPa, which is 9 percent of inherent soil strength. So from these data the soil strength attributed to root reinforcement can be as much

as 1.5 times *in situ* frictional strength or as little as 9 percent of it. On average, the *in situ* frictional strength and the median value of strength increase from Table 1-1 appear to be roughly equal. These data certainly do not explain Figure 1-1 and, in fact, raise even more questions. For example, is root reinforcement really a minority of the available soil strength (9 percent) or is it a primary source of strength? Or, are both of these numbers correct and the amount of soil strength that can be attributed to root reinforcement depends on the particular slope and situation in question? It appears that the knowledge base, at present, is inadequate to answer these questions. Therefore, to manage these steep, forested, landslide-prone sites while simultaneously considering the true effect of the management on soil strength will require more knowledge at a more refined level. Thus, a second reason to undertake this project is the need for better knowledge and management tools with which to manage forest resources, specifically the stability of steep, landslide-prone forested slopes.

OBJECTIVES

The concern about root reinforcement and its affect on slope stability has far outstripped the knowledge available upon which to base management decisions. In the Oregon Forest Practice Rules it is recommended that operators "...establish or maintain plant species that will enhance slope stability in harvested areas..." on landslide-prone sites (Oregon Department of Forestry, 1994). On certain federal forest lands in the Pacific Northwest the policy is less ambiguous. On any site with a risk of landslides, no matter how slight, management activities are eschewed.

These policies are based largely on findings which are an outgrowth of empirical data sets. There is little theoretical knowledge regarding the fundamental mechanisms that govern the behavior of root reinforcement. Through the collection of more and bigger empirical data sets, progress can be made in root reinforcement research and it will certainly be successful. Undoubtedly, over time, this research will result in an improved understanding of root reinforcement. However, this course of action also harbors shortcomings. The development of a primarily empirical database means progress is made by trial and error. For every new soil, landform, tree species, and vegetation type, a new research project is needed to set management guidelines for root reinforcement. This process could become onerous as ecosystem management

becomes a reality and results in various new and different alternative silvicultural prescriptions.

It would seem better to develop management tools based on the mechanical behavior of the soil, as described by standard parameters, the physical properties and size of the roots, and an understanding of both the failure and reinforcement mechanisms at work in the soil. This latter goal is the direction of this project.

The objectives of this project are:

1. To develop an analytical model of root reinforcement that predicts the shear strength increase of a sandy soil due to the presence of conifer roots. The model will predict the deformed shape and stresses that accompany the deformed shape of a conifer root based on the physical properties of the soil and the physical properties and size of the roots.
2. To validate or verify the model using information and data from the technical literature.
3. Use the model to calculate the magnitude of the increase in soil strength that can be attributed to reinforcement by conifer roots in sandy soils.

The balance of this dissertation is presented in four chapters. The first chapter is the Literature Review in which the development of a testable hypothesis of a root reinforcement mechanism is presented along with the research that has gone into testing the hypothesis. Then the development of both

the conceptual and analytical model for predicting root reinforcement is presented including a description of the flowpath of the model algorithm. In the chapter on results, the output from the model is compared with research results from the technical literature to determine if the output from the root reinforcement model is realistic. Also, a parameter study is presented that was used to investigate how the predicted stresses and strains in the model reinforcing element are affected by different input values of model parameters and how this, in turn, affects root reinforcement. In a final chapter, conclusions of this project are presented and their ramifications are discussed along with suggestions for future research.

LITERATURE REVIEW

The subject of timber harvesting and landslides is a relatively young area of study. Research on this subject did not appear in the technical literature until the 1950's. Even in the early references, tree roots and root reinforcement are tightly linked with the subject of landslides and timber harvesting (Croft and Adams, 1950; Flaccus, 1959). In these early references, the link between timber harvesting, landslides, and root strength is, truly, anecdotal and not the result of rigorous investigation (i.e. Croft and Adams, 1950). This illustrates the degree to which root reinforcement, timber harvesting, and landslides have been closely associated in the minds of the researchers investigating this field of study. This perceived close association has greatly influenced and continues to influence the kind and quality of research being undertaken to study the management of landslide prone forested slopes.

Debris Avalanche Inventories

Bishop and Stevens (1964) is one of the first published articles that involved timber harvesting and landslides and had more rigor than the references cited above. It is probably the single most cited reference regarding root strength, timber harvesting, and landslides. The research method used in this article is a technique that is the foundation of research into the association between timber harvesting and landslides - - the landslide or debris avalanche

inventory. A debris avalanche inventory is simply an accounting of the occurrence, and in some cases the size, of landslides within a fixed area. These inventoried landslides are then sorted and stratified by land use and other independent variables such as geology, landform, soils, and slope to name a few. The research results from debris avalanche inventories which report timber harvesting effects on landslides cover a wide range of conditions and variables. Landslide inventories have been reported from New Zealand, Alaska, British Columbia, and the Pacific Northwest over the past 30 years and thus, cover a wide range of geology, soils, precipitation regimes, and timber harvesting systems and practices.

The results from these debris avalanche inventories are usually presented in a table such as Table 3-1 (see Swanston and Swanson, 1976; Swanson, et. al., 1981). The implications of the results presented in Table 3-1 are really quite clear. Without fail, across different continents, regions, geology, and researchers, timber harvesting activities, as represented by logging roads and clearcut harvest units, have caused accelerated erosion by landslides.

The results which portray the influence of logging roads is really quite unequivocal. In every case where results have been reported, logging roads caused an increase in the frequency of landslides by at least one order of magnitude and up to four orders of magnitude. In two cases, the Oregon Coast Range and British Columbia, the average landslide volume also increased. The net results are that logging roads increased the erosion rate by landslides from 25

Table 3-1. A summary of research results from landslide inventories for forests, clearcuts, and road right-of-ways carried out in Oregon, Washington, British Columbia, and new Zealand. The number in parenthesis indicates the increase in erosion rate compared to the forest. The forest numbers from New Zealand and marked with an * indicate they are estimated.

	FORESTS			CLEARCUTS			LOGGING	ROAD	R/W
	slide rate (slides/acre)	slide volume (yd^3)	erosion rate (yd^3/acre/yr)	slide rate (slides/acre)	slide volume (yd^3)	erosion rate (yd^3/acre/yr)	slide rate (slides/acre)	slide volume (yd^3)	erosion rate (yd^3/acre/yr)
Coast Range Mtns., OR									
Ketcheson & Froehlich, 1978	1 / 28	41	0.10	1 / 21	47	0.37 (3.7)	-	-	-
Swanson, et. al., 1977	1 / 31	42	0.17	1 / 44	145	0.33 (1.9)	1 / 4	505	8.4 (49)
Schroeder & Brown, 1984	1 / 63	-	-	1 / 8.6	-	-	-	-	-
Cascade Mtns., OR									
Swanson & Dyrness, 1975	1 / 387	1,095	0.197	1 / 82	1,758	0.85 (4.3)	1 / 7	1,767	9.95 (51)
Morrison, 1975	1 / 434	2,603	0.24	1 / 62	574	0.62 (2.6)	1 / 2	1,868	82.3 (343)
British Columbia, Canada									
O'Loughlin, 1972	1 / 2,095	3,978	0.059	1 / 362	1,504	0.13 (2.2)	1 / 94	4,514	1.5 (25)
Olympic Mtns., WA									
Fiksdal, 1974	1 / 191	6,089	0.38	0	0	0	1 / 2	783	62.6 (165)
Siskiyou Mtns., OR									
Amaranthus, et. al., 1985	1 / 1,193	3,172	0.13	1 / 66	1,166	0.89 (6.8)	1 / 9	2,636	14.5 (12)
New Zealand									
O'Loughlin & Pearce, 1976	1 / 370*	719*	0.53*	1 / 16	735	11.5 (21.7)	-	-	-

implicitly or explicitly states that tree roots "bind the soil together" and "add mechanical support to the soil thus increasing soil strength". Loss of root strength after timber harvesting due to the decay of the roots of harvested trees results in decreased soil strength and an increased landslide rate (or erosion rate). Research results from debris avalanche inventories, by themselves without any other supporting research, are perceived to support the root reinforcement hypothesis by, first of all, showing an increased erosion rate in clearcut logged areas compared with forested areas. In this case, the hypothesis is supported on the basis of the argument that because only the vegetation is being manipulated, there must be a vegetative link to the increase in landsliding and that link is, most likely, through the root system. Secondly, debris avalanche inventory results show a perceived lag time between clearcut harvest and the occurrence of landsliding. This is interpreted as the time required for the small roots of the harvested trees to decay which, in turn, reduces root reinforcement and soil strength thus leading to the delayed occurrence of increased landsliding after harvest.

The data from the Oregon Coast Range landslide inventories (Ketcheson and Froehlich, 1978; Swanson, et. al., 1977) show for a forested condition the highest landslide frequency and smallest average landslide volumes illustrating that the Oregon Coast Range has the most and smallest landslides on a per unit area basis. However, these two landslide inventories are also the only ones reported in which the inventory data was collected by field traverse under the

to 342 times over background value. However, the effect of logging roads on landslides does not involve roots and root reinforcement, but rather primarily altered subsurface flow regimes on hillslopes, surface road drainage on logging roads, and altered slope geometry in the form of cut banks and side cast and fill slopes. Thus, the subject of logging roads and accelerated erosion by landslides will not be discussed further in this dissertation.

The results from the debris avalanche inventories showing the effect of clearcut harvest units on landslides is more equivocal. With the exception of the results from the Olympic Mountains (Fiksdal, 1974), the debris avalanche inventory results show an across-the-board increase in erosion rate. However, the manner in which the increase in erosion rate is attained is not consistent. For the inventories with erosion data from the Oregon Coast Range (Ketcheson and Froehlich, 1978; Swanson, et. al., 1977), the increased erosion rate is the consequence of an increase in the average size of the landslides while the landslide frequency remained, in essence, unchanged. Conversely, the balance of the landslide inventory results show a decrease in the average landslide volume and an increase in landslide frequency. This increase is often drastic, by as much as one to two orders of magnitude.

The conclusions regarding clearcut harvesting and landslides invariably drawn from the results of these debris avalanche inventories is that the stability of steep, landslide-prone forested hillslopes is inexorably linked to trees and tree roots. Based on these conclusions, a hypothesis has been developed that either

forest canopy. For the rest of the quoted studies, the inventory data for landslides in the forests were collected from either aerial photographs or from an aerial platform such as an airplane. The results from the published debris avalanche inventories clearly show that for the forested condition, field traversed landslide inventories show a higher landslide frequency and smaller average landslide volume than the aerial landslide inventories.

A possible explanation for this observation is that in forested conditions, landslide inventories carried out from aerial platforms "under sample" landslides (Pyles and Froehlich, 1987), especially small landslides, which means the results are skewed by the large landslides visible through the forest canopy. Thus, landslide frequencies can be underestimated and landslide sizes can be overestimated for forested conditions. Therefore, results like those shown in Table 3-1, especially the results in which all the inventory data was collected from aerial platforms and show increased landslide and erosion rates could, in part, result from the increased visibility of the smaller landslides. The results of landslide inventories which use aerial platforms for data collection exclusively and which show an increased incidence of landslides and landslide related erosion, may be as much the consequence of sampling methods as management effects on physical processes.

Examples of this type of result can be illustrated using landslide inventories from southeast Alaska (Bishop and Stevens, 1964) and the northern Rocky Mountains of Idaho (Megahan, et. al., 1978). In Bishop and Stevens (1964),

the authors use an examination of a chronological sequence of aerial photographs to show an increase of four and one-half times in both the number and acreage of landslides in the harvested area as compared with the same area before logging. They also report that before logging in two aerial photo sequences the average area of landslides was 4.2 and 2.3 acres and after logging the average size of landslides in three photo sequences was 0.31, 0.77, and 1.3 acres. The authors discuss that with the forest canopy removed, the smaller landslides, especially those within the small, steep, V-notch side-drainages, will become much more visible than they were under the forest canopy. Therefore, it is possible that the results could be explained, at least in part, by an increased visibility of small landslides.

In Megahan, et. al. (1978) , landslides were located using aerial reconnaissance, aerial photography, location of known slides by forest workers, and reconnaissance by road. Over the area inventoried, locating landslides was heavily dependent on aerial methods and the authors state that some landslides were probably not detected. Landslides were found to be inversely correlated to the density of both tree and shrub cover. Tree and shrub cover were used as an index of root density and this result was used to illustrate the effect of root density on landslide occurrence. However, tree and shrub density can also be correlated with landslide visibility from the air. These same results that show a correlation between landslide occurrence and root density also support a

hypothesis of a positive correlation between vegetation density and landslide visibility. Undoubtedly, both mechanisms are at work to unknown degrees.

It must be acknowledged that the cited landslide inventories were carried out by different researchers and come from different geologys and geographic provinces. Part of the differences seen in landslide size and frequency are undoubtedly true differences due to rock types, climate, and landslide measurement methods. The differences observed in the data, especially the forested data, can not be solely attributed to differences in aerial versus field methods of landslide location. However, it seems that the observed results can not be attributed totally to changes in roots either. Pyles and Froehlich (1987) present a thorough discussion of the pitfalls involved with sampling landslides in forests from aerial platforms. In light of this discussion, it is obvious that sampling methods must be considered when interpreting landslide inventory results. For the debris avalanche inventory results from the Oregon Coast Range (Ketcheson and Froehlich, 1978; Swanson, et. al., 1977) there can be no doubt that vegetation manipulation, and undoubtedly root biomass, played a role in the increase in the average landslide size and thus the increased erosion rate. However, in the debris avalanche inventories using an aerial platform for data collection, an explanation of the results must include the effect of both the sampling scheme and vegetation manipulation because both seem equally capable of effecting the results.

As stated earlier, a second, often quoted, result from debris avalanche inventories which links timber harvesting, landslides, and tree roots is a perceived lag time between the harvest of landslide prone hillslopes and the occurrence of landslides. Bishop and Stevens (1964) in southeast Alaska observed an apparent lag time between harvest and the date of slide generation and hypothesized that it may reflect root deterioration time. Also from southeast Alaska, Swanston (1974) reports a roughly 3 - 5 year period between the time of logging and the onset of debris avalanches. In the Oregon Cascades, mostly the H. J. Andrews Experimental Forest, Swanson and Dyrness (1975) and Swanston and Swanson (1976) report that most hillslope failures in clearcuts occurred within 12 years after harvest and they further state that this is apparently a period of increased susceptibility to debris avalanches. In the Oregon Coast Range, Gresswell, et. al. (1979) reported 63 percent of inventoried landslides occurred in 3 year old or younger clearcuts, 29 percent occurred in 4 - 10 year old clearcuts, and only 6 percent occurred in clearcuts greater then 11 years old. O'Loughlin, et. al. (1982) reports from New Zealand that 89 percent of landslide materials, by volume, originated from slopes clearfelled 20 to 40 months before the landslide-producing storm. Megahan et. al. (1978) reports that in the northern Rocky Mountains, on average, there is a 4 to 10 year lag between timber removal and the greatest landslide hazard. Sidle et. al. (1985) in his synthesis book reports that the 3 to 10 year lag time between forest removal and the accelerated

incidence of landsliding provides a strong indication that small tree roots (< 20 mm diameter) are the most important in slope stability.

However, all these published accounts of debris avalanche inventories fail to account for the stochastic occurrence of large storms and the effect this has on both the temporal and spatial distribution of landslides. The above-quoted authors all recognize that the widespread occurrence of landslides happens in response to large, slide-producing storms. In fact, in each article quoted above, research was carried out on the effect of timber harvest on landslides, a debris avalanche inventory was used as a research tool, and the research was undertaken only after a large, slide-producing storm. Furthermore, this research generally focused on areas that experienced widespread landslides. Comparable areas without landslides weren't studied. The authors of the quoted articles all recognize and state that large, slide-producing storms of the magnitude studied occur on a more regular basis than is expected. Large, landslide-producing storms are stated to have a recurrence interval of 5 to 10 years (Bishop and Stevens, 1964; Dyrness, 1967; Gonsior and Gardner, 1971; O'Loughlin, et. al., 1982; Schroeder and Brown, 1984). It is probably not a coincidence that the 5 to 10 year recurrence interval of slide-producing storms is the same order of magnitude and almost the same exact length of time as the 3 to 10 year lag time generally observed between harvesting and landslide occurrence. This lag time may simply represent the average time between harvesting and the occurrence of a landslide producing storm (Froehlich, 1978).

O'Loughlin, et. al. (1982) reports on the occurrence of landslides with respect to time since clearfelling during a landslide-producing storm in New Zealand. The authors report that during a landslide-producing storm, 89 percent of the landslide derived sediment produced came from harvest units that had been clearfelled 20 to 40 months prior to the storm of interest. No landslides occurred on the forested watersheds or the two watersheds that had been clearfelled only 12 and 10 months prior to the large storm. This information is summarized in Table 3-2.

O'Loughlin, et. al. (1982) also lists the maximum, instantaneous peak discharge for each experimental watershed and those values are also listed in Table 3-2. For small watersheds of this size, it is reasonable to assume that the maximum instantaneous peak discharge can be used as a surrogate for the maximum short-term precipitation intensity delivered to the watershed. If an assumption is made that the M14 watershed had the highest peak discharge, a reasonable assumption given the sediment yield, then the landslide occurrence can be correlated with storm magnitude which varied by over 100 percent from M8 to M9.

The role of root strength is emphasized in the O'Loughlin et. al. (1982) paper by comparing the occurrence of landslides during a large storm when the watersheds were unharvested with the occurrence of landslides during a large storm after harvesting. Before timber harvest, there were four landslides on all the experimental watersheds during a large storm compared with 18 landslides

Table 3-2. A summary of watershed data for the December 1979 storm for the Maimai Experimental Catchements, North Westland, New Zealand. In the column labeled Land Use, the date is when the watershed was clearfelled, B indicates it was burned, P indicates it was planted with P. radiata, and F indicates the watershed was in indigenous forest. Peak discharge for M14 was not available. Data was taken from O'Loughlin, et. al. (1982).

Catchement	Area (ha)	No. of Landslides	Landslides / ha	Land Use	Sediment Yield (m^3/ha)	Peak Discharge (l/sec/ha)
M14	4.62	7	1.5	Sept 77; B, P	108.2	--
M9	8.26	5	0.6	Feb 77; B, P	1.7	104.4
M7	4.14	4	1.0	Sept 76; B, P	0.2	84.5
M5	2.31	2	0.9	Jan 78; P	0.2	70.8
M13	4.25	0	0	Nov 78; P	0.1	60.3
M15	2.64	0	0	F	1.2	59.9
M6	1.63	0	0	F	1.0	57.1
M8	3.84	0	0	Nov 78; B, P	0.1	43.8

which occurred after timber harvest during a second large storm. All of the post harvest landslides occurred in harvested watersheds. This appears to be a strong indictment of the effect of timber harvesting on landslides. However, if instantaneous, maximum peak discharges are compared between pre- and post-harvest storms, the post-harvest peak discharges were greater. This could be interpreted as meaning that the post harvest short-term peak rainfall intensities were greater than those that occurred pre-harvest. Furthermore, for the watersheds in which landslides occurred and especially those with multiple landslides, post harvest peak discharges were significantly higher than for pre-harvest peak flows and often up to double the pre-harvest peak discharge. This reinforces the importance of short-term precipitation intensity as a causative factor in landslide occurrence especially when the precipitation occurs in conjunction with timber harvesting.

Obviously, it is not possible to say that root deterioration plays no role in the perceived lag time between timber harvest and the occurrence of landslides and the development of such a hypothesis is reasonable. However, it is just as obvious that the stochastic occurrence of large, landslide-producing storms and the spatial variability of short-term, high intensity rainfall also provides an explanation of the lag time between harvesting and landslide occurrence and the spatial distribution of landslides.

As a result of debris avalanche inventory research, the dominate hypothesis that has been reported in an attempt to explain the link between

timber harvesting, especially clearcut harvesting, and landslides is root strength or root reinforcement. This hypothesis results from the reported increase in erosion by landslides from clearcuts relative to forested sites and the perceived lag time between timber harvesting and the occurrence of landslides in harvest units. The hypothesis is that tree roots add mechanical support to soil and increase its shear strength. After timber harvest, the roots of the harvested trees decay which reduces both the biomass and strength of the roots in the soil resulting in a loss in root reinforcement and thus a decrease in soil shear strength. This hypothesized situation is analogous to the concept of reinforced earth (Vidal, 1969).

Root Strength and Biomass Changes After Timber Harvest

Results from debris avalanche inventory research has lead to the development of a root reinforcement hypothesis or reinforced earth concept to explain the perceived relationship between timber harvesting and the occurrence of landslides. A parallel line of research conducted simultaneously with debris avalanche inventories investigated the strength of roots after timber harvest. The intent of the research was to test aspects of the root reinforcement hypothesis. This research investigated the tensile strength, shear strength, and biomass of roots from uncut forests and from a series of different aged clearcuts.

As expected, the tensile strength of roots declines after the parent tree is harvested. The curve describing the decline in tensile strength over time is a negative exponential curve with a sharp decline in tensile strength in the months and years directly after harvesting. Then the curve levels off and the rate of decline in tensile strength becomes much less. The shape of this trend is illustrated in Figure 3-1.

O'Loughlin (1972, 1974) found that small, 1 to 12 mm in diameter, Douglas-fir roots from coastal British Columbia lost half their tensile strength within three years of the parent tree being cut while western red cedar roots of the same size from the same location took up to five years to lose half their tensile strength. In the Oregon Coast Range, small, less than 1.0 cm in diameter, Douglas-fir roots lost 49 percent of their tensile strength in one year and 74 percent in four years (Burroughs and Thomas, 1977). This same study showed that small Douglas-fir roots from the Northern Rocky Mountains in Idaho had weaker roots when alive but lost tensile strength much more slowly after harvesting with small roots losing only 30 percent of their tensile strength after 12 years. The decline in tensile strength of small radiata pine roots from New Zealand also exhibited an exponential decay form after timber harvest. These roots were both weaker initially and lost tensile strength more quickly with an estimated time to half strength of only 14 months (O'Loughlin and Watson, 1979).

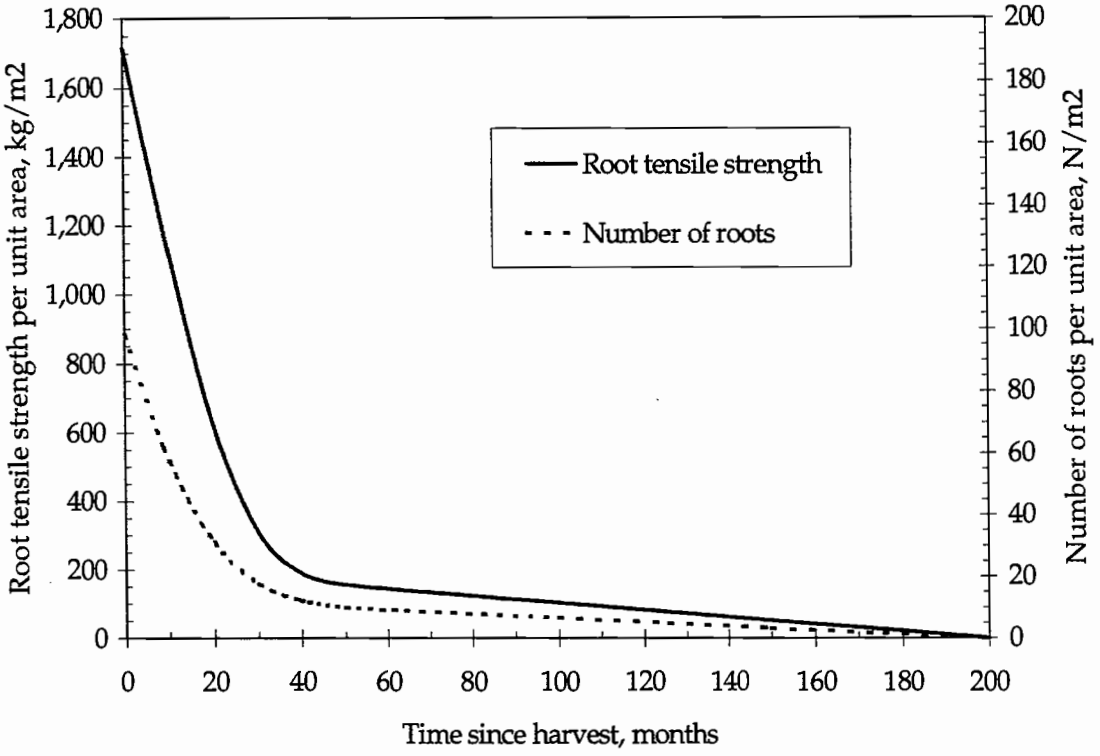

Figure 3-1. Root tensile strength per unit area, kg/m^2, and number of roots per unit area, N/m^2, for 0-1 cm diameter roots of Douglas-fir growing in the Oregon Coast Range. Data is from Burroughs and Thomas (1977).

Ziemer and Swanston (1977) also investigated the strength of tree roots, however, in their study, the shear strength of the roots was determined and used as a surrogate for tensile strength (Ziemer, 1978). The effect of time after harvest on root strength was determined for sitka spruce and western hemlock growing in southeast Alaska. The same trend was observed for this study as was observed in the previous root strength studies, root strength after harvest showed a declining trend with an exponential shape. Small hemlock roots lost approximately one third of their strength within the first two years after harvest and small spruce roots lost about one half of their strength in the same two years. By ten years after harvesting, all root sizes sampled (up to 50 mm) of all species had lost appreciable strength.

In all the studies quoted above, the authors recognized that not only was the strength of the dead roots changing after harvest, but also the biomass of the roots was declining as the smaller roots disappeared from the subsoil due to decay. While the tensile strength of the roots declined, the total number and the biomass of the conifer roots also declined after harvest. O'Loughlin (1972, 1974) recognized the biomass trends and discussed their importance but didn't study them. He did measure the diameter of 150 roots at the headscarps of each of three landslides and found the average diameters to be 1.4, 0.7, and 1.1 cm. He inferred from these measurements that this size class of roots must be the most important to stability because they were the most numerous.

Ziemer and Swanston (1977), again, did not study changes in root biomass explicitly. However, they observed an **increasing** trend in root strength over time in some species and size classes of roots. They found that in some stratifications of time, species, and size class, the sampled roots were dominated by resinous roots which had maintained their shear strength. The non-resinous roots had all decayed and were not present to be sampled so the average strength of the roots was an artifact of the roots that were available to be sampled. Thus, the combination of both root strength and biomass is perceived to be more important than simply the strength of the roots alone. Ziemer and Swanston (1977) also recognized the importance of the invasion of primary succession species to the live and total root biomass of clearcuts. In southeast Alaska, clearcuts are quickly invaded by red huckleberry *(Vaccinium parvifolium)* and because the clearcut studied supported extensive stands of red huckleberry, the authors measured the shear strength of live huckleberry roots. However, they went no further with the subject and did not measure the biomass of live huckleberry roots and didn't discuss how these roots might be important.

Burroughs and Thomas (1977) explicitly studied the effect of time since harvest on the number of roots found in the subsoil. As expected, the number of roots in the subsoil declined after harvest and the trend of the decline also described an exponential decay curve with a sharp decline in the months and years directly after harvest (Figure 3-1). In the Oregon Coast Range, the decline in the number of Douglas-fir roots was more pronounced than in the Rocky

Mountains where roots in a given size class remained intact 35 percent longer. The authors went through an exercise of combining the change in root numbers with time after harvest with the change in the tensile strength of the roots with time after harvest. This combination attempts to represent the trend of total root tensile strength available to a site as a function of time after harvest. As expected, this curve exhibited a very strong exponential decay function (Figure 3-1). For the Rocky Mountains, the estimated time to one half of the total root tensile strength was a little less than two years for all size classes. For the Coast Range, the estimated time to one half of the total tensile root strength was about one year, also for all size classes.

Ziemer (1981a) also studied the effect of forest harvest on root strength as a function of time since harvest. Ziemer (1981a) measured the total biomass of roots, both dead and alive, in an uncut forest and a chronosequence of clearcuts up to 24 years old. He studied not only the decline in the biomass of dead roots of the harvested conifer and hardwood trees but also the increase in live root biomass due to the invasion of brush species. The trend over time in the biomass of the small (< 25 mm) dead root fraction was, as expected, an exponential decay curve. For the small fraction, only two thirds of the biomass of the uncut forest remained in the 3-year old clearcut and only about 30 percent remained in the 7-year old clearcut. In the 12- to 24-year old clearcuts, all but the very largest of the dead roots had decayed. Ziemer (1981a) also measured the increase in live root biomass as primary invasion species became established in the different age

clearcuts. In the 3-year old clearcut, 10 percent of the live root biomass of the uncut forest had been recovered due to the establishment of a bracken fern *(Pteridium aquilinum)* cover. The live root biomass dropped to only 3 percent of the uncut forest biomass in the 7-year old clearcut as the bracken fern was replaced by scattered brush and herbs. The 12- to 24-year old clearcuts became fully vegetated with ceanothus *(Ceanothus velutinus)* causing the live root biomass to increase rapidly. In the 12-year old clearcut, the biomass of live roots less than 2 mm in diameter was 82 percent of that in the uncut forest. However, the biomass of the larger roots recovered more slowly. In the 12-year old clearcut, the biomass of the live roots less than 17 mm in diameter was only 30 percent of that in the uncut forest and total live root biomass was only 10 percent. So, by 12 years after harvest, the subsoil had become mostly recolonized with roots, they were just a different species and size distribution.

The live shear strength of the roots of the tree and brush species encountered at the study site in northern California were also determined. While there were differences in root shear strength by species and root size class, on average Ziemer (1981a) found that the invading brush species had the highest shear strength followed by the hardwood tree species with the conifer tree species having the lowest shear strength. The tested species listed from the strongest to the weakest in descending order are; elderberry (*Sambucus callicarpa)*, ceanothos *(Ceanothus velutinus)*, chinkipin *(Castanopsis chrysophylla)*, madrone *(Arbutus menziesii)*, Douglas-fir *(Pseudotsuga menziesii)*, incense cedar

(Libocedrus decurrens), white fir *(Abies concolor)*, sugar pine *(Pinus lambertiana)*, and ponderosa pine *(Pinus ponderosa)*.

Ziemer (1981a) did not present raw data on the trend of root biomass over time. He combined the biomass data with an empirical relationship which correlated root biomass with soil shear strength, (root biomass versus soil shear strength relationships determined by *in-situ* direct shear soil strength testing is covered in the next section of this dissertation). The empirical relationship was developed for mature, live, lodgepole pine *(Pinus contorta)* roots in a coastal sand and not for the combination of live and dead roots of the species of trees and brush encountered at the northern California site. Therefore, soil shear strength can not be predicted and, instead, Ziemer (1981a) presented the output as a relative root reinforcement index with 1.0 being the root reinforcement of the uncut stand. This relationship as presented, however, is widely cited as representing the true effect of harvesting on root strength, root biomass, or root reinforcement with time after harvest. The relationship is shown in Figure 3-2.

Strength of Soil/Root Composites

One of the research approaches used to investigate the root reinforcement hypothesis regarding timber harvesting and landslide occurrence on landslide-prone terrain has been strength testing of soil/root composites. In general, testing is carried out to determine the strength of unreinforced soils and then this

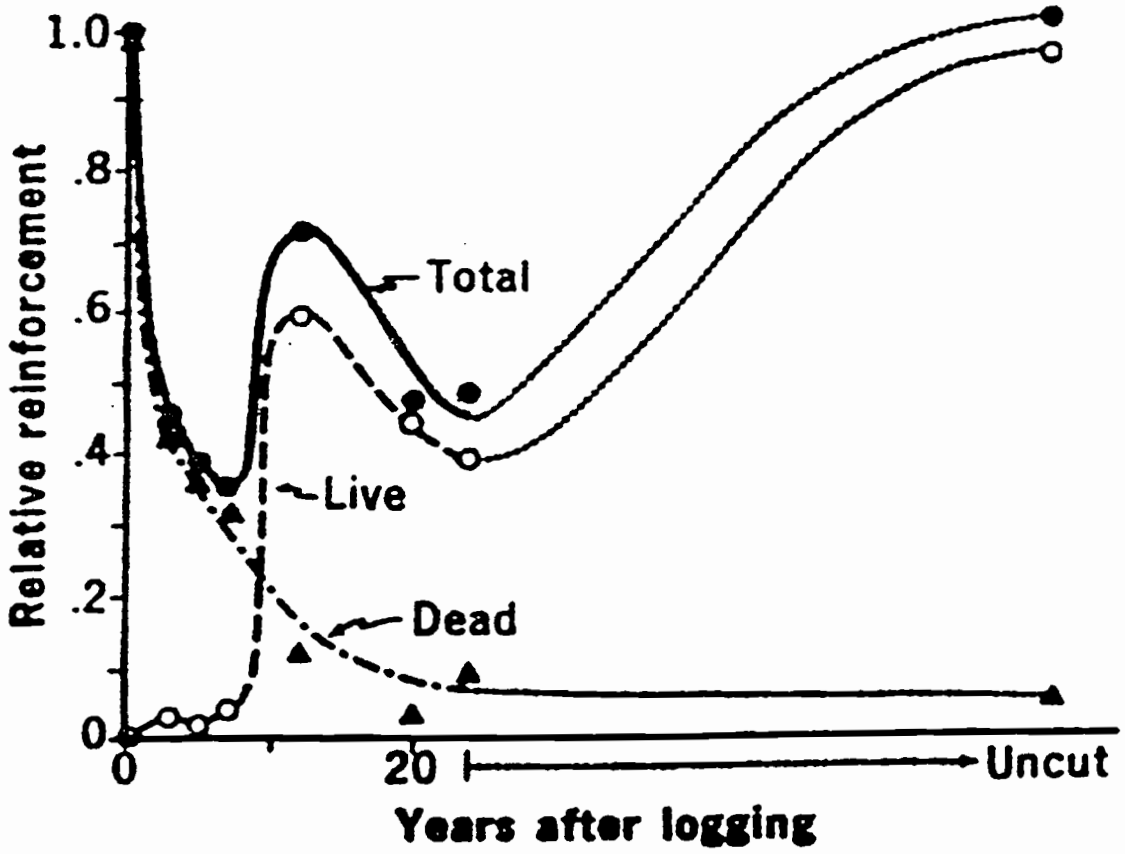

Figure 3-2. A graph showing the relative reinforcement of soil on a landslide-prone hillslope by live roots, dead roots, and the total biomass of live and dead roots as a function of time since the hillslope was harvested (from Ziemer, 1981a).

strength value is compared with the strength of the same soil only with plant or tree roots or some other fibers running through it. Results from two different types of soil strength tests are reported; direct shear tests and triaxial tests. However, two variants of the direct shear test are reported including both laboratory direct shear and field or *in-situ* direct shear. Before reporting the results of the strength testing literature, a brief discussion of the general topic of soil strength and soil strength testing will be presented.

Soil Strength

In general, when the subject of soil strength is considered, soils are divided into two broad categories: sands or cohesionless soils and clays or cohesive soils. The dominate type of residual soils formed on steep, landslide-prone slopes are sands or cohesionless soils. This same type of soil is the type of soil generally found in the colluvial deposits of headwalls or hollows in landslide-prone terrain. Most soils studied in conjunction with the stability of steep, landslide-prone terrain around the Pacific Rim are cohesionless sands. This fact has been repeatedly reported in research results from New Zealand (O'Loughlin et. al., 1982), southeast Alaska (Swanston, 1970), coastal British Columbia (O'Loughlin, 1972), the Olympic Mountains in Washington and the Oregon Coast Range (Schroeder and Alto, 1983; Schoeneman and Pyles, 1984). In general, the texture of this soil type is most often described as a sandy loam and

in the Unified system this soil is classified a silty sand (SM). Therefore, in the following discussion of soil strength and soil strength testing, only the strength and strength testing of cohesionless soils or sands will be presented.

There are several aspects of soil strength that make the discussion of this topic less than straightforward. First of all, soil strength is not a theoretically derived quantity, but rather it is empirically derived. Therefore, all soil strength values come from soil strength testing, at some point, and are thus affected by the kind and conditions of the soil strength test carried out. Secondly, for a given soil strength test and soil type, soil strength is not a constant, but a function of the effective normal stress on the failure plane at failure.

The relationship between soil shear strength and normal stress for a given soil and soil strength test can be represented by the Mohr-Coulomb strength envelope. This relationship is illustrated in Figure 3-3 and is described by the Mohr-Coulomb strength equation which takes the form,

$$S = c' + \sigma'_n \tan \phi' \qquad 3\text{-}1$$

where S is soil shear strength and is expressed in units of stress or pressure generally either kilopascals (kPa) or pounds per square inch (psi), c' is the effective soil cohesion and is expressed in the same units (kPa or psi), σ'_n is the effective normal stress also expressed in the same units (kPa or psi), and ϕ' is the effective internal angle of friction of the soil.

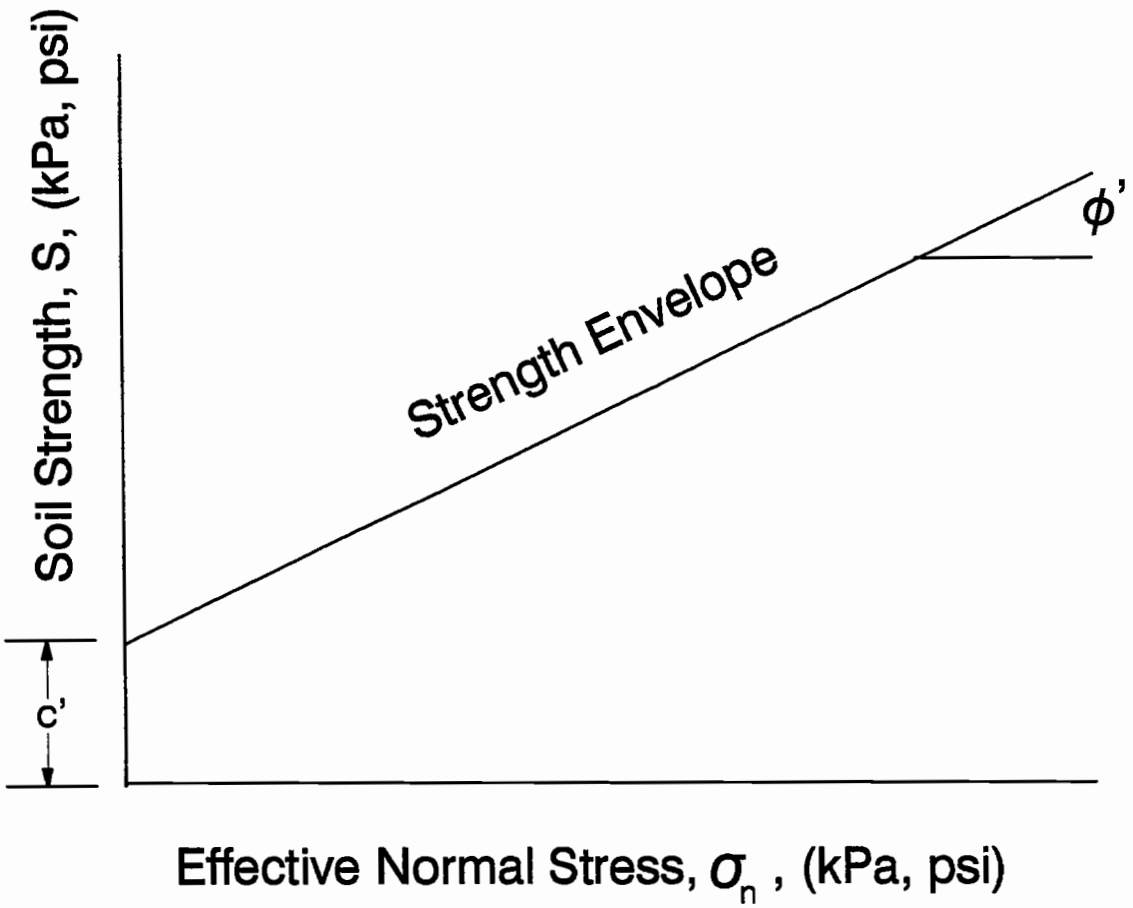

Figure 3-3. Mohr-Coulomb strength envelope.

The Mohr-Coulomb strength equation is simply the equation of a straight line. The soil cohesion, c', is the y-intercept of the line and is often referred to as the cohesion intercept and the slope of the line is $\tan \phi'$. The effective normal stress, σ'_n, and the soil strength, S, are the independent and dependent variables or x-, y- coordinates, respectively, of the relationship. The soil strength parameters c' and ϕ' are often assigned importance and characteristics beyond being simply the y-intercept and slope of the Mohr-Coulomb strength equation. The frictional component of soil strength is referred to by the internal angle of friction and is given the label ϕ'. Likewise, c' is called soil cohesion and any cohesive properties associated with soils like the electrochemical properties of clay minerals are assigned to cohesion. It is not improper to segregate and think about the different aspects of soil strength in this manner and it may even be beneficial to the understanding of soil strength to think of it in this manner. But it is important to remember that at the most elementary level, c' and ϕ' are merely the y-intercept and slope of the Mohr-Coulomb strength equation derived from soil strength testing.

The Mohr-Coulomb strength envelope is referred to as an effective strength envelope when effective strength parameters (c' and ϕ') are used which means that the relationship was developed using effective stresses. Effective stresses are determined by subtracting the pore water pressure, u, from the total normal stress, σ_n, on the failure plane. Effective strength parameters are

the preferred way to report and use soil strength values. The form of the Mohr-Coulomb strength equation using total stresses and pore water pressures is,

$$S = c' + (\sigma_n - u) \tan \phi' \qquad 3\text{-}2$$

All the parameters in the above equation have been defined previously.

A Mohr-Coulomb strength envelope is developed from a number of individual soil strength tests. Each individual soil strength test contributes a unique data point of peak soil strength and effective normal stress. Obviously, at least two soil strength tests are required to establish a Mohr-Coulomb strength envelope consisting of a straight line. The more soil strength tests the better, because more data points will more fully characterize the strength relationship and more data will extend the range of utility of the strength equation.

A soil strength test, in general, measures the ability of a soil sample to resist deformation while in a given and known stress state. The general procedure is to, first of all, secure a soil sample and install it in a testing device at a given and known state of stresses. An external load is then applied to the soil sample with the objective of causing the soil sample to shear. The deformation of the soil sample in response to the external load and the ability of the soil sample to resist the external load are recorded. The soil sample may exhibit a well-defined peak resistance at a given deformation or the sample may asymptotically approach a maximum resistance with increasing deformation. In either case, the

value of maximum resistance, expressed as a nominal shear stress, is paired with the effective normal stress state of the soil and this information is used to establish the Mohr-Coulomb strength envelope.

For the results of any soil strength test to truly reflect the strength of the soil in the field during failure, the conditions under which the soil is tested must, as closely as possible, represent the conditions in the field at failure. Some of the parameters that are important include:

- soil parameters - these include soil density, void ratio, and particle size distribution which puts a premium on testing "undisturbed" soil samples,
- *in-situ* and at-failure stress states - the most important parameters being the correct confining stress corresponding to the correct overburden pressure on the sample and the location of the water table at failure which defines the normal effective stress on the failure plane at failure, and
- the stress path to failure.

No single soil strength test can truly mimic all field conditions and each soil strength test has aspects that make its use favored as well as aspects which detract from its use. As stated previously, the results from two methods for testing soil strength will be discussed; direct shear tests and triaxial tests. The discussion will include two variants of the direct shear test; the laboratory direct shear test and the field or *in-situ* direct shear test. A brief discussion of each method for testing soil strength will be presented before the soil strength research results are presented. As each soil strength test is presented, the

strengths and weaknesses of the test relative to the determination of soil strength for shallow, cohesionless forest soils will be discussed.

Laboratory Direct Shear Test

The laboratory direct shear test is perhaps the oldest, simplest, and most inexpensive soil strength test to perform. A soil sample is placed in a direct shear device which is split horizontally into two halves. The bottom half of the direct shear device is usually fixed which allows the top half to move relative to the bottom. A load can be applied to the top of the sample which becomes, nominally, the normal stress when it is divided by the cross-sectional area of the sample. Because the failure surface will be imposed horizontally on the soil sample, the applied normal stress also becomes the normal stress on the failure plane. A lateral load can then be applied to the top half of the device and it is moved horizontally relative to the bottom half. The resistance to the horizontal movement is recorded along with the rate of horizontal deformation. The test continues until the capacity of the testing device is reached.

The soil strength is the maximum shear stress on the failure plane at failure which is defined as the peak resistance of the soil to deformation. The peak resistance to deformation is divided by the cross sectional area of the sample and the result is, nominally, the maximum shear stress. Figure 3-4 shows some idealized results for three direct shear tests run at three different effective

normal stresses. This figure also shows how that data is used to develop a Mohr-Coulomb strength envelope. Direct shear tests are covered in most geotechnical engineering texts. Dunn, Anderson, and Kiefer (1980) and Holtz and Kovacs (1981) were used as references for this discussion.

The advantages of laboratory direct shear tests are that they are easy to perform, relatively inexpensive, and can be carried out quickly. "Undisturbed" samples can be tested in laboratory direct shear, however the size of these samples is usually quite small usually 5 to 15 cm (2 to 6 inches) in diameter and 2.5 to 5 cm (1 to 2 inches) deep. This sample size rules out the inclusion of rock fragments or other inclusions larger than the sample size which, undoubtedly, affects the reported soil strength. Quite often laboratory direct shear tests will be used for disturbed or remolded samples.

The direct shear device forces a failure plane, horizontally, halfway through the sample. This tends to cause the strength of the soil sample to be overestimated due to the fact that a failure plane was forced through the soil and not allowed to develop along a zone of weakness. At the same time, because the location of the failure plane is fixed, the normal stress on the failure plane can be managed by loading the top of the sample. Other stresses in the sample besides the normal stress and the stress path to failure cannot be managed. For cohesionless, sandy soils, the direct shear test is considered a drained test meaning that pore water pressures in the sample during the test are not measured or accounted for and assumed to not impact results.

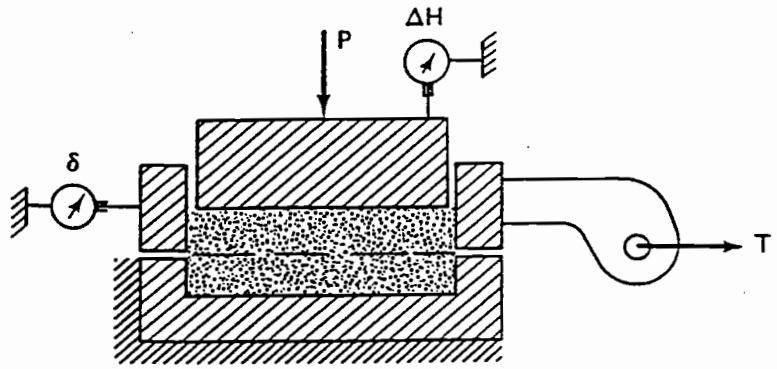

(a) Apparatus

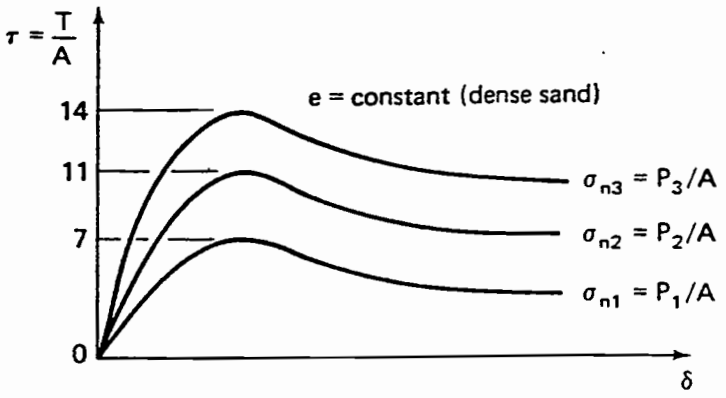

(b) Test results

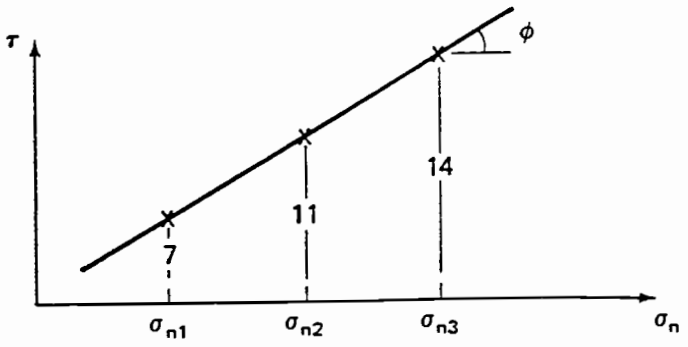

(c) Mohr diagram

Figure 3-4. (a) Schematic diagram of a laboratory direct shear apparatus; (b) typical test results for three direct shear tests of a dense sand; (c) Mohr-Coulomb strength envelope constructed from the direct shear test results (from Holtz and Kovacs, 1981).

In Situ Direct Shear Test

In situ direct shear tests are direct shear tests carried out in the field. Instead of securing a soil sample for transport back to a laboratory, a column or pedestal of soil is isolated in the field for shearing. A shear frame, of various design, is fitted onto the soil pedestal and then a lateral load is applied to the shear frame to carry out the direct shear test. Shear frames can be open only on the bottom (Endo and Tsuruta, 1969; O'Loughlin, 1972), open on two sides and not the bottom (Ziemer, 1981a) or open on two sides and the bottom (O'Loughlin, et. al., 1982). The shear frames reported in the literature are 30 cm to 1 m in length and width and 15 to 30 cm deep. The pedestal of soil to be sheared can be formed by either forcing the shear frame into the soil and then removing the soil from around it or by excavating around a column or pedestal of soil and then "trimming" the shear frame onto the pedestal. The *in situ* direct shear test can either be run at *in situ* overburden pressures, or a load can be applied to the soil at the top of the shear frame to allow the test to be run at normal stresses greater than *in situ* overburden pressures. In the reported literature, a small cable winch or hydraulic jack is used to apply a lateral load. When a lateral load is applied to the shear frame, a horizontal failure surface is forced at the base of the shear frame. The horizontal deformation of the shear frame is observed and recorded as is the resistance to deformation.

At this point, the *in situ* direct shear test becomes identical to a laboratory direct shear test. The test is continued until the lateral deformation capacity of the apparatus is reached. The maximum value of resistance is divided by the cross-sectional area of the shear frame to give the maximum shear stress which is, by definition, the shear strength of the soil at that normal stress. Maximum shear stresses and effective normal stresses for a number of these tests are plotted to yield a Mohr-Coulomb strength envelope.

The advantages of the *in situ* direct shear test is that a true undisturbed sample is tested and it is big enough to include most large soil fragments and inclusions, like tree roots. Also, the test can be run at *in situ* normal stresses or overburden pressures. The disadvantages include the fact that a failure surface is being forced instead of being allowed to develop and for a sandy, cohesionless soil the test is a drained test with no control over the stress path. Because the test is carried out in the field, data collection is often much more difficult and such tasks as applying a constant strain rate, measuring deflection, and measuring soil resistance to load become both less accurate and precise.

Triaxial Tests

Triaxial tests for soil strength represent an entirely different way to test soil strength. The strength test is performed on a cylindrical soil sample with a diameter which is nominally several centimeters and a length which is 2 to 2.5

times the diameter. The soil sample is encased in a rubber membrane and placed in a test cell which allows the sample to be surrounded by a fluid, usually water. The water can be pressurized which applies an all around consolidation pressure or confining stress to the soil sample. The cell is put in a load frame and an axial load is applied to the sample through a piston. The axial load causes deformation of the sample which is observed and recorded. The axial load is increased until the sample fails. The applied axial load is divided by the nominal cross sectional area of the sample and is called the deviator stress.

The triaxial test is fundamentally different from the direct shear test because a failure plane is not forced through the sample, but rather failure is allowed to occur on any weak plane or sometimes the sample simply bulges. Because the failure plane is not parallel to one of the principal stresses, the normal stresses on the failure plane at failure are not readily known. To find the stresses on the failure plane at failure and develop a Mohr-Coulomb strength envelope, the Mohr's circle of stresses is used. The principal stresses on the sample are known. They are the minor principal stress (σ_3) which is the confining stress and the major principal stress (σ_1) which is the confining stress plus the deviator stress. The magnitude of these two principal stresses at failure define a Mohr's circle which can be used to get the magnitude of the principal stresses on all the planes in the sample including the failure plane.

To obtain a Mohr-Coulomb strength envelope for the soil, a number of triaxial tests are performed on a number of samples all at different confining

pressures. The Mohr's circles from the tests are all plotted on the same graph and a line can be drawn which is tangent to all the Mohr's circles. The point of tangency between the line and any Mohr's circle represents the stress conditions on the failure plane at failure and the line connecting the points of tangency is the Mohr-Coulomb strength envelope. Stress-strain relationships for several triaxial tests are shown in Figure 3-5 along with a strength envelope shown tangent to three Mohr's circles. Holtz and Kovacs (1981) has an excellent discussion of Mohr's circle of stresses and the triaxial test.

The primary disadvantage of the triaxial test is the sample size. While triaxial testing apparatus exists which can test larger samples, the triaxial testing apparatus generally available is made for samples that are fairly small and it limits the inclusion of larger rock fragments and other large inclusions. "Undisturbed" samples can be run in a triaxial test but getting these samples for loose, shallow, forest soils can be difficult. Triaxial tests can also be carried out on disturbed or reconstructed samples. These disadvantages of triaxial tests are more than offset by the advantages which consist of control over both the stress states in the sample and the stress path to failure. The sample can be consolidated, even anisotropically consolidated if that is needed, before the test at very low confining pressures or high confining pressures. A failure surface is allowed to develop, it is not forced, and the correct stress path to failure can be modeled.

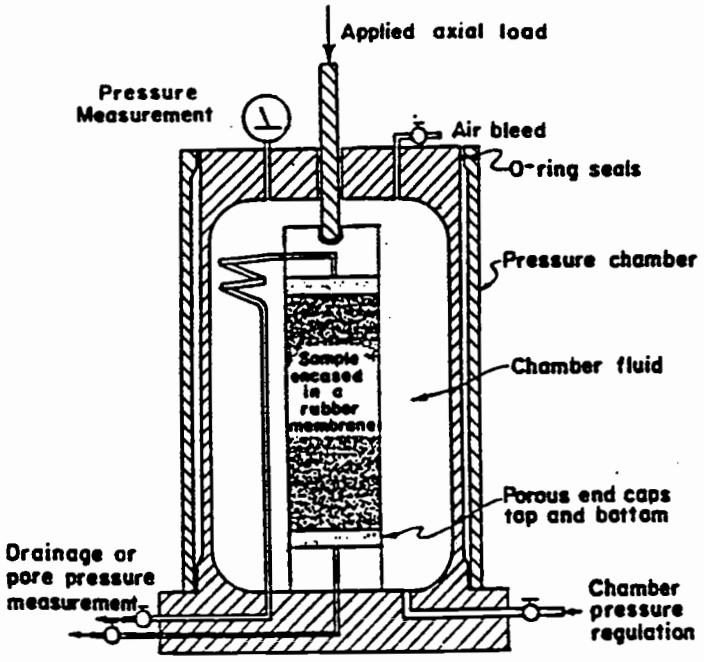

Triaxial Shear Apparatus

(a)

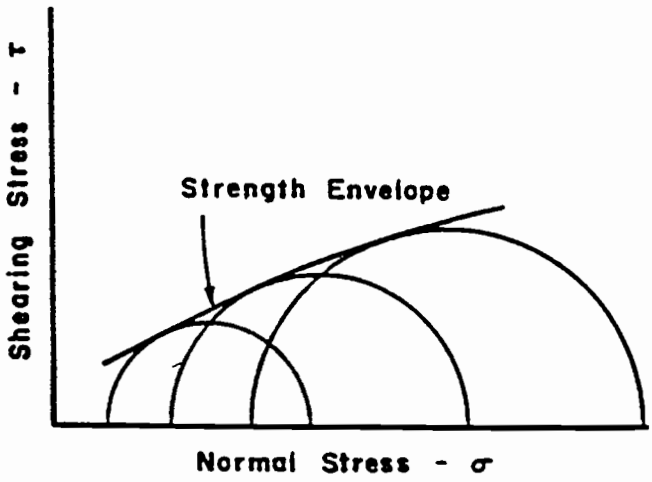

(b)

Figure 3-5. (a) Schematic diagram of a triaxial shear strength apparatus; (b) Mohr-Coulomb strength envelope shown tangent to Mohr's circles from three triaxial shear tests (from Dunn, Anderson, and Kiefer, 1980).

Soil Sampling

Obtaining adequate "undisturbed" soil samples is the bane of soil testing. Residual soils for shallow, forest soils on steeply sloping landslide prone terrain have very low densities and very high void ratios (Schroeder and Alto, 1983; Wu et. al., 1988b). The densities are so low and the void ratios so high that it is very hard, if not impossible, to recreate these conditions in a reconstructed sample. Therefore, for these soils, there is a high premium put on getting "undisturbed" soil samples for soil testing.

"Undisturbed" soil samples are not really undisturbed and thus the quotation marks. They are soil samples gathered by either driving a sampling tube into the ground and then extracting it and collecting the sample in that manner or isolating a soil column or pedestal and trimming the tube onto the soil pedestal (Schoeneman and Pyles, 1984). These "undisturbed" soil samples are then extruded into soil testing devices or further trimmed to fit a soil testing device. In getting these "undisturbed" samples for laboratory strength testing, large fragments or corestones and roots or other inclusion must be avoided because they can make getting the sample impossible. Inclusions such as rocks or roots can affect the integrity of the strength test as well. Thus, they must be avoided so soil samples are collected in areas below rooting depth or between and among roots in soil deposits, hopefully, without many large stone

fragments. Of course, exclusion of these materials from the soil sample can cause the estimate of soil strength to be non-representative.

Large stone fragments and roots can be excluded from soil samples by sieving and then reconstructing the sample for testing. This has several disadvantages, the most important of which is that the reconstructed sample will undoubtedly have different physical parameters from the *in situ* soil, most notably increased soil density and reduced void ratio, both which should affect soil strength. But one of the more important considerations is that the sample will be missing any of the relic strength that is derived from incomplete weathering of geologic material or soil structure derived from weathering in place (Yee and Harr, 1977a, 1977b). Thus the primary value of "undisturbed" samples is to preserve *in situ* physical properties like density and void ratio and allow for sampling of any relic soil strength.

Effect of Inclusions on Soil Strength

In general, adding fiber reinforcements to a sand increases soil strength by increasing the cohesion term, c, while leaving the internal angle of friction, ϕ, unchanged. While the mechanism which explains this behavior is not readily understood, this behavior is expected based on knowledge of the drained strength of sands. The primary factors that affect ϕ during strength tests are void ratio, confining pressure, particle size distribution, and angularity and surface

roughness of individual grains (Holtz and Kovacs, 1981). If all these factors are left constant and inclusions are added, the friction angle should not be affected. Inclusions will affect the internal state of stresses and strains and result in an increased deformation modulus for the soil/fiber complex (Yang, 1972; Maher and Gray, 1990). The net result of inclusions is to leave the slope of the Mohr-Coulomb strength envelope unchanged and cause the entire envelope to move upward by increasing the y-intercept of the relationship or the cohesion intercept.

This effect of increasing the cohesion intercept while leaving ϕ unchanged was clearly illustrated by Gray and Ohashi (1983) using small diameter laboratory direct shear tests on sands both unreinforced and reinforced with a variety of fiber inclusions. However, the strength tests all occurred at confining pressures higher than would be expected for shallow forest soils. Endo and Tsuruta (1969) also illustrated this concept using *in situ* direct shear tests on a prepared nursery soil with or without alders growing on it. They also carried out their tests at normal stresses greater than *in situ* overburden pressures. Dakessian (1980) showed the same effect with direct shear tests on soil samples which were either fallow or growing alfalfa or harding grass. These tests were conducted at *in situ* confining stress levels in 10 cm (4 inch) diameter by 25 cm (10 inch) long cylindrical samples. An example of these results is shown in Figure 3-6.

For the reasons presented above, the increase in strength attributed to root reinforcement is referred to as cohesion. From early research carried out on the

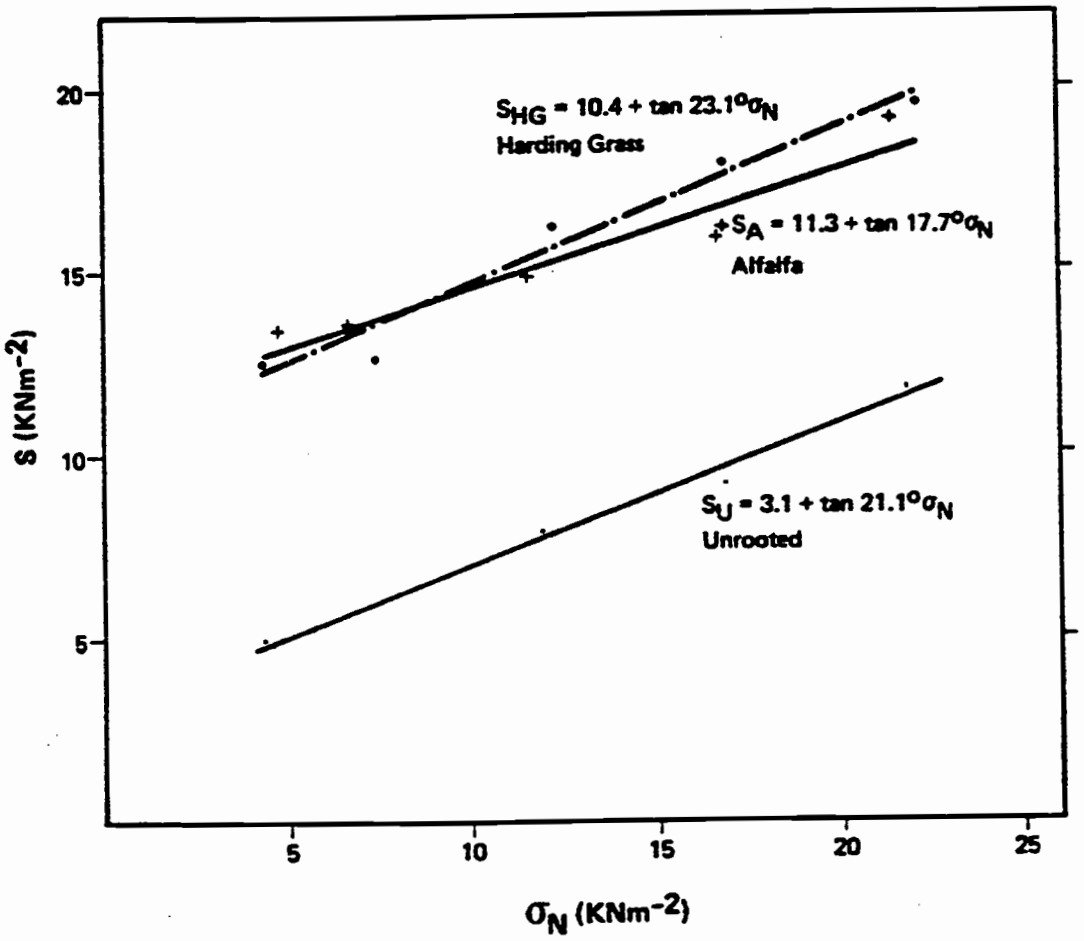

Figure 3-6. Strength envelopes for an unrooted soil and the same soil permeated with Harding grass roots and alfalfa roots. The strength envelopes illustrate the increase in soil strength associated with root reinforcement as an increase in the cohesion intercept of the strength envelopes (from Dakessian, 1980).

backanalysis of existing landslides (Swanston, 1970), the missing strength that was solved for was assigned to root reinforcement or root cohesion and given the label "apparent cohesion". This convention has been sustained and throughout the root reinforcement literature the increased soil strength attributed to root reinforcement is treated like cohesion in Mohr-Coulomb strength equations and is labeled apparent cohesion. This term is also applied to other non-organic forms of cohesion such as capillary tension. The differentiation between forms of apparent cohesion is not addressed in the root reinforcement literature and all apparent cohesion is assigned to root reinforcement.

Strength Results with Geotechnical Engineering Applications

There is a substantial body of work that exists within the geotechnical engineering community in which standard soil testing has been used to investigate the effect of fiber reinforcement on soil strength. The standard soil tests used were the laboratory direct shear test (Gray and Ohashi, 1983) and the triaxial test (Yang, 1972; Verma and Char, 1978; Maher and Gray, 1990). The objective of this research was a better understanding of the principle of reinforced earth thus, research results presented a comparison of the strength and deformation characteristics of reinforced and unreinforced cohesionless sand.

The research results show, as expected, that reinforced sand has an increased peak shear strength and decreased post peak reductions in strength (Yang, 1972; Verma and Char, 1978; Gray and Ohashi, 1983). Also, reinforcement increased the stiffness and the deformation modulus of the sand (Yang, 1972; Maher and Gray, 1990). All of this research increased the insight into the mechanics and the processes involved in the reinforcement of cohesionless sands. But, for the most part, this research is not applicable to the problem of root reinforcement of shallow forest soils because the range of the experimental parameters used during the laboratory strength tests were outside of the normally expected range of these values for shallow forest soils. These experimental parameters include soil density, the modulus of elasticity of the reinforcing elements, and soil confining stress.

The range of soil densities tested by most studies match *in situ* field values for a cohesionless forest soil better than the other experimental parameters. Verma and Char (1978) tested only one soil density which was a relatively high density (1.5 gms/cm^3) with respect to a forest soil. All the other cited authors include a low soil density treatment in which the soil has a relative density of approximately 20 percent (D_r = 20 %) which for sands yields a density of approximately 1.28 gms/cm^3 (80 lbs/ft^3).

With regard to the modulus of elasticity for the reinforcing fibers, Gray and Ohashi (1983) and Maher and Gray (1990) both included lower modulus reinforcements as a part of their experimental treatment. They included both

rubber and standard reeds as reinforcing fibers, both of which have a modulus comparable to conifer roots. The balance of the reinforcing fibers they used and the reinforcements used by Yang (1972) and Varma and Char (1978), which include Palmyra, glass, copper, aluminum, and steel, have elastic modulus values that are higher than conifer roots. Experimental results using these higher modulus reinforcements are not applicable to root reinforcement conditions.

By far the most critical experimental parameter is the confining pressure for the triaxial tests and the normal stress for the direct shear test. All of the confining stresses are very high when compared with the confining stresses that might be expected for a shallow forest soil. If a conservative soil density of 1.6 gms/cm^3 (100 lbs/ft^3) is used to convert the experimental confining pressures to soil depths, the effective soil depths modeled in the experimental tests range from a low of 1.5 m (5 ft) (Maher and Gray, 1990) to a high of greater than 4.5 m (15 ft) (Varma and Char, 1978). A soil depth of approximately 0.6 m (2 ft) is a reasonable depth for the extent of tree roots in a forest soil. Furthermore, experimental results can not be simply scaled down beyond the range of experimental values because a change in performance would be expected at smaller and smaller confining pressures. Evidence of this fact is found in Gray and Ohashi (1983) where in their direct shear tests the reinforcing elements simply pulled out of the soil samples at confining pressures below 0.72 Ksf (~0 5 psi). For these tests, the behavior at high confining pressures could not be just scaled down because at low confining pressures the behavior changed, totally.

Thus, to understand the performance of low modulus reinforcing elements at low confining pressures, they must be tested at those confining pressures.

Laboratory Direct Shear Tests

The problems which were discussed regarding the previous research, namely reinforcing elements with elastic moduli which were orders of magnitude greater than the elastic moduli of tree roots and confining pressures representing soil depths which were two to three times greater than the soil depths at which roots normally exist, were eliminated in a series of non-standard laboratory direct shear tests Waldron (1977), Waldron and Dakessian (1981; 1982), and Waldron et. al. (1983). The soil samples tested were either 10 cm x 61 cm (Waldron and Dakessian, 1982), 25 cm x 61 cm (Waldron, 1977; Waldron and Dakessian, 1981), or 1.22 m x 1.22 m (Waldron et. al., 1983) cylindrical samples. For the cylinders that were 61 cm long, failure planes were induced at depths of 15 cm, 30 cm, and 45 cm (Waldron, 1977; Waldron and Dakessian, 1981; 1982) and a failure plane was induced at 60 cm for the 1.22 m long soil samples (Waldron et. al., 1983). No additional normal loads were added to the samples so they were tested at a laboratory modeled *in situ* normal stress.

Additionally, the reinforcing elements that were tested were the roots of various plants which were grown in the soil samples. The plants included barley, grown anywhere from 90 days to 10 months, alfalfa grown for 12 to 14 months,

various grasses grown over a winter period, oak seedlings grown 35 months, and pine seedlings grown 14 and 52 months. Thus, the modulus of the reinforcing elements should be, at least, within the correct order of magnitude for the size of roots present.

Several soil types and soil profiles were also tested. There were two soil profiles common to all the research. One soil profile was composed entirely of a homogeneous clay loam taken from a local slide-susceptible soil. The second common soil profile was the same clay loam placed on top of a dense gravel with the interface at the failure plane of 45 cm for the 61 cm long samples and at 60 cm for the 1.22 m long samples. Two additional soil profiles were used for only a small part of the experimental program and they were associated with only the 61 cm long samples (Waldron, 1977). One soil profile was a homogeneous clay loam placed on top of the dense gravel with the interface at 30 cm and the other soil profile was a sandy loam, composed of 5 parts sand to 1 part of the clay loam, with a dense clay layer at 30 cm.

For this research, a subset of the samples were permeated with roots and then sheared and another subset of identical samples were treated in exactly the same manner except they remained fallow. Both of these sets of samples were sheared in direct shear leaving results in the form of a graph of shear stress versus horizontal displacement. For the purposes of this research, the increase in strength attributed to root reinforcement was calculated as the difference in shear stress between a rooted and fallow sample at a given horizontal displacement.

The results can be generally characterized by the statement that reinforced soil samples had higher peak shear stresses and higher shear stresses, in general, throughout the range of horizontal displacements. In fact, for most of the research results, the difference in shear stress increased throughout the range of displacements. In the early research (Waldron, 1977), 12 month alfalfa in the homogeneous clay loam profile gave a 290 per cent increase in strength at a displacement of 25 mm. Other profiles with other rooted mediums gave similar results with the clay loam on gravel profile yielding an average increase in strength of 170 gm/cm^2 or a 420 per cent increase at 25 mm horizontal displacement. For a variety of grasses grown over a winter, there was a threefold increase in strength at a 30 mm displacement and 14 month alfalfa yielded a fourfold increase in strength at the same displacement (Waldron and Dakessian, 1982). The results for the large, 1.22 m x 1.22 m, samples were consistent with the rest of the research. For the samples with 52 month old pines the differences in shear stress between the rooted and fallow samples increased throughout the range of displacements and at a horizontal displacement of 75 mm, the strength was almost doubled.

While this sequence of research solves some of the problems encountered in the more geotechnical engineering directed research, high modulus reinforcements and high confining pressures, some problems are still encountered which limit the utility of the research results to the problem of root reinforcement in shallow, landslide-prone, forest soils. In the initial set of

experiments (Waldron, 1977), no significant increase in soil strength was observed with the sandy loam samples where the failure surfaces were at depths of 15 and 45 cm and the samples were reinforced with four month old barley. Because this result was non-significant, the results were not included in the shear resistance increase versus root cross sectional area curve showing the effects of roots on strength increase. Also, that particular profile was not included in any of the subsequent research. This is important because this is the soil type of most interest when dealing with steeply sloping, shallow forest soils. It is not known if this is an experimental artifact or if this is a real result and the same mechanisms of root reinforcement that work for cohesive soils simply do not work for cohesionless sands. The latter hypothesis is not beyond consideration given that a cohesive and cohesionless soil would have markedly different shear-stress transfer characteristics and perhaps a 25 cm x 60 cm sample is not large enough, at these low confining pressures, to allow adequate frictional shear-stress transfer to develop. Whatever the reason, this tiny piece of research result and the fact that it wasn't explored more fully advises caution when extrapolating these research results to shallow forest soils.

This research points out a further experimental problem, strain compatibility. The authors point out repeatedly that peak soil strength occurs at a horizontal displacement of approximately 5 mm. Yet they report strength increase values at displacements of 25, 30, and even 75 mm in the case of the 52 month old pine seedlings in the large samples. Soil strength tests like the direct

shear test are strain-controlled tests where a soil sample is confined then a displacement rate is applied to the sample and the ensuing stresses are measured. This is not how the real world works. The real world is stress-controlled which means that in the real world a stress state is imposed on soil and the ensuing strains are observed. A landslide is a form of infinite strain at a fixed and critical stress state. The authors obviously believe that in a stress-controlled environment, the soil/root system can withstand a 75 mm horizontal displacement and stay intact and competent enough to allow shear-stress transfer with plant roots to occur and reinforce the soil up to double the unreinforced strength. Given that the peak strength for an unreinforced soil occurred at a horizontal displacement of only 5 mm and that there was no observable increase in strength observed for tests with the sandy loam soil, there would seem to be more than ample reason to be cautious when applying these research results to the case of shallow, cohesionless soils on steeply sloping forested terrain.

A final point of discussion deals more with the interpretation of the results than the results themselves. The authors of the results, while not stating their case emphatically, certainly imply that their research results support the root reinforcement hypothesis linking timber harvesting and landslides on landslide-prone forested terrain. In the manner and places that this work has been cited and reviewed (Sidle et. al., 1985) the case is stated much more emphatically that this research definitely supports the root reinforcement hypothesis linking

timber harvesting and landslides. This contention can not be supported. The inability to support the contention has nothing to do with the research or its quality, which is very good, but rather has to do with the almost universally accepted assumption that, in fact, the soil strength of a clear cut harvested hillslope can be modeled by a fallow soil sample. This is obviously untrue as evidenced by Ziemer (1981a) who estimated that at its lowest strength a harvested hillslope still had roughly 40 percent of its maximum root reinforcement. In fact, what Waldron (1977), Waldron and Dakessian (1981; 1982), and Waldron et. al (1983) show more than anything else is the magnitude of strength increase that can be gained on clearcut harvested slopes as a result of primary invasion species and seedlings planted after harvest.

In Situ Direct Shear Tests

In addition to laboratory direct shear, an additional method used to investigate the effect of roots on soil shear strength was *in situ* or field direct shear tests. There are two general kinds of research outputs. The most popular form of the research output was a linear regression approach in which the biomass of roots in a soil sample was regressed against the shear strength of the soil sample and the relationship was shown to have a positive and highly significant correlation (Endo and Tsuruta, 1969; O'Loughlin, 1972; Endo, 1980; Ziemer, 1981a). A second approach was to develop Mohr-Coulomb strength

envelopes for soils which were in native forest versus soils where the forest had been harvested and/or for various states of rooted versus unrooted soils and compare the strength envelopes (O'Loughlin, et. al., 1982; Abe and Iwamoto, 1985).

In general, *in situ* direct shear tests involve a larger soil sample than laboratory direct shear tests. The shear frame used to carry out the *in situ* direct shear tests ranged from 30 cm in length and width and 15 cm deep (O'Loughlin, 1972; O'Loughlin, et. al., 1982) up to 1 m in length and width and 50 cm deep (Abe and Iwamoto, 1985). The shear frames were open just on the bottom (Endo and Tsuruta, 1969; O'Loughlin, 1972; Endo, 1980; Abe and Iwamoto, 1985), on two sides and the bottom (O'Loughlin, et. al., 1982) and on just two sides (Ziemer, 1981a). Obviously, an advantage of *in situ* direct shear tests is that they can test the soils as they occur naturally at *in situ* normal stresses (O'Loughlin, 1972; O'Loughlin, et. al., 1982; Ziemer, 1981a). However, *in situ* direct shear tests are also carried out for prepared soils and the testing apparatus allows for normal stresses to be applied that are greater than the *in situ* normal stresses (Endo and Tsuruta, 1969; Endo, 1980; Abe and Iwamoto, 1985). The shear frames were all installed by evacuating a rough soil column, block, or pedestal and then the shear frame was "trimmed onto" the soil pedestal.

Endo and Tsuruta (1969) and Endo (1980) sheared prepared nursery soils in plots which were unrooted or had different numbers of various tree species growing on them. For both studies, two shear frames were used with inner

measurements of 50 cm x 50 cm and heights of 30 and 60 cm. The shear frames were open only on the bottom. Additional weight was added to the soil surface within the shear frame making the equivalent depth of the failure plane 0.6 to 1.2 m (2 to 4 ft). Endo and Tsuruta (1969) regressed total fresh weight of roots against soil strength while Endo (1980) used cross sectional area of roots per unit area. Both regressions were highly significant with r^2 values that ranged from 0.73 to 0.93.

O'Loughlin (1972) sheared *in situ* soils at ambient normal loads on two freshly clear cut slopes. He used a 30.5 x 30.5 x 15.5 cm (1 x 1 x 0.5 ft) shear frame that was open only on the bottom. The strength was the maximum shear force on soil pedestals that remained intact while soil pedestals that crumbled or collapsed were deemed unsatisfactory and not considered. There were 24 successful tests out of 40 total tests. Maximum shear strength was correlated with a number of variables believed to influence shear strength and the weight of fresh roots was the most significant variable tested. The fresh root weight alone accounted for 56 percent of the variability in soil strength.

Likewise, Ziemer (1981a) tested *in situ* sand soils in a pine forest at ambient stresses. He also tested a number of variables expected to influence shear strength and found the oven dried biomass of live roots less than 17 mm in diameter was the most significant variable and accounted for 70 percent of the variability in soil strength alone. Ziemer (1981a) used a 30 x 15 x 15 cm shear frame that was open on just the 15 x 15 cm sides and closed on the bottom. He

felt that the shear frame caused the soil strength to be underestimated by as much as 50 percent because the soil strength on the bottom of the pedestal was not included in the test.

O'Loughlin, et. al. (1982) carried out *in situ* direct shear tests for soils that were in native beech podocarp forests and soils which had been clearfelled, broadcast burned, and converted to rediata pine 36 months prior to strength testing. A 30 x 30 x 15 cm shear frame was used which was open on two sides and the bottom. The *in situ* soils were tested at a range of normal loads greater than the *in situ* overburden pressure to allow a range of normal stresses so a strength envelope could be constructed. The effective normal stress values ranged from those expected for a failure plane at approximately 0.3 m (1 ft) deep to a failure plane at 1.5 m (5 ft) deep with the average normal stress equivalent to a failure plane at approximately 0.76 m (2.5 ft). Table 3-3 shows the results of the tests. The friction angles were the same for both vegetation types, however the cohesion intercept for the harvested site was 3.3 kPa less than for the native forest site. The numbers for root content are also shown. None of the numbers presented were tested for statistical significance.

Abe and Iwamoto (1985) tested a prepared nursery soil that had plots which were both unrooted and had a single *Cruptomeria Japonica* growing on them. A shear frame that was 1 m in length and width and either 50 or 30 cm in depth was used. The shear frame was open only on the bottom. The tests were run at *in situ* normal stresses and additional weight was added to give normal

Table 3-3. The internal angle of friction, ϕ, apparent cohesion, c, and mean and standard deviation of soil block root content for soils of an intact Beech-Podocarp forest and a 36 month old radiata pine plantation in North Westland, New Zealand (O'Loughlin, et. al., 1982).

	ϕ	c	Soil Block Root Content	
	(°)	kPa	kg/m^3 soil	
			mean	std. dev.
Beech-Podocarp Forest	36	6.6	19.8	28.7
Radiata Pine Plantation	36	3.3	7.0	10.5

stresses equivalent to soil depths of between 0.6 to 1.2 m (2 to 4 ft). A Mohr-Coulomb strength envelope was developed for both unrooted and rooted soils for failure surfaces at 30 cm and 50 cm. A comparison of the strength envelopes showed that they were not parallel but had different slopes and thus different friction angles, however this aspect was not discussed. For the 30 cm failure surface at the *in situ* normal stress, the strength of the rooted soils was 11 percent greater than for the fallow soils and at the highest normal stress the strength increase was 32 percent. For the 50 cm failure surface, the rooted soils had 13 and 42 percent greater strength than for the unrooted soils for the *in situ* and highest normal stress, respectively. The authors also investigated the change in peak shear stress for individual shear stress versus horizontal displacement tests and found that peak shear stress increased for rooted versus unrooted tests and the

rooted samples could withstand greater horizontal displacement before failing. The difference in strength between the rooted and unrooted samples was correlated with the per unit area cross sectional area in roots (root area ratio) and a positive linear trend was observed. The significance and r^2 of the relationship were not reported.

In situ direct shear tests show the same general results as the laboratory direct shear tests. Soils with roots have higher shear strength than soils without roots and root biomass, or some measure of it, can be used as a predictor of soil strength. Care needs to be taken when applying these data to shallow forest soils for the same reasons as discussed for the laboratory direct shear tests. Strain compatibility at excessive displacements between soil and roots in a stress-controlled environment is still a matter of concern not addressed by this research. As evidence of this concern are the 16 out 40 *in situ* soil tests that O'Loughlin (1972) performed that crumbled and were not considered. The majority of the *in situ* direct shear test research results reviewed were generated by soil tests in which the normal stress was larger then ambient, *in situ* normal stresses which makes direct transfer of the data to shallow, forest soil conditions problematic. Most importantly, as Ziemer (1981a), O'Loughlin (1972), and O'Loughlin, et. al. (1982) illustrate with their results, the discussion regarding timber harvesting, landslides, and shallow forest soils isn't about the comparison between rooted and unrooted soils. All harvested sites have roots of some

species, size, and decay class in them. The discussion should center around the effect of the change in species, size distribution, and decay class on soil strength.

Landslide Backanalysis

A research technique that has been used to investigate both the existence and magnitude of root reinforcement in shallow forest soils is the backanalysis of existing landslides. Landslide backanalysis is routinely used in slope stability investigations to determine or deduce soil strength or other parameters related to slope stability (van Asch, 1984; Duncan and Wright, 1980). Furthermore, it is the only way to validate the estimates of parameters like soil strength used in slope stability analysis.

Landslide backanalysis is the process of doing slope stability analysis only with a slightly different objective. Slope stability analysis involves detailed knowledge of the soil mechanics of a site which results in quantifying the forces, or moments, on a failure surface or potential failure surface that are both driving and resisting the failure. The ratio of the forces, or moments resisting failure over those driving failure is the factor of safety. A factor of safety greater than one indicates a stable slope, less than one indicates an unstable slope, and a factor of safety of one indicates incipient failure. In a traditional slope stability analysis problem, the objective is to determine the factor of safety for a slope and compare that number with design objectives, thus, values are determined for all

the parameters in the slope stability analysis equation(s) and the factor of safety is the unknown. In backanalysis, the slope has already failed, and the objective is to determine the value of some parameter in the analysis. In this case, all but one of the parameters in the slope stability analysis equation(s) that describe the failed slope are determined, the factor of safety is set equal to one, and the value of the unknown is solved for. The value of a backanalysis on a landslide is that the assumption that the factor of safety was one at incipient failure can safely be made. A backanalysis can be carried out for an unfailed slope but that requires a method for assigning a factor of safety to an unfailed slope.

For the case at hand, the magnitude of the soil strength increase that can be attributed to root reinforcement in shallow forest soils is to be determined. As discussed previously, the increased strength attributed to root reinforcement is generally accepted to be and is treated as soil cohesion, c, thus it is assumed that root reinforcement does not affect the internal angle of friction, ϕ, of the soil. This cohesion term is called "apparent cohesion" and is given the symbol c_a or root cohesion and is given the symbol c_r. To determine the value of apparent cohesion contributed to a landslide, the slope stability analysis method must be chosen, the values for all the parameters in the slope stability analysis method must be determined, the factor of safety is set equal to one, and then the additional strength required for equilibrium is solved for. The strength solved for by the backanalysis is called apparent cohesion and attributed to the influence of roots in reinforcing shallow forest soils.

This process has been carried out by a number of researchers and their results are summarized in Table 3-4. Landslide backanalysis have taken place in landslide-prone terrain in southeast Alaska, coastal British Columbia, the North Cascades in Washington, and the Idaho batholith. The values of apparent cohesion or root cohesion range from a low of approximately 1.6 kPa (33 lbs/ft^2) to a high of 6.2 kPa (130 lbs/ft^2).

Table 3-4. A list of the principle investigators, geographic location, and apparent cohesion value for backanalysis research carried out to determine the existence and magnitude of the soil strength increase attributed to root reinforcement.

	Geographic Location	Apparent Cohesion, C_a
Swanston, 1970	Southeast Alaska	4.3 - 3.3 kPa
Gonsior & Gardner, 1971	Idaho Batholith	6.2 kPa
O'Loughlin, 1972; 1974	Coastal British Columbia	1.6 - 2.1 kPa
Wu, et. al., 1979	Southeast Alaska	5.9 kPa[1]
Sidle & Swanston, 1982	Southeast Alaska	2.0 kPa
Buchanan & Savigny, 1990	N. Cascades, WA	1.6 - 3.0 kPa

[1] Value derived by equation and verified by backanalysis.

Performing a landslide backanalysis requires doing slope stability analysis. Slope stability analysis requires a thorough knowledge of soil mechanics and a thorough knowledge of the site being analyzed. The first step is to locate a landslide from which the location of the critical failure surface can be

located. For an existing landslide this is pretty straightforward. To carry out backanalysis on a stable site requires a knowledge of what characteristics a landslide-prone site exhibits, the knowledge to locate the potential critical failure surface within the soil mass, and the factor of safety.

Once a landslide or potential landslide has been selected for analysis, there are a number of analysis components that have to be determined to carry out the analysis. The choices made with these components and the accuracy with which parameters are calculated will determine the accuracy and utility of the subsequent analysis. These components are:

1. The location of the critical failure surface,
2. The choice of the slope stability analysis method,
3. The loading on the critical failure surface,
4. The strength characteristics of the soil,
5. The location of the water table or piezometric surface at failure.

Each of these components will be discussed briefly. An idea will be given as to how decisions made with each component can affect the accuracy and utility of the final answer. Then the pertinent case studies cited in Table 3-4 will be critiqued in light of these discussions.

Critical Failure Surface Location

The ability to locate a critical failure surface can be either very good or very poor depending on whether a failed or stable site is being analyzed. Obviously, if an existing landslide is being analyzed, the ability to locate the critical failure surface should be very good and generally is. There is some potential error involved because the failure surface observed in the field is probably not the same failure surface that existed at failure. It is undoubtedly a surface which has formed as a result of subsequent sloughing and erosion of the slope. With landslides in shallow forest soils this is rarely a big concern because the important dimension, the depth of the failure surface generally coincides with the soil/bedrock interface and this value is fixed and its measurement reproducible. The length and width of the landslide are secondary in importance. Buchanan and Savigny (1990) located the critical failure surface at failure by using a slope stability analysis method to locate the critical failure surface within the void left by the landslide. Most researchers simply fit a rounded failure surface by eye or graphically into the void left by the landslide (Swanston, 1970) or simply use average or likely dimensions based on the site.

Finding critical failure surfaces on stable slopes without existing landslides is more problematic. Again, the problem is eased somewhat by the physical situation in which the most important dimension, depth of the critical surface, can be assumed to be fixed by the soil depth. In the articles reviewed, a

slope stability analysis method was rarely used to locate a critical surface for an unfailed site before analyzing the potential slide. The location and dimensions of a potential slide are fixed by the geometry of the problem, i.e. soil depth, and the potential slide is also assumed to have roughly the same location and dimensions as landslides at failed sites. Again, this is a reasonable assumption and shouldn't result in large errors. However, the ability to locate critical failure surfaces for unfailed sites is poorer than for failed sites and this affects the utility of the conclusions which come from a comparison of analysis results.

Choice of Slope Stability Analysis Method

The type, shape, and dimensions of the failure surface selected should drive the choice of a slope stability analysis method. There are many slope stability analysis methods available and each one treats the mechanics of the landslide differently and has different underlying assumptions. Because of the different assumptions and mechanics, the different slope stability analysis methods will yield different factors of safety, all other factors being equal. If different slope stability analysis methods can give different factors of safety, then when used to backcalculate apparent cohesion attributed to roots, they can give different estimates of that also, all other factors being equal. So the choice of a slope stability analysis method can be important.

In a slope stability analysis, the forces on the failure mass are analyzed. The forces can be analyzed for the entire soil mass, a representative section of the soil mass, or, more commonly, the failure mass can be divided up into a number of discrete slices and the forces can be analyzed on the soil slices. The rigorous slope stability analysis methods, such as Janbu's rigorous method, Spencer's method, and Moegenstern and Price's method, divide the soil mass into slices and incorporate both force and moment equilibrium in the analysis. These methods are more difficult to solve and involve the solution of multiple equations either simultaneously or iteratively. Multiple equations are used because for each individual soil slice both horizontal and vertical force equilibrium is calculated and for the overall slide mass, moment equilibrium is calculated. The slope stability analysis methods which satisfy all equilibrium conditions, horizontal and vertical force equilibrium and overall moment equilibrium, are generally considered to yield acceptable and accurate results.

There are other slope stability methods which were developed to satisfy either force equilibrium or moment equilibrium but not both. These methods are easier to solve because they involve only one equation and the factor of safety can be computed in closed form. The infinite slope and wedge methods satisfy conditions of force equilibrium while the ordinary method of slices and Bishop's method were developed around moment equilibrium only. In general, these methods which don't satisfy all conditions of equilibrium can give inaccurate

results and are often overly conservative, especially for the kind of failures expected on steeply sloping, shallow forest soils.

An example of how slope stability analysis methods, and implicit assumptions, can be conservative can be shown by conceptually comparing the infinite slope method with a slice method of slope stability analysis. The infinite slope method represents the slide mass with a two dimensional representative section of the slide mass that has a unit width. The slice method represents the slide mass with a two dimensional cross section of the slide mass which also has a unit width. Diagrams of these two concepts are shown in Figure 3-7. In general, the driving force of a landslide is a function of the mass of the soil in the landslide and is a direct function of the volume of the slide mass. The resisting force of a landslide is a function of the soil strength which is the product of the appropriate shear stress and the surface area of the slide mass. Thus the ratio of the volume of the slide mass and the area of the failure surface, as represented by the slope stability analysis method, could be a useful index for comparing these two methods.

The depth of the representative section for the infinite slope method almost always comes from the deepest part of the slide mass while the area of the failure surface of the same section is the length of the section corrected for slope angle. Thus, in the infinite slope method the volume is maximized while the failure surface area is minimized. For the slices method, the volume is calculated from both the deep slices in the middle of the slide as well as the shallower slices

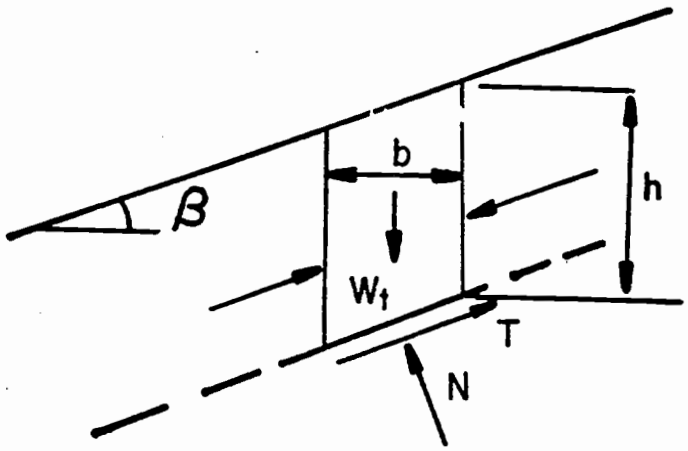

(a)

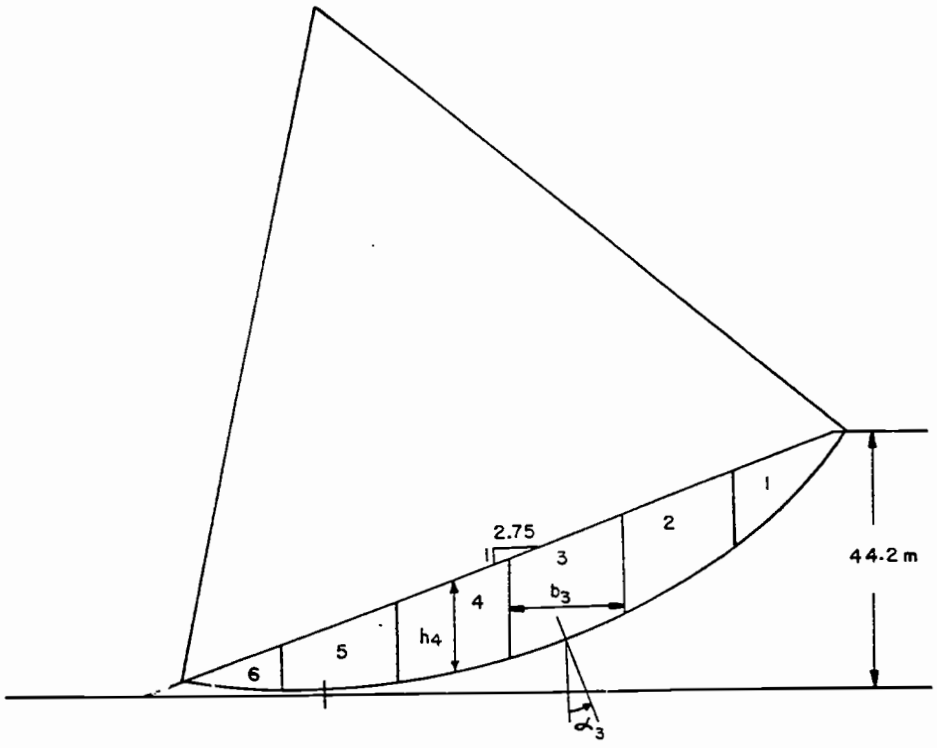

(b)

Figure 3-7. (a) Typical soil section free-body diagram for an infinite slope analysis method; (b) Typical slide cross-section for a "slices" method of analysis.

at each end of the failure while the area of the failure surface comes from, not only, the deeper slices, where the failure surface area is minimized, but also, the shallower slices where, because of the geometry of the slide, surface areas get larger. Obviously, the ratio of the slide volume to failure surface area for the slices method is more representative of the actual slide than is the infinite slope method.

This is one way in which conservatism is built into slope stability analysis methods. The infinite slope method maximizes the driving force and minimizes the strength of the actual slide. Thus if the slope is stable, by the infinite slope method, the actual factor of safety will be much larger due to assumptions regarding the ratio of slide volume to failure surface area. In landslide backanalysis to determine the apparent cohesion attributed to roots, this conservatism translates into an overestimate of the contribution of roots to the stability of the site. Thus, it can be expected that the infinite slope method will generate higher values for apparent cohesion than the ordinary method of slices.

An example of this effect is provided by Swanston (1970) who calculated apparent cohesion due to root reinforcement for three landslides in southeast Alaska using backanalysis. The slope stability analysis method used for the backanalysis was the ordinary method of slices however, the author did perform a backanalysis using the infinite slope method on a generic slope to ascertain the magnitude of his calculations. The infinite slope method was used for a generic slope with a slope angle of 37°. The apparent cohesion generated by this method

was 5.4 kPa (112.6 lbs/ft^2). The backanalysis performed using the ordinary method of slices used the exact same parameters except for slope angles where 36° and 38° were used. For these two cases the apparent cohesion calculated was 3.3 kPa (69 lbs/ft^2) and 4.0 kPa (83.9 lbs/ft^2), respectively. Therefore, the infinite slope method overestimated apparent cohesion, relative to the method of slices, by between 25 to 36 percent (1.4 to 1.9 kPa). This difference is solely a function of the choice of slope stability analysis method.

Recall that the ordinary method of slices is not a rigorous slope stability analysis method and does not satisfy all conditions of equilibrium. The ordinary method of slices can underestimate factor of safety by as much as 60 percent (Turnbull and Hvorslev, 1967; Whitman and Bailey, 1967; as quoted in Nash, 1987). Thus the errors incurred in overestimating apparent cohesion could be even greater if they were compared with a rigorous slope stability analysis method which satisfies all conditions of equilibrium.

All of the slope stability methods used in the reviewed papers were the less rigorous methods. Gonsior and Gardner (1971), O'Loughlin (1972, 1973), Wu, et. al. (1979) and Sidle and Swanston (1982) all used the infinite slope method, Swanston (1970) used the ordinary method of slices, and Buchanan and Savigny (1990) used Bishop's modified method. This is important because, as evidenced by the case study provided by Swanson (1970), the magnitude of the potential overestimates of apparent cohesion caused by using a non-rigorous slope stability analysis method may not be as large as the magnitude of the calculated

values of apparent cohesion, but they are most certainly within the same order of magnitude.

Critical Failure Surface Loading

The most important part of the loading on the critical failure surface is the weight of the soil. Once the geometry of the critical failure surface is determined, then only the soil density is needed. This information comes from laboratory analysis of field samples, is routinely carried out, and, all other details considered, is easy and straightforward to get.

It is possible to consider the weight of the trees on the failure surface, however, this routinely is not done. The primary reason it is not done is because the weight of the trees is minor compared with the total weight of the slide mass. Wu, et. al. (1979) considered the weight of the trees and found they resulted in a pressure of 5.2 kPa (~110 lbs/ft^2) on the failure surface. That value is in both the numerator and denominator of the equation so the net effect is much less than 5.2 kPa and the actual value depends on the slope angle and angle of internal friction of the soil. Bishop and Stevens (1964) also estimated the average pressure of the trees on the failure surface and came up with 2.5 kPa (~52 lbs/ft^2). Both of these examples are from old-growth forests in southeast Alaska.

A final consideration in critical failure surface loading is whether the cases studies were simply generic slopes using average values for the slope stability

analysis parameters or whether they were actual landslides for which the value of the slope stability analysis parameters were determined and substituted into the analysis. All of the cited authors except O'Loughlin (1972; 1974) analyzed existing landslides and slide-prone slopes. O'Loughlin (1972; 1974) analyzed a generic slope using average values for the analysis parameters, but even that case initiated with an actual midslope landslide. When comparing failed and unfailed landslide sites it is best to use dimensions and parameters from actual sites and not assign average values to generic slopes. A landslide, at any given site, is due to actual site conditions and not some assumed state of conditions and this will not be known unless the sites are analyzed on an individual basis with site specific parameters.

Soil Strength

Soil strength has been discussed previously. Soil strength is an empirical quantity which can only be determined through soil strength testing. Soil strength is not a constant but a function of the effective normal stress on the failure plane at failure. The relationship that relates soil strength to effective normal stress for a given soil and soil strength test is the Mohr-Coulomb strength envelope. This relationship is most often expressed as the equation of a straight line of the form,

$$S = c' + \sigma_n' \tan\phi' \qquad 3\text{-}1$$

where S is the soil strength, c' is the soil cohesion or cohesion intercept, σ_n' is the effective normal stress on the failure plane, and ϕ' is the internal angle of friction of the soil. Using this relationship, if the effective normal stress on a failure surface is known then the strength on that failure surface can be calculated.

The combined results from several strength tests are used to establish a Mohr-Coulomb strength envelope. The type of soil strength test used is important because, as discussed previously, these tests have their inherent strength and weaknesses which affects the accuracy and utility of any resulting strength envelope. For the results of soil strength tests to be as accurate and useful as possible, it is important that the conditions under which the test is carried out replicate the conditions that are expected to occur in the field at failure as closely as possible. This means that the soil physical properties, such as soil density, void ratio, and particle size distribution, should closely approximate those in the field. Thus the emphasis on collecting and testing "undisturbed" soil samples. The confining stress in the sample at the start of the strength test and the stress path to failure both should, as closely as possible, represent *in situ* field conditions. In the six articles reviewed, where apparent cohesion was determined by backanalysis of existing landslides, there are recurring problems with soil strength testing methods or the use of the soil strength data that could

affect the backanalysis sufficiently to result in incorrect values of apparent cohesion.

Undisturbed vs. Disturbed Soil Samples

Most of the authors conducted soil strength tests on "undisturbed" samples, however Gonsior and Gardner (1971) and Buchanan and Savigny (1990) performed soil strength tests on samples that were collected, air-dried, sieved and then reformed for soil testing. This process removes any large rock fragments or corestones which would add to friction but, more importantly, it removes any "relic" strength in the soil. "Relic" strength may result from strength associated with the incomplete or nonuniform weathering of bedrock that could leave residual chemical bonds or "relic" strength may also be associated with chemical bonds formed as a part of weathering which adds soil structure or aggregate stability to soil (Yee and Harr, 1977b). In either case, sample disturbance removes this "relic" strength, thus strength tests on disturbed soil samples will yield results which are not representative of true soil strength.

Soil Strength Test Method

Triaxial tests were used to determine soil strength by Swanston (1970), Gonsior and Gardner (1971), and Sidle and Swanston (1982). The triaxial test is

the preferred soil strength test because a shear plane is not forced but is allowed to develop along a zone of weakness and the triaxial test provides flexibility in modeling stress states and stress paths during the test. Swanston (1970) and Sidle and Swanston (1982) performed triaxial tests on "undisturbed" samples while Gonsior and Gardner (1971) ran their tests on disturbed, remolded samples.

O'Loughlin (1972; 1974), Wu, et. al. (1979), and Buchanan and Savigny (1990) all used direct shear tests to determine soil strength parameters. Buchanan and Savigny (1990) ran laboratory direct shear tests on disturbed, remolded samples. They did not use the strength data directly from the direct shear tests but used a weighting scheme to determine integrated peak friction angle which apparently correlates *in situ* void ratio with friction angles from the direct shear data. O'Loughlin (1972; 1974) ran *in situ* direct shear tests and, using the analogy of a sliding block, determined only friction angle, no cohesion intercept was determined, from the data. Wu, et. al. (1979) ran both laboratory direct shear tests on "undisturbed" samples and *in situ* direct shear tests. The *in situ* data resulted in strength values which were substantially higher than the laboratory direct shear data. The friction angles were comparable but the cohesion intercept for the *in situ* data was approximately three times greater, approximately 15 kPa (313 lbs/ft^2) compared to 5 kPa (104 lbs/ft^2) for the laboratory data. Because the data were dissimilar and the *in situ* data so much higher, only the laboratory data was used for the backanalysis.

It is unclear how the choice of soil test itself affected soil strength, and ultimately apparent cohesion, for the articles reviewed. In the long run, the type of soil strength test isn't as important as other related factors such as test confining pressure, piezometric surface location, and how the data was used.

Soil Sample Confining Pressure

The authors who used *in situ* direct shear tests (Wu, et. al., 1979; O'Loughlin, 1972; 1974) used *in situ* confining pressures to anchor one end of the range of normal stresses used during soil testing. These normal stresses represented a soil depth of about 0.25 m (~0.8 ft). They used different values to anchor the top end of the range of normal stresses. O'Loughlin (1972) used an upper limit value corresponding to a soil depth of approximately 0.83 m (2.7 ft) while Wu, et. al. (1979) went up to a normal stress corresponding to a soil depth of approximately 2.25 m (7.4 ft). Buchanan and Savigny (1990) did not report the normal stress range of their laboratory direct shear tests.

For the authors who used triaxial tests, only Sidle and Swanston (1982) presented sufficient information to ascertain the range of confining stresses used during their soil tests which ranged from 34.3 to 103 kPa and can be expresses in terms of an equivalent soil depth ranging from 1.8 to 5.3 m (6.0 to 17.4 ft). Gonsior and Gardner (1971) present there test results in terms of effective stress Mohr's circles and sufficient information is not presented to convert this to

equivalent soil depths, but it appears the normal stress range is very close to the range used in Sidle and Swanston (1982). Swanston (1970) presents no information at all on their soil testing except it was triaxial shear tests. However, given the time frame of the research and the fact that it was landmark research adapting geotechnical engineering to the forest environment, it is fairly safe to assume that high confining pressures were used.

In the reviewed articles where sufficient information was given to review the soil strength testing, all the soil tests were carried out using confining pressures in excess of *in situ* confining pressures. It is probably safe to assume that all the strength tests by all the authors in all the cited articles used confining pressures in excess of *in situ* levels. This is important because the Mohr-Coulomb strength envelopes are not a straight line throughout the range of stresses considered (Lambe and Whitman, 1969; Commandeur, 1989). For shallow, cohesionless soils, the strength envelope is curved which means that ϕ' gets larger and c' gets smaller as confining stresses become smaller The most important consequence of testing shallow, cohesionless soils at confining pressures higher than *in situ* conditions is that the friction angle of the soil could be underestimated (see Figure 3-8). If the frictional component of strength is considered to be the dominant component of the strength for these soils, which it is, then underestimating the friction angle results in underestimating soil strength. In the backanalysis, the strength not accounted for by the Mohr-Coulomb strength envelope shows up as apparent cohesion. So confining

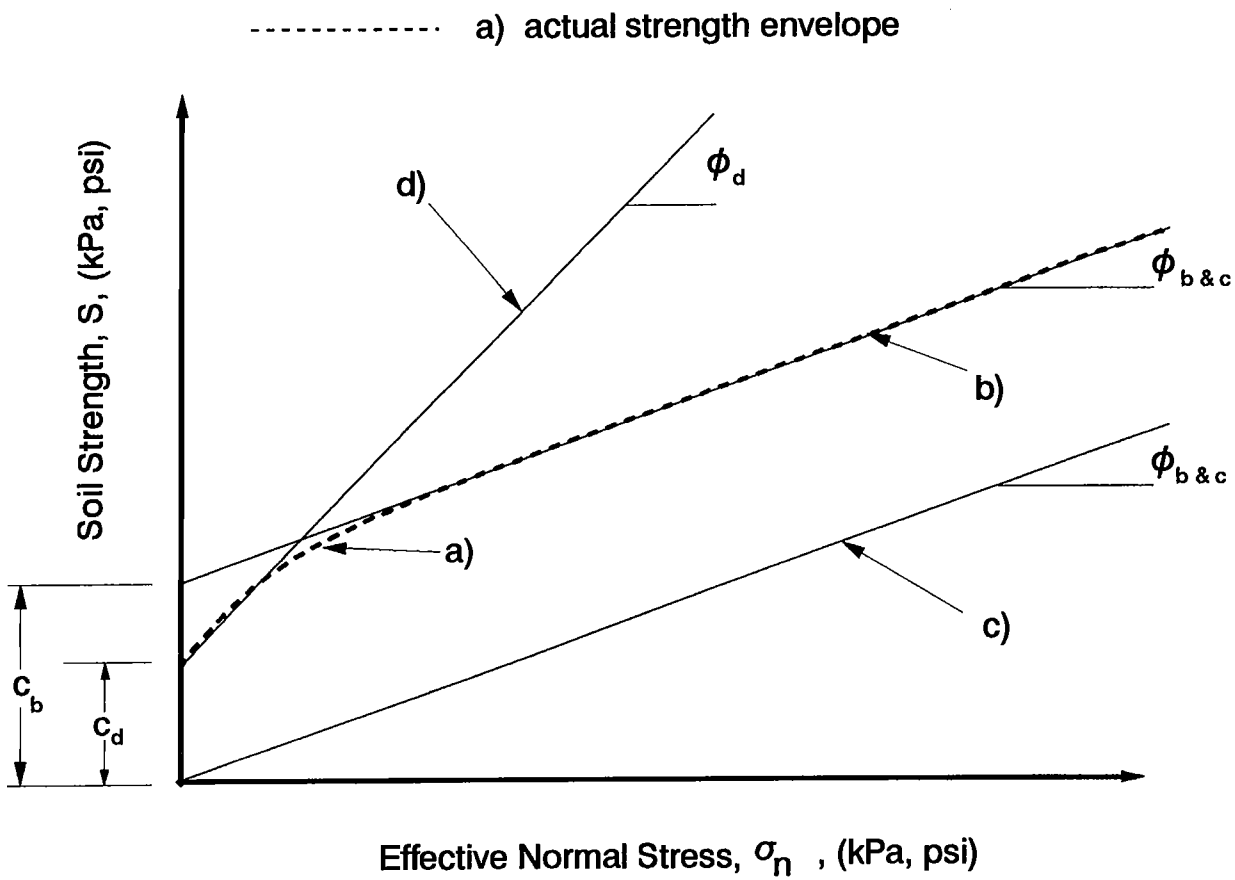

Figure 3-8. An idealized Mohr-Coulomb strength envelope for a shallow, cohesionless forest soil showing (a) the actual curved strength envelope, (b) the straight line approximation of the strength envelope for high confining pressures, (c) the strength envelope if the cohesion intercept is assumed to be zero, and (d) a straight line approximation of the strength envelope for low confining pressures illustrating the higher angle of internal friction and the smaller value for the cohesion intercept.

pressures in excess of *in situ* confining pressures could result in an overestimate of apparent cohesion attributed to roots.

Soil Strength Parameter Use

The single largest potential source of error is the use of the strength parameters derived from soil testing. A basic problem is that the concept of frictional and cohesive components of strength gets confused with the cohesion intercept and internal friction angle as the intercept and slope of a straight line. Only Wu, et. al. (1979) actually used cohesion intercept values derived from strength testing in the backanalysis equations. All of the remaining authors either assumed the soil was cohesionless and set the cohesion intercept to zero (Gonsior and Gardner, 1971; O'Loughlin, 1972; 1974; Buchanan and Savigny, 1990) or measured a cohesion intercept value in the soil strength tests and discarded it (Sidle and Swanston, 1982). Swanston (1979) used a cohesion value of zero but whether it came out of the test or was assumed isn't known.

Most soil strength tests of shallow, cohesionless soils, even those run at low or *in situ* confining pressures, result in Mohr-Coulomb strength envelopes that have some cohesion intercept. What is important is that the Mohr-Coulomb strength envelope is a unique collection of points in τ, σ' space which give a unique value of shear stress on the failure plane at failure for each value of normal stress on the failure plane. If a straight line is used to describe that

collection of points and that straight line has a y-intercept, then the y-intercept must be used whether the soil actually has any inorganic cohesion or not. If a cohesion intercept is determined but then ignored, as in the case of Sidle and Swanston (1982), or if the cohesion intercept is just ignored and a straight line is fit to the angle of internal friction without searching for a cohesion intercept, then the actual strength of the soil may be underestimated. These situations are illustrated with an idealized Mohr-Coulomb strength envelope for a shallow, cohesionless soil in Figure 3-8. The net result is that the soil strength which exists, but is not accounted for by the chosen strength envelope, becomes labeled apparent cohesion.

This is probably the single biggest potential source of error in over-estimating apparent cohesion. A triaxial test was performed on the soil that Sidle and Swanston (1982) were working with and the resulting soil cohesion, c', was 4.9 kPa (102 lbs/ft2). They assumed this meant that the soil was cohesionless and ignored that cohesion value and subsequently backcalculated a value of 2.02 kPa (42 lbs/ft2) for apparent cohesion attributed to root reinforcement. The value of the soil cohesion that was ignored is more than double the value of the apparent cohesion that was solved for. This same situation is repeated in almost all the cases where the magnitude of root reinforcement is being sought by backanalysis. Soil strength testing will yield a very small cohesion intercept value, usually in the range of 1.0 to 2.0 kPa (21 to 42 lbs/ft2) at the low end to as much as 6.0 to 8.0 kPa (125 to 167 lbs/ft^2) at the high end. These are very small

values for soil cohesion when compared to soil cohesion values encountered normally in geotechnical engineering. But, for shallow, cohesionless soils being tested at *in situ* confining pressures, they do exist and this value can represent as much as half of the total soil strength for that soil at that site. So, the determination and use of the appropriate inorganic cohesion values for shallow, cohesionless, forest soils is an important part of the problem. Straight line Mohr-Coulomb strength envelopes derived from soil tests performed at the appropriate confining pressures yields cohesion intercept values that are the same order of magnitude as apparent cohesion values attributed to roots backcalculated from existing landslides. Furthermore, these cohesion values can be as much as half of the strength of these soil at these low confining pressures. If the cohesion intercepts are real and are ignored, then this component of soil strength becomes apparent cohesion due to roots as the result of the backanalysis

Piezometric Surface Location

The single most important parameter to the slope stability process and also the most difficult parameter to ascertain correctly is the location of the piezometric surface at the landslide at the time of failure. This is an important parameter because obviously precipitation and resulting subsurface flow is the driving force triggering landslides. As the piezometric surfaces rises, in response to rainfall, from the failure surface to the soil surface, the soil strength can be reduced by as much as half, which makes the influence of water on soil strength

easily the most important of all discussed so far. This point is made in the debris avalanche inventories section where the fact is pointed out that debris avalanche inventories are routinely initiated as a consequence of large, landslide-producing storms. The location of the piezometric surface at failure is important because it allows the calculation of effective stresses on the failure plane at failure which is the parameter that really drives the process.

Measuring the location of a piezometric surface above a failure surface at failure is very difficult, if not almost impossible, to do because of the tremendous variability in both space and time of the occurrence of precipitation and consequently landslides. Landslide-producing storms occur both infrequently in time and irregularly on the landscape. So either the prediction of these stochastic precipitation events must be very good or instrumentation must be installed on a widespread basis and maintained until a landslide-producing event is sampled. A more difficult, if not impossible, problem is choosing a site to instrument that will fail during the next landslide-producing storm and produce the appropriate information. There is only one incidence reported (Sidle and Swanston, 1982) in which the researchers were fortunate enough to have a site instrumented at the time it failed.

What is done more routinely is to instrument nearby or similar sites and monitor groundwater response to large storms. Relationships are developed between rainfall and piezometric response and these relationships are applied to failed sites to help solve the backanalysis problem (Swanston, 1970; Wu, et. al.

1979; O'Loughlin, 1972; 1974). Another method is to develop a groundwater model or use an existing groundwater model. The available data on rainfall and groundwater response is used to calibrate the model and then the model is used to predict the location of the piezometric surface at failure (Buchanan and Savigny, 1990).

All of these methods have been used to predict piezometric surface location at failures. With the exception of Wu, et. al. (1979), who placed the piezometric surface at different and various depths mid-profile in the soil, all the other researchers, including Sidle and Swanston (1982), placed the ground water table at or very near the soil surface. In all these cases, except Sidle and Swanston (1982), nearby data or a groundwater model was used to place the ground water table and in the process of placing the ground water table at or near the soil surface it was necessary to extrapolate the local data or the calibration of the model beyond the range of data available.

It is unclear for this particular subject what impact the assumptions made have had on the final backcalculated value of apparent cohesion. The assumption of a saturated soil profile is conservative toward soil strength and non-conservative toward apparent cohesion. If the groundwater table is not at the soil surface at failure, then the soil strength is underestimated and attributed to apparent cohesion. The magnitude of that error for an average density forest soil is approximately 5 kPa (104 lbs/ft^2) per meter (3.3 ft) of soil depth. The

magnitude of this error is less than the magnitude of the other errors discussed, like true inorganic cohesion, but it is still within the same order of magnitude.

The possibility that the assumption of full soil profile saturation might be in error can be argued by examining available data. Finding literature which supports the existence of the widespread occurrence, in space or time, of a groundwater table is difficult. The subject of the existence of a groundwater table which would represent positive pore pressure in steeply sloping, shallow forest soils has been investigated (Harr, 1977; Yee, 1975) and their results show that such a feature is highly transient and, within the available data, does not approach the soil surface. Even the piezometric data from southeast Alaska (Swanston, 1967) and British Columbia (O'Loughlin, 1972) in the glaciated till shows water tables which, within the available data, do not approach the soil surface. The assumption of a saturated profile requires extrapolates beyond the available data.

Furthermore, for the backanalysis data on the magnitude of apparent cohesion to support the results from debris avalanche inventories, there would have to be a widespread occurrence of saturated soils. This widespread occurrence of saturated soils doesn't fit the known database. While it is accepted that there will be occasional landslide features that develop saturated profiles during large storms (Sidle and Swanston, 1982), these may be spatially isolated.

The assumption of fully saturated soil profiles could be an error. If so, it errs on the side of apparent cohesion. There is, however, no way to easily come

up with better numbers or assumptions. There are no reliable groundwater models available which can predict rainfall-piezometric relationships for steeply sloping, shallow forest soils. So either piezometric surface location values within the range of the data collected must be used, i.e. Wu, et. al. (1979), or the assumption of a fully saturated profile can be used, However, the consequences of such an assumption must be known and considered.

In conclusion, the backanalysis of existing landslides does not present convincing evidence of the occurrence of or the magnitude of apparent soil cohesion due to root reinforcement. Within the backanalysis process, there are four major places to make errors that will effect the backcalculated value of apparent cohesion. These different error locations are; 1) slope stability analysis method, 2) determination of soil strength parameters, 3) correct use of soil strength parameters, and 4) correct placement of the piezometric surface within the soil profile.

The primary slope stability analysis methods used are non-rigorous methods which tend to undervalue the amount of strength available and in a backanalysis that strength is directed toward apparent cohesion. The magnitude of the potential error is at a minimum in the single digits of kPa.

Likewise in soil strength testing. The largest potential error and the one that occurs most often is performing the soil strength test at a confining pressure that is too high. At confining pressures much greater than *in situ* for shallow forest soils, the friction angle is underestimated which underestimates available

strength when c' is ignored or set to zero. However, a confining pressure that is too high also tends to overestimate soil cohesion during the soil test. This doesn't seem to be a problem because more often than not, these soils are assumed to be cohesionless. Thus, either a soil cohesion value is not determined during the soil strength test or a value that is determined is simply ignored and not used. The errors made either during testing for soil strength or in the inappropriate or incorrect use of soil strength numbers is also in the same order of magnitude as the values of apparent cohesion that are back calculated. They are in the single digits of kPa.

Finally, in general the assumption is made that the groundwater surface is at the soil surface when landslides fail. If this assumption is incorrect, it errs by underestimating soil strength which then overestimates apparent cohesion. The order of magnitude of this error is less than the other two cases, however it is still in the lower single digits of kPa.

All the error sources for backcalculating apparent cohesion are conservative toward soil strength and non-conservative toward apparent cohesion. The magnitude of the error for all the error sources is approximately the same, in the single digits of kPa or from approximately 1 to 8 kPa (20 to 160 lbs/ft^2). Thus, in the backanalysis of the apparent cohesion values reported in the cited articles, if different, more realistic and/or non-conservative assumptions had been made regarding the backanalysis, all of the apparent cohesion values may have been reduced significantly or eliminated.

Finally, even with the values used, assumptions made, and apparent cohesion values calculated, it is impossible to make the forested system perform like we know it must. Swanston (1970) and Sidle and Swanston (1982) in their research only calculated the value of apparent cohesion for the failed landslides. No other comparisons were made. However, Gonsior and Gardner (1971), O'Loughlin (1972; 1974), Wu, et. al. (1979), and Buchanan and Savigny (1990) all concluded their research by taking the apparent cohesion values calculated and all the other stability parameters assumed, and carried out an analysis of an old-growth forested site to show it was stable and that the concept worked. The slope stability analysis carried out were for a failed site in a harvested area and a stable site in a forest area. Only Gonsior and Gardner (1971) performed a stability analysis on a stable structure that should have failed. In this case it was a road fill and what they found was that with the assumptions they had made regarding the backanalysis of the other failed structures, a similar unfailed structure should not be standing. They further admitted that in any of a number of places, including soil strength determination and the placement of the groundwater surface, assumptions could have been made differently that could account for the stable structure.

The other three cited articles all have this same situation with regard to inherent assumptions and values for slope stability analysis parameters, including a value for apparent cohesion due to roots. With these assumptions, it is not possible to have an unstable forested site or a stable harvested site.

O'Loughlin (1972) states that 71 percent of the strength of forested sites is due to roots. His apparent cohesion values don't support that statement. If that is true, then other environmental factors can only reduce the remaining 29 percent by half and without harvesting that site, it would be impossible to have it fail. Yet we know failures exist in forested areas of British Columbia. Likewise, Buchanan and Savigny (1990) put maximum root reinforcement together with worst case water tables and calculated the factor of safety of landslide-prone hillslopes supporting old-growth forests to be 2.5 to 3.0. If the water table is at worst case values, there is no way to reduce the strength of these sites and therefore they could not fail. Yet failures also occur in the forests of the Washington Cascades. While the case was not explicitly made, similar calculations can be made using the authors assumed and calculated values and it is impossible for a harvested site not to fail. Which also doesn't occur because many high risk harvested sites don't fail. Thus, landslide backanalysis as it is used in the reviewed articles does not result in parameters that can be used to correctly and consistently describe the real world. Therefore, in its present form it is not useful for helping to explain root reinforcement.

Modeling Root Reinforcement

The previous discussions regarding debris avalanche inventories, quantifying root tensile and shear strength, strength testing of soil/root

composites, and landslide backanalysis have all been directed toward the development of a root reinforcement hypothesis and then testing that hypothesis. Outside of creating awareness for the concept of root reinforcement, the developed database presents very little information that can be used as an applied management tool. To put the information into an applied management tool, the information and developed data need to be put into the form of a rough conceptual model of how root reinforcement works. That model can then be applied to forest management situations and the role of root reinforcement or the effect of alternative management strategies on root reinforcement can be evaluated.

In this section, a number of different models and modeling strategies will be discussed. The original concept embracing root reinforcement is reinforced earth theory as developed by Vidal (1969). The mechanics for designing reinforced earth walls will be discussed as well as the first cousin of reinforced earth, soil nailing. Some of the empirical models developed to explain specific data sets will also be discussed such as the root biomass model by Ziemer (1981) and the total work model by Shewbridge and Sitar (1985). Finally, the process level model of root reinforcement developed by both Wu (1976) and Waldron (1977) will be presented.

Reinforced Earth/Soil Nailing

The pioneering formal work related to imparting tensile strength to materials which do not possess innate tensile strength is in reinforced earth. In reinforced earth, reinforcing elements that are long, thin, and wide with high tensile strength and high modulus are embedded in soil, a material with low tensile strength. The composite material formed from the soil and the reinforcing elements has strength attributes of both materials including tensile strength. Reinforced earth in its contemporary form is used mainly for retaining wall structures. Reinforced earth retaining walls are structures which are constructed by alternating soil layers with layers of reinforcing elements which are usually long, flat, wide strips of steel or geotextiles. The steel or geotextile in the soil gives the composite material tensile strength thus allowing the reinforced earth wall to stand much more steeply than soil alone would.

The basic mechanics of reinforced earth which were first presented by Vidal (1969) included some basic requirements. Among these requirements are:

- the transfer of frictional force between individual soil grains and the reinforcement,
- the transfer of the subsequent shearing stress between soil grains in contact with the reinforcement element and those not in contact, and

- the reinforcement introduces a compressive force to the soil that acts parallel to the reinforcing element and whose magnitude is equal to the tension in the reinforcement.

Since the original presentation of the theory and mechanics of reinforced earth (Vidal, 1969), subsequent work has been carried out with the intent to both validate and refine the understanding of the mechanics of reinforced earth (Yang, 1972; Jewell, 1980). This research has been highly successful and with its completion a better understanding of the changes in stress states that occur in soil as a result of the inclusion of reinforcement is available. Despite this research, understanding of the mechanics of reinforced earth and the design of reinforced earth walls remains fairly straightforward. This is due to the fact that the research that has guided current design of reinforced earth structures comes primarily from observations of model reinforced earth walls, both standing and at collapse, and the observation of standing, full-size walls (Mitchell and Villet, 1987).

In a reinforced earth structure the strength added to the soil is a function of the number, size, and materials of the reinforcing elements. In the design process the objective is to match the number and size of a given reinforcing element of a known material with the strength increase needed to fulfill design objectives. Therefore, the design process incorporates the model for predicting strength increases as a result of reinforced earth.

To illustrate how a strength increase is calculated in the design process of a reinforced earth wall, a simple rectangular reinforced earth retaining wall with no external loads is considered (Figure 3-9). Sufficient data has been collected on full-size, standing, reinforced earth walls, such as the one illustrated, that the location of the critical failure surface can be predicted. The failure surface extends from the base of the wall upward at an angle of $45 + \phi/2$ until it intersects a failure surface extending vertically downward from the soil surface at a distance $0.3H$ from the edge of the wall where H is the height of the retaining wall (Figure 3-9). With the critical surface known, the maximum tensile force that will have to be resisted by a reinforcing element can be determined. That tensile force is calculated using the relationship,

$$T_{max} = K \sigma_v \, X \, Y \qquad 3\text{-}3$$

where, T_{max} = maximum developed tensile force, K = a coefficient which converts vertical to horizontal pressure, σ_v = the vertical soil pressure, and X and Y are the horizontal and vertical spacing of the reinforcements.

This maximum developed tensile force must be successfully resisted by the reinforcing elements in two modes; ultimate strength and pull-out. To design for the ultimate strength of the reinforcements, the following check must be made;

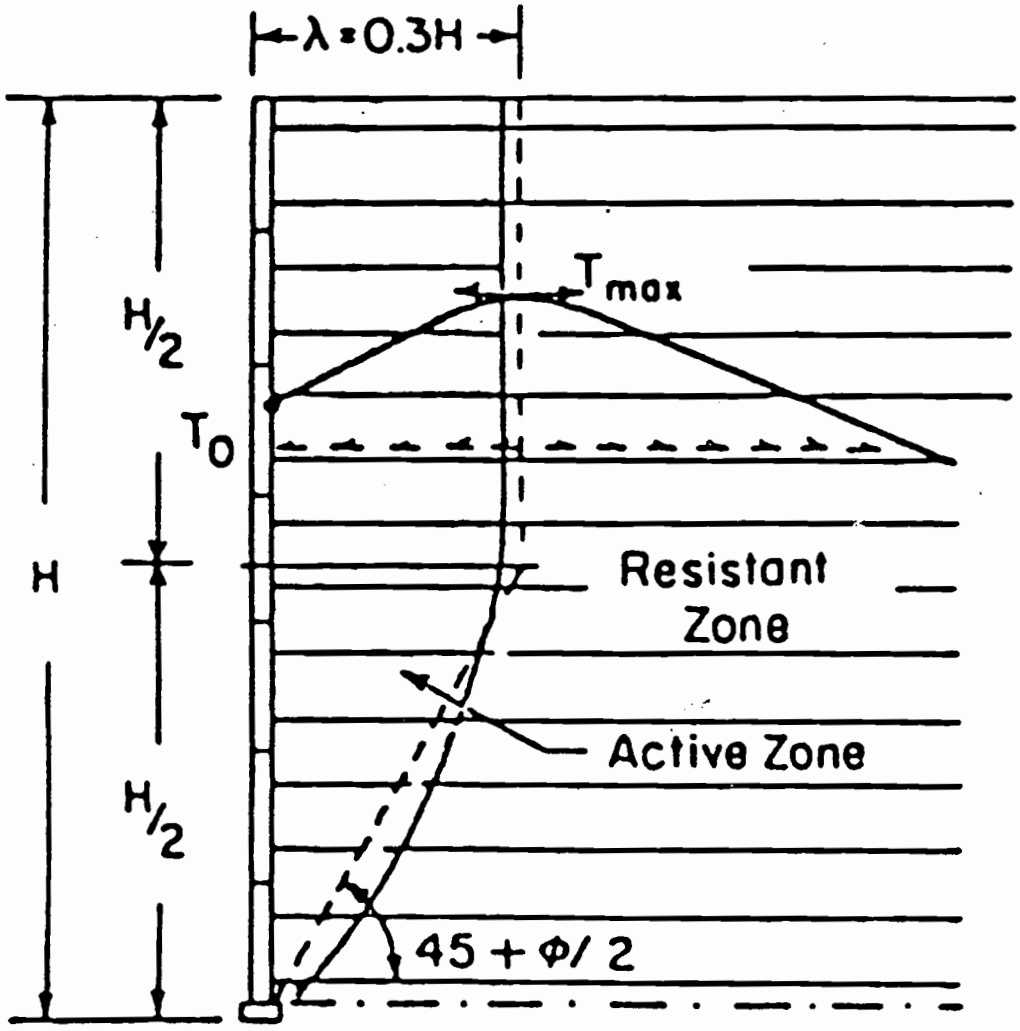

Figure 3-9. Diagram of a simple rectangular reinforced earth retaining wall with no external loads showing the location of the potential slip surface.

$$T_{\max} \leq \frac{1}{FS_R} R_t \, t \, b \qquad 3\text{-}4$$

where FS_R = required factor of safety in rupture, R_t = a maximum allowable tensile stress either an ultimate stress or yield stress, and t and b = the thickness and width of the reinforcing elements, respectively. The maximum tensile force developed must also be resisted in pull-out and the following relationship should also be checked for all the reinforcements.

$$T_{\max} = \frac{1}{FS_p} \mu^* \, \sigma_v \, 2 \, b \, L_e \qquad 3\text{-}5$$

where, FS_p = required factor of safety in pull-out, μ^* = apparent coefficient of friction between the soil and the reinforcing element, and L_e = length of the reinforcing element outside the critical failure surface. The other terms have been previously described and the 2 simply accounts for both sides of the reinforcing element.

There are many aspects of reinforced earth walls and the design procedure which separate the subject markedly from root reinforcement in shallow forest soils. Because a reinforced earth wall is constructed in place, it is possible and required to know most of the design parameters like, 1) the location of the perceived critical failure surface, 2) the mechanical properties of the stress

backfill like the density and internal angle of friction, 3) the allowable tensile and modulus of the reinforcements, 4) the apparent coefficient of friction, μ^*, between the soil and the reinforcements, and 5) the length, width, thickness, and spacing of the reinforcements (Mitchell and Villet, 1987). These same parameters are not known in the case of root reinforcement and in most cases it would not be possible to determine them easily. An example of this problem is the number, length, diameter, allowable tensile stress, modulus, and apparent friction coefficient of tree roots within a potential landslide mass.

An additional point that needs to be made is in regard to the strain compatibility of reinforced earth structures. At no place in the reinforced earth design process is the displacement of the soil and the corresponding strain of reinforcements considered. The entire problem is evaluated at peak soil strength, ultimate or rupture strength of the reinforcing elements, and ultimate pull out resistance of the reinforcing elements. These values are all modified by the appropriate safety factors. While soil strength is not explicitly dealt with in this problem, like a traditional limit equilibrium problem, the assumption is made that by using the appropriate lateral earth pressure coefficient the soil will support itself to the maximum extent possible or, in other words, the peak strength in the soil will be mobilized. A further assumption is that the soil displacement that is required to mobilize peak soil strength will also be sufficient to mobilize the required tension in the reinforcing element to result in a stable structure. The design process is driven by ultimate stress values to insure failure

of the structure will not occur and the strains needed to simply make the structure function at working stresses are not designed for but deemed acceptable to perform their task on the basis of a critical mass of data from instrumented existing structures. Thus, the strain compatibility of the dissimilar materials, which appears to be an issue with roots and shallow forest soils, is not explicitly designed for in reinforced earth structures.

A companion type of reinforced earth structure that comes closer to performing like, and is analyzed like, root reinforcement in shallow forest soils is soil nailing. Soil nailing has two primary uses, excavations and potential failing surfaces. It is an *in situ* reinforcement technique which consists of placing passive, high modulus, high tensile strength inclusions into a soil mass to give it increased shearing resistance along a potential failure surface. An example of a typical use of soil nailing is to help stabilize an excavation as illustrated in Figure 3-10. As the excavation is lowered successively, soil nails, which are usually steel bars, are driven into the soil. The objective is to drive the steel bars across any potential failure surfaces thus adding the strength of the steel bars to the shearing resistance of the soil.

The design process for soil nailed structures is different from reinforced earth structures. For soil nailed structures the global stability of the entire structure is the primary design goal and not the capacity of individual nails as in reinforced earth. The first step in the design of a soil nailed structure, like all slope stability projects, is to determine the location of a critical failure surface.

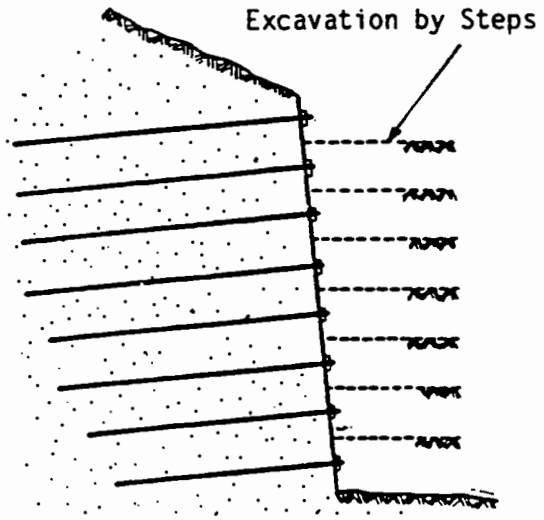

Retaining Structures

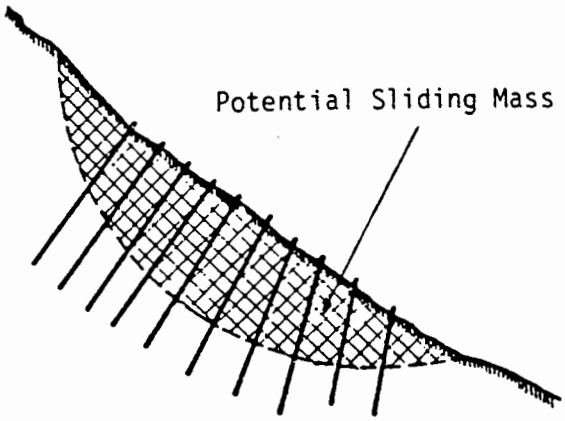

Slope Stabilization

Figure 3-10. Two examples of soil nailed reinforced earth structures; an excavation and a stabilized potential slide mass.

Soil nailing is unlike reinforced earth structures which are manufactured in placeand come with empirical performance data which delineates the location of the critical failure surface. Soil nailing requires a traditional approach to the location of the critical failure surface which includes lateral earth pressure theory and tradition slope stability analysis methods.

Once the critical failure surface is located, the design procedure consists primarily of running a limit equilibrium slope stability analysis of the failure surface with the soil nails included. A "slices" or "wedge" method of slope stability analysis is recommended (Mitchell and Villet, 1987) and the increased shearing resistance of the soil nails are included as vectors with a magnitude and direction located along the failure surface. There are several analysis methods which include different components in the increased shearing resistance. Some methods include both the increased tension in the soil nail as well as its shear capacity. Another method, the "Davis" method, deals only with the increased tension in the soil nail and it is the only method which will be discussed in detail because it is the closest analog to how root reinforcement is expected to occur.

The increased shearing resistance which is the increased tension in the reinforcements, or the soil nails, is either the allowable tensile capacity or the ultimate pull-out resistance of the portion of the nail that extends beyond the critical failure surface. The values for these quantities are calculated in a manner similar to equations 3-4 and 3-5 for reinforced earth reinforcements except the geometry is round, not thin and wide. The allowable maximum tensile capacity

is either a rupture or yielding load modified by the nail dimensions and an appropriate factor of safety. Ultimate pull-out capacity is a product of the apparent friction coefficient, effective vertical stress, surface area of the nail extending beyond the failure surface, and an appropriate factor of safety. The smaller of these two values is entered into the limit equilibrium analysis of the factor of safety.

This design method approaches more closely how root reinforcement could be handled. In comparison with the reinforced earth design procedure, the location of the critical failure surface isn't as well known but this shouldn't be an analysis problem because it can still be placed well enough for design purposes. Also, the soil is *in situ* and not manufactured so the soil properties will not be as well known but that also should not be a problem because the properties of the *in situ* soil can be determined. But, the reinforcement parameters should be much better known than working with root reinforcement. The allowable tensile stress, modulus, apparent friction coefficient with the soil, size and the number of reinforcements should all be known as a part of the design process.

The design procedure for soil nailing also involves only ultimate stresses. The assumption is made, once again, that the soil displacement will be such that the full strength of the soil will be mobilized. A further assumption is that at working stresses the displacements will develop sufficient tension to allow the nailed structure to function. The design of the nails is to keep the structure from failing and the assumption is, supported by empirical data, that if it doesn't fail

there is sufficient increased shear stress at working displacements and stresses to allow the structure to function as designed. So again, the strain compatibility issue between dissimilar materials, which appears to be an issue with root reinforcement and shallow forest soils, is not explicitly designed for.

While both limit equilibrium design methods and empirical relationships derived from observations on full scale structures work, there is ongoing interest in design methods which are "strain compatible" or "kinematically correct". There have been a series of articles by Juran and his associates which present a strain compatible design method for reinforce earth walls (Juran and Chen, 1989) and geosynthetic reinforced soil walls (Juran, et. el., 1990b). They also present a kinematical limit analysis method for soil nailed structures (Juran, et. al., 1990a). In these articles the authors present assumptions which would seem to invalidate their use in modeling root reinforcement, namely that shear zone width is unaffected by the reinforcements and that the effect of local soil-reinforcement friction on the state of stress in the soil can be neglected. The articles and the ideas they have presented also have not received universal acceptance from the geotechnical community (Leshchinsky, 1991; Leshchinsky and Boedeker, 1991; Jewell and Pedley, 1991; Shewbridge and Sitar, 1992). For these reasons, no attempt will be made to reconcile the strain compatible design for reinforced earth walls with root reinforcement in shallow forest soils.

Empirical Models

There have been several models developed to predict either the strength of soil/root composite materials or predict the strength added to soil resulting from root reinforcement. The limitation of most of these models is that they are either empirical models and thus appropriate for describing only the data set they were developed from or are more basic process models which were developed or calibrated using a limited empirical data set which limits the usefulness of the model. For example, Ziemer (1981a) developed a linear regression model predicting the strength of rooted soil columns as a function of the oven dried weight of live roots less than 17 mm in diameter. The data used to develop the model was from *Pinus contorta* growing on a beach sand in California. So while the developed model may be very good, if it is used outside of beach sand and shore pine then the predicted strength is extrapolated far beyond the data base. This fact explains why Ziemer (1981a) didn't predict increased soil strength due to root biomass changes after harvesting from his root biomass data. The equation was inappropriate for that data and he could only predict net root reinforcement.

Endo and Tsurutu (1969) also developed a regression model in which the rooted strength of prepared nursery soil was predicted as a function of the normal stress on the failure surface in the soil and the total weight of live *alnus glutinosa* roots. O'Loughlin (1972) developed a linear regression model predicting rooted soil strength as a function of fresh root weight for steeply sloping,

shallow, forest soil in coastal British Columbia. For both of these studies the value in the regression model is simply hypothesis testing because its usefulness becomes very limited when applied outside of the range of the data used to develop it.

Wu, et. al. (1988a) developed a process level model describing the interactions between soil and roots and predicts increased soil strength for the soil/root complex. The model is based on the solution for a laterally loaded pile in a flexible foundation (Scott, 1981). The authors start with the fourth order differential equation describing the behavior of a laterally loaded pile and integrate it four times to solve for four constants of integration. There are three forms to the solution. One form involves the traditional laterally loaded pile problem with small displacements at the top of the pile. A second form is the laterally load pile equation solved for the case where there are large displacements at the top of the pile. In this form, a term for the axial load in the pile is included. The final form is of the laterally loaded pile for the case when the pile can act only in tension and this form is the solution for a cable. The equations are all solved in closed form using the boundary conditions of the problem to solve for the constants of integration.

The analytical model developed by Wu, et. al. (1988a) was evaluated by the use of both laboratory model tests and *in situ* soil strength testing of a rooted forest soil (Wu, et. al., 1988b). A 30 x 15 x 15 cm shear frame was used that was only open on two sides, the bottom and the other two sides were closed off. The

same shear frame design was used by Ziemer (1981a). During the *in situ* soil tests the displacement of the ground adjacent to the shear frame was monitored and after the shear test was complete the soil in the shear box was removed and the roots in the shear box were exposed. Roots that were displaced, roots that had failed in tension, and roots that had been cut off by shear box were all considered. The size, geometry, and failure mode of the roots were used to model the contribution of the roots to the shear resistance of the soil. The authors found general agreement between the model and measured shear resistance of the soil/root complex and this research confirms, to a degree, the use of a laterally loaded pile solution method for the problem of soil-root interactions. The model is constrained from further use by the amount and quality of the input data needed from the *in situ* soil strength tests that were used to calculate the modeled shear resistance. To use the developed model without having *in situ* soil strength test results would require that that a similar quality and quantity of information regarding the number, size, geometry, and failure status of the roots in the soil would have to be known to predict soil strength *a prior*. Even though Wu, et. al. (1988a) present an analytical model to predict the strength of soil-root complexes, the model still requires the prediction of a number of characteristics of the soil sample at failure before the strength can be predicted. As a management tool then, this model is of little more value than the empirical models requiring live root weight of the soil sample.

Shewbridge and Sitar (1990) developed a deformation-based, rigid-plastic model to describe the effect of different types and numbers of reinforcements on the strength of sand in direct shear. Once again, this model was developed specifically to evaluate experimental results obtained from large-scale, direct shear tests (Shewbridge and Sitar, 1989). In fact the input for the model is in the form of output from the direct shear tests. The model is useful as a research tool to help analyze and provide insight into the direct shear results, but it should not be considered a viable management tool.

Similar comments must be made concerning the model developed by Abe and Ziemer (1991) which was developed, once again, specifically to help explain results from direct shear tests. Large-scale direct shear tests were carried out investigating the effect of different numbers and diameters of pine roots on the strength of sand in direct shear. In fact, once again, model inputs were in the form of outputs from the direct shear tests, so the model, while it may be useful as a research tool, certainly was not developed as a management tool.

Wu-Waldron Model

There is one model available which describes a mechanism of root reinforcement and was not developed around empirical data. The model was developed independently by both T. H. Wu and L. J. Waldron and is the most widely cited root reinforcement model available. The description of the model

presented here is referenced from Waldron (1977) and Wu, et. al. (1979) and has generally come to be referred to as the Wu-Waldron model.

A definition sketch for the development of the Wu-Waldron model is shown in Figure 3-11. The Wu-Waldron model assumes a shear zone of fixed width, Z. Across this shear zone a fully elastic root or some other reinforcing element is embedded with known modulus, *E*. At present, for the purposes of discussion, the assumption is made that the reinforcing element is embedded perpendicular to the shear zone. A lateral displacement or shear deformation of distance *Y* is imposed on the shear zone. It will be further assumed that the shear-stress transfer between the soil and the reinforcing element is fully engaged, thus the reinforcing element is firmly pinned at each end and can not slip. As shear deformation is imposed, the reinforcing element must stretch across the shear zone. Knowing both the shear zone width, Z, and the magnitude of the shear deformation, *Y*, the angle θ that the reinforcing element makes with the shear surface can be determined and the increase in length, Δl, of the reinforcing element can also be determined.

$$\tan\theta = Y/Z \qquad 3\text{-}6$$

$$\Delta l = \frac{Z}{\cos\theta} - Z = Z\left(\frac{1}{\cos\theta} - 1\right) = Z(\sec\theta - 1) \qquad 3\text{-}7$$

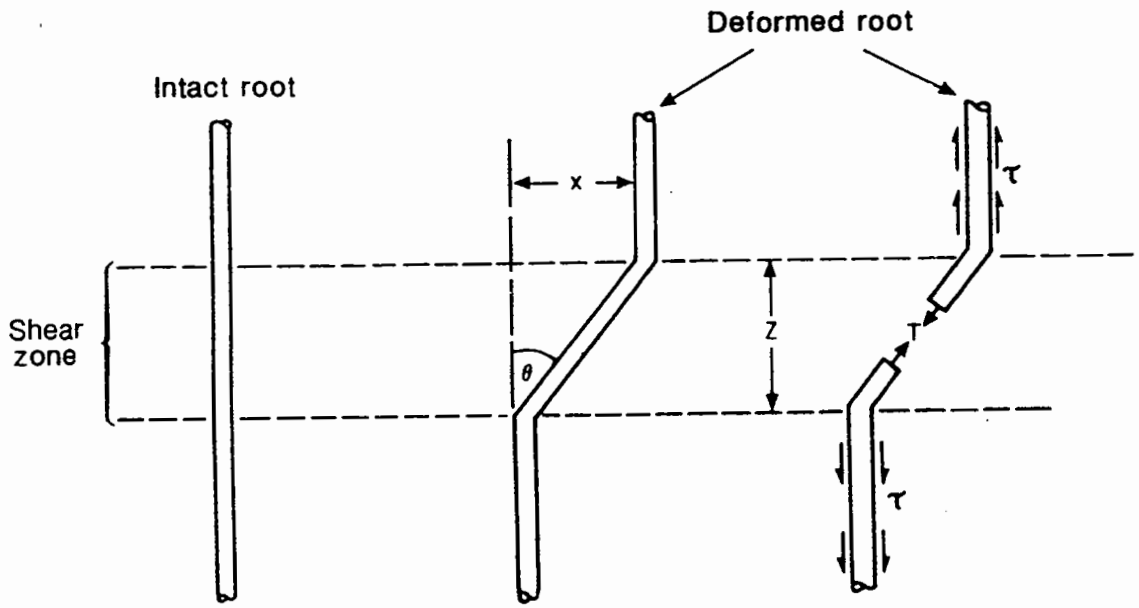

Figure 3-11. Definition sketch for the Wu-Waldron root reinforcement model (Greenway, 1987).

Thus, if the size of the reinforcing element is known, then that value along with the modulus, E, and the shear zone width, Z, allows the increased tension in the reinforcing element to be calculated using the relationship,

$$T_r = \frac{\Delta l \, E \, A}{Z} \qquad 3\text{-}8$$

where T_r is the increased tensile force in the reinforcing element due to the change in length Δl, and A is the cross sectional area of the reinforcing element. The tensile stress, t_r, is simply the tensile force, T_r, divided by the cross sectional area, A, of the reinforcing element.

The key to root reinforcement is the increase in tension or tensile force in the roots or reinforcing elements. If this is true, then equation 3-8 implies that to quantify or predict the increase in tension in reinforcing elements, a knowledge of the cross sectional area of the reinforcing elements, the modulus of the reinforcing elements, the width of the shear zone, and the shear deformation all at failure is required. This is a considerable amount of information to discern *a priori* about a particular site.

This problem can be greatly simplified by the assumption that peak soil strength and maximum reinforcement will occur when the reinforcing elements are at ultimate strength. To get the total tensile strength available to reinforce soil strength expressed on a per unit area of soil basis, the root area ratio, or the fraction of the soil cross section occupied by roots or reinforcing elements, is

needed along with the average ultimate tensile strength of the roots or reinforcing elements expressed as a stress.

$$R_t = t_{r_{ult}} \frac{A_r}{A} \qquad 3\text{-}9$$

where, R_t is the total tensile strength available to reinforce soil expressed on a per unit area of soil, $t_{r_{ult}}$ is the average ultimate stress of the reinforcing elements, and A_r/A is the root area ratio.

In Figure 3-11, the definition sketch for the Wu-Waldron model, the increase in tension in the single root can be resolved into components which directly oppose shear and which augment the normal stress. In this manner the increase in soil strength attributed to root reinforcement can be calculated by resolving the increase in tension in a single reinforcing element into its components as follows,

$$S_r = t_r(\cos\theta \tan\phi + \sin\theta) \qquad 3\text{-}10$$

where S_r is the shear strength increase in the soil due to roots and t_r is the increase in tensile stress in a single root. The other terms have been described except for ϕ which is the internal angle of friction of the soil.

This same relationship can be used to calculate the increase in soil strength due to roots on a per unit area of soil basis by using the term R_t which has been

defined as the average ultimate increase in stress due to reinforcing elements expressed on a unit soil area basis. Notice that the shear deformation angle, θ, is still in the relationship requiring knowledge of the extent of shear deformation to predict the increase in soil strength due to reinforcement. Wu (1976) and Waldron and Dakessian (1981) report, based on comparisons of output from the model to results of laboratory direct shear tests, that for both rooted and unrooted soil samples the collection of terms $(cos\,\theta\, tan\,\phi + sin\,\theta)$ is relatively insensitive to both changes in ϕ and θ within the modeled range of these values. For a range of values of ϕ between 20 and 40 degrees and θ between 40 and 70 degrees, the value of $(cos\,\theta\, tan\,\phi + sin\,\theta)$ varied from 0.92 to 1.31 (Wu, 1976 as reported in Gray and Megahan, 1981). Wu, et. al. (1979) chose a value of 1.2 as a mid-range value to model root reinforcement for his backanalysis. Gray and Megahan (1981) chose a midpoint value of 1.12 with which to model root reinforcement. The value 1.2 is found most often quoted and used in the technical literature which makes the form of the equation for calculating the increase in soil strength due to root reinforcement of the form,

$$S_r = 1.2\, R_t \qquad 3\text{-}11$$

where, S_r is the increase in soil strength due to root reinforcement and R_t is the total tensile strength available to reinforce soil expressed on a per unit area of

soil. R_t is the sum of the tensile strength of all the individual roots expressed as a stress multiplied by the root area ratio.

Equation 3-11 is the root reinforcement equivalent to ultimate stress design for both reinforced earth and soil nailed structures. There are several assumptions that have to be made in order for equation 3-11 to work. First of all, there is the assumption that peak root reinforcement will occur at ultimate stress for the reinforcing elements and secondly, there is the assumption that all reinforcing elements will reach this stress simultaneously at the same shear deformation. There is no consideration given of the strain compatibility problem between different sized roots or reinforcing elements. Furthermore, the ultimate stress in the reinforcing elements will be reached at a deformation in which the peak strength of the soil can be realized. In other words, there is no consideration of strain compatibility problems between dissimilar materials such as a loose, cohesionless forest soil and small and large roots. Some researchers have modified their estimates of root reinforcement obtained from this equation because they realize the problems inherent in assuming that all roots reach ultimate tension simultaneously. Burroughs and Thomas (1977) reduced their estimate of root reinforcement by 25 percent based on this reasoning, but the basis for that particular value was not substantiated.

Subsequent research has shown that the ultimate tension in a root is not the limiting value in root reinforcement of shallow forest soils. Waldron and Dakessian (1981) state that the shear-stress transfer at the soil-root interface is the

quantity most limiting successful modeling of root reinforcement. This finding is supported by research from the reinforced earth and soil nailing field which shows mobilization of tension in the reinforcements to be much more important in reinforcement than bending stresses (Shewbridge and Sitar, 1990; Jewell and Pedley, 1992). Despite these research advances and admonitions to the contrary, the Wu-Waldron model with the recommended factor of 1.2 can be found in numerous reports and handbooks summarizing the state-of-the-knowledge and yielding design methods (Sidle, et. al. 1985; Greenway, 1987).

An assumption of the Wu-Waldron model that was presented but not discussed is the assumption that reinforcing elements are arranged perpendicular to the shear zone. This assumption greatly simplifies the real world. The effect on soil strength increase of changing orientation of the reinforcements has been considered analytically (Wu, et. al., 1988a) and in direct shear tests (Gray and Ohashi, 1983; Jewell, 1980). Orienting the reinforcing elements normal to the shear zone is not the most optimum alignment. But, assuming that all reinforcements are aligned normal to the shear surface does not give an unreasonable average response. Gray and Ohashi (1983) in laboratory direct shear tests showed that a random orientation of fibers and a normal orientation of fibers gave comparable results.

MODEL DEVELOPMENT

Conceptual Model Development

The root reinforcement model developed as a part of this research project and described in this dissertation was developed to help quantify the effect of reinforcing elements, especially tree roots, on the strength of shallow, forest soils. The effect being modeled is the addition of reinforcing elements with high tensile strength and a high modulus, i.e. conifer roots, to a cohesionless soil which has essentially no tensile strength. The development of the model is initiated, conceptually, by embedding a reinforcing element into an isotropic block of soil as in Figure 4-1(a). To make this conceptual situation as realistic as possible, the block of soil is located within a landslide-prone goemorphic feature called a headwall or a "colluvial hollow" which is steeply sloping, forested, and has a shallow soil with a potential failure plane through it (Figure 4-2). The reinforcing element is assumed to be a conifer root which is parallel to the soil surface and perpendicular to the potential failure surface, therefore, the view of the soil block in Figures 4-1, 4-2, and 4-3 is a view normal to the hillslope and looking down on it. The soil texture is assumed to be sandy with few fines resulting in little, if any, cohesion.

As a landslide initiates on the hillslope where the conceptualized soil block is located, one half of the soil block will begin to move downslope relative to the other half. The movement of the soil will occur along a failure surface

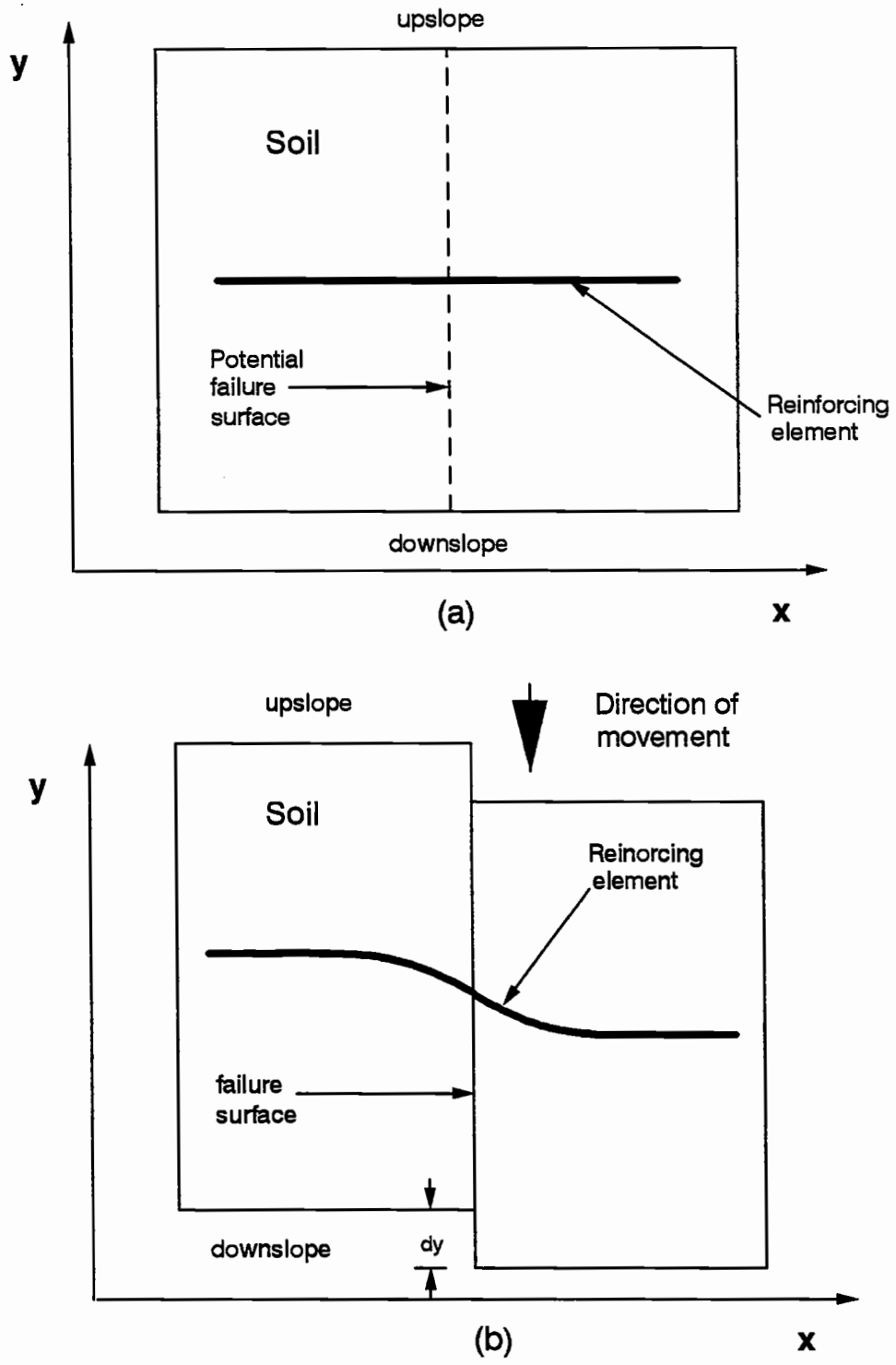

Figure 4-1. (a) An isotropic block of soil with a reinforcing element embedded in it perpendicular to a potential failure surface; (b) the block of soil with a lateral deformation, *dy*, imposed on one half of the soil relative to the other half causing deformation of the reinforcing element.

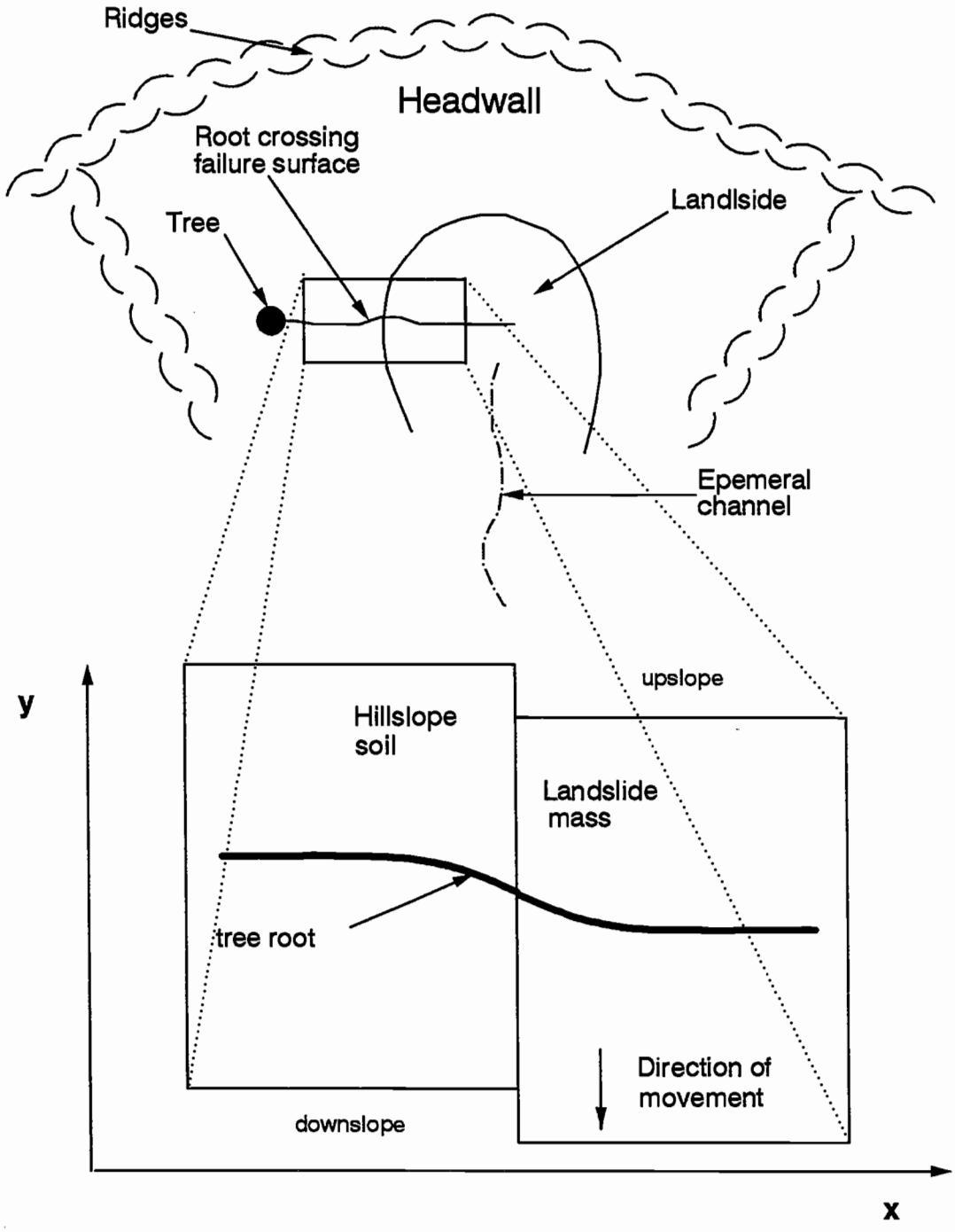

Figure 4-2. A diagram showing the context of the conceptual soil block within a headwall on a steeply-sloping, landslide-prone, forested hillslope with a shallow, cohesionless soil. The reinforcing element is portrayed as a conifer root.

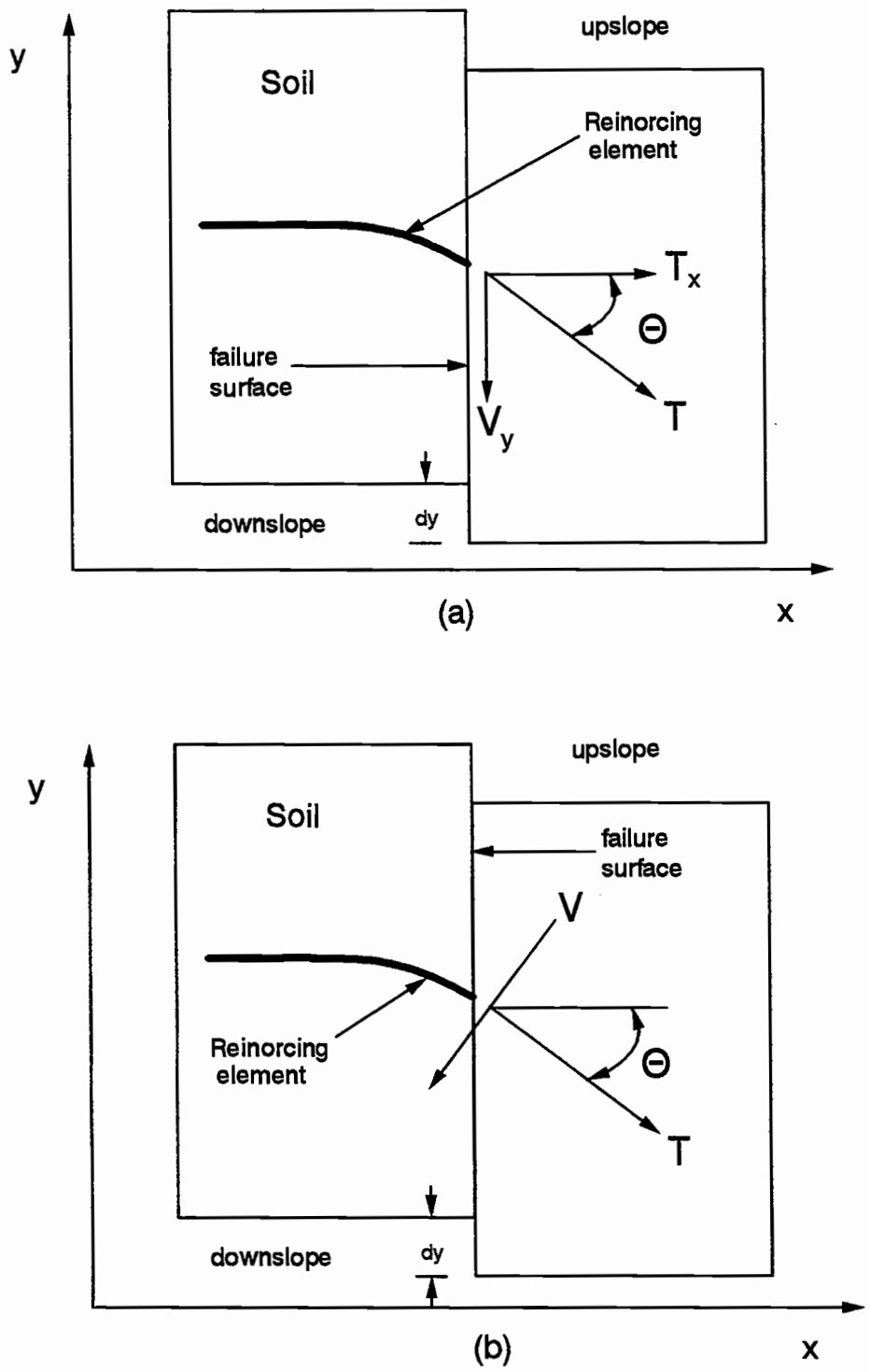

Figure 4-3. The conceptual model of root reinforcement shown with half the reinforcing element, or conifer root, replaced with an equivalent force system.

within the soil block. As the deflection between the halves of the soil block increases, the reinforcing element extending through the soil block crossing the failure surface will deform. The deformation of the reinforcing element will cause it to lengthen which will cause an increase in tension in the reinforcing element. This increased tension may cause the reinforcing element to either break in tension, pull-out, or simply continue to deform and lengthen with an accompanying increase in tension. If the reinforcing element breaks or pulls-out, the reinforcing effect will be reduced considerably, thus, a further assumption is made that the reinforcing element is sufficiently long so that shear-stress transfer between the soil and the reinforcing element will be fully engaged and allow the ultimate tensile strength of the reinforcing element to be mobilized.

At any given deflection, dy, the soil block is symmetric about the failure surface (Figure 4-1(b)). Thus, half of the soil block can be replaced by an equivalent force system. Waldron (1977) and Wu, et. al. (1979) in their separate developments of this concept have replaced the root at the failure surface with an equivalent force system comprised of a single tension vector, T, inclined at an angle, θ ,from a perpendicular to the failure surface. The tension vector is resolved into components parallel, T_y, and perpendicular, T_x, to the failure surface (Figure 4-3(a)). The component parallel to the failure surface directly opposes movement of the soil block and the component perpendicular to the failure surface contributes to the normal force. If the assumption is made that the deformation is sufficient to mobilize peak soil strength, then the components of

the tension vector can be included directly into the Mohr-Coulomb strength equation. Thus, the strength of the conceptualized soil block resisting failure becomes:

$$S = c' + \frac{T}{A} sin\theta + \left(\frac{T}{A} cos\theta + \sigma_n \right) tan\phi' \qquad 4\text{-}1$$

In this equation, S is soil strength, c' is effective soil cohesion, T is the tensile force in the reinforcing element, A is the cross-sectional area of the soil block the reinforcing element is embedded in, θ is angle the reinforcing element makes with a perpendicular to the failure surface, and ϕ' is the effective internal angle of friction of the soil. Thus, the strength the reinforcing element adds to the strength of the soil block can be given by the equation,

$$\Delta S = \frac{T}{A} (sin\theta + cos\theta \, tan\phi') \qquad 4\text{-}2$$

where, ΔS is the added strength of the soil/reinforcement composite due to the presence of the reinforcing element.

If a free body diagram of the conceptualized soil block is drawn, it becomes obvious that a shear force in the reinforcing element develops as incipient shear along the failure surface occurs. The shear vector is perpendicular to the tension vector (Figure 4-3(b)) and can also be resolved into components

parallel and perpendicular to the failure surface. This concept was developed by Jewell and Pedley (1992) and the relationship they present for the increase in strength attributed to the reinforcing element if the shear force is considered is,

$$\Delta S = \frac{T}{A} sin\theta + \frac{V}{A} cos\theta + \left(\frac{T}{A} cos\theta - \frac{V}{A} sin\theta\right) tan\phi' \qquad 4\text{-}3$$

In this expression, the terms are as previously defined and V is the shear force in the reinforcing element. If equation 4-3 is added to the Mohr-Coulomb strength equation, equation 3-1, the strength of the soil/reinforcing element matrix can be described using the resulting equation,

$$S_{comp} = \left[c' + \frac{T}{A} sin\theta + \frac{V}{A} cos\theta\right] + \left[\frac{T}{A} cos\theta - \frac{V}{A} sin\theta + \sigma_n\right] tan\phi' \qquad 4\text{-}4$$

Jewell (1980) has demonstrated that the relationship described by equations 4-1 and 4-2 predict the strength increase of sand in direct shear with different types of reinforcing elements installed at several orientations. Therefore, the model developed as a part of this project uses the relationships presented in equations 4-1 through 4-4 to predict the increased soil strength attributed to reinforcement by conifer roots. To predict these soil strength increases, it is necessary to develop analytical methods to predict the magnitude

of the tensile and shear forces developed in tree roots as they deform and stretch across failure surfaces when movement of the soil occurs.

Analytical Model Development

The purpose of the analytical model is to predict both the tensile and shear forces in the reinforcing element at the failure surface as the reinforcing element undergoes deformation due to the downslope movement of the soil block as it begins to fail as shown in Figures 4-1 and 4-2. To calculate the shear and tensile forces in the reinforcing element at the failure surface, two analytical problems must be solved. The first problem is to determine the shape of the reinforcing element that results from a given deformation of the soil block. As the two halves of the soil block move relative to each other, the reinforcing element extending across the failure surface will deform. The new shape will be a function of the size and stiffness of the reinforcing element, the depth the reinforcing element is embedded in the soil, the density and strength of the soil, and the deformation of the block of soil. The lateral force applied to the reinforcing element at the failure surface that caused the deformed shape, V_y, will also be determined as a part of the calculation of the shape of the element. The applied force and the shape of the reinforcing element will be determined using a solution technique for laterally loaded piles. The changing shape of the

reinforcing element will cause it to stretch and thus cause the tension in the reinforcing element to increase.

The second problem is to determine the applied tensile force needed to stretch the reinforcing element the amount determined by the lateral solution. The tensile force applied to the reinforcing element will be calculated using a solution technique for axially loaded piles.

Thus, the root reinforcement model resolves the problem into a lateral solution and an axial solution and the principle of superposition is used for the final solution. The applied lateral force and shape of the reinforcing element are generated using a laterally loaded pile solution, then the resulting shape of the reinforcing element is feed into an axially loaded pile solution and the tensile force applied to the reinforcing element is generated. The shape of the reinforcing element, shear force, and tensile force are then superimposed for the final solution.

Lateral Solution

The problem of determining the shape of a reinforcing element as it deforms across a failure surface in a soil is difficult and its solution involves a complex soil-structure interaction. Not only must the effects of externally applied forces on the reinforcing element be accounted for, but also the subsequent deflection of the reinforcing element into the soil and the resulting pressure on

the reinforcing element from the soil must also be accounted for. This problem is part of a class of problems dealing with beam-columns on flexible foundations and theoretical solutions to this class of problems are presented in Hetenyi (1946). The derivation of the governing differential equation for a flexible beam on an elastic foundation, which is the theoretical basis for this problem, is reproduced in Appendix A. Furthermore, as discussed in the Literature Review chapter, Wu, et. al. (1988a, 1988b) used a laterally loaded pile solution to evaluate the contribution of the tensile force in roots to the shearing resistance of reinforced soils both in laboratory tests and *in-situ* shear tests and the results were reported to be generally satisfactory.

Therefore, the solution technique for laterally loaded piles was chosen for use in the lateral portion of this analytical model. The governing differential equation for the laterally loaded pile solution, which is derived in Appendix A, is:

$$EI\frac{d^4y}{dx^4} - T\frac{d^2y}{dx^2} + E_s(y) = 0 \qquad A\text{-}17$$

In this equation, the parameters describing the reinforcing element are; E the modulus of elasticity, I the moment of inertia, T the tensile force in the reinforcing element, and y the lateral deflection of the reinforcing element at any distance x along its length. The parameter describing the soil is E_s, the secant modulus of the soil's response to the lateral defection, y.

In the analytical model that has been developed, the solution of equation *A-17*, the governing differential equation for the behavior of laterally loaded piles, is estimated using a finite-difference approximation method. The reasons for choosing this solution method are twofold. First of all, the shape of the deflected reinforcing element is needed to calculate the tension in and geometry of the reinforcing element at the failure surface so that the forces in the reinforcing element can be appropriately resolved. The second reason for choosing the finite-difference approximation method is that it is an intuitive method, computationally straightforward, has a solid base in the technical literature.

The finite-difference approximation of the governing differential equation yields the deformed shape of the reinforcing element. Wu, et. al. (1988a, 1988b) solved the laterally loaded pile differential equation in closed form by integrating the equation four times and using boundary conditions to solve for the constants of integration. In this manner, tensile forces were calculated for roots which were already deformed and the shape was known. The closed form solution allows for the determination of the forces once the shape is known but does not allow for determination of the shape given the forces.

Both Waldron (1977) and Wu, et. al. (1979) separately developed an approach to the solution of the root reinforcement problem in which the tension and geometry of the reinforcing element could be determined if the deformation of the soil and the shear zone width were known. However, as Shewbridge and

Sitar (1989; 1990) point out, a method to predict shear zone width doesn't exist and, additionally, their research along with that of Abe and Ziemer (1991) points out how difficult the development of such a method might be. Thus, the existing, known technology to predict the shape of a laterally loaded pile is a finite-difference approximation of the governing differential equation.

A finite-difference solution has been developed for the design of laterally loaded piles (Gleser, 1953; Reese, et. al., 1974; Reese, 1977), and the method is recommended by design manuals for laterally loaded piles (Reese, 1984; 1986). The development of the technology and the method is well documented in the literature and the method has a proven track record as a robust method for solving the type of problem being considered.

To solve the governing differential equation for the shape of a particular reinforcing element, it must first be discretized into n elements, each of a length h, represented by nodes. Then a finite-difference equation must be written for each node. A general finite-difference equation is written for the interior nodes, and the finite-difference form of four boundary conditions is combined with the general finite-difference equation to yield equations for the four boundary nodes, two at each end of the reinforcing element. The nodes are numbered sequentially from *1* at the failure surface to n at the end of the reinforcing element away from the failure surface. The discrete element at the failure surface is the first element and is represented by the first node. The lateral deformation of that node carries the label and subscript, y_1. The last discrete element at the end of the reinforcing

element away from the failure surface is represented by the n^{th} node and the lateral deformation of that node carries the label and subscript, y_n.

There are four boundary conditions for this problem. These boundary conditions are:

1. The end of the reinforcing element away for the failure surface will support no moment, therefore $M_n=0$.
2. Also, the end of the reinforcing element away from the failure surface will support no shear, therefore $V_n=0$.
3. The reinforcing element at the failure surface is at an inflection point and, by definition, there is no moment in the reinforcing element at that point, $M_1=0$.
4. The reinforcing element at the failure surface will support a shear force and that force is a fixed and unknown quantity, V_1.

Five finite-difference equations have been derived to describe the five different kinds of nodes requiring equations. The derivation of these five equations is presented in Appendix B. The five finite-difference equations are reproduced below.

The finite-difference equation for the first node at the failure surface is,

$$y_1\left(\frac{2EI}{h^4}+\frac{2T_1}{h^2}+E_{s_1}\right)+y_2\left(\frac{-4EI}{h^4}-\frac{2T_1}{h^2}\right)+y_3\left(\frac{2EI}{h^4}\right)=\frac{2V_1}{h} \qquad \text{B-17}$$

And, the finite-difference equation for the node at the end of the reinforcing element away from the failure surface is,

$$y_n\left(\frac{2EI}{h^4}+\frac{2T_n}{h^2}+E_{s_n}\right)+y_{n-1}\left(\frac{-4EI}{h^4}-\frac{2T_n}{h^2}\right)+y_{n-2}\left(\frac{2EI}{h^4}\right)=0 \qquad B\text{-}11$$

These finite-difference equations which are written for the nodes in the reinforcing element are a system of n simultaneous equations with n unknowns. The solution of this system of equations is very straightforward with any of a number of equation solvers available (Maron, 1987; Press, et. al., 1992). To solve the system of linear equations requires that first the system of equations be expressed in the appropriate matrix format,

$$\mathbf{[A]\,[x] = [b]}$$

where **[A]** is the coefficients matrix, **[b]** is the matrix of constants, and **[x]** is the matrix of unknowns. The coefficients matrix, **[A]**, is an $n \times n$ matrix while both the matrix of constants, **[b]**, and the matrix of unknowns, **[x]**, are $n \times 1$ matrices.

The deformed shape of the reinforcing element and the applied lateral force at the failure surface are the desired products of the solution. However, the equation for first node, equation *B-17*, has both the applied lateral force and the lateral deflection of the first node in it. One of these unknowns must be provided to drive a solution. In the root reinforcement model, the added strength of the system for a given deformation is the desired end result, so the deflection of the

The finite-difference equation for the second node, one node from the failure surface is,

$$y_1\left(\frac{2EI}{h^4}-\frac{2T_2}{h^2}\right)+y_2\left(\frac{5EI}{h^4}+\frac{2T_2}{h^2}+E_{s_2}\right)+y_3\left(\frac{-4EI}{h^4}-\frac{2T_2}{h^2}\right)+y_4\left(\frac{EI}{h^4}\right)=0 \qquad B\text{-}18$$

The finite-difference equation for the interior nodes is,

$$y_{m+2}\left(\frac{EI}{h^4}\right)+y_{m+1}\left(\frac{-4EI}{h_4}-\frac{T_m}{h^2}\right)+y_m\left(\frac{6EI}{h^4}-\frac{2T_m}{h^2}+E_{s_m}\right)+$$

$$y_{m-1}\left(\frac{-4EI}{h_4}-\frac{T_m}{h^2}\right)+y_{m-2}\left(\frac{EI}{h^4}\right)=0 \qquad B\text{-}5$$

The finite-difference equation for the next-to-the-end node away from the failure surface is,

$$y_n\left(\frac{-2EI}{h^4}-\frac{2T_{n-1}}{h^2}\right)+y_{n-1}\left(\frac{5EI}{h^4}+\frac{2T_{n-1}}{h^2}+E_{s_{n-1}}\right)+$$

$$y_{n-2}\left(\frac{-4EI}{h^4}-\frac{T_{n-1}}{h^2}\right)+y_{n-3}\left(\frac{EI}{h^4}\right)=0 \qquad B\text{-}12$$

first node is provided as a known and the applied lateral force on the reinforcing element at the failure surface for that deformation is one of the outputs. A system of simultaneous equations in matrix form representing a reinforcing element is shown in Figure 4-4.

The coefficients matrix is obviously a banded diagonal matrix (Figure 4-4). There are values in the matrix along the diagonal and for two entries each side of the diagonal. The remainder of the values in the matrix to the upper right and lower left of the diagonal are zero's. To reduce both the memory requirements of the matrix in a computer and the number of math operations, the coefficients matrix is stored in compact manner as an *nx5* matrix with the diagonal elements in the third column and the off diagonal elements stored appropriately with respect to the diagonal. A system of simultaneous equations with the coefficients matrix in compact form is presented in Figure 4-5.

The coefficients matrix is made up of the flexural rigidity or stiffness term, *EI*, the tension in the reinforcing element, T_i, the secant modulus of the soil response, E_{s_i}, and the length of the discrete elements, *h*. In the matrix of constants, the top three nodes are represented by non-zero entries and these values are made up of the same terms as the coefficients matrix except that they are multiplied by the lateral deflection of the reinforcing element at the failure surface, y_1. The matrix of unknowns is made up of the lateral deflections of all the nodes in the reinforcing element, y_2 to y_n, except for the first entry which is the horizontal force applied to the reinforcing element at the failure surface. The.

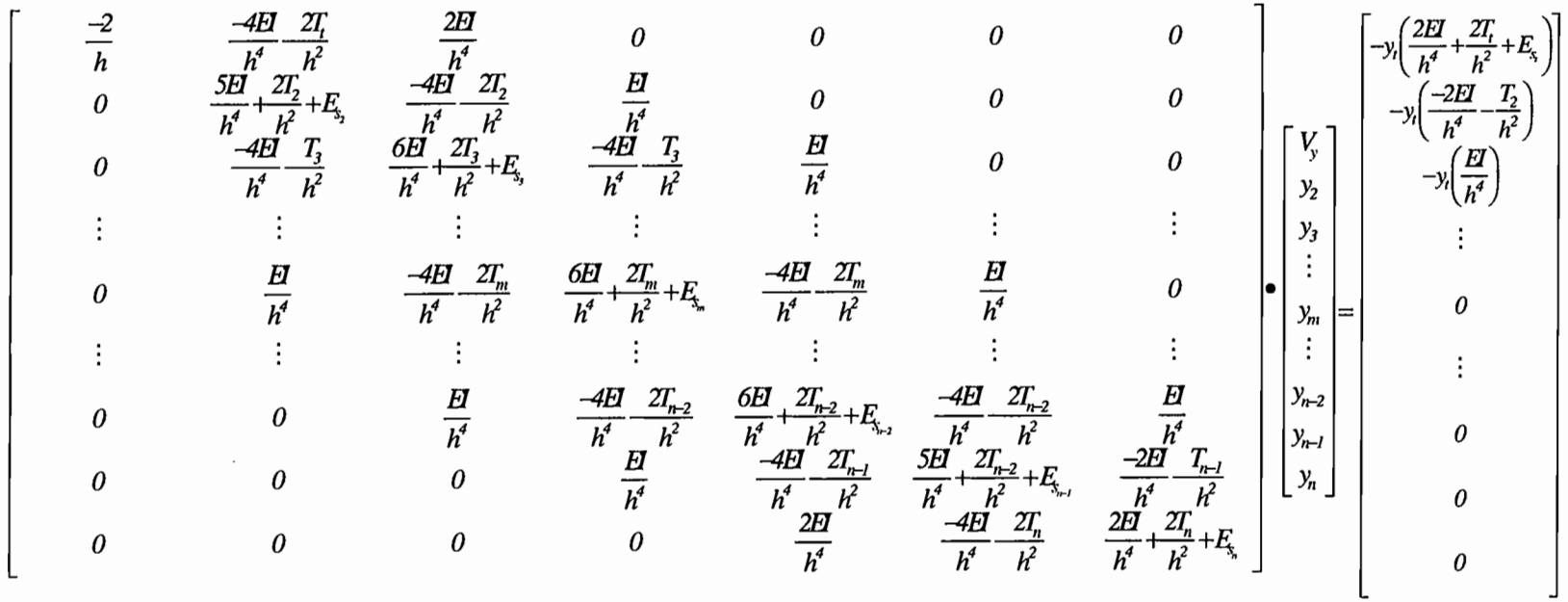

Figure 4-4. A system of simultaneous linear equations representing a reinforcing element in the root reinforcement model shown in matrix notation. The equations are of the form [A] [x] = [b], where [A] is the matrix of coefficients, [b] is the matrix of constants, and [x] is the matrix of unknowns.

$$
\begin{bmatrix}
0 & 0 & \frac{-2}{h} & \frac{-4EI}{h^4}-\frac{T_1}{h^2} & \frac{EI}{h^4} \\
0 & 0 & \frac{5EI}{h^4}+\frac{2T_2}{h^2}+E_{s_2} & \frac{-4EI}{h^4}-\frac{T_2}{h^2} & \frac{EI}{h^4} \\
0 & \frac{-4EI}{h^4}-\frac{T_3}{h^2} & \frac{6EI}{h^4}+\frac{2T_3}{h^2}+E_{s_3} & \frac{-4EI}{h^4}-\frac{T_3}{h^2} & \frac{EI}{h^4} \\
\vdots & \vdots & \vdots & \vdots & \vdots \\
\frac{EI}{h^4} & \frac{-4EI}{h^4}-\frac{T_m}{h^2} & \frac{6EI}{h^4}+\frac{2T_m}{h^2}+E_{s_m} & \frac{-4EI}{h^4}-\frac{T_m}{h^2} & \frac{EI}{h^4} \\
\vdots & \vdots & \vdots & \vdots & \vdots \\
\frac{EI}{h^4} & \frac{-4EI}{h^4}-\frac{T_{n-2}}{h^2} & \frac{6EI}{h^4}+\frac{2T_{n-2}}{h^2}+E_{s_{n-2}} & \frac{-4EI}{h^4}-\frac{T_{n-2}}{h^2} & \frac{EI}{h^4} \\
\frac{EI}{h^4} & \frac{-4EI}{h^4}-\frac{T_{n-1}}{h^2} & \frac{5EI}{h^4}+\frac{2T_{n-1}}{h^2}+E_{s_{n-1}} & \frac{-2EI}{h^4}-\frac{T_{n-1}}{h^2} & 0 \\
\frac{EI}{h^4} & \frac{-4EI}{h^4}-\frac{T_n}{h^2} & \frac{2EI}{h^4}+\frac{2T_n}{h^2}+E_{s_n} & 0 & 0
\end{bmatrix}
\bullet
\begin{bmatrix}
V_y \\ y_2 \\ y_3 \\ \vdots \\ y_m \\ \vdots \\ y_{n-2} \\ y_{n-1} \\ y_n
\end{bmatrix}
=
\begin{bmatrix}
-y_t\left(\frac{2EI}{h^4}+\frac{2T_1}{h^2}+E_{s_1}\right) \\
-y_t\left(\frac{-2EI}{h^4}-\frac{T_2}{h^2}\right) \\
-y_t\left(\frac{EI}{h^4}\right) \\
\vdots \\
0 \\
\vdots \\
0 \\
0 \\
0
\end{bmatrix}
$$

Figure 4-5. A system of simultaneous linear equations representing a reinforcing element in the root reinforcement model shown in matrix notation. The equations are of the form [A] [x] = [b] where [A] is the matrix of coefficients, [b] is the matrix of constants, and [x] is the matrix of unknowns. In this notation the matrix of coefficients, [A], is displayed in compact form.

horizontal force applied at the top of the reinforcing element in the solution vector, V_y, is the force required to deflect the reinforcing element the amount input in the constants matrix, y_1.

All of the reinforcing elements modeled during this project were assigned a round cross section (i.e. conifer roots or round wooden dowels, etc.). Thus, the centroidal moment of inertia, $I = \pi b^4/64$ was used in the coefficients and constants matrix when the moment of inertia was needed. In that equation, b is the diameter of the reinforcing element. The balance of the terms in the coefficients and constants matrix will be discussed and defined in the subsequent section.

Modulus of Elasticity, E, for Conifer Roots

One of the parameters included in both the coefficients and constants matrix is the modulus of elasticity of the reinforcing element. This value must be known if the reinforcing element is to be treated as a beam-column and its behavior both in tension and bending predicted. Of primary interest is the behavior of woody roots in shallow, loose, sandy soils, therefore, the modulus of elasticity value of most interest is for woody roots. The root reinforcement model is developed so any value of modulus of elasticity can be used, in fact, reinforcing elements of several different materials were modeled, but the primary focus remains on woody roots. The modulus of elasticity values used to

model root reinforcement in shallow forest soils were obtained from the technical literature, no tests were undertaken as a part of this project.

The literature available on modulus of elasticity values for woody roots reports on conifer roots. Three sources are reviewed in which conifer roots were tested in a standard manner in tension in a laboratory and modulus of elasticity values were determined. The results of the tests are reported in three different types of units, so all units were converted to English units for the purpose of comparison.

Waldron and Dakessian (1981) determined the modulus of elasticity of the roots of 52-month old ponderosa pine seedlings. Pine roots from 0.01 to 0.24 inches (0.25 to 6 mm) in diameter were tested and the results were presented in the form of an exponential equation. The modulus of elasticity ranged from 35,600 psi (2.5×10^6 g/cm^2) for the 0.01 inch roots to 10,200 psi (7.2×10^5 g/cm^2) for the 0.24 inch roots. No measures of variance were presented.

O'Loughlin (1972; 1974) tested both western red cedar and Douglas fir roots. They ranged from 0.04 to 0.47 inches (1 to 12 mm) in diameter and were taken from mature, living trees. For Douglas fir, the average modulus of elasticity was 124,000 psi (8,740 kg/cm^2) with a standard deviation of 85,300 psi (6,020 kg/cm^2). The western red cedar roots had an average modulus of elasticity of 137,000 psi (9600 kg/cm^2) with a standard deviation of 107,000 psi (7600 kg/cm^2).

Commandeur and Pyles (1991) also tested Douglas fir roots from young growth, living trees. The roots ranged from 0.1 to 0.79 inches (0.25 to 2 cm) in diameter. The authors reported both a form modulus, when the root was straightening out, and a material modulus when the root was strained elastically. For all roots tested, the average form modulus was 26,900 psi (185 MPa) with a standard error of 6,800 psi (47 MPa) and the material modulus was 73,000 psi (503 MPa) with a standard error of 16,000 psi (112 MPa).

The reported values of modulus of elasticity for conifer roots range from a low of approximately 10,000 psi to a high of approximately 137,000 psi. These reported values are all within an order of magnitude of each other, so for modeling purposes in this project, the material modulus from the work of Commandeur and Pyles (1991) of 73,000 psi was used as the modulus of elasticity for conifer roots.

The Secant Modulus of the Soil Reaction, Es

A parameter needed for both the coefficients and constants matrix is the soil reaction to the lateral deflection of the reinforcing element. In the derivation of the governing differential equation for this problem, the soil reaction, p, is represented in the balance of forces as a distributed force and expressed as a force per unit length of the reinforcing element. The form of the governing

differential equation using p for the soil reaction is reproduced below and derived as equation *A-16* of Appendix A.

$$EI\frac{d^4y}{dx^4} - T\frac{d^2y}{dx^2} + p = 0 \qquad A\text{-}16$$

Traditionally, the convention used to determine the soil reaction in this type of problem has been based on the Winkler spring concept. In this situation, the spring constant is called the coefficient of horizontal subgrade reaction, k_h, and it is a proportionality constant between the soil reaction, p, and the lateral deflection, y, of the reinforcing element for a given soil and reinforcing element.

$$p = k_h y \qquad 4\text{-}6$$

The soil reaction is not a linear function of lateral deflection and it is not possible to represent the coefficient of horizontal subgrade reaction as a constant over the range of deflections considered within the scope of this project. Instead, the relationship between the lateral deflection of a reinforcing element into a soil and the soil reaction is characterized by a p-y curve. An example of a typical p-y curve for a shallow, cohesionless sand is shown in Figure 4-6. In this figure, the lateral deflection of the reinforcing element is y and the soil reaction is p. The secant modulus of the soil reaction, E_s, is the ratio of the soil reaction to the lateral deflection.

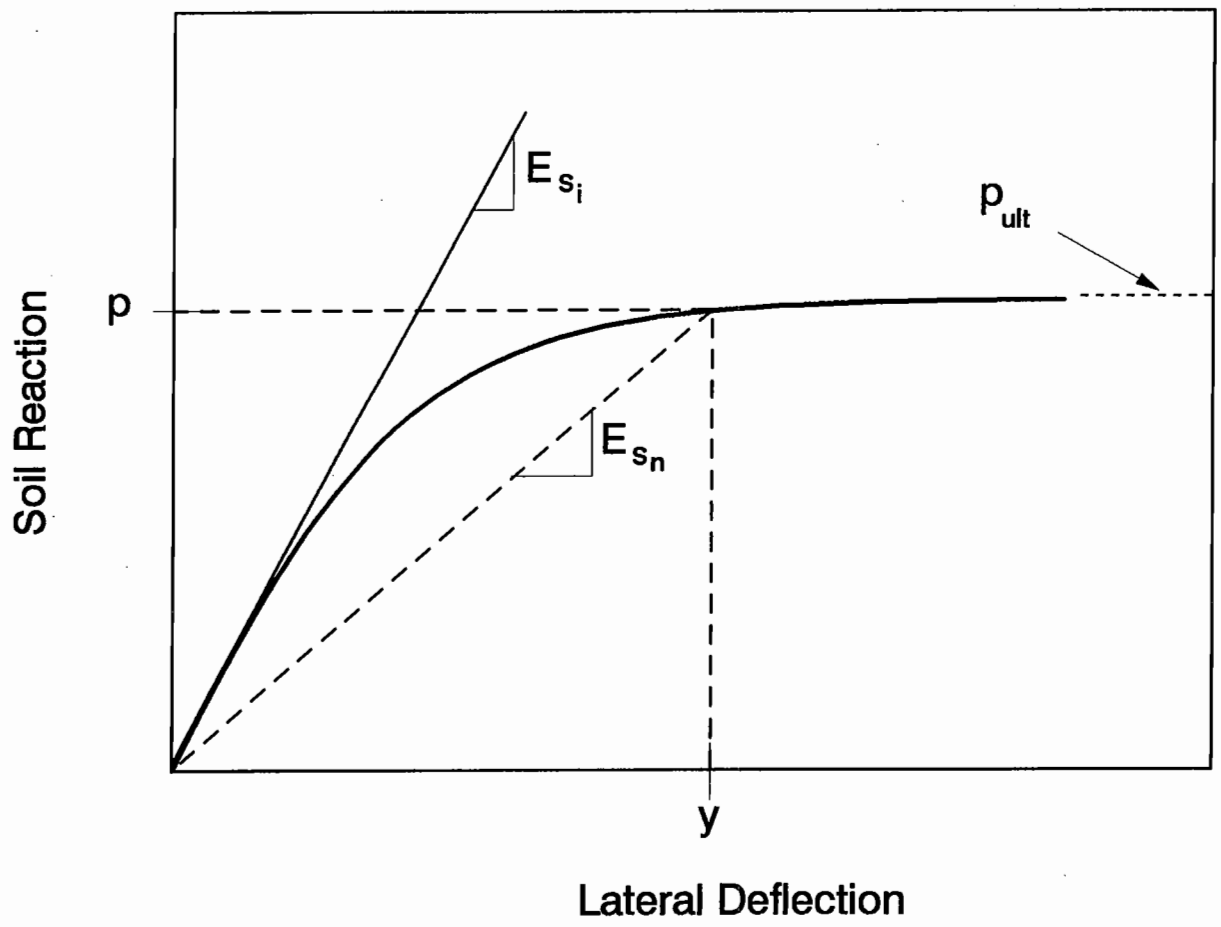

Figure 4-6. Diagram of a typical *p-y* curve for a loose, cohesionless, sand showing the initial tangent modulus, E_{s_i}, the ultimate soil resistance, p_{ult}, and the secant modulus of the soil response, E_{s_n}.

$$E_s = \frac{p}{y} \qquad 4\text{-}7$$

Figure 4-6 illustrates the concept of the secant modulus and shows that the secant modulus of the soil reaction, E_s, is larger at small deflections with the initial tangent modulus, E_{s_i}, being an upper limit. The secant modulus gets progressively smaller as the lateral deflection of the reinforcing element increases.

The final form of the governing differential equation as derived in Appendix A, can be determined by solving equation *4-7* for p and substituting that expression back into equation *A-16*.

$$p = E_s(y) \qquad 4\text{-}8$$

$$EI\frac{d^4y}{dx^4} - T\frac{d^2y}{dx^2} + E_s(y) = 0 \qquad A\text{-}17$$

If a lateral deflection, y, is known, E_s can be determined and used to generate matrix entries for the coefficients and constants matrices, if the p-y curve for the given soil type is known. The balance of this section describes methods to develop appropriate p-y curves.

p-y Curves

A wide range of soil types and conditions have had *p-y* curves developed for them (Reese, 1984; 1986). The soil types include soft clays, stiff clays, sands, and rock and the conditions include cyclic and static loading, above and below a water table, and shallow and deep soils. In selecting *p-y* curves to use in the root reinforcement model, the conceptual overview of the problem for which the model is being developed must be kept in mind. Specifically, the root reinforcement model was developed to predict the magnitude of root reinforcement in shallow, slide-prone, forest soils. The *p-y* curves used in the model should approximate those conditions, namely, shallow, cohesionless sands under static loading. These conditions represent a very narrow spectrum of the total body of work on *p-y* curves.

The process to generate *p-y* curves for shallow, cohesionless sands is fairly simple and straight forward especially when compared with the process required to generate *p-y* curves for other soil types and conditions. There are essentially three components to *p-y* curves for shallow, cohesionless sands; an initial tangent modulus, E_{s_i} an ultimate resistance, p_{ult}, and a transition curve between these two limiting values (Figure 4-6) (Parker and Reese, 1970). The initial tangent modulus, E_{s_i}, is the slope of the initial straight portion of the *p-y* curve at the origin when the response of the soil is considered linearly elastic.

The ultimate resistance, p_{ult}, is the limiting value of resistance for that soil type, soil depth, and reinforcing element width.

Initial Tangent Modulus, E_{s_i}

The procedure for determining an initial tangent modulus, E_{s_i}, for the *p-y* curve is really very simple (Parker and Reese, 1970). First, determine the density of the sand. The density can be determined subjectively (loose, moderate, or dense) or relative density can be used with loose being less than 35 percent relative density, moderate being 35 to 70 percent relative density, and dense being greater than 70 percent relative density. Next, determine whether the sand will be above or below a water table. With these two conditions known, the appropriate value of the constant of subgrade reaction, *k*, can be determined from Table 4-1. The initial tangent modulus of the *p-y* curve is simply the product of the constant of subgrade reaction and the depth of the soil where the *p-y* curve is desired.

$$E_{s_i} = k\,d \qquad 4\text{-}9$$

In the equation above, E_{s_i} is the initial tangent modulus in lbs/in^2, *k* is the constant of subgrade reaction in lbs/in^3, and *d* is the soil depth in inches.

Table 4-1. Recommended values of the coefficient of subgrade reaction, k (lbs/in^3), for three relative densities of cohesionless sands located either above or below a water table (Reese, 1986).

Relative Densities	Loose	Medium	Dense
Recommended k (lbs/in^3) for above water table	25	90	225
Recommended k (lbs/in^3) for below water table	20	60	125

A theoretical development for the basis of the of the initial tangent modulus values will not be presented here. Terzaghi (1955) first presented values for the constant of subgrade reaction, k, and suggested that the initial tangent modulus, or the coefficient of horizontal subgrade reaction, of sand should be a linear function of depth. Additional work by Reese and Matlock (1956) supported the contention that the initial tangent modulus of a p-y curve increased linearly with soil depth.

The values for the constant of subgrade reaction, k, presented by Terzaghi (1955) were used in a full scale load test of two laterally loaded piles in sand (Reese, et. al. 1974). When these values were used, the deflections were always over-estimated and the values of k obtained from the load tests were several times the values reported by Terzaghi. The authors subsequently recommended different values for k based on their research results. These values are listed in

Table 4-1 (Reese, 1984; 1986) and they are the values that were used in the root reinforcement model for developing *p-y* curves.

Ultimate Resistance, p_{ult}

In addition to the initial tangent modulus, E_{s_i}, the ultimate soil resistance, p_{ult}, is the second defining parameter needed to develop *p-y* curves for shallow, cohesionless sands (Figure 4-6). The ultimate soil resistance is the maximum resistance the reinforcing element will experience as it deflects laterally through the soil.

While the mechanics of laterally loaded piles is being used to describe the behavior of root reinforcement in shallow forest soils, there are fundamental differences in the way these two problems are approached. A pile extends into the soil perpendicular to the soil surface, thus the soil resistance for a laterally loaded pile must be represented by a family of *p-y* curves covering the depth of embedment of the pile. The shape of the *p-y* curves will change with depth and the magnitude of the soil resistance for a given deflection, including the ultimate resistance, will increase with depth. Unlike a pile, the hypothetical root being stretched across a failure surface is aligned parallel to the soil surface, at a constant depth, therefore the soil resistance to the lateral deflection of the root can be represented by a single *p-y* curve. In this case, a reinforcing element acts more like a horizontal, flexible conduit than a laterally loaded pile.

Values for the ultimate soil resistance were developed in the same manner as the initial tangent modulus. Expressions describing the different failure modes were derived and then theoretical values of the ultimate resistance were calculated using the derived expressions. The theoretical values were verified and adjusted based on results from both laboratory and full scale load tests.

Two failure modes, shallow and deep failures, need to be considered when expressions are derived for the ultimate resistance of laterally loaded piles. A shallow failure is characterized by a passive wedge developing in front of the pile and an active wedge developing in the back of the pile. A deep failure mechanism is characterized by soil flow around the pile. In laterally loaded pile analysis, the ultimate resistance of the soil is calculated using both failure mechanisms and the minimum value controls design. A transition depth, which is the depth at which the minimum value of ultimate resistance changes from a shallow to a deep failure mechanism, can be determined by equating the expressions for a shallow and deep failure mechanism. The cover ratio, the depth of cover divided by the pile diameter, for the transition depth is a function of the internal angle of friction of the soil and the calculated theoretical values range from approximately 11 to 25 for a range of friction angles between 25 and 40 degrees (Reese, 1984).

Using transition cover depths from laterally loaded pile design might not be appropriate for a root reinforcement problem because, as stated previously, the hypothetical situation presented for root reinforcement more closely

resembles a buried flexible conduit than a laterally loaded pile. Audibert and Nyman (1977) investigated horizontal soil restraint against buried pipes by conducting several laboratory trials using a physical model. The trials consisted of moving three different diameter model pipes through both a loose and dense, cohesionless sand at cover ratios ranging from 1 to 24. They found that at cover ratios less than three, the ultimate resistance of the horizontal soil reaction resulted from a failure mechanism which consisted of a passive wedge bounded by a logarithmic spiral in the direction of pipe movement and a narrow, vertical active wedged above and behind the pipe. As the cover ratio increased, the failure mechanism changed to soil flow around the pipe and at cover ratios of 12 to 24 only the soil flow failure mechanism was observed. For the hypothetical situation being modeled, root reinforcement in shallow forest soils, no situations with a cover ratio less than 12 were investigated. The lowest value of cover ratio modeled, 12, was a 0.5 inch diameter root at a soil depth of six inches. All other values of cover ratio modeled included either smaller diameter roots or deeper soil depths. Therefore, only the deep failure mechanism or the soil flow mechanism was used to calculate the ultimate resistance of *p-y* curves in shallow, cohesionless sand for this project.

There are two methods available for calculating the ultimate resistance of a deep, bearing capacity failure in shallow, cohesionless sands. Hansen (1961) derived an expression based on the balance of forces for a long, rigid pile rotating about a single point. The resulting expression treats the pile like a

horizontal footing and uses a bearing capacity factor, N_q, to calculate the ultimate load. The bearing capacity factor is a combination of earth pressure coefficients and is a function of the soil's internal angle of friction and the cover ratio of the pile. The ultimate soil resistance can be calculated using the relationship,

$$p_{ult} = \gamma\, b\, d\, N_q \qquad 4\text{-}10$$

where γ is the soil density in lbs/in^3, b is the reinforcing element diameter in inches, d is the depth in the soil of the reinforcing element in inches, and N_q is the bearing capacity factor. An expression for the bearing capacity factor has been derived (Hansen, 1961) and values of N_q can be determined using published tables (Hansen, 1961; Audibert and Nyman, 1977). In the tables, values of N_q are presented for values of cover ratio only up to 20. Because an expression for the bearing capacity factor has been developed and due to the fact that the bearing capacity factors become asymptotic to a constant value at cover ratios greater than 20, values of the bearing capacity factor can be estimated for cover ratios greater than 20.

Audibert and Nyman (1977) verified the use of Brinch Hansen's bearing capacity factor, N_q, to predict ultimate soil resistance in their work with a physical model on the horizontal soil restraint on buried conduits. They found that Hansen's bearing capacity factor, N_q, predicted the ultimate soil resistance very well, however they only tested it for cover ratios up to 24.

A second method for calculating the ultimate resistance of a shallow, cohesionless sand was developed by Parker and Reese (1970). They used the balance of forces on a single differential element of a pile moving through the soil as the soil flowed around it to derive an expression for the ultimate resistance. The resulting expression is quite similar to the one used by Audibert and Nyman (1977) to predict ultimate horizontal soil resistance in their laboratory trials of horizontal conduits. However, in the expression derived by Parker and Reese (1970), Hansen's bearing capacity factor, N_q, is replaced by a different expression which is also a combination of earth pressure coefficients. The expression for ultimate soil resistance derived by Parker and Reese (1970) is,

$$p_{ult} = \gamma bd\left(K_a\left(tan^8\,\beta - 1\right) + K_o\,tan\,\phi\,tan^4\,\beta\right) \qquad 4\text{-}11$$

where γ is the soil density in lbs/in^3, b is the reinforcing element diameter in inches, d is the depth in the soil of the reinforcing element in inches, K_a is the active earth pressure coefficient, K_o is the at-rest earth pressure coefficient, ϕ is the internal angle of friction for the soil, and $\beta = 45 + \phi/2$. By comparing equations *4-10* and *4-11*, it can ascertained quite easily that the bearing capacity factor, N_q, was replaced by the expression which is a function solely of the soil's friction angle.

Values of ultimate soil resistance predicted by the Parker and Reese (1970) equation were verified and adjusted using data from both laboratory trials using

small physical models (Parker and Reese, 1970) and full scale load tests (Cox, et.al., 1974; Reese, et.al., 1974) of laterally loaded piles. In the load tests, the piles were discretized and verification was carried out on an increment by increment or node by node basis. This verification process was different than the process carried out by Hansen (1961) and Audibert and Nyman (1977) for their derived expression for ultimate resistance which verified a single value for the whole pile or conduit structure. The results from the load tests showed that the theoretical values overestimated the actual ultimate soil resistance. For the case of static loading in deep (cover ratio > 5), cohesionless sand, Reese (1984; 1986) suggests that theoretical ultimate soil resistance values be multiplied by a coefficient of 0.88.

Both of the methods derived for predicting ultimate soil resistance of a deep, cohesionless sand give reasonable estimates and both have been verified in scale model laboratory load tests and the expression by Parker and Reese (1970) has been verified in a full scale load test. So both the methods work and estimates provided by both methods have been adjusted to be reasonably accurate. At cover ratios greater than 20, the expression derived by Parker and Reese (1970) yields an estimate of the ultimate soil resistance that is roughly twice the value predicted using Hansen's bearing capacity factor.

The method developed by Parker and Reese (1970)(Reese, 1984; 1986) was used to calculate ultimate soil resistance for this project, a model of root reinforcement in shallow forest soils. The reasons for this are several. The

validation of the Parker and Reese (1970) method was carried out for cover ratios greater than 24. The method was derived to solve for ultimate resistance on a node by node basis and not for the ultimate resistance of the whole structure. An increment by increment solution pathway fit well with the way the root reinforcement problem was being approached and solved. Finally, for cover ratios approaching the hundreds in magnitude, using the larger value of ultimate resistance was more proper than using the lower values.

Transition Curve

In the publications that describe how to develop *p-y* curves (Reese, 1984; 1986), the *p-y* curves for shallow, cohesionless sands do not include a transition curve. These curves are modeled as a perfectly elastic/perfectly plastic material with the elastic portion represented by the initial tangent modulus which extends from the origin until it intersects with the plastic portion of the curve which is the ultimate resistance. This type of *p-y* curve is shown in Figure 4-7 as a dotted line. In the laboratory trials where the theoretical *p-y* curves were compared with the actual measured curves (Parker and Reese, 1970) the authors felt that this type of curve adequately described the actual *p-y* curves.

However, Parker and Reese (1970) also suggest that the two straight line portions of the curve be fitted with a transition curve. They suggest a hyperbolic form to the transition curve because that fits the shape of the stress-strain

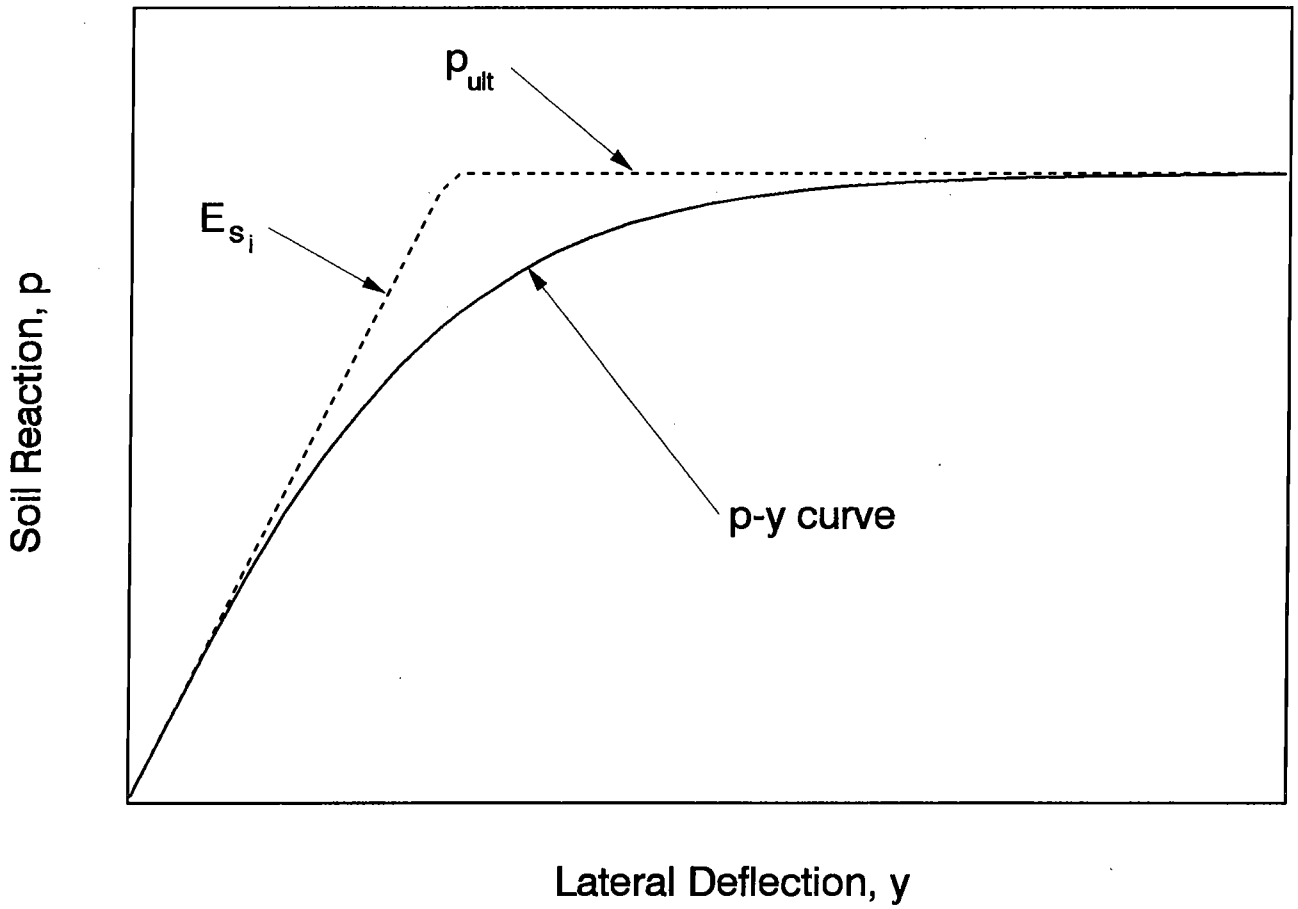

Figure 4-7. Two forms of a typical *p-y* curve for a loose, cohesionless, sand. The dotted line shows the perfectly elastic/perfectly plastic *p-y* curve defined by the initial tangent modulus and the ultimate soil resistance. The solid line shows this same *p-y* curve with a hyperbolic tangent transition curve connecting these two values.

relationship for sands. The transition curve does not affect the final values of the *p-y* curve to any great degree, thus it is recommended for purely pragmatic and cosmetic purposes. It provides a more realistic transition to the two straight line portions of the curve and, more importantly, it allows the *p-y* curve to be represented as a single continuous function in the model.

The final suggested form of the equation uses the hyperbolic tangent function and takes the form,

$$p = p_{uf}\ tanh\left(\frac{E_{s_i} y}{p_{uf}}\right) \qquad 4\text{-}12$$

where p is soil resistance in lbs/in, p_{uf} is the adjusted ultimate soil resistance and is equal to $0.88(p_{ult})$, E_{s_i} is the initial tangent modulus in lbs/in^2, and y is the lateral deflection of the reinforcing element in inches. This form of the equation yields a relationship that has a slope of E_{s_i} at $y = 0$ and becomes asymptotic to p_{uf} at large values of y. This form of the *p-y* curve was used in the analytical model for this project.

Developing *p-y* Curves

The following procedure was used to develop *p-y* curves for shallow, cohesionless sands. The *p-y* curves were used to calculate the resistance of the

shallow, cohesionless sands to the lateral deflection of reinforcing elements through the sand.

1. Determine the density, γ, and internal angle of friction, ϕ, of the soil being modeled and the depth, d, and diameter, b, of the reinforcing element.
2. Calculate the initial tangent modulus, E_{s_i}, by multiplying the depth of the reinforcing element, d, times the coefficient of subgrade reaction, k.

$$E_{s_i} = k\,d \qquad 4\text{-}9$$

The values of constant of subgrade reaction can be obtained from Table 4-1.

3. Calculate the active earth pressure coefficient, $K_a = tan^2(45-\phi/2)$, the at-rest earth pressure coefficient, $K_0 = (1-sin\,\phi)$ (Holtz and Kovacs, 1981), and $\beta = 45+\phi/2$.
4. Calculate the theoretical value of ultimate soil resistance, p_{ult}, using the equation,

$$p_{ult} = \gamma b d\left(K_a\left(tan^8\,\beta - 1\right) + K_o\,tan\,\phi\,tan^4\,\beta\right) \qquad 4\text{-}11$$

5. Calculate the final adjusted value of the ultimate soil resistance, p_{uf}

$$p_{uf} = 0.88\left(p_{ult}\right) \qquad 4\text{-}13$$

6. The soil resistance, p, for any lateral deflection, y, of the reinforcing element can be predicted using the relationship,

$$p = p_{uf} \tanh\left(\frac{E_{s_i} y}{p_{uf}}\right) \qquad 4\text{-}12$$

Figure 4-8 shows three p-y curves calculated using soil and reinforcing element parameters consistent with the concept of shallow soils on steep, landslide-prone hillslopes. These same soil and reinforcing element parameters were used to model some of the soils during the parameter study part of this project. For these three p-y curves the soil parameters were $\gamma = 90$ lbs/ft^3 and $\phi = 44°$. The width of the reinforcing element was, b = 0.5 inches. The p-y curves were calculated and graphed for three different soil depths, d = 6, 12, and 18 inches.

Once the shape, or the equation, for the p-y curves is known, the appropriate value of secant modulus of the soil resistance can be calculated simply by using the definition,

$$E_s(n) = \frac{p}{y(n)} \qquad 4\text{-}14$$

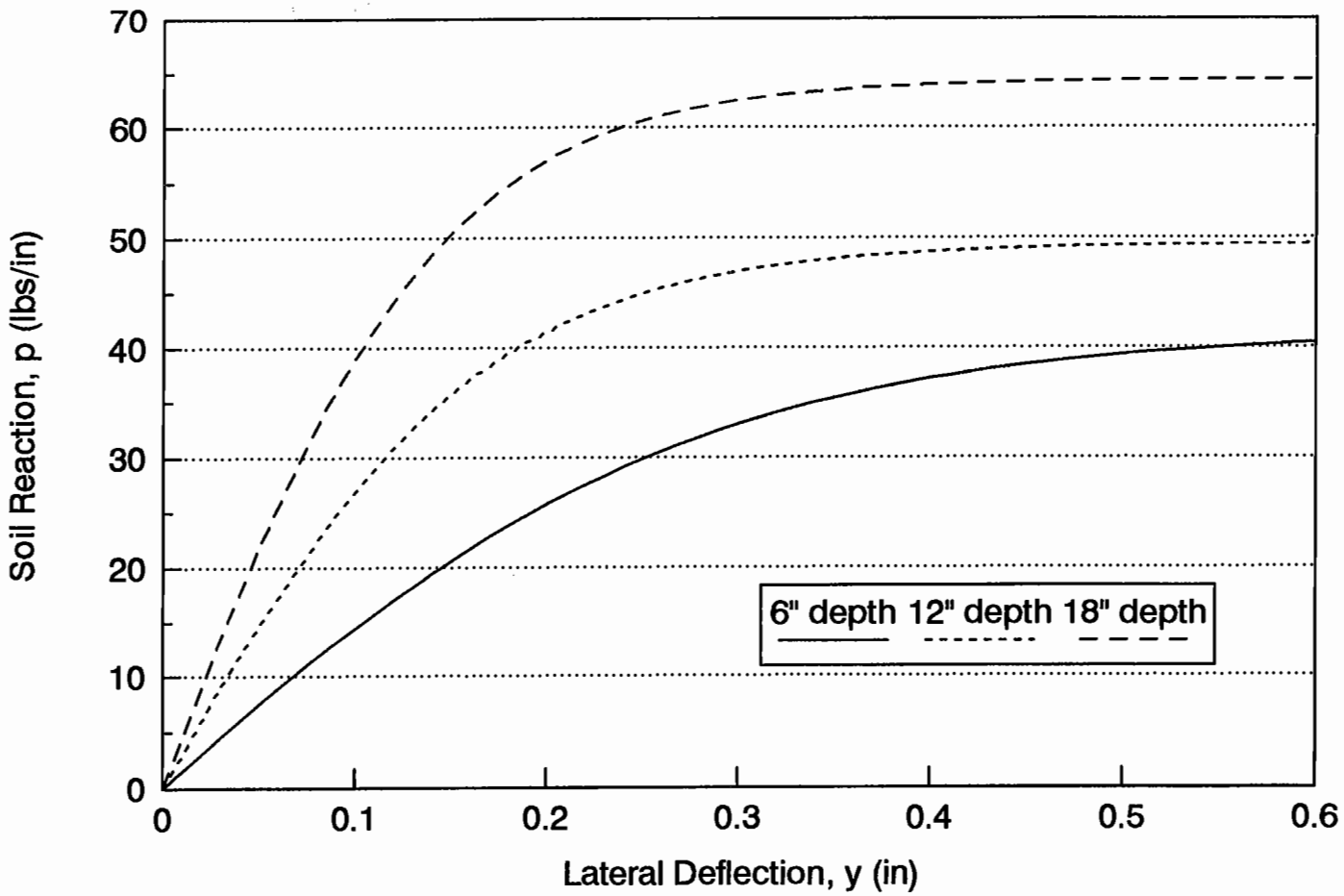

Figure 4-8. A graph showing three typical *p-y* curves used in the root reinforcement model to calculate soil resistance to lateral movement of a reinforcing element. The three curves represent soil depths of 6, 12 and 18 inches in a loose, cohesionless sand.

By substituting the expression for p in equation 4-13 into equation 4-14, the value of the secant modulus of the soil resistance is calculated using the following expression,

$$E_s(y_i) = \frac{p_{uf}\ tanh\left(\frac{E_{s_i} y_i}{p_{uf}}\right)}{y_i} \qquad 4\text{-}15$$

In this method, the secant modulus of the soil resistance, $E_s(y_i)$, is a unique value which corresponds with the lateral deflection of the reinforcing element, y_i. In this manner, a secant modulus of the soil resistance can be calculated for every discrete node in the reinforcing element for which a lateral deflection has been calculated.

Axial Solution

In modeling the magnitude of root reinforcement in shallow forest soils, one of the outputs from the model that is needed is the tensile force applied by the root, perpendicular to the failure surface, as a result of the lateral deflection. In addition to being an output of the model, the applied axial force in the reinforcing element at each node is also needed as an input to both the coefficients and constants matrices during successive iterations of the model (Figures 4-4 and 4-5).

The tension in the reinforcing element is a logical consequence of its deflected shape. The tension results from the deformation of the reinforcing element and the assumption that the end of the reinforcing element away from the failure surface does not move. If the end of the reinforcing element away from the failure surface does not move and its shape changes, then the reinforcing element must get longer. This increase in length must be accompanied by an increase in the tensile force applied to the reinforcing element at the failure surface.

The deflected reinforcing element is also in static equilibrium, thus the tensile force applied at the failure surface by the reinforcing element must be offset by an equal and opposite force. In this case, that equal and opposite applied force is the shear-stress transfer at the interface of the reinforcing element and the soil. Given the assumption that there is no movement of, and thus no applied force at, the end of the reinforcing element away from the failure surface, then the shear-stress transfer must diminish completely before the end of the reinforcing element. By reducing the shear-stress transfer along the length of the reinforcing element, the tension in the reinforcing element must diminish throughout the length of the reinforcing element. The reduction in tension along the length of the reinforcing element needs to be calculated and accounted for because it affects the lateral solution, especially at large lateral deflections.

To determine the tension in the deflected reinforcing element, the first step is to determine its length. The length of the deflected reinforcing element is

simply the sum of the lengths between successive nodes. The length between nodes is approximated as the Pythagorean distance between successive sets of node coordinates.

Each node in the reinforcing element has a unique location identified by x, y-coordinates. The x-coordinate is the node number, i, times the node length, h. This value is set at the start of the model and is maintained as a constant throughout the model. The y-coordinate is the lateral deflection of the i^{th} node. This value is set at zero when the model is initiated and is updated after every iteration of the model when a new lateral deflection is calculated. The length, l, of the deflected reinforcing element, which is the sum of the Pythagorean distances between successive nodes, is calculated using the following formula,

$$l = \sum_{i=1}^{n} \sqrt{\left(x_{i+1} - x_i\right)^2 + \left(y_{i+1} - y_i\right)^2} \qquad 4\text{-}16$$

where, n is the number of nodes, and x_i and y_i are the x-, and y-coordinates of the i^{th} node.

The change in length, z, of the deflected reinforcing element is the difference in the length of the deflected shape, l, and the original length, l_o. The original length of the reinforcing element is simply the number of nodes, n, times the node length, h.

$$z = l - l_0 = l - nh \qquad 4\text{-}17$$

Once the change in length, z, of the reinforcing element has been calculated, the tensile force necessary to cause this change in length must be calculated. This is accomplished using a technique based on a method by Coyle and Reese (1966) used to determine the load transferred from an axially loaded pile to the surrounding soil.

Two relationships are used to calculate the tensile force in the reinforcing element which occurs as a result of the deflected shape. The first relationship calculates the change in length of a discrete element of the reinforcing element given the applied tensile force in the reinforcing element. It is a basic relationship from the mechanics of materials and for use in this problem takes the form,

$$\Delta h_i = \frac{T_i h}{EA} \qquad 4\text{-}18$$

where, Δh_i is the change in length of the i^{th} node, T_i is the tensile force in the reinforcing element at the i^{th} node, h is the node length, and E and A are the modulus of elasticity and cross-sectional area of the reinforcing element, respectively. Note that h, E, and A are constants throughout the length of the reinforcing element.

For the second relationship, recall from the derivation of the laterally loaded pile problem in Appendix A, that the change in tension across a discrete element is equal to the shear-stress transfer associated with the amount of movement of the reinforcing element at that node through the soil. A governing

assumption at this point is that the amount of movement of the reinforcing element through the soil at that node is equal to the change in length of the reinforcing element at that node. The shear-stress transfer associated with the movement of the reinforcing element through the soil at a given node is calculated using the relationship,

$$F_{s_i} = \Delta T_i = \psi_i \pi b h \qquad 4\text{-}19$$

where, F_{s_i} and T_i are the shear force generated by the movement of the i^{th} node of the reinforcing element through the soil, ψ_i is a shear-stress transfer function, b is the reinforcing element diameter, and h the node length. Again, note that b and h are constants throughout the length of the reinforcing element. The shear-stress transfer functions calculate shear-stress as a function of axial displacement of the reinforcing element at a given node, soil density, and confining stress. The shear-stress transfer functions take the form,

$$\tau_i = \frac{z_i}{a_o + a_1(z_i) + a_2(z_i)^2} \qquad 4\text{-}20$$

where, τ_i is the shear-stress at node i, z_i is the axial deformation of the i^{th} node, and a_0, a_1, and a_3 are empirically derived coefficients. The shear-stress transfer

functions were derived by Commandeur (1989) and will be presented in greater detail in a subsequent section.

The solution of the axial problem requires that both the increased length of the reinforcing element and an estimate of the applied tensile force required to cause that increased length be known. The solution technique proceeds by taking an estimate of the applied tensile force, calculate an increased length associated with the estimated applied tensile force, and then compare that value with the increased length calculated from the lateral solution. If the two values do not agree, then a new value of the applied tensile force is estimated and an increased length is calculated and this process continues until the two values of increased length match.

The solution technique proceeds by first taking the calculated increase in length of the reinforcing element, z, and assume that it represents the distance the first node moves through the sand. This value, z, is used in equation 4-20 to calculate the shear force which is due to the shear-stress transfer associated with the movement of the first node through the soil. This calculated shear force is equal to the change in tensile force across the element.

$$\Delta T_1 = \left(\frac{z_1}{a_o + a_1 z_1 + a_2 (z_1)^2} \right) \pi b h \qquad 4\text{-}21$$

The tensile force in the first node is used to calculate the elongation of the first node by substituting the appropriate values into equation 4-18.

$$\Delta h_1 = \frac{\Delta T_1 h}{EA} \qquad 4\text{-}22$$

The change in tensile force across the first element is subtracted from the estimate of axial force applied at the first element and the difference is the estimated axial force applied at the second element. Similarly, the change in length associated with the first element is subtracted from the change in length of the reinforcing element and the difference becomes the change in length of the reinforcing element at the second node. This, in turn, becomes the axial deformation of the reinforcing element at the second node.

$$T_2 = T_1 - \Delta T_1 \qquad 4\text{-}23$$

$$z_2 = z_1 - \Delta h_1 \qquad 4\text{-}24$$

These values are then used to calculate the shear-stress and, thus, the change in tension across the second element and the corresponding change in length of the second element. These values, in turn, are subtracted from the applied axial force at the second element and the change in length of the

reinforcing element at the second element to get the applied force at the third element and the change in length and, thus, the axial deformation of the reinforcing element at the third node. This process continues down the reinforcing element until either the applied tensile force or the increase in length of the reinforcing element equals zero.

The solution to the axial portion of the problem is achieved when both the increased length of the reinforcing element and the estimated applied tensile force reach zero simultaneously. This never occurs on the initial estimate, therefore the process is iterative with successive estimates of the applied tensile force until the solution is achieved. If the estimate of the applied axial force causes the increased length of the reinforcing element to reach zero before the axial force, the estimate of axial force was too large and a smaller estimate is needed. Conversely, if the estimate of the applied axial force reaches zero before the increase in reinforcement element length, then the estimate was too small and a larger estimate of applied axial force is needed.

The estimate of the increased length of the reinforcing element comes from the lateral solution. The initial estimate of the applied tensile force was always one pound. Given the size roots being modeled, this initial estimate worked very well. The estimate of applied force was always low so it adjusted upward in increments of one pound until the transition between too little and too much applied tensile force was achieved. At this point, the applied tensile force was incremented by 0.5 pounds and once this addition had been made,

increments of 0.1 pounds were subsequently added or subtracted until the transition between too much and too little applied tensile force was reached. This process continued with each iteration adding a significant digit of precision.

Given the precision of contemporary personal computers, the estimated applied axial force and the increased length of the reinforcing element will never equal zero at the same time. The process simply continues with the estimate of the applied tensile force becoming more and more precise until the computer runs out of significant digits. For this reason, an arbitrary closure had to be defined. That arbitrary point was when the applied tensile force and the increased length of reinforcing element equaled zero at the same time and the precision of the estimate of applied tensile force was seven significant digits. The other portions of the solution which depended on the estimate of applied tensile force, namely the calculated lateral deflection, were not affected within single precision accuracy by an estimate of applied tensile force with a precision of seven significant digits.

In addition to the final estimate of the applied tensile force, which is a solution of the model and an output, the applied tensile force at each node is calculated and stored. These values are inputs to both the coefficients and constants matrices in subsequent iterations of the lateral solution.

Shear-Stress Transfer Functions

In the previous section, the process to calculate the applied tensile force in the reinforcing element at the failure surface was described. A crucial step in the process, the shear-stress transfer functions, was mentioned but was not discussed in detail. Shear-stress transfer is the process of transmitting tensile force in the reinforcing element to the surrounding soil through friction between the soil and the reinforcing element. In the conceptual model, as one soil block attempts to pull the reinforcing element from the soil through increased applied force at the failure surface, the attempt is resisted by the shear-stress transfer between the reinforcing element and the soil. To determine a solution to the model and estimate the applied tensile force at the failure surface, shear-stress transfer functions must be known.

The concept and quantification of shear-stress transfer is encountered regularly in civil engineering practice with reinforced earth and soil nailed structures. However, shear-stress transfer in these applications is quantified only at ultimate strength levels. This ultimate strength can be either the ultimate rupture strength of the reinforcing element or the ultimate pullout resistance. The ultimate pullout resistance is designed to be greater than a design load on the reinforcing element or the ultimate tensile strength of the reinforcing element. The calculation of ultimate pullout resistance is similar for both soil

nails and for metal reinforcing strips. To calculate the frictional component of the pullout resistance, the following equation is used,

$$P_f = \mu^* \sigma_n A_s \qquad 4\text{-}25$$

where P_f is the ultimate pullout capacity due to friction, μ^* is an apparent friction coefficient between the soil and reinforcing element, σ_n is a normal stress which can be the vertical overburden pressure or can include an at-rest horizontal earth pressure component, and A_s is the surface area of the reinforcing element which includes its length. In this process, the critical piece of information is the apparent coefficient of friction, μ^*. The value of this parameter is determined during pullout tests in which a reinforcing element of known characteristics is embedded in a soil of known characteristics and a tensile load is applied to the end of the reinforcing element until it pulls out. All the known parameters are entered in the above equation and an apparent friction coefficient is solved for. The technical literature is replete with the results of pullout tests for reinforcing materials used in reinforced earth structures (Schlosser and Elias, 1978)

It is important to remember that this is an ultimate strength value. The assumption is made that something approaching ultimate axial deformation has been reached in the reinforcing element which has resulted in the ultimate shear-stress transfer being mobilized between the reinforcing element and the soil

throughout most of the length of the reinforcing element. These assumptions may be valid in manufactured, high density, high strength soils reinforced with high modulus, steel reinforcing elements. The assumptions have less validity when dealing with loose, shallow, cohesionless soils reinforced with low modulus conifer roots.

Due to the concern that ultimate displacements in shallow forest soils may not be sufficient to mobilize ultimate shear-stress transfers in conifer roots, there is interest in shear-stress transfer at smaller displacements than ultimate. Shear-stress transfer functions which relate shear-stress transfer throughout a range of displacements not just at the ultimate displacement are of interest. What is of most interest is information on shear-stress transfer functions for shallow, cohesionless sands reinforced with low modulus reinforcing elements (i.e. conifer roots). For this information, the work of Commandeur (1989) was used.

Commandeur (1989) conducted pullout tests using Douglas-fir roots buried in a clean, uniform, cohesionless silica sand. He conducted 58 pullout tests on 24 Douglas-fir roots with diameters ranging from 0.18 to 0.50 inches. The soil used during the pullout tests had an average density of 90.3 lbs/ft^3 (14.22 kN/m^3) and a relative density of 63.3 percent which corresponded to a void ratio of 0.83. The pullout tests were conducted at confining stresses of 0.31, 0.45, and 0.63 lbs/in^2 (2.1, 3.1, and 4.3 kPa) corresponding to soil depths of 6, 9, and 12 inches.

For each of the 54 pullout tests, load and displacement data were collected and a graph of shear-stress transfer versus displacement was prepared. The data was fitted to a three parameter, hyperbolic, shear-stress transfer versus displacement function of the form,

$$\tau = \frac{z}{a_o + a_1 z + a_2 z^2} \qquad 4\text{-}26$$

where, τ is the shear-stress transfer between the reinforcing element and the soil in lbs/in^2, z is the axial displacement of the reinforcing element, and a_0, a_1, and a_2 are empirical coefficients.

The results from the pullout tests by Commandeur (1989) were stratified by soil density and depth. The empirical coefficients were determined by multiple linear regression of z/τ on z and z^2 for a transformed equation,

$$\frac{z}{\tau} = a_o + a_1 z + a_2 z^2 \qquad 4\text{-}27$$

for each group of data.

Table 4-2 shows the regression coefficients generated by Commandeur (1989) for 6 and 12 inch soil depth classes and for three soil density classes. The shear-stress transfer curves for the three soil depth classes for the 89 to 91 lbs/ft^3 soil density class are shown in Figure 4-9. These shear-stress transfer functions

Table 4-2. Empirical regression coefficients for quadratic shear-stress transfer functions for three soil density classes for two confining stress conditions represented by soil depth from Commandeur (1989).

Soil Depth	Soil Density Class (lbs/ft^3)	a_0	a_1	a_2
6 inches	88 to 89	0.0505	1.10	0.363
	89 to 91	0.0562	0.770	0.667
	91 to 92	0.1420	0.818	0.511
12 inches	88 to 89	0.0428	0.761	0.277
	89 to 91	0.0300	0.596	0.325
	91 to 92	0.0667	0.223	0.421

were used in the root reinforcement model to calculate the applied tensile force in the reinforcing element for a given lateral deflection, and thus axial deformation, of the reinforcing element.

Commandeur (1989) experienced a similar problem that other researchers have experienced during pullout tests. The apparent friction angle between the reinforcing element and the soil at the ultimate shear-stress transfer was larger than the internal angle of friction for the soil. For Commandeur (1989), the internal angle of friction of the soil at the confining stresses tested was 45°. The apparent friction angle that was experimentally derived between the Douglas-fir roots and the sand ranged from a low of 50° to as high as 85°. This friction angle

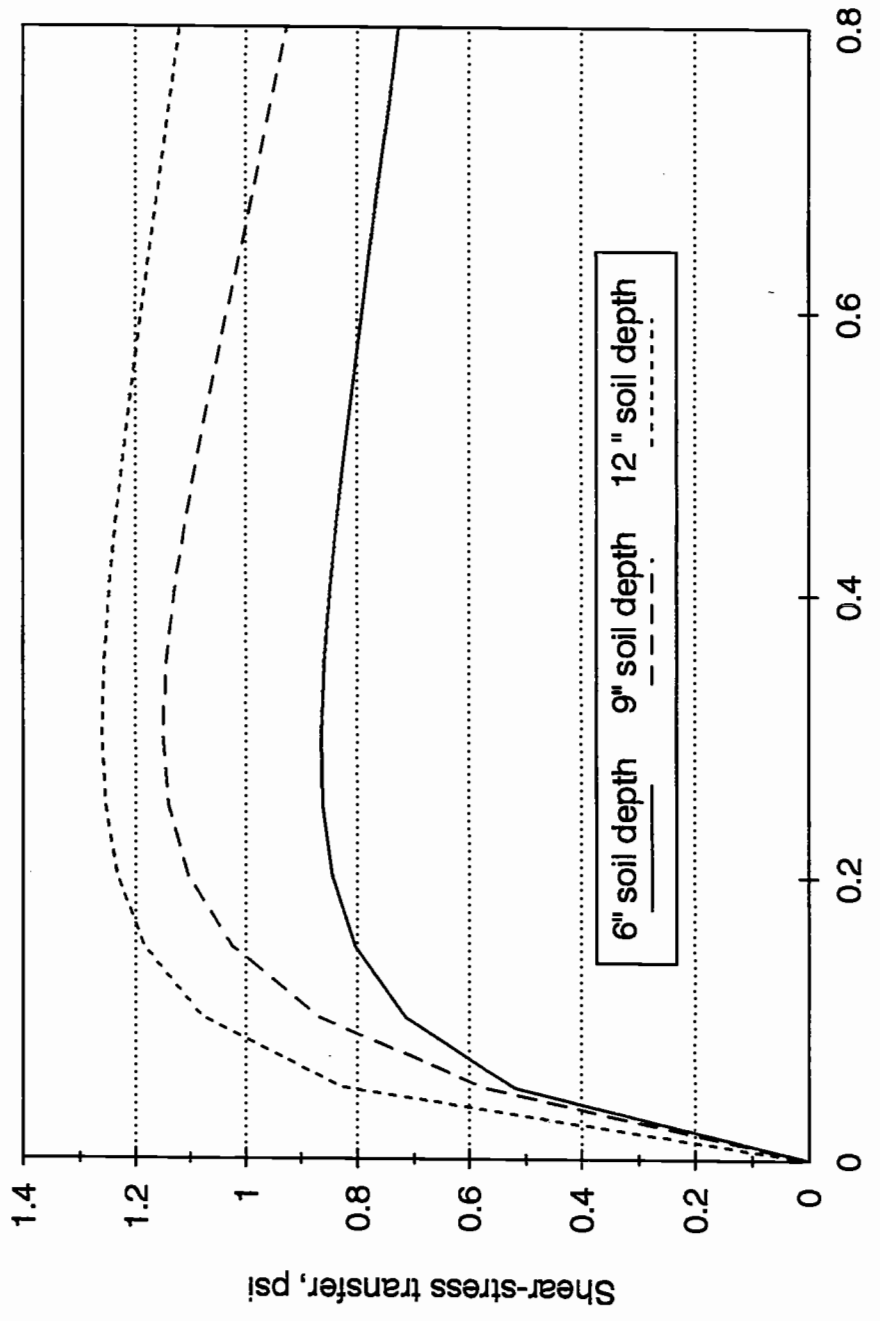

Figure 4-9. The shear-stress transfer functions used in the root reinforcement model for a loose, cohesionless sand. The curves represent funtions for soil depths of 6, 12 and 18 inches for a sand with a dry density of 89 to 91 lbs/ft^3.

is called an apparent friction angle and is given the symbol δ. The apparent friction coefficient, given the symbol μ^*, is the tangent of the apparent friction angle and is defined by the following relationship,

$$\mu^* = tan\,\delta = \frac{\tau_{ult}}{\sigma_n} \qquad 4\text{-}28$$

Using this relationship, the apparent friction angles from Commandeur's (1989) study translated to apparent friction coefficients of approximately 1.2 to greater than 11.0.

This effect has been observed and reported in other studies (Schlosser and Elias, 1978; Mitchell and Villet, 1987). The apparent friction angle between soils and different reinforcing element materials in shear box tests is 0.5 to 0.8 times the internal angle of friction of the soil (Mitchell and Villet, 1987). In pullout tests, apparent friction coefficients have been reported ranging from 0.5 to considerably greater than 1.0. Apparent friction coefficient values that correspond to apparent friction angles which are larger than 80 percent of a soil's internal angle of friction are reported to occur with rough or ribbed reinforcing elements and at small confining pressures (Schlosser and Elias, 1978; Mitchell and Villet, 1987). Commandeur's (1989) work supports these findings. He was working with very low confining pressures and in addition to the roughness of the surface of a root, which was considered micro-roughness, the tortuous shape

of the root also caused macro-roughness. The tortuous shape of the roots were believed to cause zones of passive earth pressure during pullout tests and make the roots appear very rough.

In the case of ribbed reinforcing elements tested in dense soils with small confining pressures, the large apparent friction coefficients have been blamed on soil dilatency (Mitchell and Villet, 1987). Commandeur (1989) hypothesized that the large apparent friction coefficients could arise from two mechanisms. First of all, they could be the effect of the development of a shear zone about a soil/root cylinder which had an effective diameter equal to the tortuosity of the root. By including only the root surface area instead of the surface area of the soil/root cylinder in apparent friction angle calculations, the apparent friction angle might appear to be larger than it really was. A second mechanism was a hypothesized interaction with the testing equipment which would cause an increased pressure distribution about the root. Attempts were made to account for these mechanisms. After accounting for these mechanisms, Commandeur (1989) still had apparent friction coefficients ranging from 0.79 to 1.32 which corresponds to friction angles between the soil and reinforcing elements ranging from 38° to 53°.

While these values are more reasonable than the initial values, they, at times, still exceed the internal angle of friction of the soil and therefore the validity of the findings in the real world is questioned. To account for this uncertainty, the shear-stress transfer functions were incorporated into the axial solution of the root reinforcement model in two ways. One way was to leave the

shear-stress functions exactly as they appeared in Commandeur (1989). These equations consist of the coefficients which were experimentally determined and appear in Table 4-2. A second way was to incorporate a scaling coefficient.

To use a scaling coefficient, the first step was to assume the friction angle between the root and the soil was $(2/3)\phi$ which results in an apparent friction coefficient of 0.58. Using this friction angle, the ultimate shear-stress transfer between the reinforcing element and the soil was calculated using the relationship,

$$\tau_{ult} = \sigma_n \tan \delta \qquad 4\text{-}29$$

where, $\delta = (2/3)\phi$ and σ_n is an average of the vertical overburden pressure and the horizontal at-rest earth pressure. This term becomes,

$$\sigma_n = \frac{\gamma d}{2}\left(1 + (1 - \sin\phi)\right) \qquad 4\text{-}30$$

where γ is the soil density and d is the soil depth.

For each stratification of soil density and depth for which coefficients for shear-stress transfer functions were determined, an ultimate shear-stress transfer value was experimentally determined. The scaling coefficient was calculated by expressing the ultimate shear-stress transfer determined using $\delta = (2/3)\phi$ as a

decimal fraction of the ultimate shear-stress transfer determined experimentally by Commandeur (1989) for each soil density/depth stratification. For example, for the group with a soil density of 90 lbs/ft^3 and a soil depth of 12 inches the ultimate shear-stress determined experimentally 1.26 lbs/in^2. The calculated ultimate shear-stress using the assumed apparent friction angle of $(2/3)\phi$ is 0.404 lbs/in^2. Thus, the scaling coefficient is,

$$SC = \frac{0.404}{1.26} = 0.32 \qquad 4\text{-}31$$

In the axial solution of the root reinforcement model when a scaling coefficient is used, the entire shear-stress transfer function is adjusted by the scaling coefficient. Thus, the shear-stress transfer function becomes,

$$\tau = (SC)\frac{z}{a_0 + a_1(z) + a_2(z)^2} \qquad 4\text{-}32$$

For the particular case of the example discussed above which consists of a 12 inch deep soil with a density of 90 lbs/ft^3, the shear-stress transfer function with the appropriate scaling coefficient is,

$$\tau = (0.32)\frac{z}{0.03 + 0.596(z) + 0.325(z)^2} \qquad 4\text{-}33$$

Commandeur's (1989) original shear-stress transfer function and the function shown above using the scaling coefficient are graphed together in Figure 4-10.

Using the scaling coefficient with the shear-stress transfer functions allows the magnitude of the ultimate shear-stress to be scaled within values that are more intuitively correct. At the same time it allows for the full range of experimental data and the full shape of the shear-stress transfer curve to be used. There is no reason to believe that the scaled version of the shear-stress transfer function is not a good approximation of the process going on in the field.

When root reinforcement was modeled for a soil deeper than 12 inches, the same adjustments were applied. The coefficients for the shear-stress function were for a soil 12 inches deep and from the appropriate density group. The ultimate shear-stress transfer for the deeper soil was calculated using $(2/3)\phi$ as described above. Then the shear-stress transfer function for a 12 inch deep soil was used except that the scaling coefficient incorporated the calculated ultimate shear-stress transfer for the deeper soil.

Analytical Model Flowpath

The root reinforcement analytical model has three parts. First the model prompts the user for the needed inputs and calculates the balance of the needed parameters from these inputs. A final input implicit to the solution is the request for the lateral deformation of the reinforcing element at the failure surface.

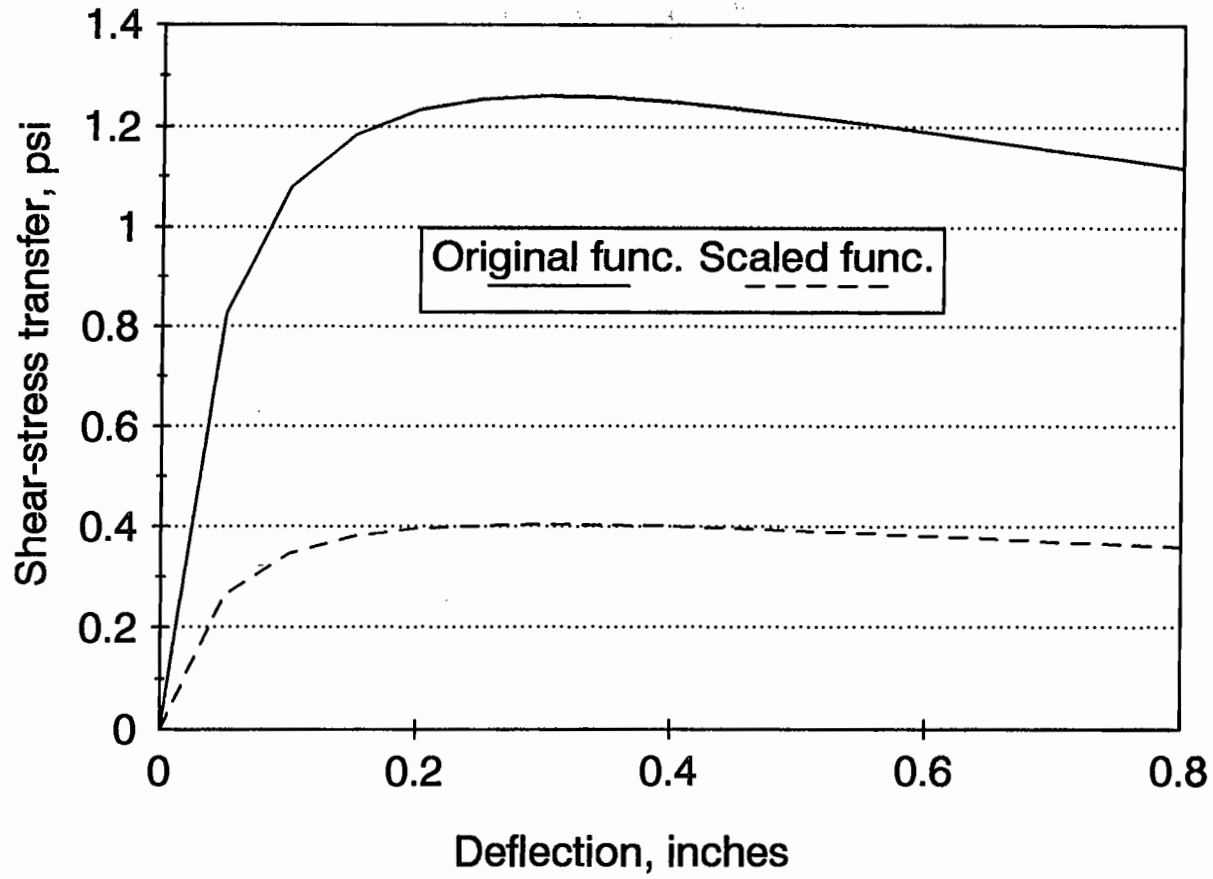

Figure 4-10. Shear-stress transfer functions for a loose, cohesionless sand with a density of 90 lbs/ft^3 at a soil depth of 12 inches. The solid line represents the shear-stress transfer function without using a scaling coefficient. The dotted line represents the shear-stress transfer function using a scaling coefficient.

After the inputs are completed, the model solves the lateral problem. This solution yields a deflected shape of the reinforcing element and the applied horizontal force at the failure surface to cause the deflected shape. Finally, the model solves the axial problem and calculates the applied tensile force needed to lengthen the reinforcing element the amount required for the lateral deflection. Because the tensile force determined in the axial solution affects the shape of the reinforcing element in the lateral solution, subsequent solutions from each part of the problem are input back into the model and the solution is iterated until it does not change. In this case, that means that the largest change in the calculated deflection at any node is less than 10^{-4} inches between successive iterations.

The final output of the model is the applied horizontal force at the failure surface, V_y, the applied tensile force at the failure surface, T_x, and the deflected shape of the reinforcing element. The flow path for the model is shown in Figure 4-11 and the following sections describe the model algorithm in more detail

Data Input Subroutine

The model is initiated with a subroutine that prompts for and allows the input of the appropriate soil and reinforcing element parameters and then calculates other needed parameters from this input. The inputs are prompted and required in English units and in pounds and inches except where the normal convention is different.

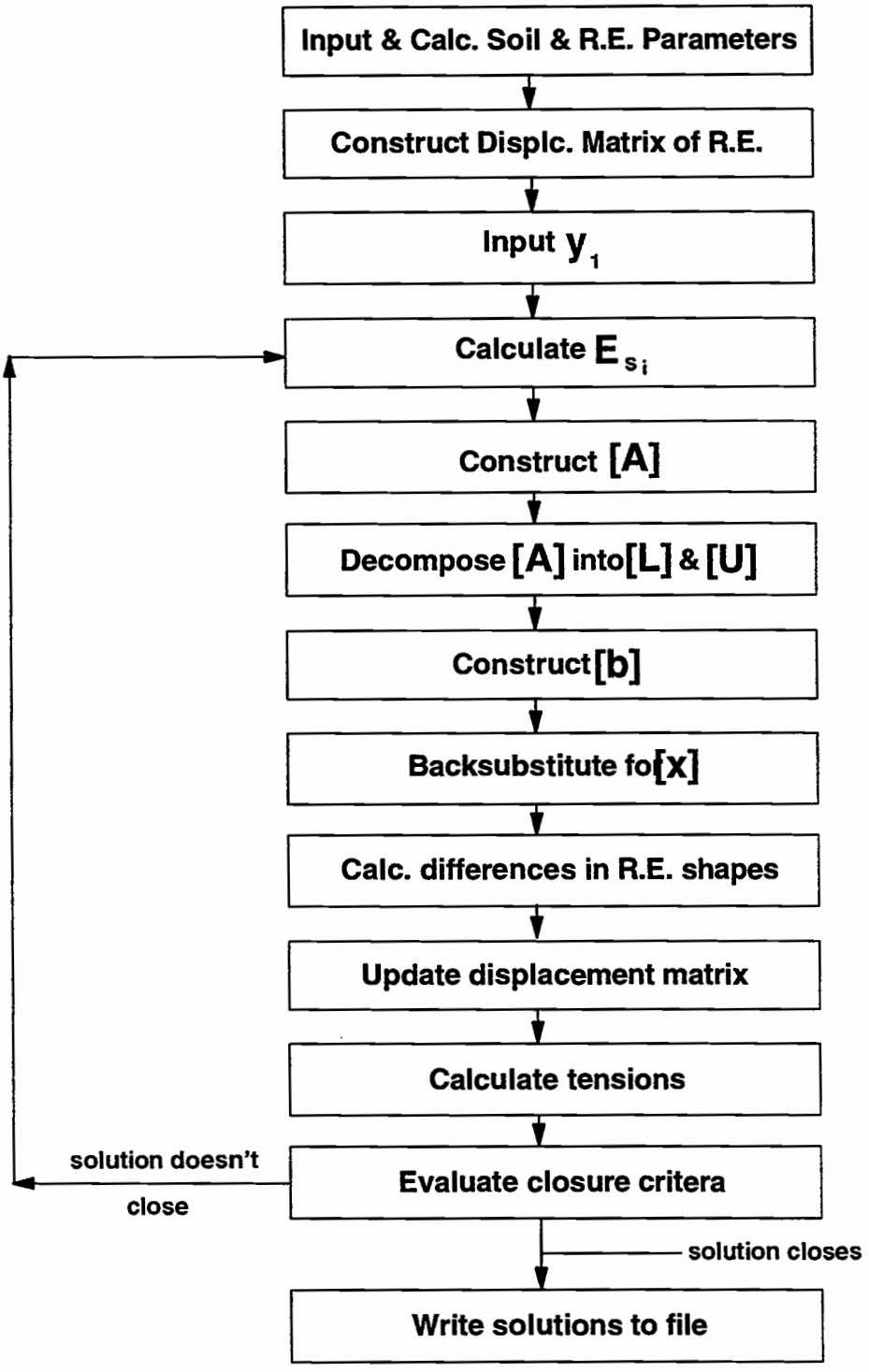

Figure 4-11. The structure of the root reinforcement model showing the flowpath of the algorithm.

The soil parameters are input first. The following soil parameters are requested;

- soil density, γ, in lbs/ft^3 (converted to lbs/in^3 in the subroutine),
- internal angle of friction, ϕ, in degrees,
- soil cohesion, c, is assumed to be zero,
- coefficient of subgrade reaction, k, in lbs/in^3 is either input or assigned (Table 4-1).

Next the reinforcing element parameters are input. These parameters are;

- modulus of elasticity, E, in lbs/in^2,
- the diameter of the reinforcing element, b, in inches,
- the depth in the soil the reinforcing element is embedded, d, in inches.

From these input parameters, a number of parameters needed for the model are calculated. These include both soil and reinforcing element parameters. The parameters are:

- moment of inertia, $I = \pi b^4/64$,
- active earth pressure coefficient, $K_a = tan^2(45 - \phi/2)$,
- at-rest earth pressure coefficient, $K_o = (1 - sin\,\phi)$,
- the argument of the passive earth pressure coefficient, $\beta = 45 + \phi/2$.

Three other parameters have to be calculated. They are the length of the discrete element length, h, reinforcement element length, l, and the number of nodes, n. The number of nodes is quite easy to determine, it is simply the length of the

reinforcing element divided by the node length, $n = l / h$. However, determining the length of the reinforcing element to model and the length of the discrete element were not as straight forward.

Reinforcing Element Length

Determining the length of the reinforcing element to be modeled was far from a straight forward exercise. Initially, during development of the model, a method was sought that would allow the length of the reinforcing element to be modeled to be calculated *a priori*. The reasons for this were that a calculated length was sought, instead of just assigning a conservative fixed length which would always work, due to concerns about computer memory and performance. An initial length was sought that would be long enough such that subsequent calculations of the length of the reinforcing element in tension would not exceed the initial estimated length. An attempt was made to balance computer memory and performance with the performance of the root reinforcement model.

Originally, the calculation of an optimum length revolved around the concept of the ultimate tensile strength of the reinforcing element. Using an ultimate shear-stress transfer concept, the length of the reinforcing element to be modeled should, at a minimum, be long enough to develop enough tensile force from shear-stress transfer to allow the reinforcing element to fail in tension. This would certainly be an upper limit value of needed reinforcing element length.

However, the criteria of reinforcing element ultimate tensile strength as a limiting value became moot as modeling proceeded because even at the maximum lateral deformation of 2 inches, the ultimate tensile strength of the roots was seldom reached. Due to the realities of the diameter distribution of roots in a soil for a landslide-prone forested slope, only a limited number of root diameters were modeled. These diameters are reported in Burroughs and Thomas (1977) and this subject is discussed in the parameter study section of the results chapter. The root diameters modeled extensively were 0.1, 0.25, and 0.5 inches. The only instances when the modeled tensile stress of a root exceeded its ultimate strength was for a 0.1 inch diameter root with a scaling coefficient at lateral deflections of 1.75 and 2.0 inches and for the same root without using a scaling coefficient at all defections greater than 1.0 inch. For the rest of the situations in which roots were modeled, the ultimate tensile strength of the root was not exceeded.

The problem with the modeled length of the root was not in the axial solution but in the lateral solution. In the lateral solution of this model, the modeled deflections oscillate about the original shape of the root. The lateral deformation is initially positive, then it passes through a zero deflection point and becomes negative, and then continues to oscillate between positive and negative deflections along the root. The maximum calculated deflection between each zero deflection point is reduced by approximately an order of magnitude for each oscillation as the process proceeds along the reinforcing element away

from the failure surface. The accuracy of the solution to the lateral problem doesn't improve if the length of the modeled pile extends beyond the second zero deflection point (Reese, 1984). Therefore, a suggested procedure was to set the length of the reinforcing element to be long enough to include two zero deflection points in the lateral solution.

A problem occurs because the lateral and axial solution techniques require different lengths for the reinforcing element. The two length requirements are different by approximately an order of magnitude. The axial solution can have several tens of inches and, at times, several hundred inches of root in tension which translates into several thousand to, at times, over ten thousand nodes for the axial solution. Conversely, the lateral solution requires only several inches of root length and generally not more than one hundred nodes. There is no downfall, in terms of accuracy of the solution, from including hundreds of inches of root and thousands of nodes in the lateral solution, but there is considerable downfall in computing time and power. Using thousands of nodes in the matrix conversion subroutine, even with the efficient banded storage of the matrices, often overran memory capability and required long calculation times. Obviously, the entire length of the root in tension did not need to be carried through the entire lateral solution.

Ultimately, the model was written so that the length of the reinforcing element modeled as a laterally loaded pile was set at approximately seven inches. This number is not arbitrary but comes from experience running the

model. This length allows the large diameter roots at the maximum lateral deformation to have two zero deflection nodes in the solution and, at the same time, doesn't overrun memory capacity and make computation time exceedingly long for the smaller roots at small lateral deformations. For the bulk of the modeling the seven inch length resulted in less than 100 nodes in the lateral solution calculations. For the axial solution, the total length of the root in tension still involved thousands of nodes and these calculations were carried out and a final tensile load was calculated and recorded. However, the tension at each node was stored only for the nodes used in the lateral solution.

Thus, the length of the reinforcing element that was to be modeled was set at seven inches. This value is based simply on experience running the model in the range of values associated with landslides in shallow forest soils. The length is long enough to allow large roots at large deflections to have two zero deflection points modeled but short enough not to exceed computer memory or make computation time exceedingly long.

Discrete Element Length

A second problem dealt with the length of the discrete elements that the reinforcing element would be divided into. This, again, is a compromise between model accuracy and computing time and power. In general, as the length of each discrete element becomes smaller, the solution will become more accurate. As the

length of the discrete elements becomes smaller, there are more of them resulting in increased computing time and memory requirements. The objective was to find a length for the discrete elements that gives the required accuracy but also allows for expedient computations.

The literature on modeling laterally loaded piles suggests that a discrete element length equal to one half the diameter of the reinforcing element be used (Reese, 1984). This suggestion is for large diameter, high modulus piles in which an axial force is either ignored or treated as a constant. Furthermore, not only is the modulus high but the stiffness, *EI*, which is a product of the modulus and the moment of inertia of the pile is also high. In the root reinforcement model a low modulus, small diameter root is modeled which will have a small stiffness value and will not perform like a steel pile.

To investigate this problem, the model was run with a range of discrete element lengths while all other variables were held constant. The modeled soil was a clean, loose, cohesionless soil with an internal angle of friction of 44°. The reinforcing elements were conifer roots, 0.5 inches in diameter, embedded 12 inches in the soil, and possessing a modulus of elasticity of 73,000 lbs/in^2. The shear-stress transfer function was used without a scaling coefficient and that function with the appropriate coefficients is,

$$\tau = \frac{z}{0.03 + 0.596(z) + 0.325(z)^2} \qquad 4\text{-}34$$

where, τ is the shear-stress transfer in lbs/in^2 and z is the axial deformation of the reinforcing element in inches. This equation is for a confining stress equal to 12 inches of sand with a density of 90 lbs/ft^3 (Commandeur, 1989). The model was run for a full range of lateral deformations from 0.01 inches to 2.0 inches (see Table 5-2).

At each deformation that the model was run, the length of the discrete element was varied as a function of the diameter of the reinforcing element. The lengths of the discrete element modeled were $3b$, $2b$, b, $b/2$, $b/5$, and $b/10$ where b is the reinforcing element diameter. The results of the modeling are illustrated in Figures 4-12 and 4-13. The figures show a graph of force versus length of the discrete elements. The forces graphed are the model output forces the horizontal force applied parallel to the failure surface, $V_{y'}$, and the applied tensile force perpendicular to the failure surface, $T_{x'}$. Figures 4-12 and 4-13 show results for only the element lengths b, $b/2$, $b/5$, and $b/10$ and the lateral deflections illustrated only go through 0.5 inches. The purpose is to show that the modeled output forces do not change with a decrease in element length. A discrete element length of $b/2$ was used for the root reinforcement model.

Displacement Matrix Subroutine

After the needed parameters to run the model have been either input or calculated, a displacement matrix is created to store the current shape of the reinforcing element being modeled. The matrix is an $nx2$ matrix where n is the

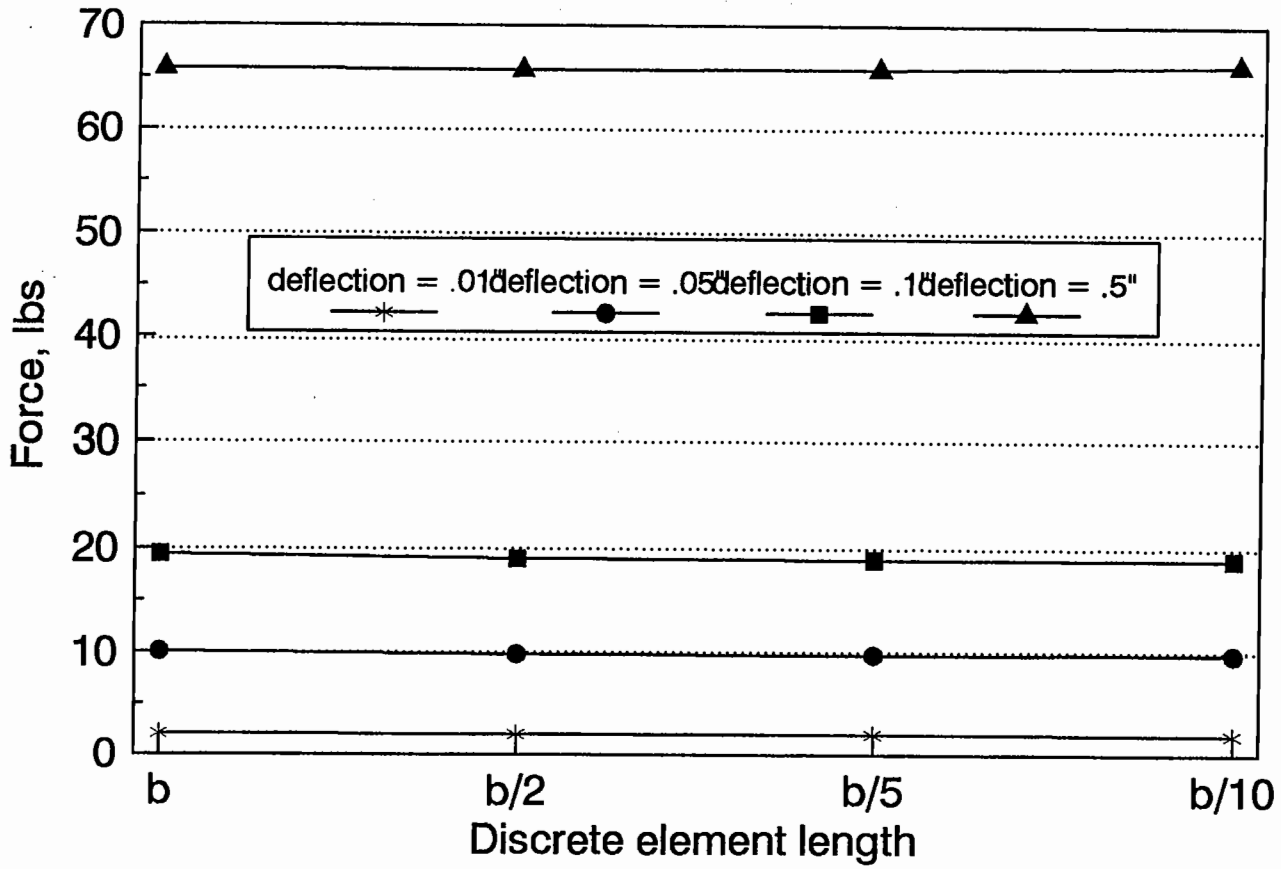

Figure 4-12. A graph of the applied lateral force, V_y, versus the length of the discrete elements where the discrete elements lengths range from b to b/10 where b is the diameter of the reinforcing element. The four lines show the effect of discrete element length on applied lateral force for four deflections of the reinforcing element at the failure surface ranging from 0.01 to 0.5 inches.

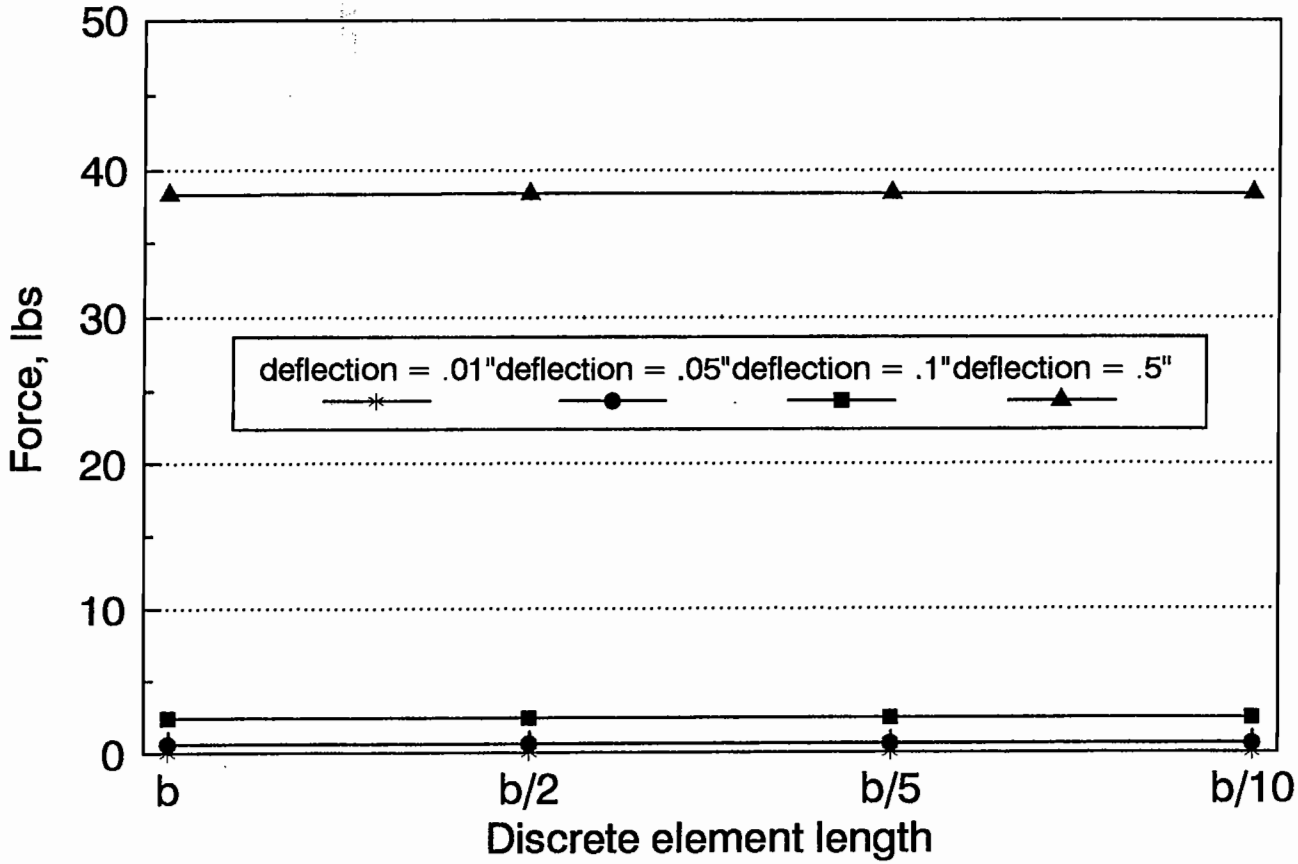

Figure 4-13. A graph of the applied tensile force, T_x, versus the length of the discrete elements where the discrete elements lengths range from b to b/10 where b is the diameter of the reinforcing element. The four lines show the effect of discrete element length on applied lateral force for four deflections of the reinforcing element at the failure surface ranging from 0.01 to 0.5 inches.

number of nodes being modeled in the calculations and the 2 indicates that the displacement matrix is a two-dimensional array where the two dimensions are the x- and y-coordinates, $[x_i, y_i]$ of the centroids of the discrete elements or the nodes of the modeled root.

When the displacement matrix is created, the x-value of the array for each node is the node number, n_i, times the node length, h.

$$x_i = n_i(h) \qquad 4\text{-}35$$

This value doesn't change and is carried throughout the model. The y-value is the lateral deflection of that node. When the displacement matrix is created, the y-values are all set to zero except for the first node. The lateral deflection of the first node, y_1, the node right at the failure surface, is an input to initiate the model. The model prompts for the lateral deflection of the reinforcing element at the failure surface to be input when this subroutine is encountered.

The x-values of the displacement matrix remain constant throughout subsequent iterations of the model. The y-values are updated during each iteration of the model and the latest values are always placed in the displacement matrix. The final form of the displacement matrix, which is the final shape of the reinforcing element, is an output of the root reinforcement model.

Calculating the Secant Modulus of the Soil Response

After the displacement matrix has been created, the program enters the iteration loop (Figure 4-11). The first step after entering the loop is the calculation of the secant modulus of the soil response. The theory behind the calculation has been presented in a previous section. The equations are complete in that section and won't be restated here. This subroutine is a simple one which takes the lateral deflection of the reinforcing element at each node from the displacement matrix, y_i, and calculates the value of the secant modulus of the soil response, E_{s_i}, for that node given that displacement. The secant modulus values are then stored in a one-dimensional array. The values of the secant modulus of the soil response are recalculated for every iteration of the root reinforcement model.

The Coefficients Matrix

At this point in the program, the coefficients matrix for the solution of the lateral problem is constructed. Recall that the lateral solution follows a traditional form for solving systems of simultaneous equations. This discussion is presented previously in this document and will be recounted briefly here. The system of simultaneous equations is represented in matrix notation by the identity **[A] [x] = [b]** where **[A]** is the coefficients matrix, **[b]** is the constants matrix, and **[x]** is the matrix of unknowns. The content of all of these matrices are shown in Figures 4-4 and 4-5.

All of the terms needed to construct **[A]** are known. The components of the stiffness term, *EI*, are constants as is the element length, *h*. The values for secant modulus of the soil response, E_{s_i}, were calculated previously and stored in a one-dimensional array. The array for the tensile force at each node, T_i, was declared initially in the program and stores zeros until other values are assigned. Therefore, during the first iteration, zeros are used for tensile force in the coefficients matrix. As deflected shapes and the subsequent values of tensile force for each node are calculated and stored in the appropriate array during subsequent iterations, these values will be used to construct the coefficients matrix. The values in the coefficients matrix are updated during each iteration of the root reinforcement model.

The coefficients matrix is an *nxn* square matrix. As illustrated previously, it is a banded diagonal matrix with the only nonzero values being two places to the left and right of the main diagonal. The storage and computation of a banded diagonal matrix can be made very efficient by just storing and using the numeric values and eliminating the zeros. This is done routinely and there are numerous coded algorithms available in the technical literature to help develop this part of the solution. The coefficients matrix becomes an *nx5* matrix where *n* is the number of nodes being modeled. The main diagonal values become the third column and the two values on each side of the diagonal become the other four columns.

Decomposing the Coefficients Matrix

The equation solver used to solve the system of linear equations for the lateral solution of the problem performs an LU-Decomposition. LU-Decomposition is a variant of basic Gaussian elimination (Press, et.al., 1992). The initial step in LU-Decomposition is to decompose the coefficients matrix **[A]** into two triangular matrices. One is a lower triangular matrix with values on and below the diagonal and nothing above the diagonal and this matrix is labeled **[L]**. For this method, ones are substituted into the diagonal values of the lower matrix. The other matrix is an upper triangular matrix with values on and above the diagonal and nothing below it and this matrix is labeled **[U]**. A requirement of the method is that **[L][U] = [A]**. Decomposing the coefficients matrix into upper and lower triangular matrices whose product is the coefficient matrix is carried out using a procedure called *Crout's Method*. The specific procedure used in the root reinforcement model is *Crout's Method* with partial pivoting. The coded algorithm for the subroutine, called **bandec**, which was used in the model was taken from Press, et.al. (1992).

The algorithm, **bandec**, takes an nxn banded diagonal matrix stored in compact form and performs an LU-Decomposition. The upper triangular matrix, **[U]**, is replaced back in **[A]** and the lower triangular matrix is returned to an $nx2$ matrix **[al]**.

Constructing the Constants Matrix

To solve the lateral portion of the problem, a constants matrix is needed to multiply the coefficients matrix, or the two decomposed triangular matrices, by to solve for the solution matrix. The composition of the constants matrix is shown in Figures 4-4 and 4-5. It is an *nx1* matrix with values for only the top three entries of the matrix, the balance of the entries are zero. The components of the entries, the stiffness, *EI*, the element length, *h*, the tension for that node, T_i, the secant modulus of the soil response for that node, E_{s_i}, and the lateral deflection of the first node, y_1, are all known. The values in the constants matrix are updated for each iteration.

Backsubstitution Routine

The next subroutine performs the backsubstitution on **[L]** and **[U]**, the lower and upper triangular matrices decomposed from **[A]**, the coefficients matrix, with **[b]**, the constants matrix. The subroutine solves the linear set

$$\mathbf{[A][x] = ([L][U])[x] = [L]([U][x]) = [b]}$$

by solving for a vector which can be called **[y]** such that

$$\mathbf{[L][y] = [b]}$$

and then solving

$$\mathbf{[U][x] = [y].}$$

The advantage of the LU-Decomposition is that both the solution vector **[x]** and the vector **[y]** can be solved for by forward- and back-substitution without row or column operations. This significantly reduces the number of operations that needs to be carried out and reduces the opportunity for roundoff error (Press, et.al., 1992).

Once again, a coded algorithm from Press, et.al. (1992) was used. The subroutine is called **banbks** and is used in combination with **bandec** as an equation solver. The subroutine writes the solution vector into the constants vector **[b]**. The **[L]** and **[U]** matrices are left intact should another solution be sought with the same coefficients matrix.

At this point in the model, the shape of the reinforcing element generated by the most recent solution of the lateral portion of the problem is compared with the previous shape of the reinforcing element. The difference in the deflections from the two solutions is calculated for each node and the largest difference among all the nodes is stored.

Then there is a subroutine to transfer the lateral deflections from the solution vector, which is the most recent solution to the lateral problem, to the displacement vector. Recall that the solution vector, **[x]**, is written into the constants vector array, **[b]**. By transferring the latest lateral deflections to the displacement vector, the constants vector space is freed up for the next construction of the constants vector and for the next iteration. Also, the latest deflected shape of the reinforcing element is stored in the displacement vector to

allow calculation of the quantities that come from that shape in subsequent iterations. This includes both the tension in the reinforcing element and the secant modulus of the soil response.

Tension Subroutine

The final subroutine is the one that calculates the axial solution to the problem. The output of the tension subroutine is the applied tensile force perpendicular to the failure surface and the tension in the reinforcing element at each node. The subroutine calculates the output quantities by first calculating the increased length of the deflected shape of the subroutine. Then the force required to cause the increased length is calculated by summing the shear-stress transfer values associated with each node given its movement through the soil.

Iteration Criteria

At the end of the tension subroutine, the decision is made whether to accept the current solution or calculate one more iteration of the solution. The decision is made based on the difference in the deflected shape of the reinforcing element from successive iterations of the model. If the maximum difference between any two successive deflections for any node is greater than 10^{-4} inches, then another iteration is calculated. In each subsequent iteration the shape of the reinforcing element and the tension values at each node are updated. Then the

entire procedure from the beginning of the loop, which starts at the calculation of the secant modulus of the soil response, is carried out again (see Figure 4-11). If the maximum difference in deflections between successive iterations is smaller then 10^{-4} inches, then the loop is exited. The header information, including the soil and reinforcing element parameters of the test, is written to a disk file along with the final displacement vector, or the final shape of the deflected reinforcing element, and the forces parallel to and perpendicular to the failure surface that caused the deflection.

The root reinforcement model has proven to be quite robust. The solution technique is initiated by simply offsetting the top node by the amount of lateral deformation desired in the final solution. The iteration technique is simply to take the answer from the previous iteration and use it as input for the current iteration. For the smaller lateral deflections the model closed within three or four iterations. For the larger reinforcing elements and large deflections the model took seven or eight iterations to close. Thus the criteria for a robust model, one that takes a very crude shape and minimal input and moves very quickly to a solution.

Initially, based on suggestions and examples from numerical methods texts and other numerical methods programs, a value of 10^{-6} inches was used as the closure criteria. This often lead to several iterations where the model output was not changing within five or six significant digits. A closure criteria of 10^{-4} inches was reached by trial and error. A range of values for closure criteria were

tested and the solutions for each were compared. A closure criteria of 10^{-4} inches speeded up calculation time, especially for problems with large lateral deflections, but didn't affect the value of the answer to within five significant digits. This was deemed acceptable for the problem being tested.

RESULTS

Model Verification

Verification is a critical part of the development of any model. It is important that the output of the model be considered correct, or in other words, the model must be able to correctly predict the behavior of the modeled phenomena in the real world. Model output does not have to exactly mimic real world behavior of the modeled phenomena to be useful, but it must come close enough to satisfy the objectives driving the development of the model in the first place.

The charge for the development of the root reinforcement model was to develop a model which was based primarily on physical principles, not empiricism. The requirements on the accuracy of the root reinforcement model are that the output forces be within the correct order of magnitude, model output should respond properly and intuitively to changes in input, and the model be responsive enough to allow "what if" scenarios to be run with differing input parameters.

To verify the accuracy of the model, results generated by the model have to be compared with real world results generated by a process similar to the one being modeled. Independent field or laboratory trials for the expressed purpose of verifying this model were not conducted. Therefore the real world results with

which to compare the model output have to come from research results in the technical literature. The applied tensile force, applied shear force, and shape of the reinforcing element as it is stretched across a failure surface are output from the root reinforcement model. The model was constructed to generate this output for reinforcing elements, including conifer roots, in shallow, cohesionless, sandy soils. There are no research results available in the technical literature which give these outputs for the environmental conditions described. Thus, technical literature was examined which reported results on either field or laboratory trials where reinforced earth structures or theory were tested. Reinforced earth is used in its broadest sense to describe any situation where high tensile strength inclusions, including steel rods and tree roots among other materials, are embedded in soil with the reported result that the strength of the soil/reinforcement was increased relative to the strength of the soil alone.

The most applicable type of information from the technical literature comes from case studies of reinforced earth walls. In these case studies, the reinforced earth wall is instrumented to measure the movement of the wall and the reinforcing elements are instrumented to measure the extension, and thus the tensile stress, in the reinforcing elements. With this type of data, the actual increase in stresses in the reinforcing elements in response to a movement of soil are known, which is the information being sought. The type of reinforced earth structures most applicable to the situation being modeled are reinforced earth walls and soil nailed walls. Soil nailed walls are the type of reinforced earth

structure that most closely resembles the situation being modeled by root reinforcement. An example of the type of information and literature available for case studies of reinforced earth walls is Shen et. al. (1981a & 1981b). Shen et. al. report on the performance of two soil-nailed walls, a prototype model wall and a full-scale wall. The reported results include both the observed movement of the wall and the increase in the tensile forces in the soil nails. There are a great number of reinforced earth wall case studies available in the literature. Many of the case studies are reviewed in Mitchell and Villet (1987).

Case studies of reinforced earth walls should be a valuable source of data to validate the root reinforcement model, however, the data are not useful for several reasons. First of all, even short reinforced earth walls are several meters tall and the first row of reinforcing elements are installed at a depth of 1 to 2 meters which makes the confining stress on these reinforcing elements considerably greater than the confining stress associated with shallow landslides. Secondly, the reinforcing elements are high modulus. They are, at minimum, steel reinforcing bars and, more often, are steel bars encased in grout which makes their modulus of elasticity much different than that of conifer roots. Finally, the soil in most reinforced earth walls is either a manufactured soil which would be a high density, compacted, granular fill or an *in situ* soil which may have considerable cohesion. These conditions do not adequately replicate the environmental conditions modeled, so reinforced earth case studies are not used to validate the root reinforcement model.

Waldron and his associates published a series of articles describing a research program studying the strength of soils reinforced with plant roots (Waldron, 1977; Waldron and Dakessian, 1981; 1982; Waldron et. al., 1983). In this research, direct shear strength tests were used to measure the strength of a soil/root matrix. Failure surfaces imposed on the tested soil columns were all less than 1 meter deep, thus confining stress on the failure surface was consistent with a shallow soil. Only plant roots were used for the reinforcing elements so the modulus of elasticity of the reinforcing elements was consistent with the root reinforcement model. Some of the soils that the plants were grown in, and later tested, were the same textures as a shallow forest soil. However, a lot of the published testing was carried out on a clay loam which had more cohesion than was considered in the root reinforcement model. During strength testing, only external displacements and forces were measured and recorded, so the numbers and orientation of the plant roots, both before and after testing, and stresses in the roots were not studied and can not be deduced from the article. Therefore, this information was also not used to validate the root reinforcement model.

Gray and Ohashi (1983) ran a series of laboratory direct shear tests using various materials as reinforcing elements in a cohesionless sand. Both the texture of the sand and the modulus of elasticity of most of the reinforcing elements were within the modeled range of these parameters. However, the confining stresses used during the direct shear tests, which corresponded to soil depths greater than 2 m, could not be considered shallow. Additionally, only external

displacements and forces were measured and recorded and, while the initial geometry of the reinforcing elements were known, the final geometry was not. For all of these reasons, but primarily because the confining stresses were too high, this data was also not used for validation of the root reinforcement model

Wu, et. al. (1988b) conducted *in situ* direct shear tests on small blocks of forest soil with conifer roots embedded. Obviously, the soil type, modulus of elasticity of the reinforcing elements, and the confining stress were all acceptable and their values were in the range being modeled. Once again, the direct shear tests give only the external displacements and forces except the tension in some of the roots was monitored during the test. The final geometry of the roots after the test were completed was known, but root geometry was not known before the test was initiated, so the change in geometry of the root is not known. This particular test would seem to be ideal for testing the root reinforcement model, but insufficient information was given in the article to allow validation of the root reinforcement model to be carried out.

Jewell (1980) performed laboratory direct shear tests on sand reinforced with either steel or brass bars or grids. A cohesionless sand was used for the tests, but is was a dense sand and the applied normal force made the confining stress on the reinforcing elements too large for the modeled soil depth to be considered shallow. The geometry of the reinforcing elements, both before and during the tests, was known, however only external displacements and forces

were measured and recorded. Primarily due to the large confining stresses, data from this source was also not used to validate the root reinforcement model.

Shewbridge and Sitar (1985; 1989) and Abe and Ziemer (1991) also used laboratory direct shear tests to determine the strength of sand reinforced with different types of reinforcing elements. A clean, cohesionless sand was used for the direct shear tests at a confining stress on the reinforcing elements that was equivalent to a soil depth of less than two feet which is a shallow soil. The reinforcing elements included parachute cord, aluminum and steel bars, wooden dowels, and conifer roots, so the direct shear tests were conducted with reinforcing elements which had an appropriate modulus of elasticity. The geometry of the reinforcing elements before the test were known and great care was taken to determine the final geometry of the reinforcing elements at the completion of the tests. Only external displacements and forces were measured during the direct shear tests. The displacements and forces in the reinforcing elements during the direct shear tests were not measured. Despite the fact that the internal forces in the reinforcing elements during the strength tests are not known, which are outputs of the root reinforcement model, everything else about the tests matched quite well. The direct shear tests used a shallow, cohesionless sand, the modulus of elasticity of the reinforcing elements was appropriate, and the geometry of the reinforcing elements both at the beginning and the completion of the tests were measured and recorded. Research results

from these articles and this series of direct shear tests were used to validate the root reinforcement model.

As a first step in validating the root reinforcement model, the conditions in which the direct shear tests were conducted were converted into input parameters for the root reinforcement model. Both Shewbridge and Sitar (1985) and Abe and Ziemer (1991) used the same direct shear device but they used slightly different test conditions and different reinforcing elements. Shewbridge and Sitar (1985) used bungy cords, parachute cord, wooden dowels, steel rods, and aluminum rods as reinforcing elements while Abe and Ziemer (1991) tested actual conifer roots (*Pinus contorta*) as reinforcing elements.

Shewbridge and Sitar (1985) used a clean, dry cohesionless sand with an internal angle of friction of 40^0 in their direct shear tests. The relative density of the sand was 71 percent and the dry unit weight was 104 lbs/ft^3. Based on the relative density, the sand was medium density so a coefficient of subgrade reaction of 90 lbs/in^3 was assigned. Based on the reported confining stress on the reinforcing elements and the density of the sand, the reinforcing elements were embedded at an equivalent soil depth of 24.7 inches. The extent of the lateral deformation of the reinforcing element at the completion of the direct shear test was 85 mm. Recall that the root reinforcement model is symmetric about the failure surface so only half the problem is modeled. Thus, the lateral deformation used in the model was 42.5 mm or 1.67 inches. The diameters and modulus of

elasticity of the reinforcing elements used in the root reinforcement model were taken from Shewbridge and Sitar (1985) and are listed in Table 5-1.

Abe and Ziemer (1991) also used a cohesionless sand in their direct shear tests. It had a dry unit weight of approximately 92 lbs/ft^3 and a moisture content of 19.5 percent making the moist unit weight approximately 110 lbs/ft^3. No angle of internal friction was given, so one of 40° was assumed. The sand was also assumed to be medium density and based on the unit weight of the sand a coefficient of subgrade reaction of 90 lbs/in^3 was assigned. Based on the confining stress on the reinforcing elements and the moist unit weight of the sand, the reinforcing elements were embedded at an equivalent soil depth of approximately 21.5 inches. The total lateral deformation of the reinforcing elements in these direct shear tests was 88 mm, thus the displacement distance used in the root reinforcement model was 44 mm or 1.73 inches.

The reinforcing elements used by Abe and Ziemer (1991) were pine roots. Three root diameters and three modulus of elasticity values were used in the root reinforcement model during model validation. Three root diameters were used because the roots tested by Abe and Ziemer (1991) fell into three convenient size classes. A representative diameter from each of these size classes was included in the root reinforcement model validation. The diameters that were used are listed in Table 5-1. Abe & Ziemer (1991) did not determine a modulus of elasticity for the pine roots they tested and used an assumed value instead. The value they assumed was no better or worse than any of a number of other values that could

Table 5-1 Summary of properties for reinforcing elements used in validation of the root reinforcement model. Summary data taken from Shewbridge and Sitar (1985; 1989) and Abe and Ziemer (1991).

Reinforcing Element Type	Diameter (inches)	Modulus of Elasticity (lbs/in^2)	Apparent Friction Angle	Ultimate Shear-Stress Transfer (lbs/in^2)	Scaling Coefficient	b (1/inches)
Parachute Cord	0.13	213,000	39°	0.82	0.46	1.04
Small Wooden Dowel	0.13	1,730,000	35°	0.71	0.39	0.91
Large Wooden Dowel	0.31	1,730,000	35°	0.71	0.39	0.61
Steel Rod	0.13	29,500,000	24°	0.45	0.25	0.69
Aluminum Rod	0.37	10,600,000	24°	0.45	0.25	0.51
Pine Root - Small[1]	0.32	73,000[2]	35°	0.65	0.37	0.51
Pine Root - Medium[1]	0.44	392,000[3]	35°	0.65	0.37	0.41
Pine Root - Large[1]	0.54	1,730,000[4]	35°	0.65	0.37	0.41

1 All three diameters of pine roots were modeled using all three modulus values for pine roots

2 Commanduer and Pyles, 1991

3 Abe and Ziemer, 1991

4 Shewbridge and Sitar, 1989

have been used. Their assumed value was bracketed by both a larger and smaller value of modulus of elasticity for conifer roots to allow a range of modulus values to be tested. The largest value used in the root reinforcement model for a conifer root was 1,730,000 psi. This was the modulus of elasticity value used by Shewbridge and Sitar (1985; 1989) for the wooden dowels in their direct shear tests. The modulus of elasticity value assumed by Abe and Ziemer (1991) was 392,500 psi and was taken from modulus of elasticity tests performed on *Cryptomeria japonica* by the senior author. The smallest value of modulus of elasticity used in the root reinforcement model was 73,000 psi which came from work done by Commandeur and Pyles (1991) on Douglas-fir roots and this value of modulus of elasticity is the default value used for conifer roots throughout this dissertation. These modulus values are also listed in Table 5-1.

In addition to setting the input parameters for the soil and reinforcing elements, the shear-stress transfer functions were also set. During validation of the root reinforcement model, as well as during all simulations using the root reinforcement model, Commandeur's (1989) shear-stress transfer equations were used. The equivalent soil depths for the two situations being modeled were 24.7 and 21.5 inches and the corresponding soil densities were 104 and 110 lbs/ft^3 The shear-stress transfer function developed by Commandeur (1989) with the most extreme soil depth and density was for a 12 inch soil depth and a 92 lbs/ft^3 soil density. This shear-stress transfer function was used because no better data

exists. Therefore, the shear-stress transfer coefficients in Table 4-2 of this dissertation were used for the following shear-stress transfer function,

$$\tau = \frac{z}{0.0667 + 0.223(z) + 0.421(z)^2} \qquad 5\text{-}1$$

where, τ is the calculated shear-stress transfer in lbs/in^2 and z is the displacement of the root. The coefficients are empirical constants for the case of a 12 inches soil depth and a 92 lbs/ft^3 soil density.

There is more to the process than just assigning a shear-stress transfer function, the shear-stress transfer function must be scaled to account for discrepancies between the empirically measured ultimate shear-stress, τ_{ult}, in Commandeur (1989) and a reasonable estimate of the same value. The ultimate shear-stress transfer measured during the laboratory trials to develop the above shear-stress transfer function was 1.79 lbs/in^2. During the verification of the root reinforcement model, a scaling coefficient was used in the root reinforcement model to reduce the value of shear-stress transfer predicted by the above equation. The scaling coefficient was a ratio between the calculated reasonable estimate of ultimate shear-stress and the value of ultimate shear-stress measured by Commandeur (1989). To determine a reasonable estimate of the ultimate shear-stress, the first step is to assume an apparent friction angle between the reinforcing element and the sand. For the reinforcing elements tested by

Shewbridge and Sitar (1985; 1989), the apparent friction angles were given and are listed in Table 5-1. For the pine roots tested by Abe and Ziemer (1991), no apparent friction angles was given so one was assumed. The assumed apparent friction angle was 35° which is the same as the apparent friction angle for the wooden dowels from Shewbridge and Sitar (1985). These values are also listed in Table 5-1. Once the apparent friction angles had been assigned, the ultimate shear-stress value was calculated by averaging the vertical overburden pressure and the horizontal at-rest earth pressure and then multiplying that value by the tangent of the apparent friction angle. The calculated ultimate shear-stress values and the resulting scaling coefficients are also listed in Table 5-1 with all the other input parameters.

Model validation was carried out by comparing the shape of the modeled reinforcing element with the direct shear results reported in the literature (Shewbridge and Sitar, 1985; 1989; Abe and Ziemer, 1991). This task was made easier due to the way that the deformed shape of the reinforcing elements in direct shear tests were reported. The procedure, initiated by Shewbridge and Sitar (1985) and used by Abe and Ziemer (1991), was to make a map or drawing of the shape of the deformed reinforcing elements at the completion of the direct shear test. The shape of half of the reinforcing elements were fitted to an exponential function of the form:

$$y = B - B^{-b|x|} \qquad 5\text{-}2$$

where, y is the lateral deflection of the reinforcing element parallel to the failure surface at a distance x from the failure surface and perpendicular to it. B is half of the total lateral deformation of the reinforcing element during the test. So B is 1.67 inches for tests run by Shewbridge and Sitar (1985)and 1.73 inches for the tests run by Abe and Ziemer (1991). The constant that describes the curve is b. To recreate the shape of a deformed reinforcing element for the purpose of comparing that shape with output from the root reinforcement model, the constant, b, for the reinforcing element is determined and the shape of the curve is calculated and graphed.

In the root reinforcement model, only one reinforcing element is modeled at a time. In the direct shear tests run by both Shewbridge and Sitar (1985) and Abe and Ziemer (1991), the reinforcement effect of multiple reinforcing elements was tested during each direct shear test. In none of the direct shear tests used to validate the root reinforcement model was a single reinforcing element tested. The authors reported interference with multiple reinforcing elements especially at the high concentrations of reinforcing elements, thus b-values were not constant for a given reinforcing element material over several direct shear tests. It was important to choose the most appropriate b-value for comparisons with the root reinforcement model. The direct shear tests that were chosen for the most appropriate b-value for comparisons with the root reinforcement model, in every case, were direct shear tests in which the minimum number of reinforcing elements were used. In some cases, direct shear tests with the same material and

number of reinforcing elements had differing b values. Although there was not a great difference in the b-values, they, nonetheless, were different. In these cases, a representative value was chosen which was usually not an extreme value but some intermediate value. The b-values used for model validation are listed in Table 5-1.

The results of the model verification exercise are shown in Figures 5-1 through 5-8. The model was run to generate output for parachute cord, small wooden dowels, large wooden dowels, steel rods, aluminum rods, and small-, medium-, and large- pine roots. A problem was encountered regarding the modeled tension in the reinforcing elements. The reinforcing elements used in the direct shear tests were 750 mm long. Only one half of the reinforcing element on one side of the failure plane could be modeled in the root reinforcement model which made the length of the modeled reinforcing element 375 mm or approximately 15 inches long. The maximum length of the reinforcing element that could be in tension was 15 inches. Shewbridge and Sitar (1985) note that shear-stress transfer between the soil and the reinforcements, with a corresponding increase in tension in the reinforcing elements, must be mobilized significantly beyond the zone of shear displacements. They also noted that the complete length of the reinforcing elements in the direct shear tests were in tension by the completion of the direct shear tests and often before completion of them. The force-displacement curves show this to be the case (Shewbridge and Sitar, 1989) and output from the root reinforcement model confirms this.

The amount of tension in the reinforcing elements in the direct shear tests could be drastically overestimated in the root reinforcement model if the model is allowed to assume an infinitely long reinforcing element and account for all the potential increase in tension by shear-stress transfer between the soil and reinforcing element. The tension in the reinforcing element affects the lateral deformation of the reinforcing element and over estimating the actual tension available in the direct shear tests could affect how well direct shear test results and root reinforcement model output compare. This problem was accounted for by running the root reinforcement model using a range of values o tension. Because it was not possible to know the actual values of tension in the reinforcing elements during the direct shear tests, values of one half and/or one quarter of the maximum calculated tension were used in the root reinforcement model. All output from the root reinforcement model was graphed to allow visual comparisons. The use of multiple tension values in the root reinforcement model explains the multiple curves for each reinforcing element per graph.

During the direct shear tests for the pine roots, a modulus of elasticity value was assumed, not measured (Abe and Ziemer, 1991). When the root reinforcement model was run to generate output to compare with these direct shear tests, a range of modulus values were used. The range of shapes associated with multiple values of modulus for the pine roots offers more insight into the function of the root reinforcement model than multiple values of reinforcing element tension, therefore for the root reinforcement model comparisons with

the direct shear tests involving pine roots, the multiple curves are associated with various values of modulus.

An attempt was made to fit the output from the root reinforcement model to exponential decay curves so *b*-values could be assigned to the shape of the model output and numerical comparisons between the direct shear tests and model output could be made. The deformed shape of the reinforcing elements produced by the root reinforcement model did not easily or nicely fit an exponential decay function. Therefore, the primary mode of model verification was visual comparison.

The worst fit between output from the root reinforcement model and the direct shear test results was for the high modulus reinforcing elements, the steel and aluminum rods. In both cases there was a poor fit between model output and test results regardless of the value of tension used in the root reinforcement model. The root reinforcement model over predicted the deflection of the reinforcing element throughout its length compared with the direct shear test results. Figures 5-1 and 5-2 show the envelope of shapes associated with the range of tension values modeled for the reinforcing elements. The outcomes are different enough that it seems reasonable to expect that the forces which would be required to create the different shapes would probably not be in close agreement either.

The success modeling the pine roots was mixed (Figures 5-3 to 5-5). The smallest value of modulus, 73,000 psi, resulted in shapes that didn't match very

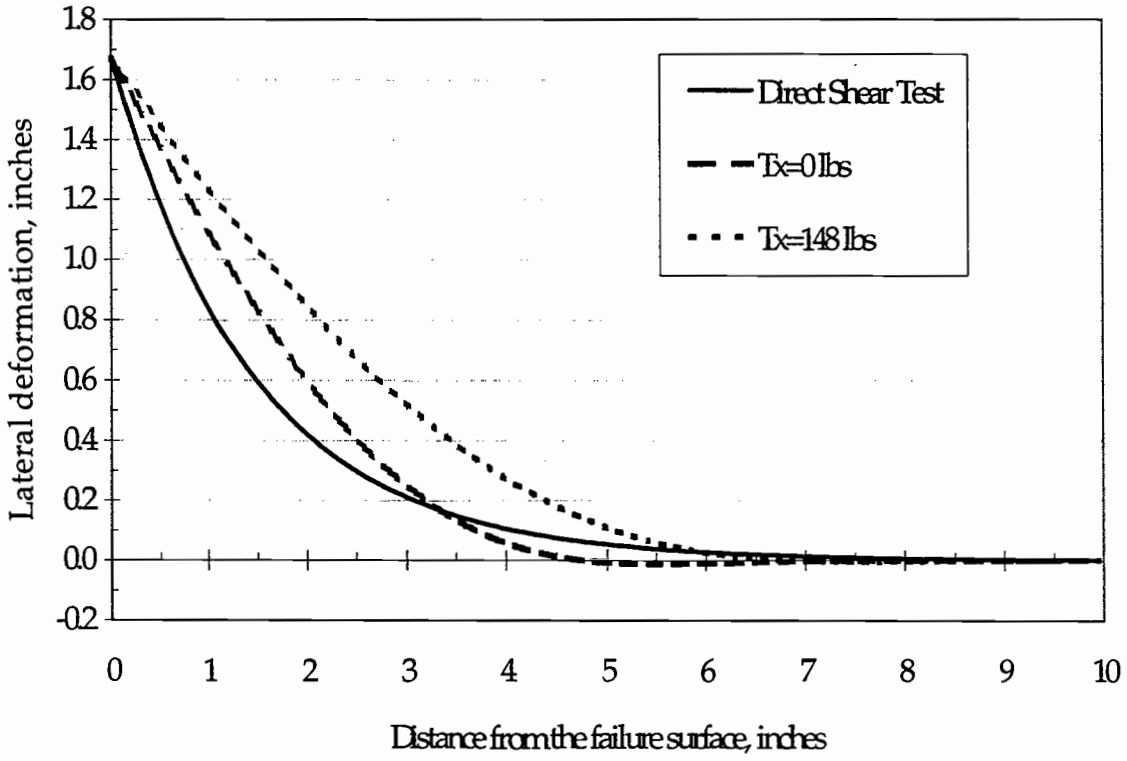

Figure 5-1. A graph of distance from the failure surface versus lateral deflection for a steel rod reinforcing element embedded in a cohesionless sand. The graph shows the results from a laboratory direct shear test (Shewbridge and Sitar, 1985) compared with output from the root reinforcement model run with no axial tension and the maximum calculated axial tension shown in the legend.

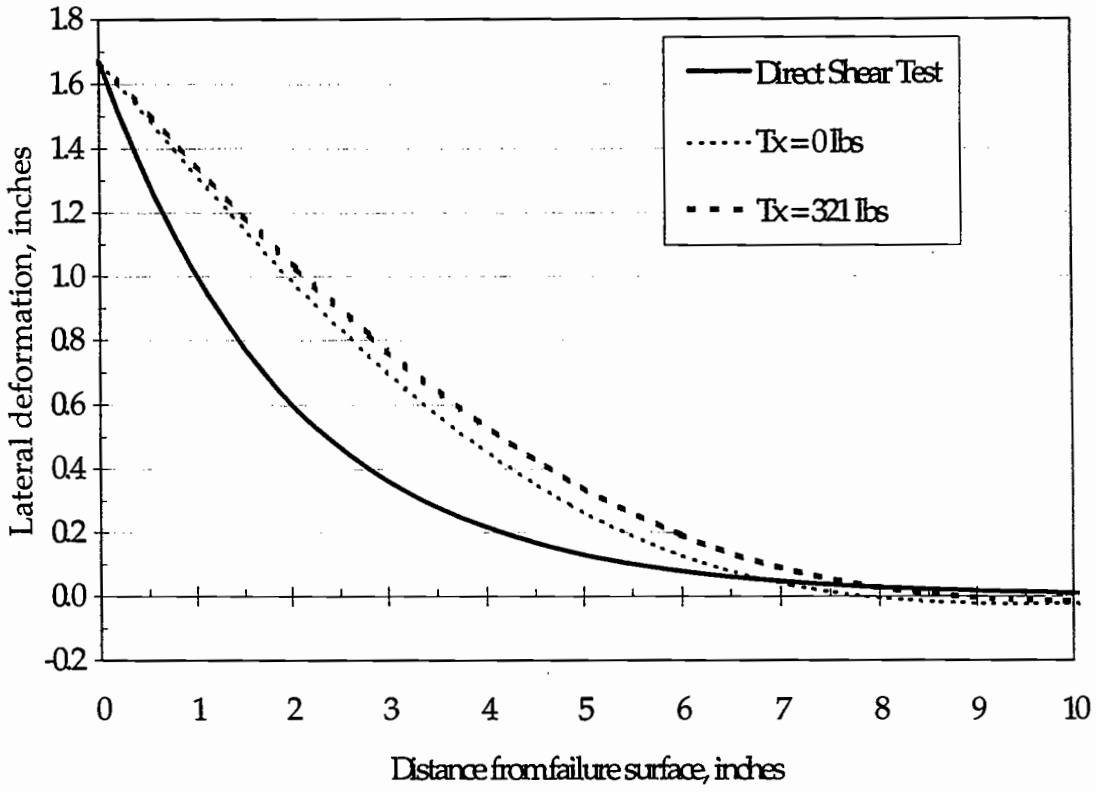

Figure 5-2. A graph of distance from the failure surface versus lateral deflection for an aluminum rod reinforcing element embedded in a cohesionless sand. The graph shows the results from a laboratory direct shear test (Shewbridge and Sitar, 1985) compared with output from the root reinforcement model run with no axial tension and the maximum calculated axial tension shown in the legend.

well for the three diameters modeled. The root reinforcement model underestimated the deflections when compared with direct shear test results throughout the length of the reinforcing element. The agreement between shapes was best for the largest value of modulus, 1,730,000 psi. Using this value of modulus with all the root diameters tested, the deflections were overestimated close to the failure surface and underestimated away from the failure surface. For the intermediate modulus value, 392,500 psi, the comparisons were also intermediate but, in general, were not good. The shape of the modeled root matched the direct shear test results very closely right at the failure surface but then very quickly the deflection was underestimated for the remainder of the length of the tested root. It is unclear why the stiffer modulus associated with wooden dowels would model the direct shear test results better than the other two values which are derived from actual tree roots and, in the case of the smallest modulus value, green tree roots.

The comparisons between deformed shapes for direct shear test results and root reinforcement model output for the wooden dowels are very good. The graphs are shown in Figures 5-6 and 5-7. The figures show an envelope of curves for a range of tensions for both of the diameters of wooden dowels tested. The breadth of the envelope associated with the different values of tension is an indicator of the relative importance of reinforcing element tension to the deflected shape of the reinforcing element. A comparison of the range in deflected shapes in the two graphs (Figures 5-3 and 5-4) indicate the importance

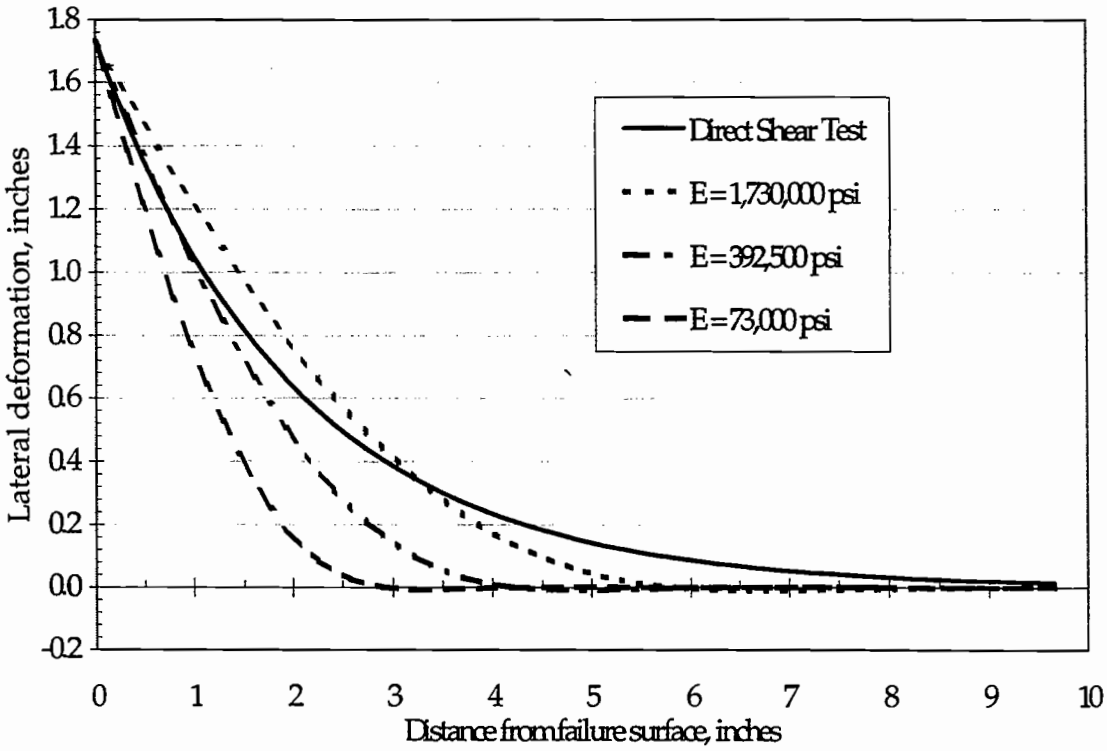

Figure 5-3. A graph of distance from the failure surface versus lateral deflection for a 0.32 inch diameter pine root reinforcing element embedded in a cohesionless sand. The graph shows the results from a laboratory direct shear test (Shewbridge and Sitar, 1985) compared with output from the root reinforcement model run with the three modulus of elasticity values shown in the legend.

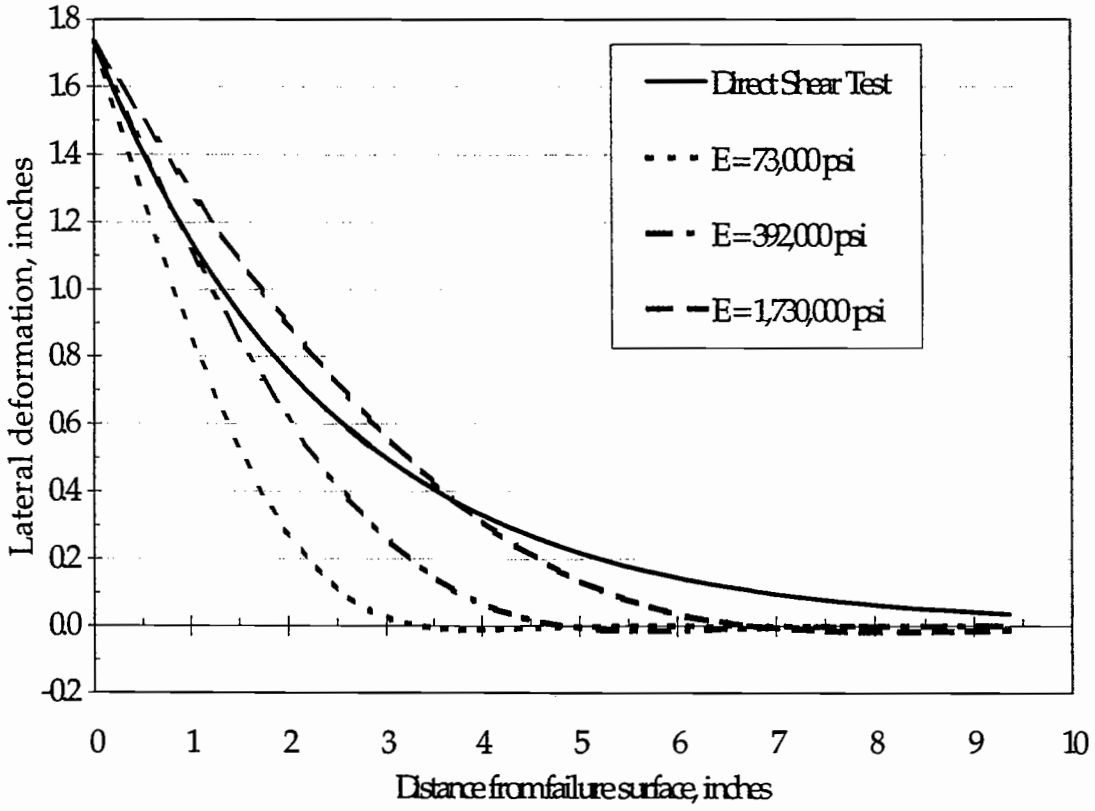

Figure 5-4. A graph of distance from the failure surface versus lateral deflection for a 0.43 inch diameter pine root reinforcing element embedded in a cohesionless sand. The graph shows the results from a laboratory direct shear test (Shewbridge and Sitar, 1985) compared with output from the root reinforcement model run with the three modulus of elasticity values shown in the legend.

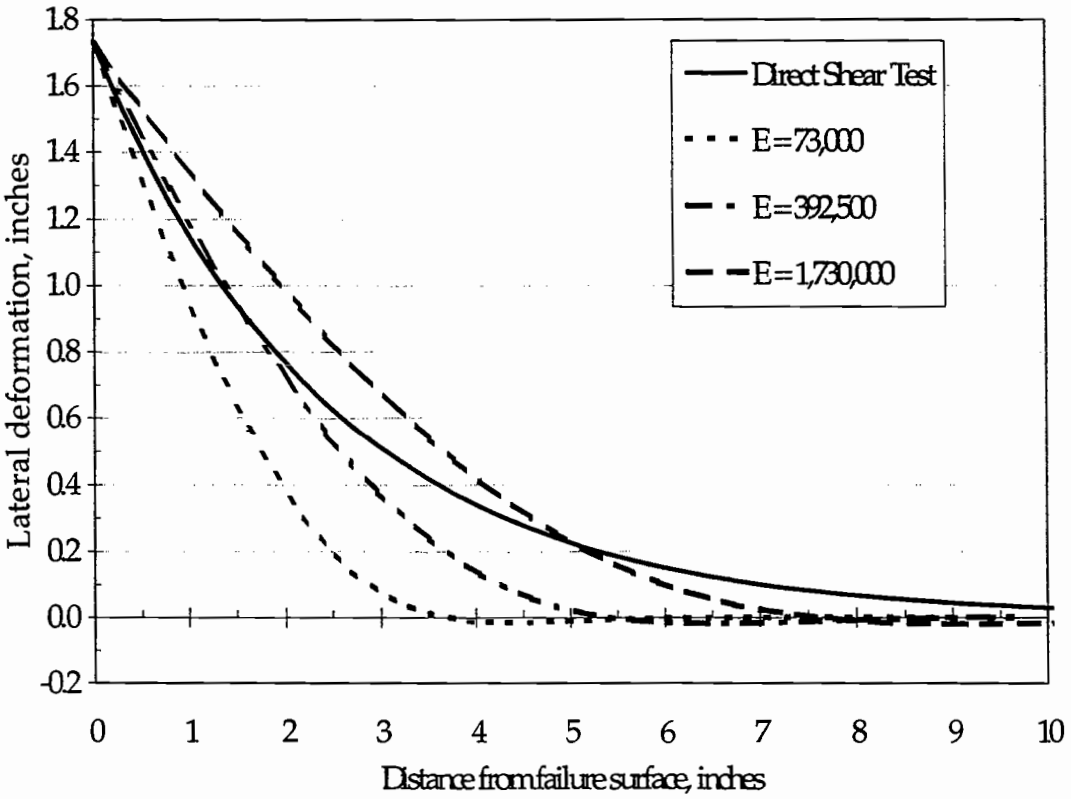

Figure 5-5. A graph of distance from the failure surface versus lateral deflection for a 0.54 inch diameter pine root reinforcing element embedded in a cohesionless sand. The graph shows the results from a laboratory direct shear test (Shewbridge and Sitar, 1985) compared with output from the root reinforcement model run with the three modulus of elasticity values shown in the legend.

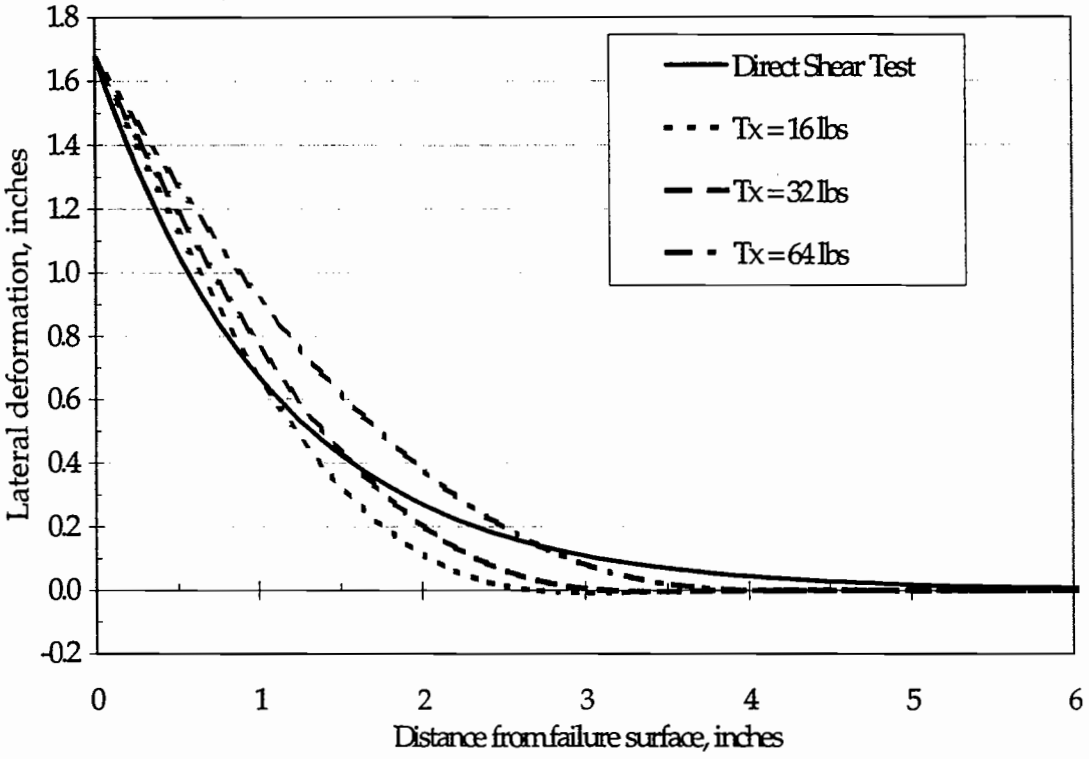

Figure 5-6. A graph of distance from the failure surface versus lateral deflection for a small, 0.13 inch diameter, wooden dowel reinforcing element embedded in a cohesionless sand. The graph shows the results from a laboratory direct shear test (Shewbridge and Sitar, 1985) compared with output from the root reinforcement model run with the three different axial tensions imposed on the solution. These three values are listed in the legend.

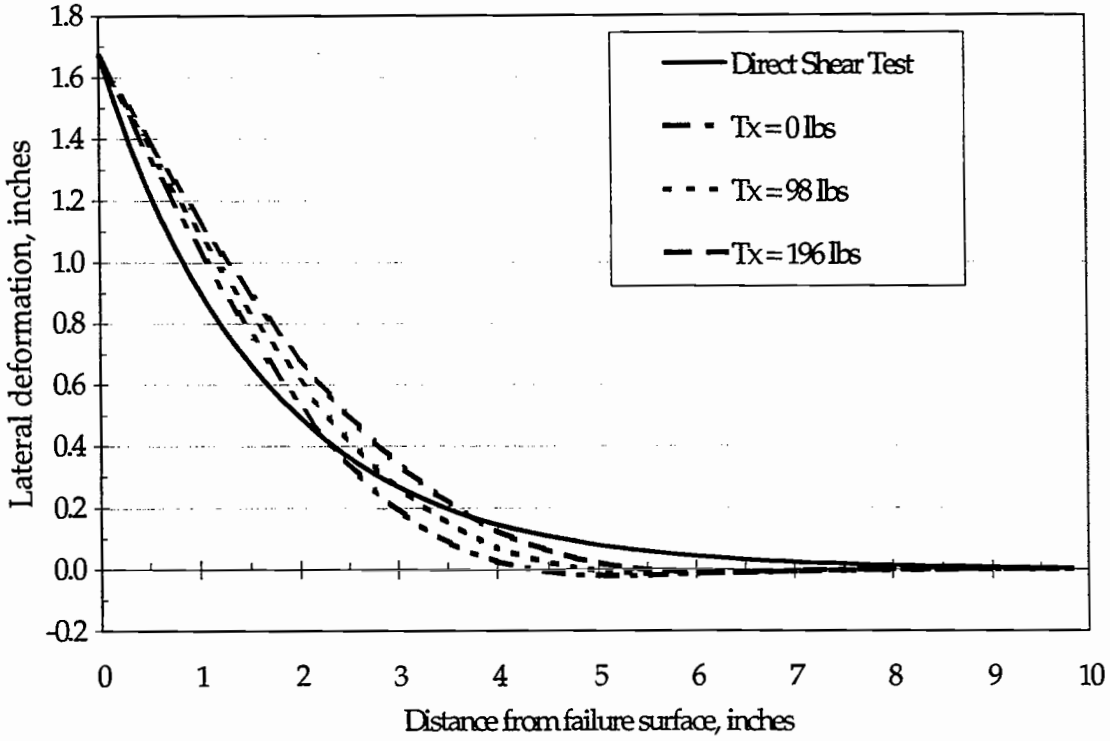

Figure 5-7. A graph of distance from the failure surface versus lateral deflection for a large, 0.31 inch diameter, wooden dowel reinforcing element embedded in a cohesionless sand. The graph shows the results from a laboratory direct shear test (Shewbridge and Sitar, 1985) compared with output from the root reinforcement model run with the three different axial tensions imposed on the solution. These three values are listed in the legend.

of the interaction between tension in the reinforcing element and its diameter. With both the large and small diameter wooden dowels, the predicted shapes straddle the results from the direct shear tests. Initially, the predicted deflections are greater than the actual deflections directly adjacent to the failure surface, then the trend reverses and the predicted deflections are less than the actual deflections. The trend is similar for all the predicted curves, the crossover just occurs in different locations. When the vagaries associated with generating the exponential decay curves from the deformed shape of reinforcing elements and the root reinforcement modeling process are considered, the model verification results for the wooden dowels is really quite good.

The model verification results for the parachute cord are also quite good (Figure 5-8). This is an important result because in all the previous results the only situation that gave acceptable results was wooden reinforcing elements with a modulus of 1,730,000 psi and an apparent skin friction of 35°. This included the results for both large and small wooden dowels and all three diameters of pine roots at the highest modulus value. The results from high modulus, low skin friction metal reinforcing elements and for the low modulus pine roots did not compare well with the direct shear results. However, the parachute cord has a low modulus, 213,000 psi, and a high apparent skin friction and the model output compared very well with the direct shear results. This increases the comfort level that the root reinforcement model is a valid tool and can be used to interrogate the root reinforcement process.

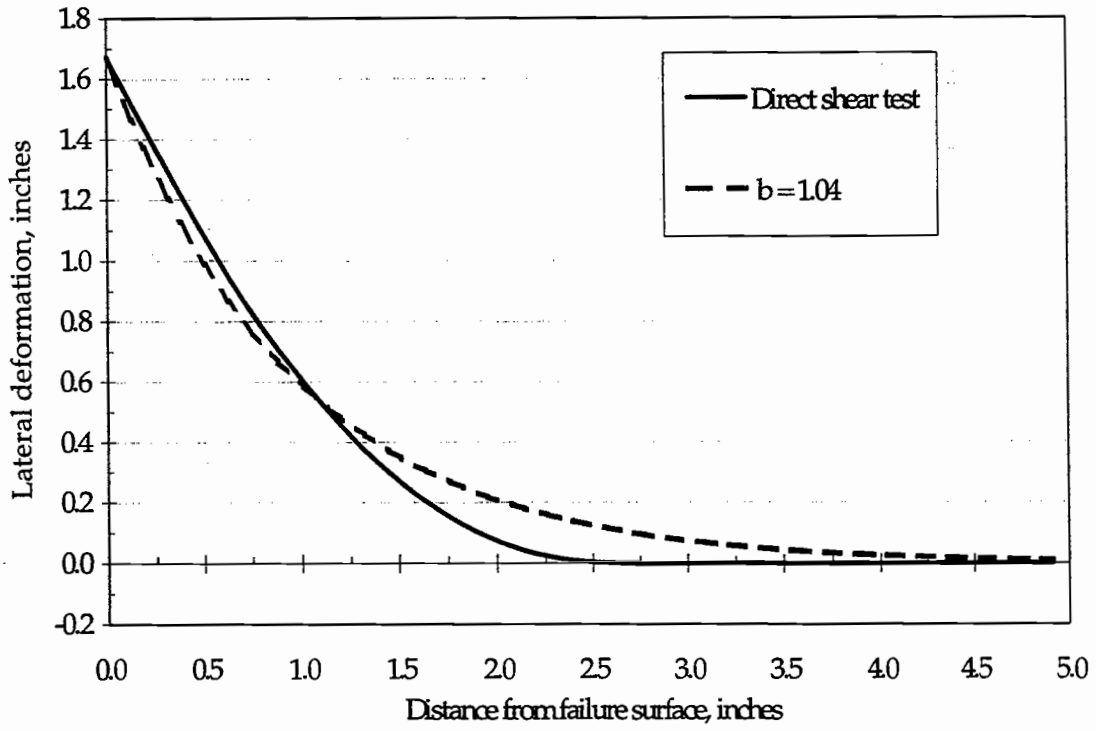

Figure 5-8. A graph of distance from the failure surface versus lateral deflection for a parachute chord reinforcing element embedded in a cohesionless sand. The graph shows the results from a laboratory direct shear test (Shewbridge and Sitar, 1985) compared with output from the root reinforcement model.

The verification of the root reinforcement model has proceeded in a manner that was not quantitatively rigorous, however there is no doubt that it can perform adequately for the task required. The modeled output for the wooden reinforcing elements compared very well with direct shear results from both Shewbridge and Sitar (1985;1989) and Abe and Ziemer (1991). While the model output did not overlap the direct shear results exactly, it was certainly within order-of-magnitude accuracy. Furthermore, any existing mismatch could just as easily be associated with the process that generated exponential curves from direct shear test results (Shewbridge and Sitar, 1989; Abe and Ziemer, 1991) as with the root reinforcement model. For those situations where the model output and the direct shear results were a good match, it seems reasonable to expect that the forces calculated by the root reinforcement model that would cause the calculated deflections should match the forces required to generate the deflected shape in the direct shear tests. It is comforting that the situations where the model seems to have performed the best, namely, wooden reinforcing elements with constant modulus properties and constant shear-stress transfer values throughout their length, are those situations of most interest to this project.

The goal of model verification was to determine if the model would generate output which was within correct order-of-magnitude range, if model output would respond intuitively to changes in input parameters, and if model output would be responsive enough to allow "what-if" scenarios. The output

from the root reinforcement model has certainly shown order-of-magnitude accuracy with the overlap of modeled and deflected shapes. It is hard to believe that with the overlap of the deflected shapes, that the forces generated from the shapes wouldn't have similar levels of accuracy. Furthermore, a range of reinforcing element diameters, elastic modulus values, and reinforcing element tensions have been modeled and the model has responded appropriately and intuitively to these changes in input. The root reinforcement model has performed well enough for this project to continue with the parameter study.

Parameter Study

The purpose of this part of the dissertation is to investigate how the output of the model responds to changes in selected input parameters. Input parameters that are expected to have a normal range of values, such as root diameter and the root's depth in the soil, were varied, while parameters that are expected to remain constant, like the modulus of elasticity of roots, soil density, and internal angle of friction of the soil, were not varied. Those input parameters that were varied, were tested over a range of values normally expected for a shallow, cohesionless soil on a landslide-prone forested slope.

One of the parameters that was not varied was soil type. The soil was assumed to be a clean, cohesionless, loose sand with a dry density of 90 lbs/ft^3.

Soil strength was representative of how it would vary normally. There was no cohesion so *c* was zero throughout this parameter study (as well as all other runs of the model). The internal angle of friction was assumed to be 44° for soil depths of 12 and 18 inches and was 47° for the 6 inch depth. The variation in internal angle of friction is a consequence of lower confining stresses at shallow depths. In cohesionless soils at low confining pressures, the internal angle of friction is a function of the confining stress and increases with decreasing confining pressure (Lambe and Whitman, 1969; Holtz and Kovacs, 1981). As reported by Commandeur (1989), at a confining stress equivalent to a 6 inch depth of loose, 90 lbs/ft^3 dry sand, the internal angle of friction is 47°.

The type of reinforcing elements and the modulus of elasticity of the reinforcing elements were also held constant. The reinforcing elements were assumed to be Douglas-fir roots with a modulus of elasticity of 73,000 lbs/in^2.

The input values that were varied are the diameter of the reinforcing elements, the soil depth the reinforcing elements were modeled at, and the shear-stress transfer functions. Three root diameters were modeled; 0.1, 0.25, and 0.5 inches. These three diameters were chosen as representative of the distribution of diameters available in shallow, landslide-prone, forest soils. Burroughs and Thomas (1977) studied the distribution of diameters for Douglas-fir roots in a shallow, forest soil in the Oregon Coast Range. Their data is listed in Table 5-2 which shows the number of Douglas-fir roots per unit area of soil for six diameter size classes. These data are the best available to indicate the number

and diameter distribution of tree roots most likely be found in failure surfaces of naturally occurring landslides. Table 5-2 shows that 90 percent of the roots are

Table 5-2. The number of roots per square meter and square foot of forest soil for six diameter size classes for a Douglas-fir forest in the Oregon Coast Range (Burroughs and Thomas, 1977).

Diameter size class	N/m^2	N/ft^2
0 - 4 mm (0 - 0.16 in)	90.42	8.4
4 - 10 mm (0.16 - 0.39 in)	7.90	0.75
1.1 - 2 cm (0.39 - 0.78 in)	1.59	0.147
2.1 - 4 cm (0.79 - 1.59 in)	0.409	0.038
4.1 - 6 cm (1.6 - 2.38 in)	0.106	0.00987
6.1 - 8 cm (2.39 - 3.17 in)	0.104	0.00971
Total	100.53	9.35

0-4 mm in diameter, 8 percent are between 4 and 10 mm in diameter, and the remaining 2 percent of the roots are 1 to 8 cm in diameter. The three root diameters modeled were chosen to represent these three size classes. The 0.1 inch (2.5 mm) diameter root represents the 0 to 4 mm size class, the 0.25 inch (6.4 mm) diameter root represents the 4 to 10 mm size class, and the 0.5 inch (12.7 mm) diameter root represents all roots greater than 1 cm in diameter. The choice of just three root diameter classes is, admittedly, a compromise between accuracy of the output and workload. More root diameter size classes would model the

actual situation more accurately but would also take more time to complete the required runs of the root reinforcement model for each size class. The choice of the three size classes, hopefully, optimizes the combination of workload and accuracy.

The roots were modeled at three soil depths; 6, 12, and 18 inches. These three depths represent the range of soil depths that conifer roots are found in shallow, forest soils. Finally, the shear-stress transfer functions used in the root reinforcement model were used both with and without scaling coefficients. One run of the model was made with the shear-stress transfer functions as reported by Commandeur (1989) and a second run of the model was made with the appropriate scaling coefficient for the shear-stress transfer function with all other parameters remaining fixed. The shear-stress transfer function that was used for the 6-inch soil depth is:

$$\tau = \frac{z}{.0562 + (0.770)z + (0.667)z^2} \qquad 5\text{-}3$$

and the shear-stress transfer function used for both the 12- and 18- inch soil depths is:

$$\tau = \frac{z}{0.03 + (0.596)z + (0.325)z^2} \qquad 5\text{-}4$$

The scaling coefficients for the three depths are 0.14085, 0.1819, and 0.26808 (all the significant digits were used in the model) for the 6-, 12-, and 18-inch depths, respectively.

In this parameter study, the roots were modeled through a series of lateral deflections. Unlike the model verification, where information was known only at the extreme deflections, the objective of this portion of the study was to model how the roots will perform through a series of deflections from very slight to extreme. The lateral deflections of the root at the failure surface used in the parameter study are; 0.05, 0.1, 0.25, 0.5, 0.75, 1.0, 1.25, 1.5, 1.75, and 2.0 inches (Figure 5-9). All the input values used in the parameter study are listed in Table 5-3.

The information needed to calculate the increase in soil strength attributed to the reinforcing elements is the tensile and shear force in the reinforcing element and the angle of reinforcing element at the failure surface. This model output is different than the information required to calculate the increase in soil strength and must be converted. The lateral and tensile force applied to the reinforcing element are applied perpendicular and parallel to the failure surface and must be converted to the tensile and shear force in the reinforcing element (Figure 4-3). The following section describes and illustrates the process of converting the root reinforcement model output to a more usable form followed by a description of how different model inputs affect model output.

Table 5-3. Input values used in the parameter study of the root reinforcement model.

Input Parameter	Parameter Value
Soil Type	clean, loose, and cohesionless
Soil Strength	c = 0; $\phi = 44^o$
Soil Density	90 lbs/ft^3
Depth of Reinforcing Elements	6-, 12-, & 18-inches
Modulus of Reinforcing Elements	73,000 lbs/in^2
Diameter of Reinforcing Elements	0.1-, 0.25, 0.5-inches
Scaling Coefficients for Shear-Stress Transfer Functions	6" depth- 0.14085 12" depth- 0.1819 18" depth- 0.26808
Reinforcing Element Deflections	.05, .1, .25, .5, .75, 1.0, 1.25, 1.5, 1.75, & 2.0 in.

Output generated by the root reinforcement model, as discussed previously, is the deformed shape of the reinforcing element and the forces applied to the reinforcing element parallel and perpendicular to the failure surface that produce the deformed shape. Model output for the force parallel to the failure surface is labeled V_y and the model output perpendicular to the failure surface is labeled T_x. The angle the root makes with its original, undeflected

shape is labeled θ (Figure 4-3). All of these quantities were calculated for a 0.25 inch diameter root embedded one foot deep in a sandy soil with a scaling coefficient of 0.1819. The modeled shape of the 0.25 inch diameter root deformed through the complete sequence of lateral deflections is shown in Figure 5-9. A graph of V_y and T_x versus the lateral deflection of the reinforcing element at the failure surface is shown in Figure 5-10. Both quantities show, in essence, a linear increase in magnitude as a function of increasing deflection. The force parallel to the failure surface, V_y, starts out greater than the axial force, T_x, and stays higher throughout the range of deflections.

The shear and tensile force in the reinforcing element are calculated using the following relationships,

$$V = V_y \cos\theta - T_x \sin\theta \qquad 5\text{-}5$$

$$T = T_x \cos\theta + V_y \sin\theta \qquad 5\text{-}6$$

The applied force parallel to the failure surface is V_y and the applied force perpendicular to the failure surface is T_x and both are outputs from the root reinforcement model. The values are converted to tension, T, and shear, V, in the reinforcing element. From the deflected shape of the reinforcing element, θ, the angle the root makes with its original, vertical position at the failure surface, is

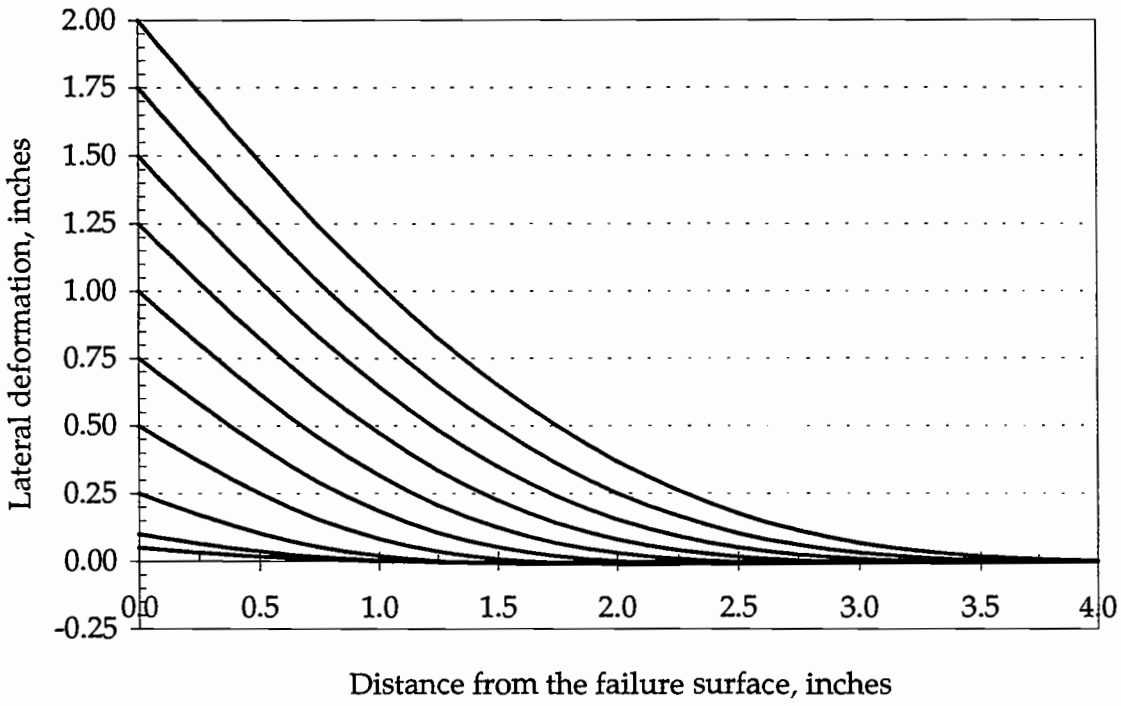

Figure 5-9. The deformed shapes of a 0.25 inch root deflected through the complete sequence of lateral deformations. The input parameters for the root reinforcement model resulting in this sequence of shapes is listed in Table 5-2.

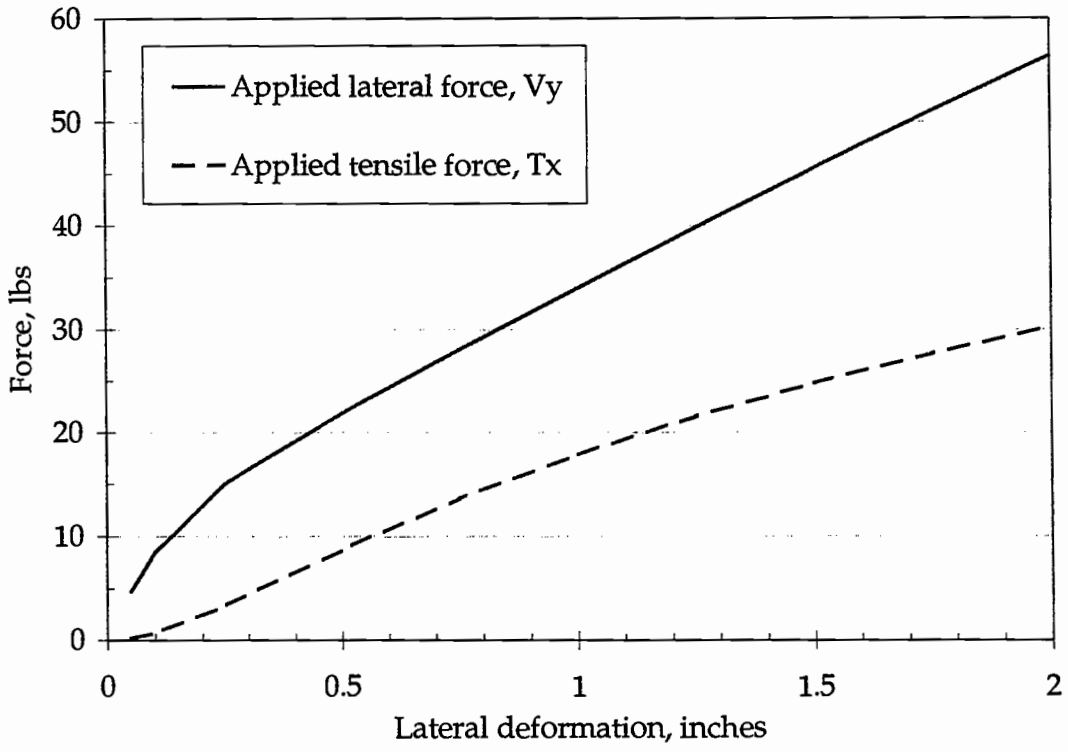

Figure 5-10. A graph of output from the root reinforcement model of applied lateral force, V_y, and tensile force, T_x, on a root versus lateral deformation at the failure surface for a 0.25 inch diameter root in a one foot deep sandy soil.

calculated. This angle is used to convert the forces parallel and perpendicular to the failure surface to forces parallel and perpendicular to the reinforcing element cross-section. It is these forces that are used to calculate the increased strength of the soil due to the reinforcing element.

As observed in Figure 5-11, initially the shear force, *V*, is greater than the tensile force, *T*, however, these two forces crossover very quickly and after the crossover the tensile force increases linearly with increasing deflection and the shear force decreases slightly but, essentially, settles on a single value with increasing deflection. This output clearly shows the importance of the tensile force in adding strength to reinforced soil when low modulus reinforcing elements are used. While there is a shear force component in the reinforcing element which adds strength to the reinforced soil as the geometry of the reinforcing element changes with increasing deflection, the shear force remains essentially constant while the tensile force increases linearly. This leads to the observation that increasing deflection will cause the reinforcing element to fail in tension while failure of the reinforcing element in shear probably will not occur.

The effect of root diameter on increased soil strength by root reinforcement was investigated by modeling tensile and shear forces in 0.1, 0.25, and 0.5 inch diameter roots at a 12 inch soil depth using scaling coefficients with shear-stress transfer functions. The effect of root diameter on the tensile and shear forces in the root as a function of deflection are shown in Figures 5-12.

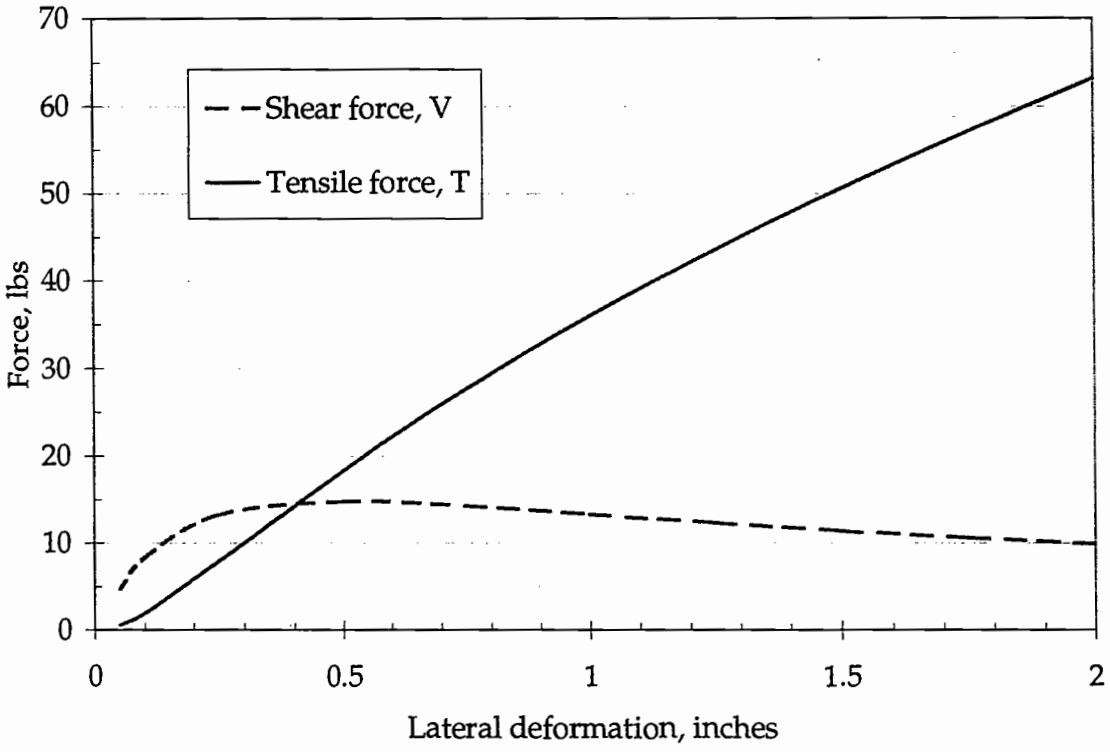

Figure 5-11. A graph of output from the root reinforcement model of the tensile force, T, and shear force, V, in a root at the failure surface versus lateral deformation for a 0.25 inch diameter root in a one foot deep sandy soil.

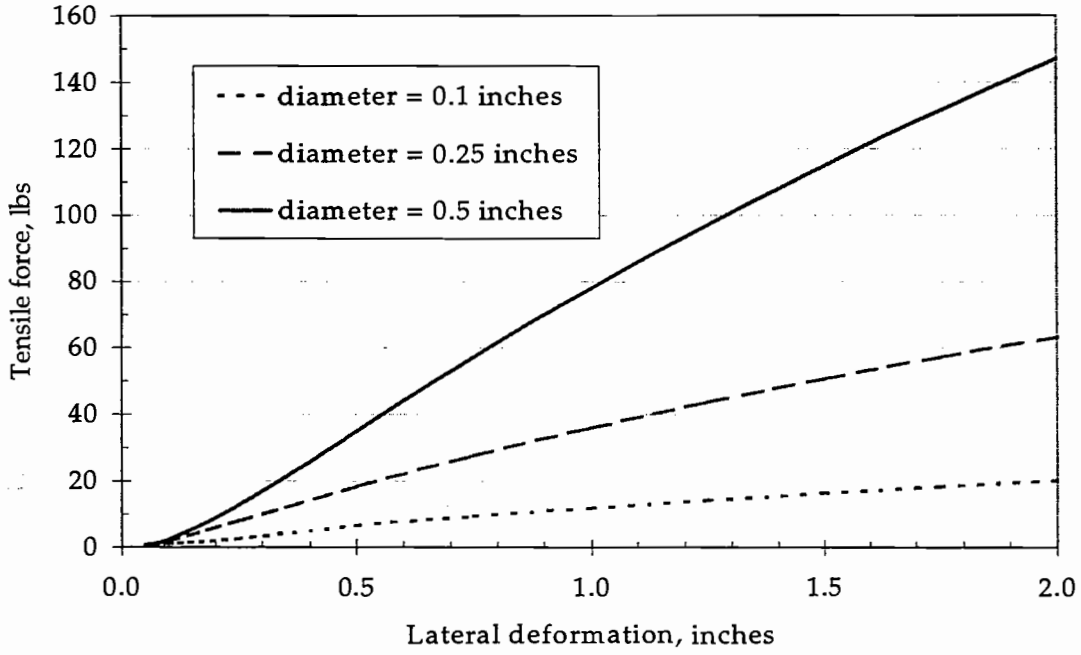

(a)

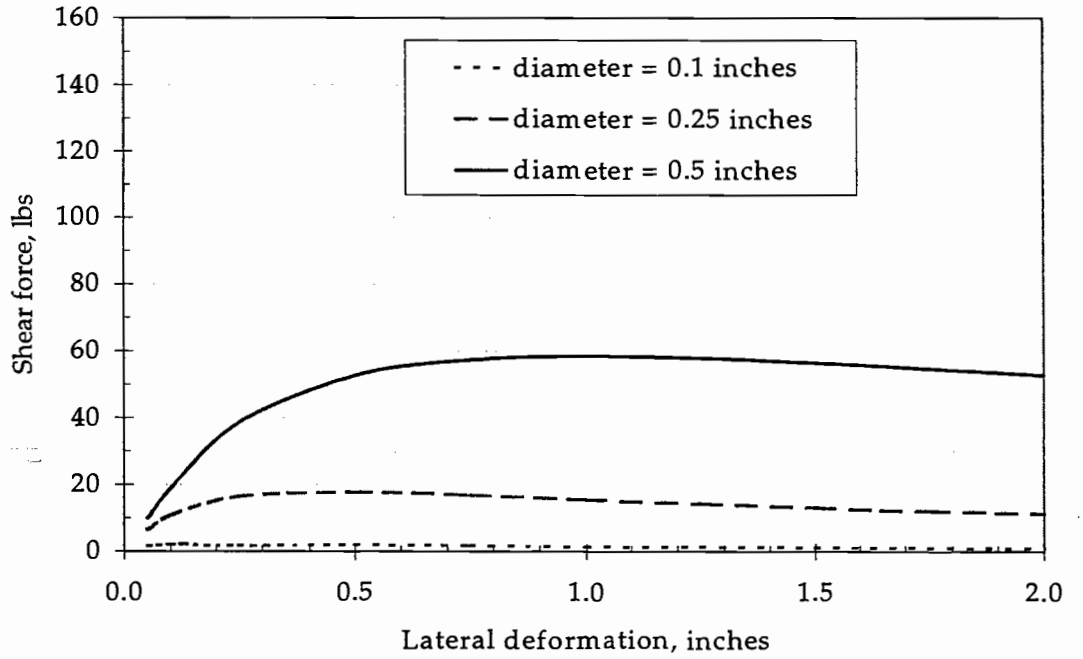

(b)

Figure 5-12. The effect of root diameter on (a) the modeled tensile forces and (b) the modeled shear forces as a function of lateral deformation for three different diameter roots (0.1, 0.25, and 0.5 inches) embedded one foot deep in a sandy soil.

For the tensile force, the shape of the curves are the same with a linear increase in tensile force throughout the range of modeled deflection. For a given deflection, the tensile force increases with increasing diameter. Larger diameter roots develop proportionately more tensile force than smaller diameter roots. For the shear force, the curves for all three diameter roots are shaped similarly. The maximum shear force occurs at larger deflections for larger diameter roots. The maximum shear force or, for a given deflection, the increase in shear force also increases with increasing root diameter. The larger diameter roots develop proportionately more shear force than smaller diameter roots.

Figure 5-13 shows the effect of soil depth on the tensile and shear forces in the modeled root. To show the effect of soil depth, a 0.25 inch diameter root was modeled at 6, 12, and 18 inch soil depths and scaling coefficients were used with the shear-stress transfer functions. Once again, for the tensile force the curves are all similarly shaped. The effect of soil depth on tensile force is less than the effect of root diameter and at any deflection the increase in tensile force appears to be a linear function of soil depth which is an expected result. The effect of soil depth on the shear force is similar to its effect on tensile force. The shape of the curves are all similar and the maximum shear force appears to occur at a deflection of approximately 0.5 inches. At deflections up to 1.0 to 1.2 inches, the shear force appears to be a linear function of depth but beyond a deflection of about 1.2 inches, the curves do not maintain their relationship.

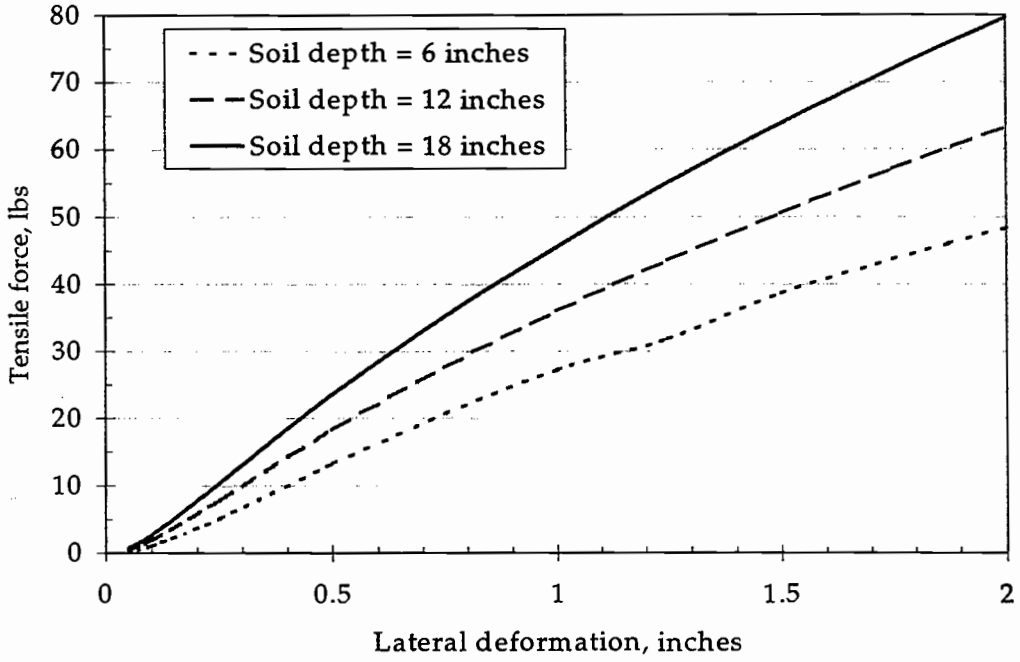

(a)

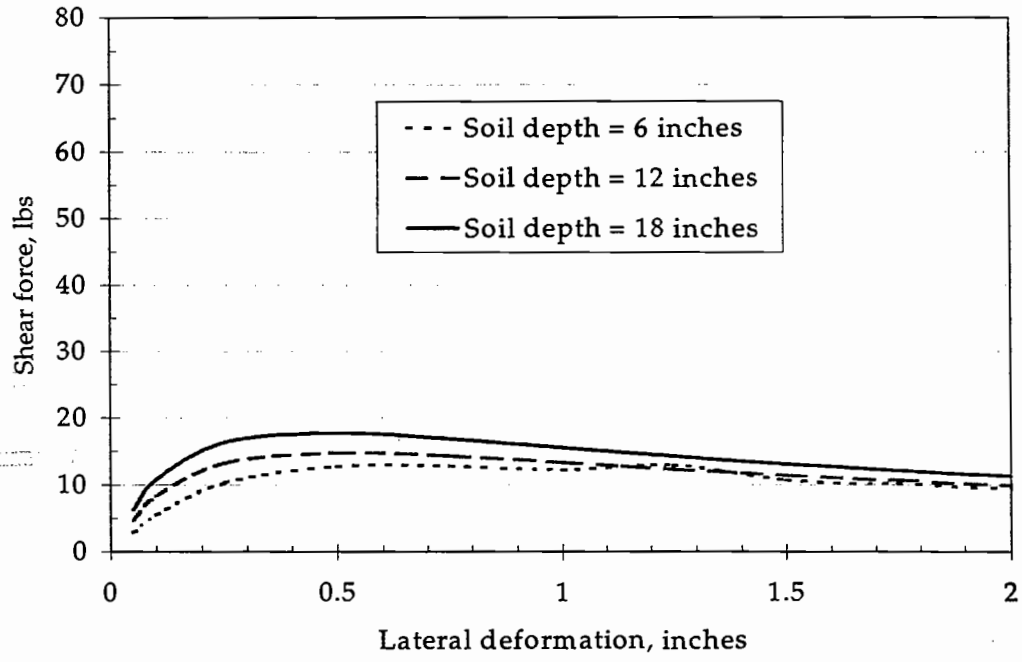

(b)

Figure 5-13. The effect of three soil depths, 6, 12, and 18 inches, on the modeled tensile (a) and shear (b) forces in a 0.25 inch root as a function of lateral deformation.

The effect of using a scaling coefficient with the shear-stress transfer functions on the shear and tensile forces in the reinforcing element is shown in Figure 5-14. For most of the situations, root reinforcement was modeled both with and without using scaling coefficients. The results all showed a consistent pattern which is illustrated with the 0.25 inch root at a 12 inches soil depth. The use of the scaling coefficient has an effect, although it is minor, on the geometry of the deflected root. The use of a scaling coefficient means less tension is developed in the reinforcing element at a given deflection. Less tension in the reinforcing element translates into a more flexible root which will result in the root making greater angle with vertical at the failure plane. This greater angle translates accordingly during the force conversions to tension and shear in the reinforcing element. However, the modeled increase in the angle of the reinforcing element which is brought about by a more flexible root is insufficient to offset the primary effect. The primary effect is that without a scaling coefficient greater shear and tensile forces are generated at any deflection. This effect is shown in Figure 5-14. Without a scaling coefficient the model output had increased tension perpendicular to the failure surface which means a stiffer root which requires greater force parallel to the failure surface to achieve a given deflection. During the conversion of model output to tensile and shear force in the reinforcing element, the increased applied forces translate into a much greater tensile force in the reinforcing element root and a slightly increased shear

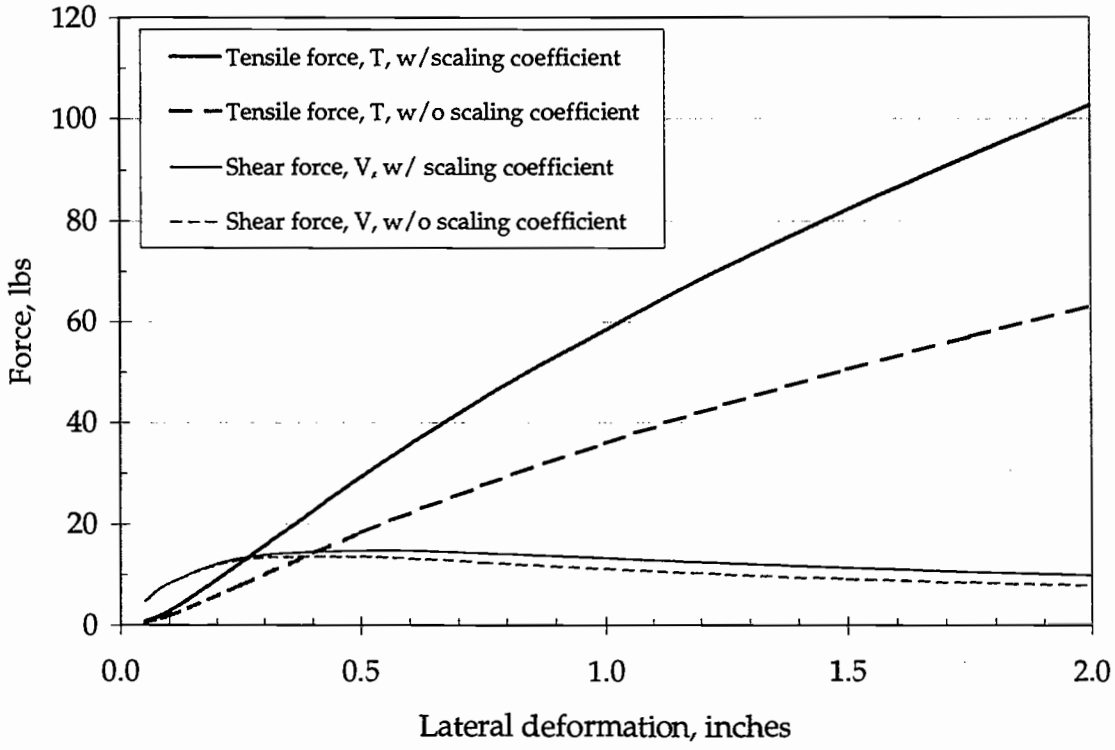

Figure 5-14. The effect of using a scaling coefficient with the shear-stress transfer functions in the root reinforcement model on the computed tensile and shear forces in a 0.25 inch diameter root embedded one foot deep in a sandy soil.

force. The greatest effect is to the tensile force, however, which has the greatest influence on the values of root reinforcement.

Once the tension and shear in the reinforcing element have been calculated, then the increase in soil strength attributed to the reinforcing element can be calculated. This is done using equation 4-3, which is shown below.

$$\Delta S = \frac{T}{A}\sin\theta + \frac{V}{A}\cos\theta + \left(\frac{T}{A}\cos\theta - \frac{V}{A}\sin\theta + \sigma_n\right)\tan\phi' \qquad 4\text{-}3$$

This equation calculates the increase in soil strength ΔS, given tension, T, and shear, V, in the reinforcing element, the angle, θ, that the reinforcing element has deformed from its original vertical position, and the cross sectional area of soil, A, that the strength is spread over.

A composite soil strength can be calculated using equation 4-4. This equation is,

$$S_{comp} = S + \Delta S = \left[c' + \frac{T}{A}\sin\theta + \frac{V}{A}\cos\theta\right] + \left[\frac{T}{A}\cos\theta - \frac{V}{A}\sin\theta + \sigma_n\right]\tan\phi' \qquad 4\text{-}4$$

which incorporates the soil cohesion, c', and the normal stress of the soil σ_n, into equation 4-3.

This simple exercise was carried out for the test case being modeled. The increase in strength was calculated for each of the three different diameter roots

embedded in a shallow cohesionless soil one foot deep. The calculation was carried out for the range of lateral deflections listed in Table 5-1.

The increase in soil strength attributed to one root of each diameter embedded in one square foot of sand is shown in Figure 5-15. For the model output shown in Figure 5-15 (a), the soil strength increase due to root reinforcement was calculated using a scaling coefficient with the shear stress transfer functions and for Figure 5-15 (b), the soil strength increase was calculated without using a scaling coefficient. As discussed, without a scaling coefficient, the calculated increase in tension is greater and thus at any given deflection the calculated increase in strength is greater.

The strength increases are minor at the small deflections. At the smallest lateral deflection, the 0.1 inch diameter root caused a calculated increase in soil strength of 1.8 lbs/ft^2 (0.09 kPa). For the 0.25 inch root the calculated increase in soil strength was 5.2 lbs/ft^2 (0.25 kPa) and for the 0.5 inch root the calculated increase in soil strength was 10.4 lbs/ft^2 (0.5 kPa). As lateral deflection increases, the magnitude of the increase in soil strength increases, in essence, linearly.

For the 0.1 inch diameter root, the graphs terminate at deflections of 1.5 and 0.75 inches for the cases of with and without a scaling coefficient, respectively. The graphs terminate at these deflections because the root reached its ultimate strength. The ultimate strength of a 0.1 inch diameter root was calculated using Commandeur's (1989) relationship, $T_R=1750.9(DIB)^2$, where T_R is the ultimate load at rupture and *DIB* is the diameter inside bark for the root.

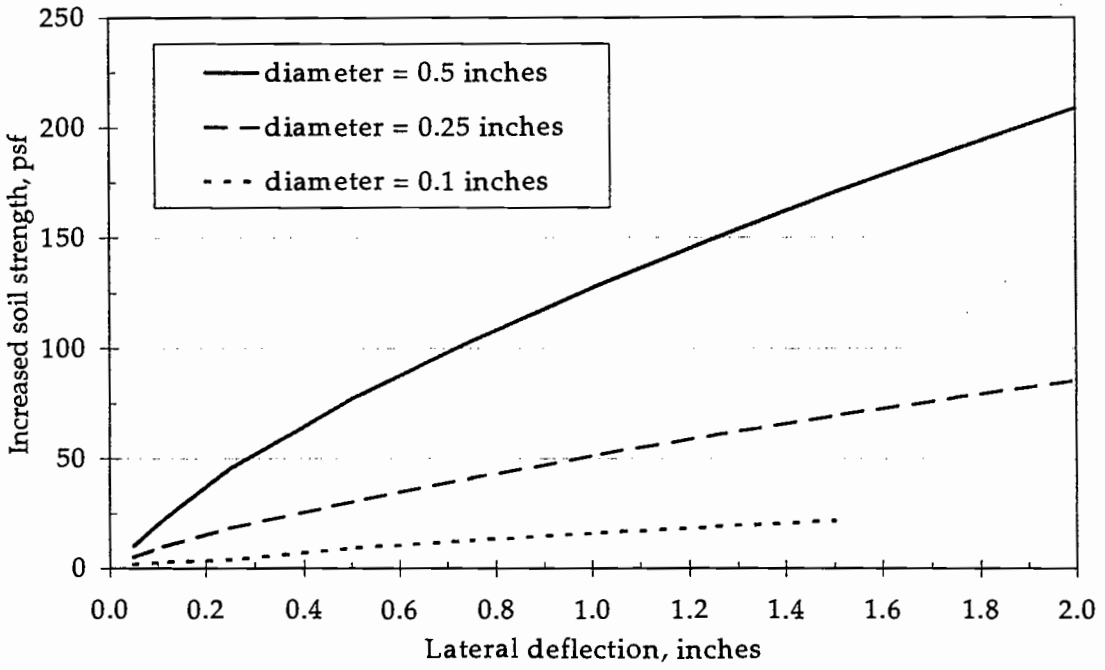

(a)

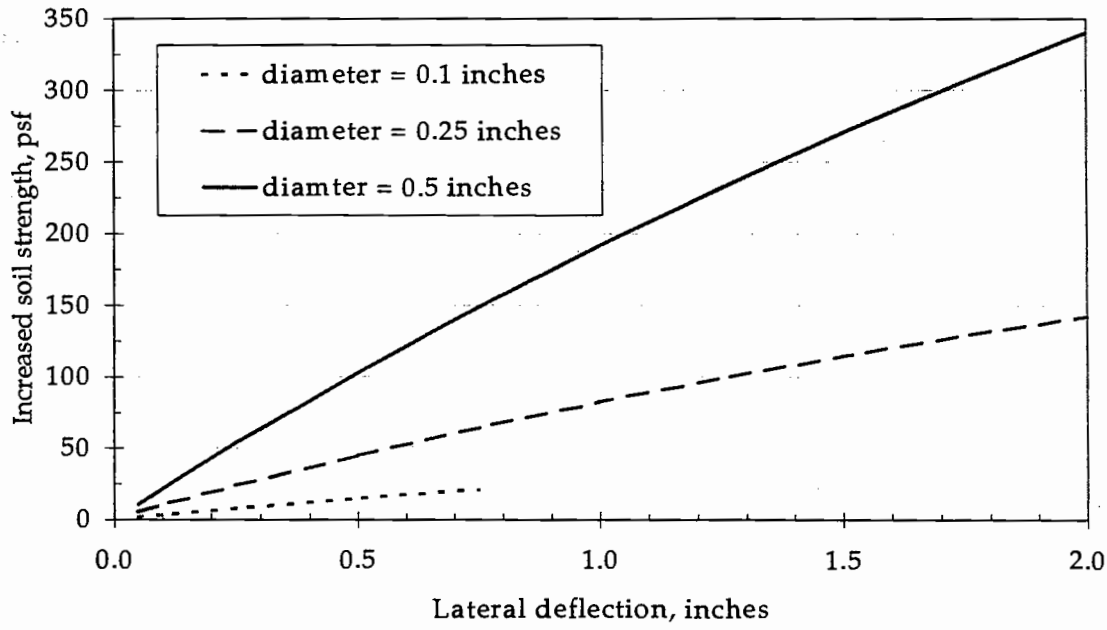

(b)

Figure 5-15. The effect of root diameter on the modeled increase in soil strength of one root per size class in one square foot of soil. A scaling coefficient was used with the shear-stress transfer functions in (a) and no scaling coefficient was used in (b). The roots were embedded in a sandy soil one foot deep.

Assuming the 0.1 inch diameter is inside bark, the rupture load is 17.5 pounds. At rupture, a single 0.1 inch diameter root per square foot of soil increased the soil strength 21.6 and 20.9 lbs/ft^2 (1.03 and 1.0 kPa) for the case of with and without a scaling coefficient, respectively.

At a maximum lateral deflection of 2.0 inches, a single 0.25 inch diameter root per square foot of soil increased soil strength by 85.6 lbs/ft^2 (4.1 kPa) with a scaling coefficient and by 142.6 lbs/ft^2 (6.8 kPa) without a scaling coefficient. A single 0.5 inch diameter root per square foot of soil increased soil strength by 209.0 and 340.1 lbs/ft^2 (10.0 and 16.3 kPa) for with and without a scaling coefficient, respectively. Recall that the lateral deflection of the root is only one half the lateral deflection of the soil block. Rupture strength was not approached by either the 0.25 or 0.5 inch diameter roots.

The increased soil strength values reported above are not really representative of how forested soils will perform because the diameter distribution of roots in a forest soil is not a single diameter root per square foot of soil. Increased soil strength values were calculated that were more representative of true field conditions. The model results for the single diameter roots were weighted by the number of roots that diameter class represented. Table 5-2 lists the diameter class and number of roots per unit area expected for a mature, late seral stage, Douglas-fir forest in the Oregon Coast Range (Burroughs and Thomas, 1977).

To calculate the total increase in soil strength attributed to the number and diameter distribution of roots in the representative forest soil, the model output for each diameter root was multiplied by the number of roots that size represented from Table 5-2. The output from the 0.1 inch diameter root was multiplied by 8.4, the output for the 0.25 inch diameter root was multiplied by 0.7, and the output for the 0.5 inch diameter root was multiplied by 0.2.

The output from these calculations is shown in Figures 5-16. The results from calculations using a scaling coefficient are shown in Figure 5-16 (a) and Figure 4-16 (b) shows the results from calculations made without using a scaling coefficient.

The graphs show clearly how dependent the increased strength is on the smallest size fraction root. This, of course, is simply a matter of numbers. Approximately 90 percent of the roots are in the smallest size class. The increased soil strength is initially low at the smallest lateral deflection, an approximate increase in soil strength of 21 lbs/ft^2 (1.0 kPa) for both with and without a scaling coefficient. The increase in soil strength does not increase linearly throughout the range of lateral deflections, but peaks at the rupture strength of the smallest sized roots. After the small roots rupture, the strength decreases and then increase again but do not return to peak strength levels within the range of lateral deflections tested. The peak increase in soil strength for both cases is similar. For the case where a scaling coefficient was used the peak increase in strength was 264 lbs/ft^2 (12.6 kPa) and for the case where a scaling coefficient

was not used the peak increase in soil strength was 250.5 lbs/ft^2 (12.0 kPa). Even though the lateral deflections at the peak increase in soil strength are different by a factor of 2, the peak increase in soil strength is essentially the same due to the fact that the peak soil strength is governed by the rupture strength of the small roots.

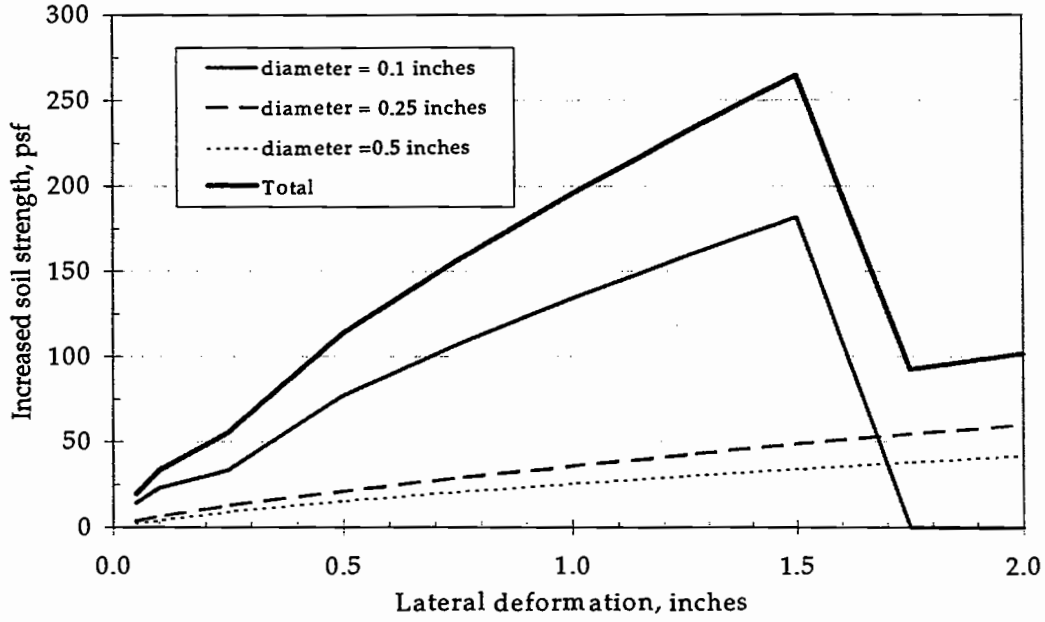

(a)

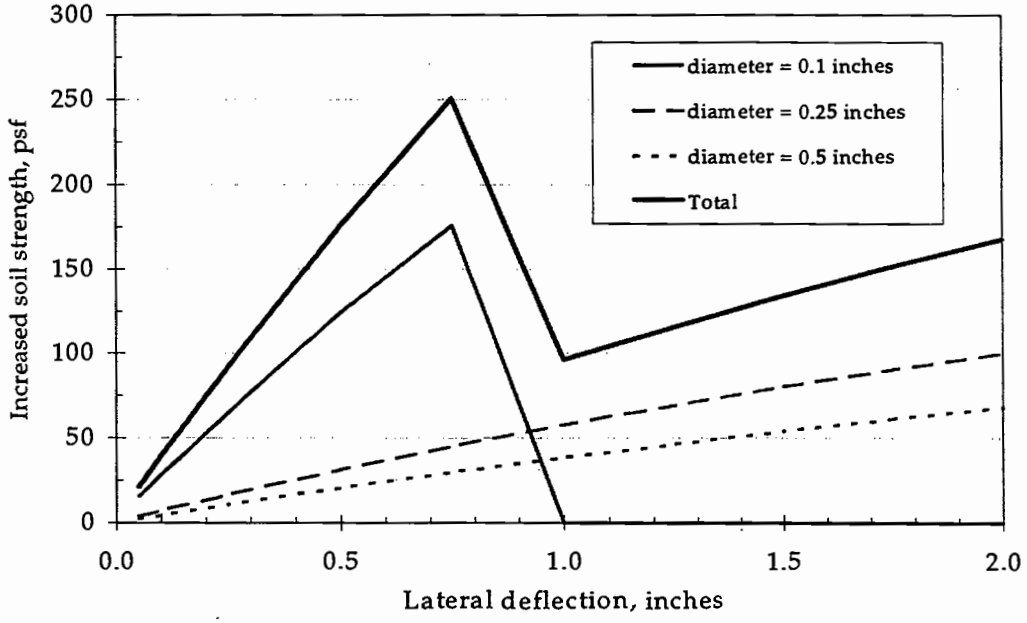

(b)

Figure 5-16. The modeled increase in soil strength for a forest soil in the Oregon Coast Range using root number and diameter distribution from Burroughs and Thomas (1977). A scaling coefficient was used with the shear-stress transfer functions in (a) and no scaling coefficient was used in (b). The roots were embedded in a sandy soil one foot deep.

CONCLUSIONS & DISCUSSION

An analytical model that predicts the increase in the strength of shallow, cohesionless forest soils due to the reinforcement of roots has been developed. The model is physically based and predicts the deflected shape and the tensile and shear forces in the deflected root as the soil deforms and these outputs are predicted as a function of the physical properties of the soil and the root.

Output from the root reinforcement model was compared with direct shear test results in which different materials were tested as reinforcing elements in a shallow, moderately dense sand. The shapes of the deflected reinforcing elements, as predicted by the root reinforcement model, were compared with the shapes of the deflected reinforcing elements which resulted from direct shear tests and the comparison was generally satisfactory. It was not possible to compare the predicted forces in the reinforcing elements with experimental results because such data do not exist.

The root reinforcement model has solved one of the problems with the Wu-Waldron model which is the need to know *a priori* the width of the shear zone before a soil strength increases associated with root reinforcement can be predicted. The model can deflect roots and calculate tensile and shear load increases without knowing a shear zone width.

Output from the model clearly shows that the increase in strength associated with root reinforcement soil is not a fixed quantity but varies as a

function of soil deformation. The strength of root reinforced soil is not a function of the type of reinforcement and the soil type alone, but a function of the deformation of the soil block, also. The predicted strength of the reinforced soil will increase as deformation increases as long as the soil/root composite structure remains competent. If the competence of the composite structure is lost at a small deflection then the predicted strength increase will be less than if competence is lost at a larger deflection.

The output from the root reinforcement model clearly illustrates the problem of strain incompatibility between the large and small roots. The model output shows that it is not appropriate to simply sum the ultimate strength of all the roots in a potential slide surface to calculate reinforced soil strength. Figures 5-15 and 5-16 show that small roots will reach ultimate tensile strength while large roots are still stretching elastically. The model output also illustrates the importance of the smallest sized roots (0 to 4 mm) to the strength of the root reinforced soil. Their importance is a consequence of their abundance.

Thus, models which predict the increase in strength of root-reinforced soils by simply summing the ultimate tensile strength of the roots and use that number as the increased strength due to root reinforcement are inappropriate. Small diameter roots will fail in tension while large diameter roots are still well below their tensile capacity. If this approach, the summation of the ultimate strength of all roots in the soil, is to be used to predict the strength of root-reinforced soils, it would be more appropriate to consider just the smallest

diameter fraction of the roots. In this manner, the estimate of root reinforcement would always be conservative and underestimate the true value.

Thus, the root reinforcement model has fulfilled one of the primary expectation of it when the project was initiated. The root reinforcement model is physically based and predicts the increased strength in soils associated with root reinforcement through calculation of the shape of a deflected root and the accompanying tensile and shear forces in the deformed root. These calculations are based on the physical and mechanical properties of the soil and roots. Output from the model clearly demonstrates that the increase in soil strength can not be calculated by summing the ultimate tensile strength of the roots in a soil. This conclusion comes from the clear illustration of strain incompatibility between the large and small diameter roots which is illustrated by output from the model. The output from the model also clearly illustrates that root reinforced strength is not a fixed quantity but deformation based.

While the root reinforcement model has fulfilled expectations, it is important to understand its limitations. Because the predicted strength increase is not empirical, it is important to use the value in an appropriate manner. Also, the model contains conceptual flaws which need to be discussed. Finally, the model can not predict the actual failure mechanism in shallow forest soils, so depending on the what the true failure mechanism is, the predicted strength values may or may not be appropriate.

The root reinforcement model clearly predicts an increase in soil strength as a consequence of root reinforcement in shallow forest soils. Recall from the results section that the predicted increase in soil strength due to root reinforcement for a clean, dry, cohesionless sand with Douglas-fir roots embedded in it was approximately 250 lbs/ft^2 (12.0 kPa). It is not appropriate to use this value as the strength that would be lost if the trees were harvested from the site. The lost strength would be less than 250 lbs/ft^2 because the soil would not become unrooted but have a shift in the species and size distribution of the roots. What would be the true effect on a per unit area of soil basis? It is hard to know and not possible to calculate because numbers for species and diameter distribution shift are not readily available. Ziemer (1981a) predicts that at its lowest point the soil will have 40 percent net root reinforcement. If Ziemer's (1981a) value is used in this example, the loss in soil strength due to root reinforcement of the hypothetical modeled slope is approximately 150 lbs/ft^2 (7.2 kPa). However, for this value of increased soil strength to be meaningful, it must be compared with the inherent soil strength of the site. This can not be done without considering the soil strength at a landslide site because tree roots are not distributed evenly throughout a landslide mass.

To carry out this portion of the example, a relatively small, approximately 10 yd^3, hypothetical landslide will be considered. The soil strength of the landslide will be considered in three dimensions because two dimensional landslide analysis doesn't allow for the root reinforcement effect to be correctly

modeled. The main body of the landslide is rectangular, 3 feet deep by 6 feet wide and 12 feet long, and the upslope end of the landslide is shaped like a semicircle. Assume that roots exist down to two feet below the soil surface. The rest of the surface of the landslide, the bottom and one foot along the edges, will not be affected by roots. Total failure surface area is approximately 186 ft^2 and total volume is approximately 258 ft^3. The area of the failure surface under the influence of roots is approximately 67 ft^2.

Assume that the area represented by the landslide is a shallow forest soil on a landslide-prone slope and the trees from the slope were harvested at such a time that this analysis is occurring when root biomass is at its lowest point. Assume further that the soil characteristics are the same as those that were used to model root reinforcement, namely the soil is a clean, cohesionless sand with a dry density of 90 lbs/ft^3 and an internal angle of friction of 44°. The force resisting failure for the surface area of the landslide without considering roots is approximately 35,000 lbs. Approximately 67 ft^2 of the landslide surface area will have an increase in strength due to root reinforcement which will be 100 lbs/ft^2, about 40 percent of maximum root reinforcement, which is approximately 6,700 lbs of additional strength. The same 67 ft^2 of landslide surface area will have a reduction in soil strength due to loss of root reinforcement. The value of lost strength mentioned above was 150 lbs/ft^2 and when multiplied by the appropriate surface area come to approximately 10,000 lbs of lost strength. In this example the harvesting attributed loss in soil strength due to the decay of the

roots of harvested trees is approximately 19 percent of the inherent strength that would have existed had harvesting not occurred.

Instead of assuming only frictional strength, a nominal value for soil cohesion can be considered to reflect more accurately the true results of soil strength testing for shallow, cohesionless soils. Assume a value of 105 lbs/ft^2 (5 kPa) for the cohesion value. This cohesion value will result in an additional 19,000 pounds of strength to be added to the failure surface area making the reduction in strength due to root reinforcement 14 percent of the inherent strength that would have existed had harvesting not occurred.

The 14 and 19 percent reduction in soil strength can not be interpreted to equate to a 14 and 19 percent reduction in stability or factor-of-safety. To determine the effect of the soil strength reduction on the stability of the landslide, a slope stability analysis would have to be performed and this would require knowledge of the other factors that affect slope stability like the steepness of the hillslope and location of the piezometeric surface. This example was presented to illustrate how values for soil strength increase due to root reinforcement could and should be used. It was not intended to be a definitive calculation of the effect of harvesting on slope stability. These values for soil strength can be used in slope stability analysis equations for a particular site and the effect of harvesting on slope stability can be modeled.

This example was carried out using dry unit weights and effective stresses were equal to total stresses. Buoyant unit weights and resulting effective stresses

were not used for two reasons. First of all, the root reinforcement model was run using dry unit weight. This exercise could be carried out in a saturated soil but all the root reinforcement values would have to be recalculated using buoyant unit weights in the ultimate soil resistance of the *p-y* curves and a below the water table condition for the coefficient of subgrade reaction. These changes would cause the values of strength attributed to root reinforcement to change. This exercise could be carried out, however. More importantly, dry densities were used because no shear-stress transfer functions exist for saturated soils. Rather than try to estimate the effect of saturation on shear-stress transfer, the model was run with only dry unit weight values. The example does give an idea of how to use the root reinforcement model and model output and this was the intent.

It is possible that the root reinforcement model as used still overestimated the contribution of root reinforcement to soil strength. The fault is not necessarily in the root reinforcement model but in the quality of the root biomass, and more importantly, root size data. Recall from Burroughs and Thomas (1977), that 90 percent of all root biomass for a Oregon Coast Range Douglas-fir forest was in the 0 to 4 mm diameter range. This was modeled using a 0.1 inch (2.5 mm) diameter root which has a modeled ultimate strength of approximately 17.5 pounds.

Assume that the root biomass in the 0 to 4 mm range is evenly distributed, then just under one half of the total root biomass is less than 2 mm in diameter.

The ultimate strength of 1 mm and 2 mm diameter roots is approximately 2.7 and 10.8 pounds, respectively. The ultimate strength of this size root would be reached sooner than was modeled in Figures 5-15 and 5-16. The net result would be that the modeled peak strength would be brought down and the peak strength illustrated in Figures 5-15 and 5-16 would be less and occur at a smaller deformation. The magnitude of the reduction in strength isn't know and no effort will be made to estimate it.

Finally, the distribution of root biomass in the 0 to 4 mm range is, most likely, not linear but exponential. This means that probably more than half of the total root biomass in a soil is less than 2 mm in diameter which would tend to reduce the modeled peak strength value even more. So the values of the modeled increase in soil strength attributed to root reinforcement shown in Figures 5-15 and 5-16 should be considered maximum values. The true values could be even less.

As mentioned previously, there are flaws in the conceptual development of the root reinforcement model. The root reinforcement model is simplified in its formulation. The axial problem and the lateral problem are uncoupled and the problem is solved by superimposing the solutions of the two problems as the last step. A node in the model root is not allowed to move in x direction. The only stretching is done as it changes shape due to lateral deflection. Furthermore, the root element right at the failure surface can not, by definition, move axially through the soil. Yet the assumption is made that it moves axially by the amount

of elongation. So the assumptions and calculations for the model, especially in the vicinity of the failure surface are simply not correct. Beyond the failure surface at the point where there is no lateral deformation and only the axial processes are going on, the formulation of the problem is probably more correct but in the vicinity of the failure surface, the superimposed solution isn't correct. A model which would be more correct would treat all the forces in a root element at the same time and allow the element to deform in accordance with both lateral and axial forces at the same time. This undoubtedly could become very complex because in the direct vicinity of the failure surface, the forces being put on the root are from the soil moving past the root (Jewell, 1980) and not the root moving through the soil which means that a kinimatically correct solution which can handle the stresses and strains in the soil, as well as the root, is needed. This is a task which appears to have eluded even the geotechnical community, so far.

The shear-stress transfer functions, as used in the model, are undoubtedly underestimated. Commandeur (1989) ran shear stress transfer on roots with and without rootlets attached. As expected, the roots with rootlets had increased shear-stress transfer and even that modified system still undoubtedly underestimated shear-stress transfer in the real world. Yet, shear stress transfer functions without rootlets were used in the root reinforcement model because they represented the highest quality data available. How the magnitude of the shear-stress transfer functions might effect the magnitude of root reinforcement

was inadvertently modeled by the use of scaling coefficients. The scaling coefficients used in the root reinforcement model resulted in values of shear-stress transfer that were approximately one fifth of the value of shear stress transfer without scaling coefficients. The use of these two different values for shear-stress transfer still doesn't tell us what the real world shear-stress transfer is. The use of scaling coefficients, however, does give the root reinforcement model the ability to change the shear-stress transfer function and allows different scenarios to be evaluated.

The model can't predict the lateral deformation at which the soil/root composite material will lose its competence. It can only strain the system until the roots start to break in tension and that constitutes failure of the composite material. This behavior has been observed in direct shear strength tests, most notably Waldron, et. al.(1983) in which the strength of a soil/root composite increased throughout the range of the experimental test. This behavior in a strain-controlled strength test is unlikely to occur in a stress-controlled environment like the real world. Obviously, in the real world soil/root composite materials fail and they fail at relatively small lateral deflections certainly at deflections less than those observed in experimental strength tests. This can be stated with a fair amount of certainty because tension cracks of the magnitude of 2 to 4 inches, such as those in strain-controlled strength tests and in model results, are not observed in shallow forest soils where landslides are most likely. There is some evidence that the traditional soil strength failure mechanism

may not be appropriate for this problem. Kramer and Seed (1988) and Anderson and Sitar (1994) have investigated the failure mechanism of static liquefaction. They have found that the conditions that exist in shallow forest soils, i.e. loose soils with a high void ratio, high *in situ* shear stresses due to steep slopes, and a potential undrained failure mechanism make these sites prone to failure by static liquefaction. Iverson and LaHusen (1989) observed shear induced pore pressures in experimental landslides which would indicate static liquefaction is indeed a viable failure mechanism for these sites. Learning the failure mechanism of these soils and sites is critical to understanding root reinforcement.

FUTURE RESEARCH NEEDS

If modeling root reinforcement in shallow forest soils remains a high priority area for research, there are a number of projects that are needed to advance the current state of knowledge.

1. The most important research priority is to determine the failure mechanism of shallow forest soils. Current thinking regarding root reinforcement including the model developed for this project, assumes sufficient lateral deflection of roots to develop sufficient tensile force in the roots. Small diameter roots must be allowed to develop their ultimate tensile capacity. This may be giving the soil more strength than it is capable of. Shallow forest soils and conifer roots have a tremendous strain compatibility problem. Roots have a large strain capability and soil has none. If soil strain is very small and then a failure occurs by static liquefaction, this needs to be known because it changes the concept of root reinforcement, how to think about it, and model it. The failure mechanisms of shallow forest soils and the strain compatibility of shallow forest soils and tree roots needs to be known.
2. If current models calculating root reinforcement are to be used in a meaningful and rigorous fashion, a much better database of root biomass and diameter distributions needs to be obtained. There is currently very little data at all on diameter and species distributions of roots in shallow forest soils. This is true even of forested sites where the best information is known. For

harvested and reforested sites, there is essentially no raw data available that would work with slope stability or root reinforcement models. A very serious data gap for root reinforcement modeling and understanding how root reinforcement might occur is an understanding of both species, biomass, and diameter distribution dynamics of harvested sites as a function of time. Even an understanding of seasonal dynamics is critical. Model output from this project points out the importance of the very smallest diameter roots. From Burroughs and Thomas (1977), the fact that 90 percent of the root biomass is smaller than approximately 4 mm is known but how diameters are distributed within this range is not known. It is known that there is a significant die-off and turnover of roots less than 1 mm in diameter during the winter. Yet all *in situ* strength testing and biomass work has been carried out during the summer when this diameter class is at a maximum. How seasonal dynamics of root biomass affects root reinforced soil strength is a subject which has never been addressed.

3. A much better process-based, analytical model of root reinforcement than Wu-Waldron or the root reinforcement model created by this project is needed. Most importantly, the axial and lateral components of the problem must be coupled and the root must be allowed to respond correctly. This may require a "kinimatically correct" model which also accounts for soil stresses and strains. But an improved model is needed if modeling root reinforcement is to be advanced.

BIBLIOGRAPHY

Abe, K., and M. Iwamoto. 1985. Effect of tree roots on soil shearing strength. Proceedings of an Interntional Symposium on Erosion, Debris Flow and Disaster Prevention. Sept. 3-5, 1985, Tsukuba, Japan. p.341-346.

Abe, K. and R. R. Ziemer. 1991. Effect of tree roots on a shear zone: modeling reiforced shear stress. Canadian Journal of Forest Research, Vol 21, p. 1012-1019.

Amaranthus, M. P., R. M. Rice, N. R. Barr, and R. R. Ziemer. 1985. Logging and forest roads related to increased debris slides in Southwester Oregon. Journal of Forestry, Vol. 83, p. 229-233.

Anderson, S. A. and N. Sitar. 1995. Analysis of rainfall-induced debris flows. ASCE Journal of Geotechnical Engineering, Vol. 121, No. 7. p. 544-552.

Audibert, J. M. E. and K. J. Nyman. 1977. Soil restraint against horizontal motion of pipes. Proceedings of the American Society of Civil Engineers, Journal of the Geotechnical Engineering Division, Vol.103, No. GT 10 p. 1119-1142.

Bishop, D. M., and M. E. Stevens. 1964. Landslides on logged areas in southeast Alaska. USDA Forest Service, Northern Forest Experiment Station, Research Paper NOR-1. 18 p.

Bowles, J. E. 1969. Foundation Analysis and Design. McGraw-Hill, Inc. 659 p.

Buchanan, P. and K. W. Savigny. 1990. Factors controlling debris avalanche initiation. Canadian Geotechnical Journal Vol. 19, No. 2, p 167-174.

Burroughs, E. R. and B. R. Thomas. 1977. Declining root strength in Douglas-fir after falling as a factor in slope stability. USDA Forest Service, Intermountain Forest and Range Experiment Station, Research Paper INT-190,.27 p.

Commandeur, P. R. 1989. Shear stress transfer between roots and soil Msc. thesis, Department of Forest Engineering, Oregon State University, Corvallis, OR. 126 p.

Commandeur, P. R. and M. R. Pyles. 1991. Modulus of elasticity and tensile strength of Douglas-fir roots. Canadian Journal of Forest Research, 21:48-52.

Coyle, H. M. and L. C. Reese. 1966. Load transfer for axially loaded piles in clay. Journal of the Soil Mechanics and Foundations Division, Proceedings of the American Society of Civil Engineers, Vol. 92, No. SM2, p.1-26.

Cox, W. R., L. C. Reese, and B. R. Berry. 1974. Field testing of laterally loaded piles in sand. Sixth Annual Offshore Technology Conference, Houston, Texas.

Croft, A. R., and J. A. Adams. 1950. Landslides and sedimentation in the North Fork of Ogden river, May 1959. USDA Forest Service, Intermountain Forest and Range Experiment Station, Research Paper No. 21. 4 p.

Dakessian, S. 1980. Strength characteristics of root-reinforced soils. Ph.D. dissertation, University of California, Berkeley, CA, 187 p.

Duncan, J. M. and S. G. Wright. 1980. The accuracy of equilibrium methods of slope stability analysis. Engineering Geology, 16(1), 5-17.

Dunn, I. S., L. R. Anderson, and F. W. Kiefer. 1980. Fundamentals of Geotechnical Analysis. John Wiley & Sons, Inc.

Dyrness, D. T. 1967. Mass soil movements in the H. J. Andrews Experimental Forest. USDA Forest Service, Pacific Northwest Forest and Range Experiment Station, Research Paper PNW-42, 12 p.

Endo, T. 1980. Effect of tree roots upon the shear strength of soil. JARQ, Vol 14, No. 2, p. 112-115.

Endo, T., and T. Tsuruta. 1969. The effect of the tree's roots upon the shear strength of soil. IN: 1968 Annual Report of the Hokkaido Branch,Forest Experiment Station, p. 167-182.

Fiksdal, A. J. 1974. A landslide survey of the Stequaleho Creek watershed. Supplement to Final Report UW-7404, Fisheries Research institute, University of Washington, Seattle. 7 p.

Flaccus, E. 1959. Landslides and their revegetation in the White Mountains of New Hampshire. Ph.D. thesis, Duke University, Durham, N.C. 187 p.

Froehlich, H. A. 1978. The influence of clearcuting and road building activities on landscape stability in western United States. Preceedings of the 5th North American Forest Soils Conference, Colorado State Universtiy, Fort Collins, CO. p. 165-173.

Gleser, S. M. 1953. Lateral load tests on vertical fixed-head and free-head piles. Symposuim on Lateral Load Tests on Piles, ASTM Special Technical Publication No. 154, p. 75-101.

Gonsior, M. J. and R. B. Gardner. 1971. Investigation of slope failures in the Idaho Batholith. USDA Forest Service, Intermountain Forest and Range Experiment Station, Research Paper INT-97. 33 p.

Gray, D. H. and W. F. Megahan. 1981. Forest vegetation removal and slope stability in the Idaho Batholith. USDA Forest Service, Intermountain Forest and Range Experiment Station, Reserach Paper INT-271, 23 p.

Gray, D. H., and H. Ohashi. 1983. Mechanics of fiber reinforcement in sand. Journal of Geotechnical Engineering, Vol. 109, No. 3, p. 335-353.

Greenway, D. R. 1987. Vegetation and slope stability. IN: Slope Stability, Edited by M. G. Anderson and K. S. Richards, John Wiley & Sons Ltd., Chapter 6, p. 187-230.

Gresswell, S., D. Heller, and D. N. Swanston. 1979. Mass movement response to forest management in the central Oregon Coast Range. USDA Forest Service, Pacific Northwest Forest and Range Experiment Station, Resources Bulletin PNW-84. 26 p.

Hansen, J. B. 1961. The ultimate resistance of rigid piles against transversal forces. The Danish Geotechnical Institute, Bull. No. 12, Copenhagen. 16 p.

Harr, R. D. 1977. Water flux in soil and subsoil on a steep forested slope. Journal of Hydrology, Vol. 33, p. 37-58.

Hetenyi, M. 1946. Beams on elastic foundation. University of Michigan Press, Ann Arbor, Michigan and Oxford Universtiy Press, London, England.

Holtz, R. D. and W. D. Kovacs. 1981. An Introduction to Geotechnical Engineering. Prentice-Hall, Inc. Englewood Cliffs, NJ.

Iverson, R. M. And R. G. LaHusen. 1989. Dynamic pore-pressure fluctuations in rapidly shearing granular materials. Science, Vol. 246, p. 796-799.

Jewell, R. A. 1980. Some effects of reinforcement on the mechanical behaviour of soils. Ph.D. dissertation. Cambridge University

Jewell, R. A. and M. J. Pedley. 1991. Discussion "Kinematical limit analysis for design of soil nailed structures". ASCE Journal of Geotechnical Engineering, Vol. 117, No. 11, p. 1821-1824.

Jewell, R. A. and M. J. Pedley. 1992. Analysis for soil reinforcement with bending stiffness. ASCE Journal of Geotechnical Engineering, Vol. 118, No. 10, p. 1505-1528.

Juran, I. and C. L. Chen. 1989. Strain compatibility design method for reinforced earth walls. ASCE Journal of Geotechnical Engineering, Vol. 115, No. 4, p. 435-456.

Juran, I., G. Baudrand, K. Farrag, and V. Elias. 1990a. Kinematical limit analysis for design of soil-nailed structures. ASCE Journal of Geotechnical Engineering, Vol. 116, No. 1, p. 54-72.

Juran, I., H. M. Ider, and K. Farrag. 1990b. Strain compatibility analysis for geosynthetics reinforced soil walls. ASCE Journal of Geotechnical Engineering, Vol. 116, No. 2, p. 312-329.

Ketcheson, G. and H. A. Froehlich. 1978. Hydrologic factors and environmental impacts of mass soil movements in the Oregon Coast Range. Water Resources Research Institute, WRRI-56, Oregon State University, Corvallis, OR. 94 p.

Kramer, S. L. and H. B. Seed. 1988. Initiation of soil liquefaction under static loading conditions. ASCE Journal of Geotechnical Engineering, Vol. 114, No. 4, p. 412-430.

Lambe, T. W. and R. V. Whitman. 1969. Soil Mechanics. John Wiley & Sons, Inc.

Leshchinsky, D. 1991. Discussion "Kinematical limit analysis for design of soil nailed structures". ASCE Journal of Geotechnical Engineering, Vol. 117, No. 11, p. 1821-1824.

Leshchinsky, D. and R. H. Boedeker. 1991. Closure "Geosynthetic reinforced soil structures. ASCE Journal of Geotechnical Engineering, Vol. 117, No. 10, p. 1644-1652.

Maher, M. H., and D. H. Gray. 1990. Static response of sands reinforced with randomly distributed fibers. Journal of Geotechnical Engineering, Vol. 116, No. 11, p. 1661-1677.

Maron, M. J. 1987. Numerical Analysis - A Practical Approach. 2nd Edition. Macmillan Publishing Company, New York. Collier Macmillan Publishers, London.

Megahan, W. F., N. F. Day, and T. M. Bliss. 1978. Landslide occurrence in the western and central Northern Rocky Mountain Physiographic Province in Idaho. Proceedings of the 5th North American Forest Soils Conference, Colorado State University, Fort Collins, CO. p.116-139.

Mitchell, J. K. and W C. M. Villet. 1987. Reinforcement of earth slopes and embankments. Transportation Research Board, National Research Council. National Cooperative Highway Research Program, Report 290, 323 p.

Morrison, P. H. 1975. Ecological and geomorphological consequences of mass movements in the Alder Creek watershed and implications for forest land management. B. A. Thesis, University of Oregon, 102 p.

Nash, D. 1987. A comparative review of limit equilibrium methods of stability analysis. Slope Stability, Edited by M. G. Anderson and K. S. Richards, John Wiley & Sons Ltd., Chapter 2, p. 11-75.

O'Loughlin, C. L. 1972. An investigation of the stability of the steepland forest soils in the coast mountains, southwest British Columbia. Ph.D. thesis, University of British Columbia, Vancouver, 147 p.

O'Loughlin, C. L. 1974. The effect of timber removal on the stability of forest soils. Journal of Hydrology (N. Z.), Vol. 13, No. 2, p 121-134.

O'Loughlin, C. L. and A. J. Pearce. 1976. Influence of Cenozoic geology on mass movement and sediment yield response to forest removal, North Westland, New Zealand. Bulletin of the International Association of Engineering and Geology, Vol. 14, p. 41-46

O'Loughlin, C. L. and A. Watson. 1979. Root-wood strength deterioration in radiata pine after clearfelling. New Zealand Journal of Forest Science 9(3):284-293.

O'Loughlin, C. L., L. K. Rowe, and A. J. Pearce. 1982. Exceptional storm influences on slope erosion and sediment yield in small forest catchments, North Westland, New Zealand. IN: Poceeding of the First National Symposium on Forest Hydrology. Melbourne, Autralia, May, 1982. The Institute of Engineers, Australia, National Conference, Publication No. 82/6, Barton, ACT, Autralia.p. 84-91.

Oregon Department of Forestry. 1994. Oregon Forest Practice Rules and Statutes. Salem, OR. December 1, 1994. 130 p.

Parker, F. P. and L. C. Reese. 1970. Experimental and anlytical studies of behavior single piles in sand under lateral and axial loading. Center For Highway Research, The University of Texas at Austin, Research Report 117-2, 251 p.

Press, W. H., S. A. Teukolsky, W. T. Vetterling, and B. P. Flannery. 1992. Numerical Recipes in Fortran - The Art of Scientific Computing. 2nd Edition, Cambridge University Press.

Pyles, M. R. and H. A. Froehlich. 1987. Discussion "Rates of landsliding as impacted by timber management activities in norwestern California. Bulletin of the Association of Engineering Geologists. Vol. XXIV, No. 3, p 425-431.

Reese, L. C. 1977. Laterally loaded piles: program documentation. ASCE Journal of the Geotechnical Engineering Division, Vol. 103, No. GT4, p. 287-305.

Reese, L. C. 1984. Handbook on design of piles and drilled shafts under lateral load. U.S. Department of Transportation, Federal Highway Administration, FHWA-IP-84-11, 386 p.

Reese, L. C. 1986. Behavior of piles and pile groups under lateral load. U.S. Department of Transportation, Federal Highway Administration, FHWA/RD-85/106, 311 p.

Reese, L. C. and H. Matlock. 1956. Non-dimensional solutions for laterally loaded piles with soil modulus assumed proportional to depth. Proceedings, Eighth Texas Conference on Soil Mechanics and Foundation Engineering, Austin, Texas.

Reese, L. C., W. R. Cox, and F. D. Koop, 1974. Analysis of laterally loaded piles in sand. Fifthe Annual Offshore Technology Conference, Paper No. OTC-2080, Houston, Texas. p. 473-483.

Schlosser, F. and V. Elias. 1978. Friction in reinforced earth. Proceedings of a Symposium on Earth Reinforcement, ASCE Annual Convention, Pittsburg, Pennsylvania, April 27, 1978. p.735-763

Schoenemann, M. R. and M. R. Pyles. 1984. Statistical description of shear strength in residual soils. Presented at the Symposium on the Effects of Forest Land Use on Erosion and Slope Stability, May 7-11, 1984, Honolulu, Hawaii. p. 73-82.

Schroeder, W. L. and J. V. Alto. 1983. Soil properties for slope stability analysis; Oregon and Washington coastal mountains. Forest Science, Vol. 29, No. 4, p. 823-833.

Schroeder, W. L. and G. W. Brown. 1984. Debris torrents, precipitation, and roads in two coastal Oregon watersheds. Presented at the Symposium on the Effects of Forest Land Use on Erosion and Slope Stability. May 7-11, Honolulu, Hawaii, p.117-122.

Scott, R. F. 1981. Foundation Analysis. Prentice-Hall, Inc. Englewood Cliffs, NJ.

Shen, C. K., S. Bang, K. M. Romstad, L. Kulchin, and J. S. DeNatale. 1981a. Field measurements of an earth support system. Proceedings of the American Society of Civil Engineers, Journal of the Geotechnical Engineering Division, Vol. 107, No. GT12, p. 1625-1642.

Shen, C. K., L. R. Herrmann, K. M. Romstad, S. Bang, Y. S. Kim, and J. S. DeNatale. 1981b. An *in situ* earth reinforcement lateral support system. Department of Civil Engineering, Report No. 81-03, University of California, Davis. 188 p.

Shewbridge, S. E. and N. Sitar. 1985. The influence of fiber properties on the deformation characteristics of fiber-soil composite. Geotechnical Engineering Report No. UCB/GT/85-02. University of California, Berkeley, CA.

Shewbridge, S. E. and N. Sitar. 1989. Deformation characteristics of reinforced sand in direct shear. ASCE Journal of Geotechnical Engineering, Vol. 115, No. 8, p. 1134-1147.

Shewbridge, S. E. and N. Sitar. 1990. Deformation-based model for reinforced sand. ASCE Journal of Geotechnical Engineering, Vol. 116, No. 7, p. 1153-1170.

Shewbridge, S. and N. Sitar. 1992. Discussion, "Strain compatibility design method for reinforced earth walls. ASCE Journal of Geotechnical Engineering, Vol. 118, No. 2, p. 318-321.

Sidle, R. C. and D. N. Swanston. 1982. Analysis of a small debris slide in coastal Alaska. Canadian Geotechnical Journal, Vol. 19, No. 2, p. 167-174.

Sidle, R. C., A. J. Pearce, and C. L. O'Loughlin. 1985. Hillslope Stability and Land Use. American Geophysical Union, Water Resources Monograph No. 11, 140 p.

Swanson, F. J. and C. T. Dyrness. 1975. Impact of clear-cutting and road construction on soil erosion by landslides in the western Cascades Range, Oregon. Geology 3(7):393-396.

Swanson, F. J., M. M. Swanson, and C Woods. 1977. Inventory of mass erosion in the Mapleton Ranger District Siuslaw National Forest. Final Report, Siuslaw National Forest and Pacific Northwest Forest and Range Experiment Station, Forestry Sciences Laboratory, Corvallis, OR

Swanson, F. J., M. M. Swanson, and C. Woods. 1981. Analysis of debris-avalanche erosion in steep forest lands: An example from Mapleton, Oregon, USA. In: Erosion and sediment transport in Pacific Rim steeplands. IAHS Publication No. 132. Christchurch, N. Z. p. 67-75.

Swanston, D. N. 1967 Soil-water pieziometry in a southeast Alaska landslide area. USDA Forest Service, Pacific Northwest Forest and Range Experiment Station, Research Note PNW-68. 17 p.

Swanston, D. N. 1970. Mechanics of debris avalanching in shallow till soils of southeast Alaska. USDA Forest Service, Pacific Northwest Forest and Range Experiment Station, Institute of Northern Forestry, Research Paper PNW-103, 17 p.

Swanston, D. N. 1974. Slope stability problems associated with timber harvesting in mountainous regions of the western United States. USDA Forest Service, Pacific Northwest Forest and Range Experiment Station, General Technical Report PNW-21, 14 p.

Swanston, D. N., and F. J. Swanson. 1976. Timber harvesting, mass erosion, and steepland forest geomorphology in the Pacific Northwest. Geomorphology and Engineering. D. R. Coates, ed. Dowden, Hutchinson & Ross, Inc. Stroudsburg, Pa. p. 199-221.

Terzaghi, K. 1955. Evaluation of coefficients of subgrade reaction. Geotechnique, Vol. 5, p.297-326.

Turnbull, W. J. and M. L. Hvorslev. 1967. Special problems in slope stability. ASCE, Journal of the Soil Mechanics and Foundation Division, Vol. 93,No. SM4, p. 499-528.

van Asch, Th. W. J. 1984. Landslides: The deduction of strength parameters of materials from equlibrium analysis. CATENA, Vol. 11, p. 39-49.

Verma, B. P., and A. N. R. Char. 1978. Triaxial tests on reinforced sand. Proceedings of a Symposium on Soil Reinforcing and Stabilising Techniques, Sydney, Australia. October 16-19, 1978. p. 29-39.

Vidal, H. 1969. The principle of reinforced earth. Highway Research Record. No. 282, p. 1-16.

Waldron, L. J. 1977. The shear resistance of root-permeated homogeneous and stratified soil. Soil Science Society of America Journal, Vol. 41, p. 843-849.

Waldron, L. J., and S. Dakessian. 1981. Soil reinforcement by roots: Calculation of increased soil shear resistance from root properties. Soil Science, Vol. 132, No. 6, p. 427-435.

Waldron, L. J., and S. Dakessian. 1982. Effect of grass, legume, and tree roots on soil shearing resistance. Soil Science Society of America Journal, Vol. 46, p. 894-899.

Waldron, L. J., S. Dakessian, and J. A. Nemson. 1983. Shear resistance enhancement of 1.22-meter diameter soil cross sections by pine and alfalfa roots. Soil Science Society of America Journal, Vol. 47, p. 9-14.

Whitman, R. V. And W. A. Bailey. 1967. Use of computers for slope stability analysis. ASCE Journal of the Soil Mechanics and Foundation Division, Vol. 93,No. SM4, p. 475-498.

Wu, T. H., 1976. Investigation of Landslides on Prince of Wales Island. Geotechnical Engineering Report 5, Civil Engineering Dept., Ohio State University, Columbus, Ohio, USA. 94 p.

Wu, T. H., W. P. McKinnell III, and D. N. Swanston. 1979. Strength of tree roots and landslides on Prince of Wales Island, Alaska. Canadian Geotechnical Journal, Vol. 16, p. 19-33.

Wu, T. H., R. M. McOmber, R. T. Erb, and P. E. Beale. 1988a. Study of soil-root interaction. ASCE Journal of Geotechnical Engineering, Vol. 114, No. 12, p. 1351-1375.

Wu, T. H., P. E. Beale, and C. Lan. 1988b. In-situ shear test of soil-root systems. ASCE Journal of Geotechnical Engineering, Vol. 114, No. 12, p. 1376-1394.

Yang, Z. 1972. Strength and deformation characteristics of reinforced sand. Ph.D. thesis, University of California, Los Angeles, CA. 236 p.

Yee, C. S. 1975. Soil and hydrologic factors affecting stability of natural slopes in the Oregon Coast Range. Ph.D. thesis, Oregon State University, Corvallis, OR, 204 p.

Yee, C. S. and R.D. Harr. 1977a. Effect of wetting mode on shear strength of two aggregated soils. USDA Forest Service,Pacific Northwest Forest and Range Experiment Station, Research Note, PNW-303, 9 pp.

Yee, C. S. and R. D. Harr. 1977b. Influence of soil aggregation on slope stability in the Oregon Coast Ranges. Environmental Geology, Vol. 1, p. 367-377.

Ziemer, R. R. 1978. An apparatus to measure the crosscut shearing strength of roots. Canadian Journal of Rorest Research, Vol. 8, p. 142-144.

Ziemer, R. R. 1981a. Roots and the stability of forested slopes. IN: Erosion and Sediment Transport in Pacific Rim Steeplands. International Association of Hydrologic Sciences Publication No. 132, p. 343-361.

Ziemer, R. R. 1981b. The role of vegetation in the stability of forested slopes. International Union of Forestry Research Organizations, XVII World Congress, Kyoto, Japan, September, 1981.

Ziemer, R. R. and D. N. Swanston. 1977. Root strength changes after logging in southeast Alaska. USDA Forest, Pacific Northwest Forest and Range Experiment Station, Research Note PNW-306, 9 p.

APPENDICES

Appendix A

Appendix A

Derivation of the Governing Equation for Laterally Loaded Piles

The derivation of the governing equation for laterally loaded piles is based on beam-column theory. Specifically, it is based on the theory for an elastic beam on an flexible foundation. This derivation is essentially reproduced from Hetenyi (1946). The differential element for the derivation is shown in Figure *A-1*. The forces on and the dimensions of the differential element are:

- T = tensile force,
- V = shear force,
- M = moment
- P = the force of the soil on the element = $p\,dx$, where
- p = distributed force, and
- dx = length of the differential element
- F_s = soil shear force on the element, and
- dy = differential lateral deflection of the differential element.

In Figure *A-1(a)*, the forces at the ends of the differential element are drawn parallel to the coordinate axis. However, the soil shear force, F_s, is drawn parallel to the line of deflection. The components of the soil shear force in the x- and y-direction would be,

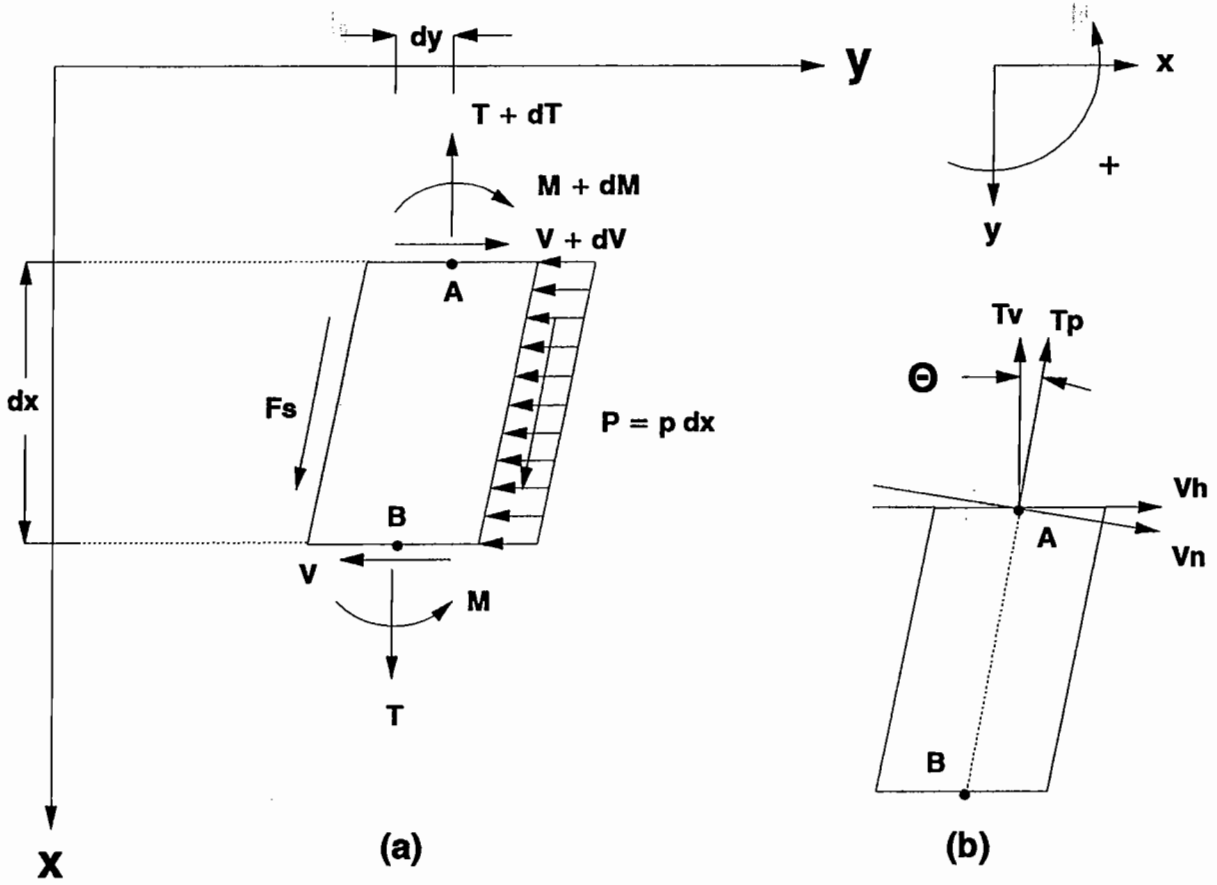

Figure A-1. A differential element from an elastic beam on a flexible foundation used to derive the governing differential equation for a laterally loaded pile.

$$F_{s_y} = F_s \cos\theta, \text{ and} \qquad A\text{-}1$$

$$F_{S_x} = F_s \sin\theta \qquad A\text{-}2$$

Likewise, the shear and tensile force at the ends of the element could be expressed as parallel or normal to the line of deflection. As illustrated in Figure *A-1(b)*, The expression for the shear would be

$$V_n = V_h \cos\theta - T_v \sin\theta \qquad A\text{-}3$$

Likewise the tensile force parallel to the line of deflection would be expressed as,

$$T_p = T_v \cos\theta + V_h \sin\theta \qquad A\text{-}4$$

For this derivation, the assumption will be made that the angle of deflection will be sufficiently small such that the approximations $\cos\theta = 1$ and $\sin\theta = 0$ can be used. However, F_{s_y}, F_{s_x}, V_n, and T_p can be computed using expressions *A-1* through *A-4* should that assumption become inappropriate.

First, sum the forces in the x-direction.

$$\sum F_x = 0 = V + dV - p\,dx - V \qquad A\text{-}5$$

This leads to the identity,

$$p = \frac{dV}{dx} \qquad A\text{-}6$$

Then, sum the forces in the y-direction.

$$\sum F_y = 0 = \left[-(T + dT)\right] + F_s + T \qquad A\text{-}7$$

This leads to the identity,

$$dT = F_s \qquad A\text{-}8$$

Next, sum the moments about point A.

$$\sum M_A = 0 = \left[-(M + dM)\right] - p\,dx\frac{dx}{2} - V\,dx + T\,dy + M \qquad A\text{-}9$$

With elimination of the higher order terms, subsequent algebraic manipulation leads to the expression,

$$-dM - V\,dx + T\,dy = 0 \qquad A\text{-}10$$

Expression *A-10* can be checked by summing the moments about B.

$$\sum M_B = 0 = \left[-(M + dM)\right] + p\,dx\frac{dx}{2} - (V + dV)\,dx + (T + dT)\,dy + M \qquad A\text{-}11$$

Again, by eliminating the higher order terms and with the appropriate algebraic manipulations, the expression in *A-10* can be derived.

$$-dM - V\,dx + T\,dy = 0 \qquad A\text{-}10$$

Differentiate both sides of the expression by x.

$$-\frac{dM}{dx} - \frac{V\,dx}{dx} + T\frac{dy}{dx} = 0 \qquad A\text{-}12$$

From beam-column theory the definition of moment is,

$$M = E\,I\left(\frac{d^2y}{dx^2}\right) \qquad A\text{-}13$$

Substituting, *A-13* into *A-12* results in,

$$-\frac{d}{dx}\left(E\,I\frac{d^2y}{dx^2}\right) - V + T\left(\frac{dy}{dx}\right) = 0$$

$$-EI\left(\frac{d^3y}{dx^3}\right)-V+T\left(\frac{dy}{dx}\right)=0 \qquad A\text{-}14$$

Once again, differentiate both sides with respect to x.

$$-EI\left(\frac{d^4y}{dx^4}\right)-\frac{dV}{dx}+T\left(\frac{d^2y}{dx^2}\right)=0 \qquad A\text{-}15$$

Substitute the identity $p = dV/dx$ (from equation *A-6*) into *A-15*.

$$-EI\left(\frac{d^4y}{dx^4}\right)-p+T\left(\frac{d^2y}{dx^2}\right)=0 \qquad A\text{-}16$$

The identity $p = E_s(y)$ can be substituted into equation *A-16* and when both sides of the equation are multiplied by a (-1), the equation becomes,

$$EI\left(\frac{d^4y}{dx^4}\right)-T\left(\frac{d^2y}{dx^2}\right)+E_s(y)=0 \qquad A\text{-}17$$

Equation *A-17* is the governing differential equation for the behavior of laterally loaded piles.

Appendix B

Appendix B

Derivation of the Finite-Difference Form of the Governing Differential Equation for Laterally Loaded Piles

This appendix presents the derivation of the finite-difference form of the governing differential equation for laterally loaded piles. This derivation is essentially reproduced from Reese (1977). The governing differential equation for laterally loaded piles was derived in Appendix A and is reproduced below as equation *(A-17)*.

$$E I \frac{d^4 y}{dx^4} - T \frac{d^2 y}{dx^2} + E_s(y) = 0 \qquad A\text{-}17$$

In this equation, the parameters describing the reinforcing element are; E = modulus of elasticity, I = moment of inertia, T = tensile force, and y = the lateral deflection of the reinforcing element at some length x along it. The parameter describing the soil is; E_s = secant modulus of the soil response to the lateral deflection, y.

To solve the above equation in finite-difference form, the length of the reinforcing element must first be divided into a finite number of discrete elements each with a fixed length, h, (Figure *B-1)*. The centroid of the discrete

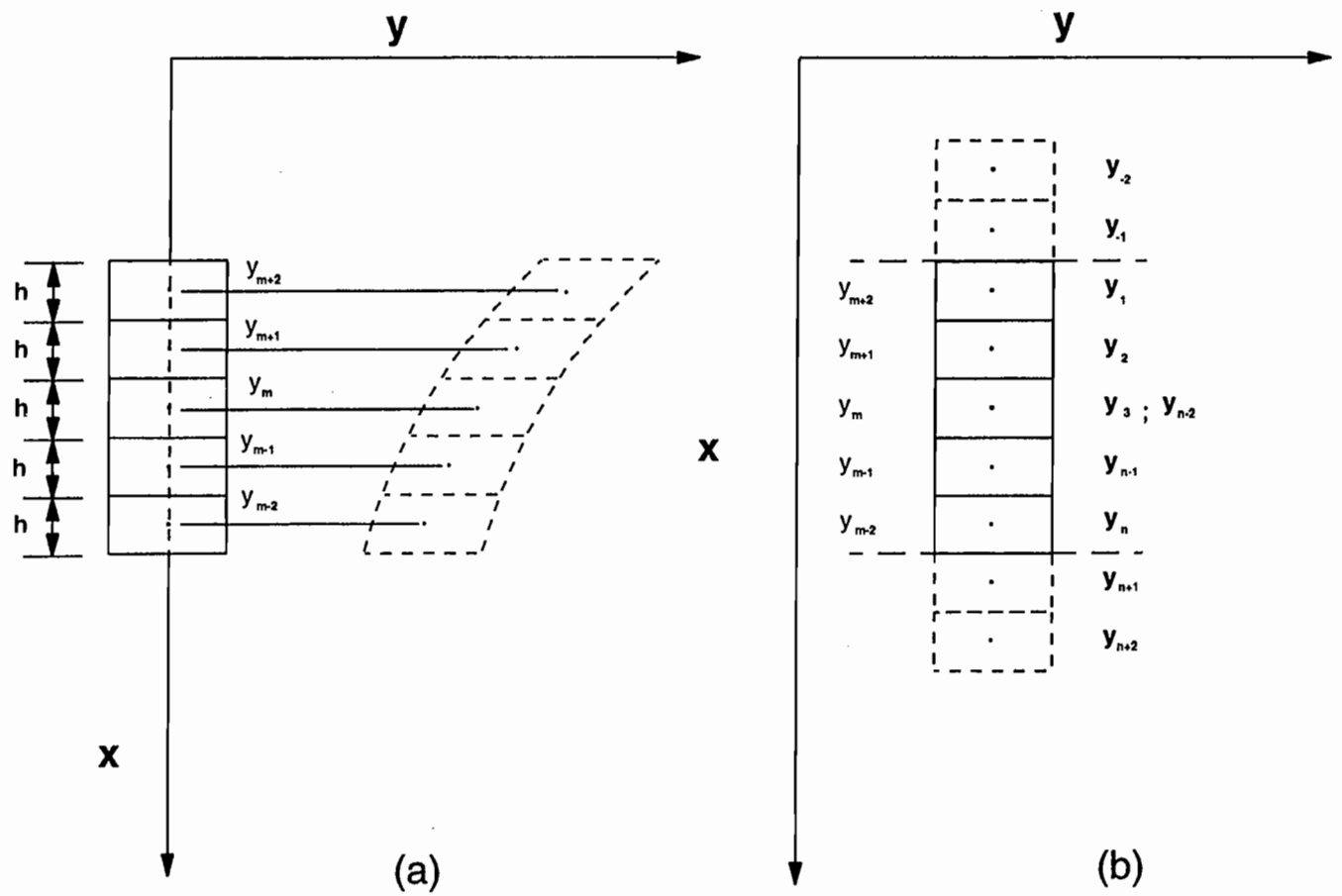

Figure B-1. Definition sketches showing the reinforcing element represented by discrete elements. The figure in (a) shows how the deflection, y_i, is represented and the figure in (b) shows the phantom nodes at each end of the reinforcing element.

elements are labeled with the *x*-, *y*-coordinates which identify each discrete element and they are called nodes. The following finite-difference definitions can then be applied to the differential equation (Bowles, 1968).

$$\frac{dy}{dx} = \frac{(y_{m-1} - y_{m+1})}{2h} \qquad B\text{-}1$$

$$\frac{d^2y}{dx^2} = \frac{(y_{m+1} - 2y_m + y_{m-1})}{h^2} \qquad B\text{-}2$$

$$\frac{d^3y}{dx^3} = \frac{(-y_{m+2} + 2y_{m+1} - 2y_{m-1} + y_{m-2})}{2h^3} \qquad B\text{-}3$$

$$\frac{d^4y}{dx^4} = \frac{(y_{m+2} - 4y_{m+1} + 6y_m - 4y_{m-1} + y_{m-2})}{h^4} \qquad B\text{-}4$$

The meaning of the subscripts are illustrated in Figure *B-1(a)*. If equations *B-2* and *B-4* are substituted into *A-17*, the general equation becomes,

$$\frac{(EI)_m}{h^4}\left[y_{m+2} - 4y_{m+1} + 6y_m - 4y_{m-1} + y_{m-2}\right] - \frac{T_m}{h^2}\left[y_{m+1} - 2y_m + y_{m-1}\right] + E_{s_m}(y) = 0 \qquad B\text{-}4$$

If the reinforcing element is composed of a material with constant properties and a non-changing cross section, then the flexural rigidity term, *EI*, becomes a constant. The tension in the reinforcing element and the secant modulus of the soil response vary throughout the length of the reinforcing element and maintain the subscript of the node they are associated with. Multiply through equation *B-4* then collect and gather terms and the finite-difference form of the governing differential equation becomes,

$$y_{m+2}\left(\frac{EI}{h^4}\right)+y_{m+1}\left(\frac{-4EI}{h^4}-\frac{T_m}{h^2}\right)+y_m\left(\frac{6EI}{h^4}-\frac{2T_m}{h^2}+E_{s_m}\right)+$$

$$y_{m-1}\left(\frac{-4EI}{h^4}-\frac{T_m}{h^2}\right)+y_{m-2}\left(\frac{EI}{h^4}\right)=0 \qquad B\text{-}5$$

The finite-difference equations for the end nodes of the reinforcing element are derived using the boundary conditions at each end of the reinforcing element. Two phantom nodes are created at each end of the reinforcing element to aid in deriving the finite-difference equations. The use of the phantom nodes is illustrated in Figure *B-1(b)*. The nodes are number sequentially starting with the node at the failure surface and extending to the end of the reinforcing element away from the failure surface. The node right at the failure surface is called the first node and is given the subscript *1* with the second node being *2* and so on

until the end of the reinforcing element away from the failure surface is reached. The last node at the end of the reinforcing element away from the failure surface is given the subscript *n* and the next to the last node is given the subscript *n-1* and so on.

The assumption is made that there is no movement at the end of the reinforcing element away from the failure surface and that it will not support a moment. Thus, the reinforcing element will support neither moment nor shear at the end away from the failure surface. Using the definition of moment from beam-column theory, the finite difference form of the boundary condition for the moment at the end of the reinforcing element away from the failure surface is,

$$M = EI\frac{d^2y}{dx^2} = \frac{EI}{h^2}\left(y_{n-1} - 2y_n + y_{n+1}\right) = 0 \qquad B\text{-}6$$

Multiply through equation *B-6* and then collect and gather terms and solve for the phantom node, y_{n+1}.

$$y_{n+1} = 2y_n - y_{n-1} \qquad B\text{-}7$$

Using the definition of shear from beam-column theory, the differential equation for shear at the end of the reinforcing element away from the failure surface is,

$$V = -EI\frac{d^3y}{dx^3} + T\frac{dy}{dx} = 0 \qquad B\text{-}8$$

In finite difference form equation *B-8* becomes,

$$V = \frac{-EI}{2h^3}\left(y_{n-2} - 2y_{n-1} + 2y_{n+1} - y_{n+2}\right) + \frac{T_n}{2h}\left(y_{n-1} - y_{n+1}\right) = 0 \qquad B\text{-}9$$

Again, multiply through equation *(B-9)*, then collect and gather terms and solve for the phantom node, y_{n+2}.

$$y_{n+2} = y_{n+1}\left(2 - \frac{T_n h^2}{EI}\right) - y_{n-1}\left(2 - \frac{T_n h^2}{EI}\right) + y_{n-2} \qquad B\text{-}10$$

Substitute the equations for the phantom nodes, *B-7* and *B-10*, into the finite-difference form of the governing differential equation, *B-5*, with the subscript n replacing m. The result is the following finite difference equation for the node at the end of the reinforcing element away from the failure surface.

$$y_n\left(\frac{2EI}{h^4} + \frac{2T_n}{h^2} + E_{s_n}\right) + y_{n-1}\left(\frac{-4EI}{h^4} - \frac{2T_n}{h^2}\right) + y_{n-2}\left(\frac{2EI}{h^4}\right) = 0 \qquad B\text{-}11$$

Likewise, the finite difference equation for the next-to-the-end of the reinforcing element can derived by substituting equation *B-7* into the general equation, *B-5*. The m subscripts are again replaced by n and the equation becomes,

$$y_n\left(\frac{-2EI}{h^4}-\frac{2T_{n-1}}{h^2}\right)+y_{n-1}\left(\frac{5EI}{h^4}+\frac{2T_{n-1}}{h^2}+E_{s_{n-1}}\right)+$$

$$y_{n-2}\left(\frac{-4EI}{h^4}-\frac{T_{n-1}}{h^2}\right)+y_{n-3}\left(\frac{EI}{h^4}\right)=0 \qquad \textit{B-12}$$

This process can be repeated for the boundary conditions at the end of the reinforcing element at the failure surface. The forces in the reinforcing element are considered at the failure surface which is a point of inflection in the deformed shape of the reinforcing element. Therefore, by definition, there is no moment and the shear is a fixed quantity which will be denoted by V. Again, using the definition of moment from beam-column theory, the finite difference form of the boundary condition for the moment at the end of the reinforcing element at the failure surface can be derived exactly like the moment at the end of the reinforcing element away from the failure surface. The subscript, *1*, is used to denote the node at the failure surface. The finite difference equation for the phantom node y_2 is identical to *B-7* except the subscript n is replaced with *1*.

$$y_{-1} = 2y_1 - y_2 \qquad B\text{-}13$$

Again, using the definition of shear from beam-column theory, the differential equation for the shear in the reinforcing element at the failure surface is,

$$V = EI\frac{d^3y}{dx^3} - T\frac{dy}{dx} \qquad B\text{-}14$$

The finite difference form of equation *B-14* is,

$$V = \frac{EI}{2h^3}\left(y_3 - 2y_2 + 2y_{-1} - y_{-2}\right) - \frac{T_1}{2h}\left(y_2 - y_{-1}\right) \qquad B\text{-}15$$

An equation for the phantom node y_{n-2} is derived by multiplying through equation *B-15* then collecting and gathering terms. That expression is,

$$y_{-2} = y_3 + y_2\left(-2 - \frac{T_1h^2}{EI}\right) + y_1\left(2 + \frac{T_1h^2}{EI}\right) - \frac{2Vh^3}{EI} \qquad B\text{-}16$$

Substitute the equations for the two phantom nodes at the end of the reinforcing element at the failure surface, *B-14* and *B-16*, into the finite-difference form of the governing differential equation, *B-5*, except substitute the subscript *1* for *m*. The resulting equation is the finite difference equation for the first node of the reinforcing element at the failure surface. That equation is,

$$y_1\left(\frac{2EI}{h^4}+\frac{2T_1}{h^2}+E_{s_1}\right)+y_2\left(\frac{-4EI}{h^4}-\frac{2T_1}{h^2}\right)+y_3\left(\frac{2EI}{h^4}\right)=\frac{2V}{h} \qquad B\text{-}17$$

Once again, the finite difference equation for the second node of the reinforcing element is derived by substituting equation *B-14* into the general equation, *B-5*. The subscript m is replaced by *1*. The equation becomes,

$$y_1\left(\frac{-2EI}{h^4}-\frac{2T_2}{h^2}\right)+y_2\left(\frac{5EI}{h^4}+\frac{2T_2}{h^2}+E_{s_2}\right)+y_3\left(\frac{-4EI}{h^4}-\frac{T_2}{h^2}\right)+y_4\left(\frac{EI}{h^4}\right)=0 \qquad B\text{-}18$$

The five equations *B-5*, *B-11*, *B-12*, *B-17*, and *B-18* can be used to describe the lateral deflection of a laterally loaded pile or the deformation of half of a reinforcing element stretched across a failure surface in a block of soil. The equations take into account the boundary conditions of the reinforcing element at the failure surface and away from the failure surface. Equations *B-17* and *B-18* account for the boundary conditions of the reinforcing element at the failure surface and equations *B-11* and *B-12* account for the boundary conditions at the end of the reinforcing element away from the failure surface and the general equation *B-5* accounts for all of the interceding nodes unaffected by the boundary conditions.

Appendix C

```
REM DAMODEL
DEFINT I-N

DECLARE SUB amatrix (a(), modulus!, inertia!, h, Tx#(), Es(), n)
DECLARE SUB subgradereaction ()
DECLARE SUB datainput (D2R#, pi#)
DECLARE SUB dispmatrix (n, h, D())
DECLARE SUB secantmodulus (k!, b, gamma, phi, depth, pi#, e#, Ka!, Ko!, beta, n, D(), Es())
DECLARE SUB tension (D(), pi#, n, b, h, modulus!, Tx#(), k, b(), Zx#())
DECLARE SUB bmatrix (modulus!, inertia!, h, Es(), Tx#(), n, D(), b())
DECLARE SUB bandec (a(), n, m1, m2, np, mp, al(), mpl, indx(), D)
DECLARE SUB banbks (a(), n, m1, m2, np, mp, al(), mpl, indx(), b())
DECLARE SUB Increment (Zx#, b, h, modulus!, k, Tx#, mud)

CONST pi# = 3.1415926536#
CONST e# = 2.718281828459045#
CONST tiny = .001
CONST D2R# = pi / 180

np = 200
mp = 5
DIM indx(np), D(np, 2), Es(np), al(np, 2)
DIM b(np), a(np, mp), Tx#(np), Zx#(np), Txo(np)

CALL datainput(D2R#, pi#)
CALL dispmatrix(n, h, D())

'Set tension matrix to zero
FOR i = 1 TO n
  Tx#(i) = 0
NEXT i

iter = 1

DO
  DO
    CALL secantmodulus(k!, b, gamma, phi, depth, pi#, e#, Ka!, Ko!, beta, n, D(), Es())
    CALL amatrix(a(), modulus!, inertia!, h, Tx#(), Es(), n)
    CALL bandec(a(), n, m1, m2, np, mp, al(), mpl, indx(), D)
    CALL bmatrix(modulus!, inertia!, h, Es(), Tx#(), n, D(), b())
    CALL banbks(a(), n, m1, m2, np, mp, al(), mpl, indx(), b())

    'Calculate the difference in the last set of y-deflections and the current
    'y-deflections.
    maxdiff! = 0
    FOR i = 2 TO n
      diff = ABS(b(i) - D(i, 2))
      IF diff > maxdiff! THEN maxdiff! = diff
    NEXT i

    'Print the solution vector
    CLS
    FOR i = 1 TO n
      PRINT USING "####.######"; b(i);
```

```
    NEXT i
    PRINT
    PRINT
    PRINT iter, maxdiff!
    'DO
    'LOOP WHILE INKEY$ = ""


    'Exchange the solution vector with the y displacements in the
    'displacement matrix.
    FOR i = 2 TO n
      D(i, 2) = b(i)
    NEXT i

  LOOP UNTIL maxdiff! < tiny

  'Write the tension values into a different array
  FOR i = 1 TO n
    Txo(i) = Tx#(i)
  NEXT i

  CALL tension(D(), pi#, n, b, h, modulus!, Tx#(), k, b(), Zx#())

  Txmaxdiff = 0!
  FOR i = 1 TO n
    Txdiff = ABS(Tx#(i) - Txo(i))
    IF Txdiff > Txmaxdiff THEN Txmaxdiff = Txdiff
  NEXT i

  iter = iter + 1


LOOP UNTIL iter = 10 OR Txmaxdiff < .01

'Print the solution vector
'CLS
'FOR i = n TO 1 STEP -1
'   PRINT USING "####.######"; b(i); CSNG(Tx#(i))
'NEXT i
'PRINT

'Print out the displacement matris
CLS
FOR i = n TO 1 STEP -1
  FOR j = 1 TO 2
    PRINT USING "####.######"; D(i, j);
  NEXT j
  PRINT
NEXT i
PRINT
PRINT CSNG(b(1)); CSNG(T#); iter; maxdiff!; Txmaxdiff
DO
LOOP WHILE INKEY$ = ""

CLS
```

```
INPUT "What is the name of the output file; Include the full path"; file$
ext$ = ".dat$"
finalfile$ = file$ + ext$
INPUT "What is the title for the output file"; title$
OPEN finalfile$ FOR OUTPUT AS #1
PRINT #1, title$
PRINT #1, "Top deflection, yt ="; yt
PRINT #1, "Soil density, gamma ="; gamma * 1728
PRINT #1, "Angle of internal friction, phi ="; phi * (180 / pi)
PRINT #1, "Effective soil depth, depth ="; depth
PRINT #1, "Loose soil density"
PRINT #1, "Diameter ="; b
PRINT #1,
PRINT #1, "Ft ="; b(1); "lbs"
PRINT #1, "Tx ="; T#; "lbs"
PRINT #1,
FOR i = 1 TO n
  FOR j = 1 TO 2
    PRINT #1, D(i, j);
  NEXT j
  PRINT #1,
NEXT i
CLOSE #1



PRINT
PRINT "All Done Now"

DO
LOOP WHILE INKEY$ = ""

SUB amatrix (a(), modulus!, inertia!, h, Tx#(), Es(), n)

'This is a subroutine to build the A-matrix for the reinforcing element
'system of equations. The A-matrix uses the convention A(x)=b. The
'A-matrix is the coefficient matrix. The x-matrix is the matrix of knowns.
'The answer is returned in the b-matrix. The A-matrix is a band diagonal
'matrix stored in compact form. It has n rows and 5 columns.

R1 = (modulus! * inertia!) / (h * h * h * h)
R2 = (2 * modulus! * inertia!) / (h * h * h * h)
R3 = -R2
R4 = (-4 * modulus! * inertia!) / (h * h * h * h)
R5 = (5 * modulus! * inertia!) / (h * h * h * h)
R6 = (6 * modulus! * inertia!) / (h * h * h * h)

FOR i = 1 TO n
  IF i = 1 THEN
    FOR j = 1 TO 5
      IF j = 3 THEN
        a(i, j) = -2 / h
      ELSEIF j = 4 THEN
        a(i, j) = R4 - ((2 * Tx#(i)) / (h * h))
      ELSEIF j = 5 THEN
```

```
      a(i, j) = R2
    ELSE : a(i, j) = 0
    END IF
  NEXT j
ELSEIF i = 2 THEN
  FOR j = 1 TO 5
    IF j = 3 THEN
      a(i, j) = R5 + ((2 * Tx#(i)) / (h * h)) + Es(i)
    ELSEIF j = 4 THEN
      a(i, j) = R4 - (Tx#(i) / (h * h))
    ELSEIF j = 5 THEN
      a(i, j) = R1
    ELSE : a(i, j) = 0
    END IF
  NEXT j
ELSEIF i = 3 THEN
  FOR j = 1 TO 5
    IF j = 2 OR j = 4 THEN
      a(i, j) = R4 - (Tx#(i) / (h * h))
    ELSEIF j = 3 THEN
      a(i, j) = R6 + ((2 * Tx#(i)) / (h * h)) + Es(i)
    ELSEIF j = 5 THEN
      a(i, j) = R1
    ELSE : a(i, j) = 0
    END IF
  NEXT j
ELSEIF i = n - 1 THEN
  FOR j = 1 TO 5
    IF j = 1 THEN
      a(i, j) = R1
    ELSEIF j = 2 THEN
      a(i, j) = R4 - (Tx#(i) / (h * h))
    ELSEIF j = 3 THEN
      a(i, j) = R5 + ((2 * Tx#(i)) / (h * h)) + Es(i)
    ELSEIF j = 4 THEN
      a(i, j) = R3 - (Tx#(i) / (h * h))
    ELSE : a(i, j) = 0
    END IF
  NEXT j
ELSEIF i = n THEN
  FOR j = 1 TO 5
    IF j = 1 THEN
      a(i, j) = R2
    ELSEIF j = 2 THEN
      a(i, j) = R4 - ((2 * Tx#(i)) / (h * h))
    ELSEIF j = 3 THEN
      a(i, j) = R2 + ((2 * Tx#(i)) / (h * h)) + Es(i)
    ELSE : a(i, j) = 0
    END IF
  NEXT j
ELSE
  FOR j = 1 TO 5
    IF j = 1 OR j = 5 THEN
      a(i, j) = R1
    ELSEIF j = 2 OR j = 4 THEN
```

```
        a(i, j) = R4 - (Tx#(i) / (h * h))
      ELSE
        a(i, j) = R6 + ((2 * Tx#(i)) / (h * h)) + Es(i)
      END IF
    NEXT j
  END IF
NEXT i

'Print out the A-matrix
'CLS
'  FOR i = 1 TO n
'    FOR j = 1 TO 5
'      PRINT USING "########.#######"; a(i, j);
'  NEXT j
'  PRINT
'NEXT i
'DO
'LOOP WHILE INKEY$ = ""
END SUB

SUB banbks (a(), n, m1, m2, np, mp, al(), mpl, indx(), b())

'Given the arrays a, al, and indx as returned from bandec, and given a
'right-hand side vector b(n), solves the band diagonal linear equations
'A(x) = b. The solution vector x overwrites b(n). The other input arrays
'are not modified, and can be left in place for successive calls with
'different right-hand sides.

mm = m1 + m2 + 1
l = m1
FOR k = 1 TO n
  i = indx(k)
  IF i <> k THEN
    dum = b(k)
    b(k) = b(i)
    b(i) = dum
  END IF
  IF l < n THEN l = l + 1
  FOR i = k + 1 TO l
    b(i) = b(i) - al(k, i - k) * b(k)
  NEXT i
NEXT k
l = 1
FOR i = n TO 1 STEP -1
  dum = b(i)
  FOR k = 2 TO l
    dum = dum - a(i, k) * b(k + i - 1)
  NEXT k
  b(i) = dum / a(i, 1)
  IF l < mm THEN l = l + 1
NEXT i

END SUB

SUB bandec (a(), n, m1, m2, np, mp, al(), mpl, indx(), D)
```

```
'Given an n x n band diagonal matrix A with m1 subdiagonal rows and
'm2 superdiagonal rows, compactly stored in the array a(n, m1+m2+1) as
'described in the comment for routine banmul, this routine constructs an LU
'decomposition of a rowwise permutation of A. The upper triangular matrix
'replaces a, while the lower triangular matrix is returned in al(n, m1).
'indx(n) is an output vector which records the row permutation effected by
' the partial pivoting; d is output as +-1 depending on whether the number
'of row interchanges was even or odd, respectively. This routine is used in
'combination with banbks to solve band-diagonal sets of equations.

CONST tiny = 1E-20
mm = m1 + m2 + 1

l = m1
FOR i = 1 TO m1                 'Rearrange the storage a bit
  FOR j = m1 + 2 - i TO mm
    a(i, j - l) = a(i, j)
  NEXT j
  l = l - 1
  FOR j = mm - l TO mm
    a(i, j) = 0
  NEXT j
NEXT i
D = 1
l = m1
FOR k = 1 TO n                  'For each row
  dum = a(k, 1)
  i = k
  IF l < n THEN l = l + 1
  FOR j = k + 1 TO l            'Find the pivot element
    IF ABS(a(j, 1)) > ABS(dum) THEN
      dum = a(j, 1)
      i = j
    END IF
  NEXT j
  indx(k) = i
  IF dum = 0 THEN a(k, 1) = tiny
     'Matrix is algorithmically singular, but proceed anyway with TINY
     'pivot (desirable in some applications).
  IF i <> k THEN                'Interchange rows
    D = -D
    FOR j = 1 TO mm
      dum = a(k, j)
      a(k, j) = a(i, j)
      a(i, j) = dum
    NEXT j
  END IF
  FOR i = k + 1 TO l
    dum = a(i, 1) / a(k, 1)
    al(k, i - k) = dum
    FOR j = 2 TO mm
      a(i, j - l) = a(i, j) - dum * a(k, j)
    NEXT j
    a(i, mm) = 0
```

```
  NEXT i
NEXT k
END SUB

SUB bmatrix (modulus!, inertia!, h, Es(), Tx#(), n, D(), b())

'This subroutine builds the known value or constants vector.  It follows
'the convention A(x)=b where A is the coefficient matrix and b is the
'solution vector.  The x-matrix is call the b-matrix and is changed in
'the subroutine banbks.  It has three nonzero values in the initial
'three rows.  The balance of the entries are zero.

R1 = (modulus! * inertia!) / (h * h * h * h)
R2 = (2 * modulus! * inertia!) / (h * h * h * h)
R3 = -R2

FOR i = 1 TO n
  IF i = 1 THEN
    b(i) = (-1 * D(1, 2)) * (R2 + ((2 * Tx#(i)) / (h * h)) + Es(i))
  ELSEIF i = 2 THEN
    b(i) = (-1 * D(1, 2)) * (R3 - (Tx#(i) / (h * h)))
  ELSEIF i = 3 THEN
    b(i) = (-1 * D(1, 2)) * R1
  ELSE
    b(i) = 0
  END IF
NEXT i

'Print out the b-matrix
'CLS
'FOR i = 1 TO n
'  PRINT b(i),
'NEXT i

END SUB

SUB datainput (D2R#, pi#)

'This subroutine is used to input raw data and calculate other parameters
'needed by the model.

SHARED gamma, phi, k!, Ko!, Ka!, beta, modulus!, inertia!
SHARED b, depth, sigmault, h, n, m1, m2

CLS
'Input the soil variables first.
LOCATE 3, 30: PRINT "INPUT SOIL VARIABLES."
LOCATE 6, 5: PRINT "CAUTION:  At this time, this model can only work with cohesionless"
LOCATE 7, 15: PRINT "soils or sands."
VIEW PRINT 10 TO 25

'Input soil density
LOCATE 11, 5: PRINT "For the soil that you are working with:"
LOCATE 13, 10: INPUT "What is the density (lbs/ft^3)", gamma
  gamma = gamma / 1728
```

```
CLS

'Input soil strength parameters
LOCATE 11, 25: PRINT "Soil Strength Parameters"
LOCATE 14, 10: PRINT "Soil cohesion, c, equals 0 (c = 0)"
  c = 0
LOCATE 16, 10: INPUT "What is the internal angle of friction (degrees)?", phi
  phi = D2R * phi
CLS

'Either input or calculate a coefficient of subgrade reaction or k value
DO
  LOCATE 11, 22:
  PRINT "Coefficient of Subgrade Reaction"
  LOCATE 13, 10:
  PRINT "For the coefficient of subgrade reaction or k value, you may either:"
  LOCATE 15, 10:
  PRINT "(1)  Input a k value now, or"
  LOCATE 17, 10:
  PRINT "(2)  Have the program select an appropriate value for you."

  LOCATE 19, 5: INPUT "Select either (1) or (2) now"; choice

  IF choice = 1 THEN
    LOCATE 21, 2
    INPUT "What is the coefficient of subgrade reaction or k value (lbs/in^3)"; k!
    EXIT DO
  ELSEIF choice = 2 THEN
    CALL subgradereaction
    EXIT DO
  ELSE
    BEEP: PRINT "Please enter a 1 or 2"
  END IF
LOOP

VIEW PRINT
CLS

'Now enter the input parameters of the reinforcing element(s)
LOCATE 5, 21
PRINT "INPUT REINFORCING ELEMENT VARIABLES"
LOCATE 10, 5: INPUT "What is the modulus of elasticity (lbs/in^2)", modulus!
LOCATE 12, 5: INPUT "What is the width or diameter (inches)", b
LOCATE 14, 5: INPUT "What is their depth in the soil (inches)", depth

'Calculate the ultimate tensile stress of the reinforcing element
IF b > .19 THEN
    sigmault = (4 * 1750.9) / pi
  ELSE
    sigmault = (25.4 - (20 * 2.54 * b)) * 1000 / 6.895
END IF

'Calculate the length of the nodes
h = b / 2
```

```
'Calculate the polar moment of inertia for the reinforcing element
inertia! = (pi * b ^ 4) / 64

'Calculate the at-rest earth pressure coefficient
Ko! = 1 - SIN(phi)

'Calculate the active earth pressure coefficient
Ka! = (TAN(45 * D2R - phi / 2)) ^ 2

'Calculate beta
beta = 45 * D2R + phi / 2

'Calculate a first cut at the length of the reinforcing element. Take the
'sigmault value multiply by area and divide by an average Tau (.864) and
'the circumference. This value will be replaced by the length in tension
'later in the program.
'l! = sigmault * b / 3.456
l! = 10

'Calculate the number of nodes
'n = CINT(l! / h)
m1 = 2
m2 = 2
n = l! / h

'Print out the input parameters
CLS
LOCATE 2, 30: PRINT "SOIL PARAMETERS"
LOCATE 4, 5: PRINT "Soil density ="; gamma * 1728; "lbs/ft^3"
LOCATE 5, 5: PRINT "c ="; c; "lbs/in^2"
LOCATE 6, 5: PRINT "phi ="; phi * (180 / pi); "degrees"
LOCATE 7, 5: PRINT "k ="; k!; "lbs/in^3"
LOCATE 8, 5: PRINT "Ko ="; Ko!
LOCATE 9, 5: PRINT "Ka ="; Ka!
LOCATE 10, 5: PRINT "Beta ="; beta; "radians"

LOCATE 13, 23: PRINT "REINFORCEING ELEMENT PARAMETERS"
LOCATE 15, 5: PRINT "modulus ="; modulus!; "lbs/in^2"
LOCATE 16, 5: PRINT "diameter ="; b; "inches"
LOCATE 17, 5: PRINT "depth ="; depth; "inches"
LOCATE 18, 5: PRINT "sigmault ="; sigmault; "lbs/in^2"
LOCATE 19, 5: PRINT "h ="; h; "inches"
LOCATE 20, 5: PRINT "I ="; inertia!; "inches^4"
LOCATE 21, 5: PRINT "Length ="; l!; "inches"
LOCATE 22, 5: PRINT "Number of nodes ="; n
LOCATE 25, 2: PRINT "Press any key to continue"

END SUB

SUB dispmatrix (n, h, D())

'This subroutine builds an initial displacement matrix. The matrix
'notation is d(x, y). The x-value is the vertical or x distance of
'the node centroid from the axis. The y-value is the calculated displacement.
'x = n * h & y at the top is assumed (yt). Subsequent values of y will
```

```
'be calculated.

SHARED yt

'Calculate the x-values of the displacement matrix
FOR i = 1 TO n
  IF i = 1 THEN
    D(i, 1) = 0
  ELSE
    D(i, 1) = (i - 1) * h
  END IF
NEXT i

'Get displacement of y at the top
CLS
LOCATE 10, 5
INPUT "What is the assumed or given displacement of the top node"; yt
D(1, 2) = yt

'Set the rest of the y-displacements to 0
FOR i = 2 TO n
  D(i, 2) = 0
NEXT i

'Print out the displacement matrix
'CLS
'FOR i = 1 TO n
'  FOR j = 1 TO 2
'    PRINT USING "####.####"; d(i, j);
'  NEXT j
'  PRINT
'NEXT i

END SUB

SUB Increment (Zx#, b, h, modulus!, k, Tx#, mud)
SHARED length#, Told#
k = 0
DO
  dT# = (.14085 * (Zx# / (.0562 + (.77 * Zx#) + (.667 * Zx# ^ 2)))) * pi# * b * h
  dz# = (Tx# * h) / (modulus! * pi# / 4 * b ^ 2)
  Tx# = Tx# - dT#
  Zx# = Zx# - dz#
'  k = k + 1
LOOP UNTIL Tx# < 0 OR Zx# < 0
IF Tx# < 0 THEN
  mud = 1
ELSEIF Zx# < 0 THEN
  mud = 2
END IF
length# = (k - 1) * h

END SUB

SUB secantmodulus (k!, b, gamma, phi, depth, pi#, e#, Ka!, Ko!, beta, n, D(), Es())
```

```
'Given a displacement, y, this function will calculate the secant modulus
'from a know p-y curve presented in a hyperbolic-tangent form.  Inputs
'required are k, depth, gamma, phi, and d.  Inputs calculated are Ko, Ka, and
'beta = 45 + phi/2.

Esi = k! * depth
Pult = gamma * b * depth * ((Ka! * ((TAN(beta) ^ 8) - 1)) + (Ko! * TAN(phi) * (TAN(beta) ^ 4)))
Puf = .88 * Pult

FOR i = 1 TO n
  IF D(i, 2) = 0 THEN
    Es(i) = 0
  ELSE
    x = (Esi * D(i, 2)) / Puf
    P = Puf * (((e ^ x) - (e ^ -x)) / ((e ^ x) + (e ^ -x)))
    Es(i) = P / D(i, 2)
  END IF
NEXT i

'Print out the Es values
'CLS
'  FOR i = 1 TO n
'  PRINT Es(i)
'NEXT i
'DO
'LOOP WHILE INKEY$ = ""
END SUB

SUB subgradereaction

SHARED k!

CLS
VIEW PRINT 10 TO 25
DO
  LOCATE 11, 10
  INPUT "Is the soil: (1) loose, (2) medium, or (3) dense"; density%
  LOCATE 15, 10
  INPUT "Is the soil: (1) submerged or (2) above a water table"; water%

    IF density% = 1 AND water% = 1 THEN
       k! = 20
       EXIT DO
     ELSEIF density% = 1 AND water% = 2 THEN
       k! = 25
       EXIT DO
     ELSEIF density = 2 AND water% = 1 THEN
       k! = 60
       EXIT DO
     ELSEIF density% = 2 AND water% = 2 THEN
       k! = 90
       EXIT DO
     ELSEIF density% = 3 AND water% = 1 THEN
       k! = 125
```

```
      EXIT DO
    ELSEIF density% = 3 AND water% = 2 THEN
      k! = 225
      EXIT DO
    ELSE
    BEEP
    PRINT "Please enter only a 1, 2, or 3 when requested."
   END IF
LOOP
END SUB

SUB tension (D(), pi#, n, b, h, modulus!, Tx#(), k, b(), Zx#())

DIM length(n) AS DOUBLE
SHARED T#

'Print out the displacement matris
'CLS
'FOR i = n TO 1 STEP -1
'  FOR j = 1 TO 2
'    PRINT d(i, j),
'  NEXT j
'  PRINT
'NEXT i
'DO
'LOOP WHILE INKEY$ = ""

'First calculate the increase in length of the reinforcing element due
'to the change in shape.
l# = 0
FOR i = 2 TO n
  length#(i - 1) = SQR((D(i - 1, 1) - D(i, 1)) ^ 2 + (D(i - 1, 2) - D(i, 2)) ^ 2)
  l# = l# + length#(i - 1)
NEXT i
l# = l# + h
z# = l# - (n * h)

'LOCATE 22, 5: PRINT "z ="; z#
'LOCATE 23, 5: PRINT "l ="; l#
'LOCATE 24, 5: PRINT "Ft ="; b(1)

'DO
'LOOP WHILE INKEY$ = ""

tenshun# = 1#
inc# = tenshun#
Tx# = tenshun#
Zx# = z#
i = 1

DO
  CALL Increment(Zx#, b, h, modulus!, k, Tx#, mud)

  SELECT CASE mud
    CASE 1
```

```
      DO
        lengthold# = length#
        Told# = tenshun#
        tenshun# = Told# + inc#
        Tx# = tenshun#
        Zx# = z#
        CALL Increment(Zx#, b, h, modulus!, k, Tx#, mud)
      LOOP UNTIL mud = 2
    CASE 2
      DO
        lengthold# = length#
        Told# = tenshun#
        tenshun# = Told# - inc#
        Tx# = tenshun#
        Zx# = z#
        CALL Increment(Zx#, b, h, modulus!, k, Tx#, mud)
      LOOP UNTIL mud = 1
  END SELECT

  T# = (Told# + tenshun#) / 2#
  inc# = inc# / 10#
  i = i + 1
  tenshun# = T#
  Tx# = tenshun#
  Zx# = z#

LOOP UNTIL i = 7

i = 0
Tx#(0) = tenshun#
Zx#(0) = z#
FOR i = 1 TO n
  dT# = (.14085 * (Zx#(i) / (.0562 + (.77 * Zx#(i)) + (.667 * Zx#(i) ^ 2)))) * pi# * b * h
  dz# = (Tx#(i) * h) / (modulus! * pi# / 4 * b ^ 2)
  Tx#(i) = Tx#(i - 1) - dT#
  Zx#(i) = Zx#(i - 1) - dz#
NEXT i


CLS
'FOR l = 0 TO n
'  PRINT l * h, Tx#(l), Zx#(l)
'NEXT l
'PRINT
'FOR l = kold - 1 TO kold
'  PRINT l * h, Tx#(l), Zx#(l)
'NEXT l
'PRINT
'PRINT kold, kold * h, CSNG(T#), CSNG(z#)
'DO
'LOOP WHILE INKEY$ = ""

END SUB
```